58-1931-5-019
DESIGN OF A PROTOTYPE IN
LINE INSPECTION SYSTEM FOR
APPLES
USDA-AFRS
PREPARED: DJ ANESHANSLEY

FINAL REPORT

Agreement Number 58-1931-5-019
Oct. 1, 1995 – June 30, 2000
Design of a Prototype In-Line Inspection System For Apples

Prepared by:
Daniel J. Aneshansley, Assoc. Prof.
Cornell University

The agreement continued the collaborative work between the Appalachian Fruit Research Station and Cornell University with techniques to segment fresh and stored apple bruising on the same apple (Throop et. al. 1995). Studies for either positioning the stem/calyx ends in a known position by orientation (Throop et. al. 1995, Throop et. al. 1997, Throop et. al. 1999) or identifying the stem and calyx (Campins et. al. 1997) to avoid detection as a defect were pursued. Spectra to determine the reflectance properties of the many different defects that can occur on the different cultivars that grow in Eastern United States were recorded. Statistical and neural network analysis was used to find the best wavelengths for identifying 22 different defects on 10 cultivars (Aneshansley et. al. 1997, Miller et. al. 1998). Methods to segment defects were developed for each of the identified wavelengths or combination of wavelengths (Throop and Aneshansley, 1997a and 1997b). Orientation, reflectance spectra, and methods of segmentation were incorporated into an inspection station to find defects on apples at a rate of 5 apples per second (Throop and Aneshansley, 1999a and 1999b). With the possibility of orientation, investigations using body transmittance to detect internal browning were conducted (Upchurch et. al. 1996). Further work needs to be done to bring this work on line.

Papers and patents associated with this project are listed below:

Throop, J. A., D. J. Aneshansley, and B. L. Upchurch. 1995. An image processing algorithm to find new and stored apple bruises. Applied Engineering in Agriculture of the American Society of Agricultural Engineers. 11(5):751-757.

Throop, J. A., D. J. Aneshansley, and B. L. Upchurch. 1995. Apple orientation on automatic sorting equipment. ASAE Paper 956176. ASAE, St. Joseph, MI 49085-9659

Throop, J. A., D. J. Aneshansley, B. L. Upchurch. 1997. Apple orientation on automatic sorting equipment. Proceedings from the Sensors for Nondestructive Testing International Conference, Orlando Florida. pp324-342.

Aneshansley, D. J., J. A. Throop, and B. L. Upchurch. 1997. Reflectance spectra of surface defects on apples. Proceedings from the Sensors for Nondestructive Testing International Conference, Orlando Florida. pp143-160.

Campins, J., J. A. Throop, and D. J. Aneshansley. 1997. Apple stem and calyx identification for automatic sorting. ASAE Paper 973079. ASAE, St. Joseph, MI 49085-9659

Throop, J. A., D. J. Aneshansley. 1997a. Inspection of processed fruit before and after peeling. ASAE Paper 976044. ASAE, St. Joseph, MI 49085-9659

Throop, J. A., D. J. Aneshansley. 1997b. Apple Damage Segmentation utilizing reflectance spectra of the defect. ASAE Paper 973078. ASAE, St. Joseph, MI 49085-9659

Upchurch, B. L., J. A. Throop, and D. J. Aneshansley, 1997. Detecting internal breakdown in apples using interactance measurements. Postharvest Biology and Technology 10(1997)15-19.

Miller, W. M., J. A. Throop, and B. L. Upchurch. 1998. Pattern recognition models for spectral reflectance evaluation of apple blemishes. Postharvest Biology and Technology 14(1998)11-20.

Throop, J. A., D. J. Aneshansley, and B. L. Upchurch. 1999a. Fruit orienting device. U. S. Patent No. 5,855,270. 19p. Commissioner of Patents and Trade Marks, Washington, D.C.

Throop, J. A., D. J. Aneshansley, and B. Anger. 1999b. Inspection station detects defects on apples in real time. ASAE Paper 993205. ASAE, St. Joseph, MI 49085-9659

An Image Processing Algorithm to Find New and Old Bruises

J. A. Throop, D. J. Aneshansley, B. L. Upchurch

Abstract. *Stored 'Red Delicious' apples can have old and new bruises. Previous studies have shown the near-infrared (NIR) reflection of bruised tissue with respect to unbruised tissue to be darker in new (24 h) bruises and lighter in old (four to six weeks) bruises. An algorithm was developed to identify both old and new bruises in the same NIR image. Apple images were low pass filtered to remove small surface characteristics (lenticels) and normalized. Absolute difference between these images and a standard (delrin sphere) representing unbruised tissue were also low pass filtered. A binary image of bruised/unbruised tissue was formed based upon a user defined threshold level. Shapes of the bruised areas were evaluated and, based upon a shape factor, either dismissed or counted as bruised areas. The algorithm detected both old and new bruises except for large 25 to 35 mm (0.98 to 1.38 in.) diameter old bruises. These bruises had areas within their boundaries where NIR reflectance had not changed completely from darker to lighter than unbruised tissue. This patterning altered the bruise shape causing the algorithm to discount them.* **Keywords.** *Apples, Apple quality, Bruise, Bruise detection, Image analysis, Image processing.*

Algorithms to separate bruise information from the rest of the NIR image of an apple have been attempted by only a few researchers. Digital matrix camera images of apple NIR reflectance have been processed with an algorithm using a multivariable linear statistical classifier that classified bruised from unbruised apple tissue as well as a human inspector (Graf et al., 1981).

A digital linescan camera captured images of apple NIR reflectance eliminating both spatial distortion in one dimension and image background (Taylor, 1985). However, the pixel grey level nonuniformity caused data variability requiring a time-consuming data normalization process for a quadratic statistical classifier to operate.

A nonstatistical algorithm for linescan images of apple NIR reflectance was developed (Throop et al., 1988) and tested on experimentally machine-harvested apples (Rehkugler et al., 1989). This algorithm creates a new image from the original by averaging a plurality of adjacent pixel values of the same row. The original image is subtracted from the averaged image. The resulting image is inverted and converted to a binary image by thresholding. The black pixel clusters are evaluated for their shape by finding the relationship of their area with respect to their perimeter (shape factor). Only elliptical- to circular-shaped clusters (shape factor 0.7 to 1.5) are counted as bruises.

The above algorithm was only applied to apple images of NIR reflectance which were bruised and held at room temperature for 24 h. NIR reflectance has been shown to change with extended storage (Rehkugler et al., 1976; Upchurch et al., 1992). NIR reflectance of bruised tissue is less than unbruised tissue 24 h after bruising, but slowly increases to be equal and exceed the reflectance of unbruised tissue over time (one to two months) during cold storage. The problem of sorting fruit which could have both old (stored) bruises and new bruises, acquired during removal from storage, has not been addressed.

Objectives

The first objective is to develop an algorithm which can separate old and new bruised tissue from stored apples by using NIR reflectance. The second objective is to demonstrate an experimental method to estimate the value of user supplied variables, minimum shape factor, and threshold factor required in the algorithm for optimal bruised tissue classification.

Materials and Methods

A 512 diode array line scan camera (EG&G Reticon LC1901FAN-011, Sunnyvale, Calif.) with a 25 mm (0.98 in.) lens using an aperture setting of f2.0 and with a longpass filter (Wratten 89B, Kodak, Rochester, N.Y.) in front of the lens captured the images. Image digitization was performed by a line scan processor (DT2856, Data Translation, Marlboro, Md.) set for externally triggered single line per trigger acquisition mode, clocked at 156.25 kHz, 525 counts per line, a line transfer value of 20, and a total line count of 360. The intensity value for every

Article has been reviewed and approved for publication by the Information and Electrical Technologives Div. of ASAE. Presented as ASAE Paper No. 93-6534.

Mention of specific products is for the information of the reader and is not considered an endorsement by Cornell University, USDA-Agricultural Research Service, or the authors.

The authors are **James A. Throop**, ***ASAE Member Engineer,*** Research Support Specialist, **Daniel J. Aneshansley**, ***ASAE Member Engineer,*** Associate Professor, Cornell University, Dept. of Agricultural and Biological Engineering, Ithaca, N.Y.; and **Bruce L. Upchurch**, ***ASAE Member Engineer,*** Agricultural Engineer, USDA-Agricultural Research Service, Appalachian Fruit Research Station, Kearneysville, W.V. **Corresponding author:** James A. Throop, Dept. of Agriculture and bilogical Engineering, Cornell University, Riley-Robb Hall, Ithaca, NY 14853; e-mail: <jat12@cornell.edu>.

five counts per line were averaged so that a 360V × 105H pixel image of the apple surface was formed. The microcomputer (Gateway 386SX/25 mHz, North Sioux City, S.D.) provided a pulse to trigger both the stepper motor and the line scan camera. Subroutine functions (DT_Linescan, Data Translation) and the "C" programming language (Microsoft C 6.0, Microsoft Corp., Redmond, Wash.) were used for algorithm development.

Illumination consisted of eight standard incandescent lamps (model 40A, 40W, General Electric, Cleveland, Ohio) placed between an outer reflective chamber surface and an inner white acrylic diffuser [254 μm (10 mil)]. Apples were rotated by a stepper motor (ABS 3008-006, 12V, 1.0°, Hurst, Princeton, Ind.) driven spindle on the opposite side of the acrylic diffuser.

A custom turned 7.62 cm (3.0 in.) diameter white delrin sphere (Great Lakes Plastics, Buffalo, N.Y.) is known to be a good standard to represent unbruised 'Red Delicious' apple tissue (Throop et al., 1993).

Algorithm Description

Load and Process Image of Delrin Sphere

The delrin sphere image (fig. 1c), captured for the same lighting and camera setup as for capturing the apple images (figs. 1a and 1b), is normalized to a grey level intensity of 200. The average intensity of each 360 pixel column is found and divided into 200. The product of the resulting scaling factor and each pixel value in that column is substituted in the delrin sphere image (fig. 1d).

Load and Low Pass Filter Apple Image

Each apple image (figs. 1a and 1b) is loaded and a 5 × 5 mean filter convolution is performed. The need for this process was to smooth the intensities of the brighter lenticels visible in the image background so that a more uniform background average can be found for background normalization.

Normalize Background of Apple Image

The sum of the center column pixel intensities of the upper 180 pixel rows is found. All columns of 180 pixel rows whose sum is equal or greater than 80% of the central column sum are normalized. The remaining pixels are set to 0. The average pixel intensity for each 180 pixel column to be normalized is found and divided into 200. Each pixel intensity for that column is multiplied by the resulting scale factor (fig. 2a). A similar operation is performed on rows 181 to 360 resulting in the apple image background

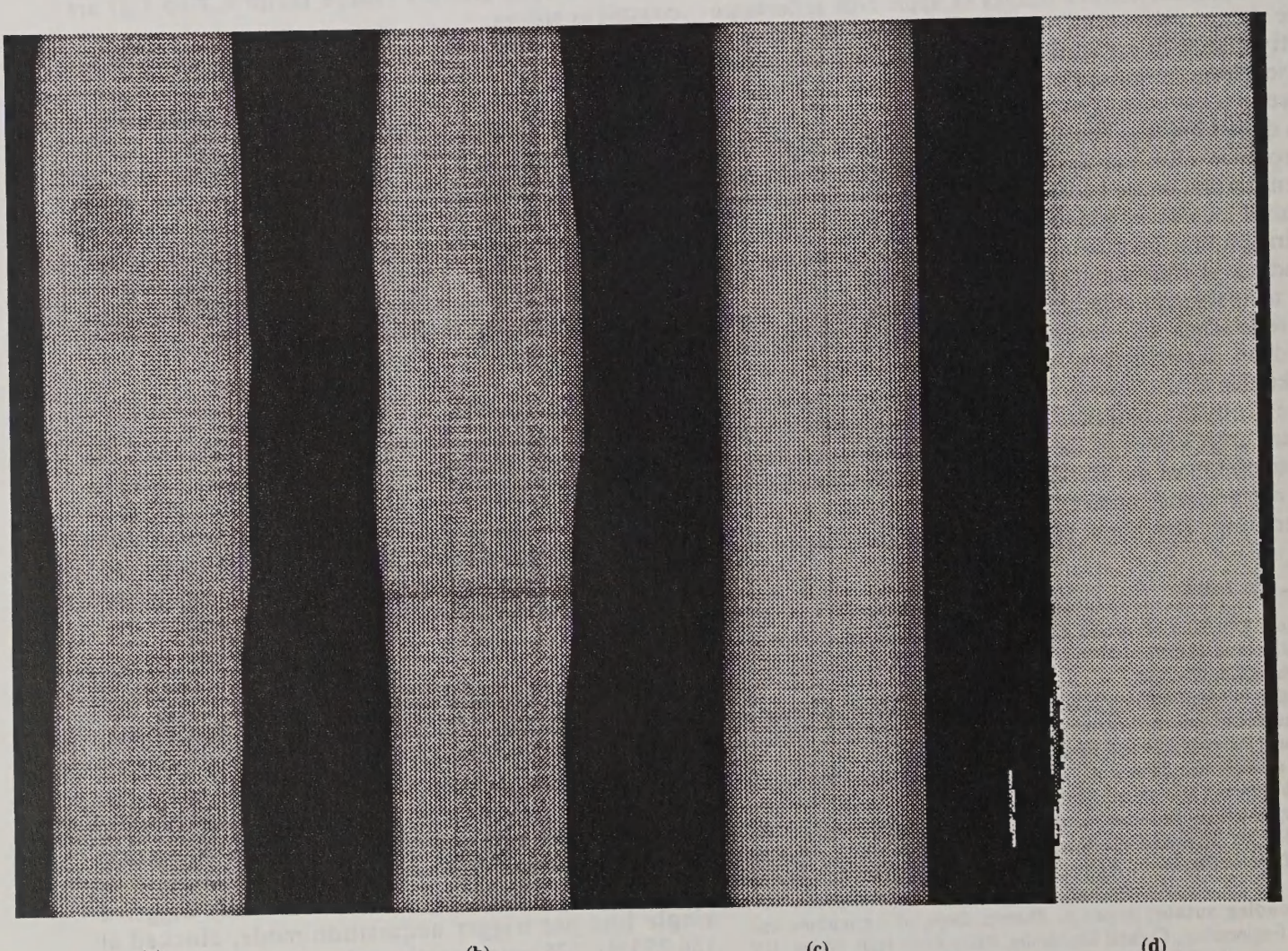

(a) (b) (c) (d)

Figure 1–Composite NIR grey tone digital linescan image: (a) apple with 24-h-old bruise, (b) apple with 2-month-old bruise, (c) delrin sphere unnormalized, and (d) delrin sphere normalized to grey level 200.

(fig. 2b) being of approximately equal intensity as the normalized delrin sphere standard (fig. 1d).

Subtract Apple Image From Normalized Delrin Image

By normalizing the backgrounds of both the apple and delrin images, their absolute difference results in an image of the high frequency intensity changes, brighter and darker, appearing as light pixels. Each pixel of the resulting image is multiplied by 10 (fig. 2c).

Low Pass Filter the Resulting Image

The image is smoothed by a 5 × 5 mean filter convolution to even out any small pixel areas of sharp contrast. This causes a slight blurring which is visible in figure 2d.

Threshold Image to Convert to a Binary Image

The average grey level for the first 180 rows of each column is calculated and multiplied by a user supplied multiplier (threshold factor). Any pixel grey level greater than this value is set to 0, otherwise the pixel is set to 255 (fig. 3a). This process is repeated on each column for rows 181 to 360. The resulting binary image has black pixels at all of the previous brighter areas and white pixels for the darker background (fig. 3b). The threshold factor value can be estimated by the user processing a small representative sample of bruised fruit. Examination of the resulting thresholded images to determine if the bruised areas have been segmented from the surrounding unbruised tissue can be used as a measure to approximate the value of the threshold factor.

Closing of the Image

The mathematical morphological process (Haralick et al., 1987) of closing black pixel objects with a 5 × 5 structuring element eliminated details in the image that were smaller than the structuring element size and produced little change in the size of larger black pixel clusters (fig. 3c).

Find Pixel Cluster Shape From Area and Perimeter

The area and perimeter of each black pixel cluster in figure 3c is found and the cluster shape factor is found (Rehkugler et al., 1989). If the shape factor (1.0 for a circle) is greater than a user selected minimum and less than 1.5, the pixel cluster is counted as a bruise and the area is recorded; otherwise, the algorithm discounts the dark cluster as a bruise and continues. The final processed

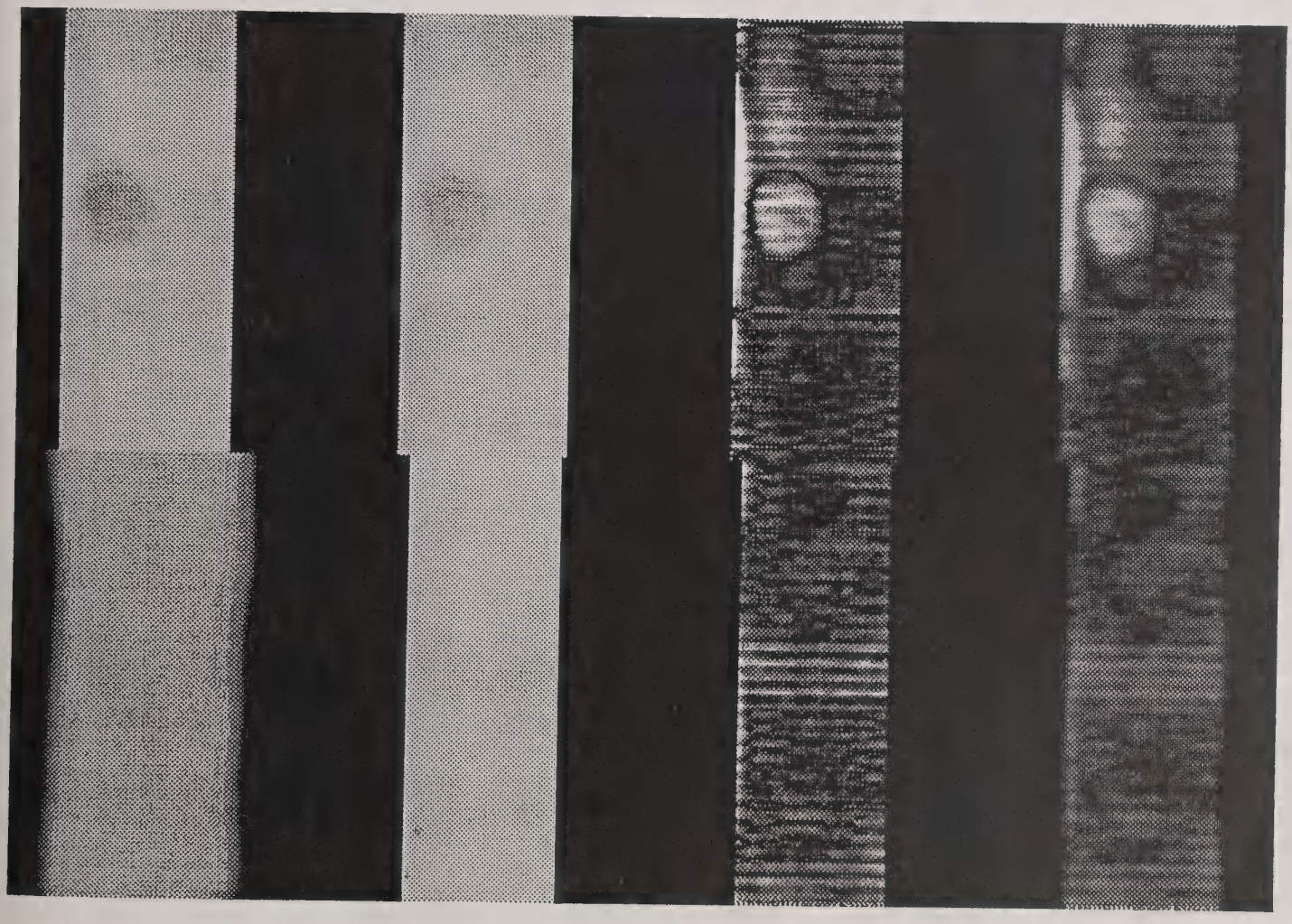

(a) (b) (c) (d)

Figure 2–Processed NIR images of an apple with a 24-h-old bruised apple: (a) background normalized to grey level equal to 200 for half of the apple surface, (b) all of background normalized to grey level 200, (c) absolute difference of normalized sphere and apple image, and (d) 5 × 5 low pass filtered image of c.

image shows that the algorithm has successfully segmented the bruised area from the unbruised areas (fig. 3d).

Load a New Apple Image and Repeat Image Process

Figure 1a is a NIR image of a 24-h-old bruise on a 'Red Delicious' apple. Figure 1b is the same apple bruise after two months in storage. Figures 4 and 5 show a sequence of images as processing occurs for the two-month-old bruise. The results are very similar to the same apple 24 h after bruising (figs. 2 and 3) except that the final processed image shows three small false clusters that were counted as bruises (fig. 5d).

Selection of Threshold and Shape Factors in the Algorithm

Eighty-seven 'Red Delicious' apples, harvested during the 1992 harvest season, were used to evaluate the algorithm. The apples were removed from cold storage in December 1992, and allowed to warm to room temperature (6 h). The apples were divided into three groups of 29 apples. Each apple of the first group was dropped 5 cm (1.97 in.) [bruise diameters = 11 to 15 mm (4.33 to 5.91 in.)], the second group was dropped 15 cm (5.91 in.) [bruise diameters = 19 to 25 mm (7.48 to 9.84 in.)], and the third group was dropped 25 cm (9.84 in.) [bruise diameters = 25 to 35 mm (9.84 to 13.77 in.)] onto a flat steel plate. Images were captured 24 h and 2 months after bruising with the apples held in cold storage between image captures.

The algorithm was used to process the three groups of 'Red Delicious' apples using three different threshold factors (1.2, 1.4, 1.6) and three different minimum shape factors (0.8, 0.9, 1.0).

Results and Discussion

A number of pixel clusters which were not bruise pixels were retained after the algorithm processed the apple images 24 h after bruising. Table 1 shows the average number of false bruise pixel clusters per apple and their average area in pixels which were included as bruised tissue for three drop heights, three minimum shape factors, and three threshold factors. For any minimum shape factor selected, as the threshold factor increased, the average number of false bruise pixel clusters decreased. Also for any threshold factor selected, as the minimum shape factor increased, the number of false bruise pixel clusters decreased.

Figure 3–Further processing of an apple with a 24-h-old bruise: (a) binary threshold of top half of image based on the product of column average and threshold factor, (b) binary threshold of bottom half of image based on the product of column average and threshold factor, (c) closed binary image, and (d) pixel cluster counted as a bruise based on shape.

An Image Processing Algorithm to Find New and Old Bruises

J. A. Throop, D. J. Aneshansley, B. L. Upchurch

Abstract. *Stored 'Red Delicious' apples can have old and new bruises. Previous studies have shown the near-infrared (NIR) reflection of bruised tissue with respect to unbruised tissue to be darker in new (24 h) bruises and lighter in old (four to six weeks) bruises. An algorithm was developed to identify both old and new bruises in the same NIR image. Apple images were low pass filtered to remove small surface characteristics (lenticels) and normalized. Absolute difference between these images and a standard (delrin sphere) representing unbruised tissue were also low pass filtered. A binary image of bruised/unbruised tissue was formed based upon a user defined threshold level. Shapes of the bruised areas were evaluated and, based upon a shape factor, either dismissed or counted as bruised areas. The algorithm detected both old and new bruises except for large 25 to 35 mm (0.98 to 1.38 in.) diameter old bruises. These bruises had areas within their boundaries where NIR reflectance had not changed completely from darker to lighter than unbruised tissue. This patterning altered the bruise shape causing the algorithm to discount them.* **Keywords.** *Apples, Apple quality, Bruise, Bruise detection, Image analysis, Image processing.*

Algorithms to separate bruise information from the rest of the NIR image of an apple have been attempted by only a few researchers. Digital matrix camera images of apple NIR reflectance have been processed with an algorithm using a multivariable linear statistical classifier that classified bruised from unbruised apple tissue as well as a human inspector (Graf et al., 1981).

A digital linescan camera captured images of apple NIR reflectance eliminating both spatial distortion in one dimension and image background (Taylor, 1985). However, the pixel grey level nonuniformity caused data variability requiring a time-consuming data normalization process for a quadratic statistical classifier to operate.

A nonstatistical algorithm for linescan images of apple NIR reflectance was developed (Throop et al., 1988) and tested on experimentally machine-harvested apples (Rehkugler et al., 1989). This algorithm creates a new image from the original by averaging a plurality of adjacent pixel values of the same row. The original image is subtracted from the averaged image. The resulting image is inverted and converted to a binary image by thresholding. The black pixel clusters are evaluated for their shape by finding the relationship of their area with respect to their perimeter (shape factor). Only elliptical- to circular-shaped clusters (shape factor 0.7 to 1.5) are counted as bruises.

The above algorithm was only applied to apple images of NIR reflectance which were bruised and held at room temperature for 24 h. NIR reflectance has been shown to change with extended storage (Rehkugler et al., 1976; Upchurch et al., 1992). NIR reflectance of bruised tissue is less than unbruised tissue 24 h after bruising, but slowly increases to be equal and exceed the reflectance of unbruised tissue over time (one to two months) during cold storage. The problem of sorting fruit which could have both old (stored) bruises and new bruises, acquired during removal from storage, has not been addressed.

Objectives

The first objective is to develop an algorithm which can separate old and new bruised tissue from stored apples by using NIR reflectance. The second objective is to demonstrate an experimental method to estimate the value of user supplied variables, minimum shape factor, and threshold factor required in the algorithm for optimal bruised tissue classification.

Materials and Methods

A 512 diode array line scan camera (EG&G Reticon LC1901FAN-011, Sunnyvale, Calif.) with a 25 mm (0.98 in.) lens using an aperture setting of f2.0 and with a longpass filter (Wratten 89B, Kodak, Rochester, N.Y.) in front of the lens captured the images. Image digitization was performed by a line scan processor (DT2856, Data Translation, Marlboro, Md.) set for externally triggered single line per trigger acquisition mode, clocked at 156.25 kHz, 525 counts per line, a line transfer value of 20, and a total line count of 360. The intensity value for every

Article has been reviewed and approved for publication by the Information and Electrical Technologives Div. of ASAE. Presented as ASAE Paper No. 93-6534.

Mention of specific products is for the information of the reader and is not considered an endorsement by Cornell University, USDA-Agricultural Research Service, or the authors.

The authors are **James A. Throop**, ***ASAE Member Engineer***, Research Support Specialist, **Daniel J. Aneshansley**, ***ASAE Member Engineer***, Associate Professor, Cornell University, Dept. of Agricultural and Biological Engineering, Ithaca, N.Y.; and **Bruce L. Upchurch**, ***ASAE Member Engineer***, Agricultural Engineer, USDA-Agricultural Research Service, Appalachian Fruit Research Station, Kearnesville, W.V. **Corresponding author:** James A. Throop, Dept. of Agriculture and bilogical Engineering, Cornell University, Riley-Robb Hall, Ithaca, NY 14853; e-mail: <jat12@cornell.edu>.

  0883-8542 / 95 / 1105-0751

five counts per line were averaged so that a 360V × 105H pixel image of the apple surface was formed. The microcomputer (Gateway 386SX/25 mHz, North Sioux City, S.D.) provided a pulse to trigger both the stepper motor and the line scan camera. Subroutine functions (DT_Linescan, Data Translation) and the "C" programming language (Microsoft C 6.0, Microsoft Corp., Redmond, Wash.) were used for algorithm development.

Illumination consisted of eight standard incandescent lamps (model 40A, 40W, General Electric, Cleveland, Ohio) placed between an outer reflective chamber surface and an inner white acrylic diffuser [254 μm (10 mil)]. Apples were rotated by a stepper motor (ABS 3008-006, 12V, 1.0°, Hurst, Princeton, Ind.) driven spindle on the opposite side of the acrylic diffuser.

A custom turned 7.62 cm (3.0 in.) diameter white delrin sphere (Great Lakes Plastics, Buffalo, N.Y.) is known to be a good standard to represent unbruised 'Red Delicious' apple tissue (Throop et al., 1993).

Algorithm Description

Load and Process Image of Delrin Sphere

The delrin sphere image (fig. 1c), captured for the same lighting and camera setup as for capturing the apple images (figs. 1a and 1b), is normalized to a grey level intensity of 200. The average intensity of each 360 pixel column is found and divided into 200. The product of the resulting scaling factor and each pixel value in that column is substituted in the delrin sphere image (fig. 1d).

Load and Low Pass Filter Apple Image

Each apple image (figs. 1a and 1b) is loaded and a 5 × 5 mean filter convolution is performed. The need for this process was to smooth the intensities of the brighter lenticels visible in the image background so that a more uniform background average can be found for background normalization.

Normalize Background of Apple Image

The sum of the center column pixel intensities of the upper 180 pixel rows is found. All columns of 180 pixel rows whose sum is equal or greater than 80% of the central column sum are normalized. The remaining pixels are set to 0. The average pixel intensity for each 180 pixel column to be normalized is found and divided into 200. Each pixel intensity for that column is multiplied by the resulting scale factor (fig. 2a). A similar operation is performed on rows 181 to 360 resulting in the apple image background

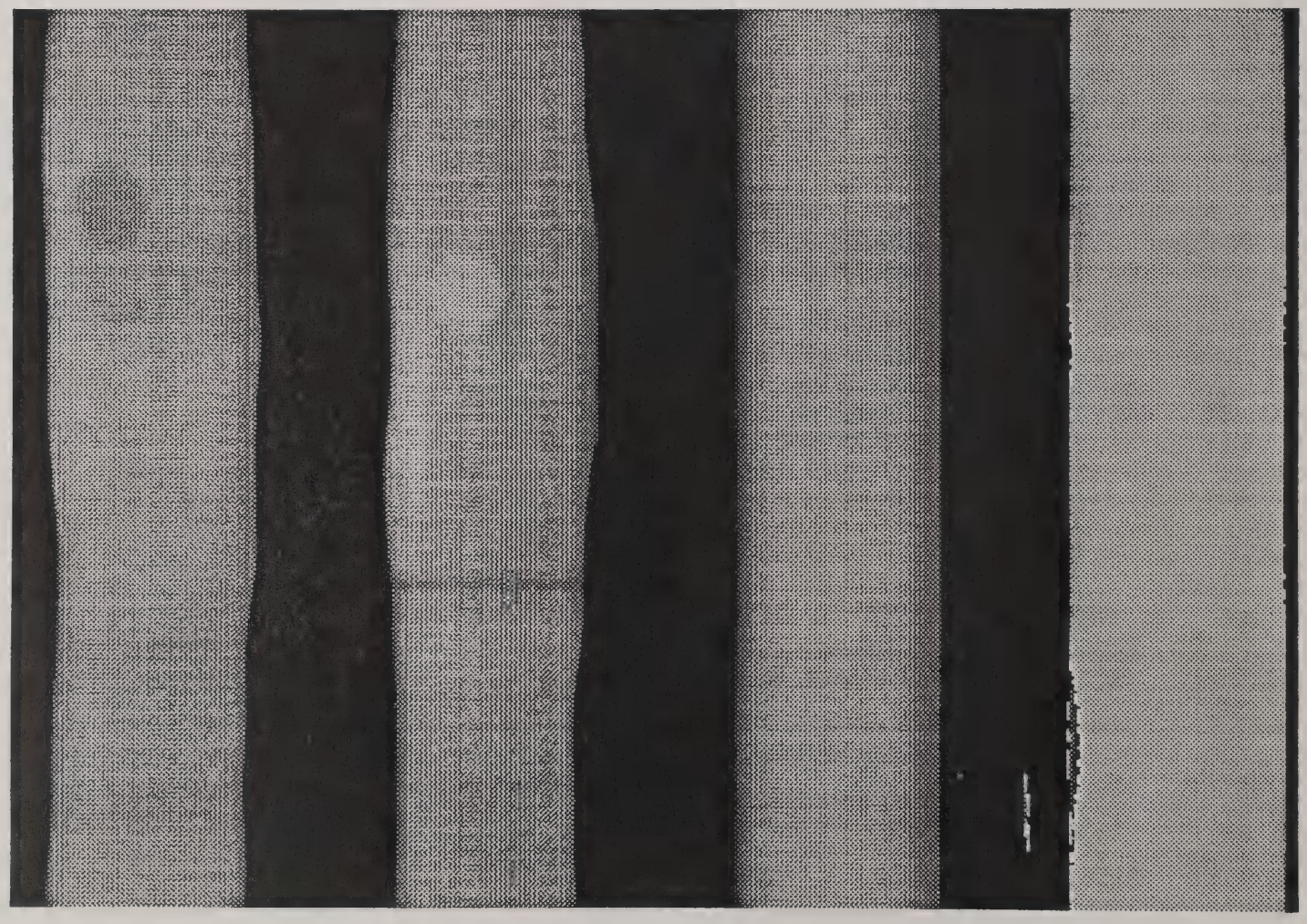

(a) (b) (c) (d)

Figure 1–Composite NIR grey tone digital linescan image: (a) apple with 24-h-old bruise, (b) apple with 2-month-old bruise, (c) delrin sphere unnormalized, and (d) delrin sphere normalized to grey level 200.

(fig. 2b) being of approximately equal intensity as the normalized delrin sphere standard (fig. 1d).

Subtract Apple Image From Normalized Delrin Image

By normalizing the backgrounds of both the apple and delrin images, their absolute difference results in an image of the high frequency intensity changes, brighter and darker, appearing as light pixels. Each pixel of the resulting image is multiplied by 10 (fig. 2c).

Low Pass Filter the Resulting Image

The image is smoothed by a 5 × 5 mean filter convolution to even out any small pixel areas of sharp contrast. This causes a slight blurring which is visible in figure 2d.

Threshold Image to Convert to a Binary Image

The average grey level for the first 180 rows of each column is calculated and multiplied by a user supplied multiplier (threshold factor). Any pixel grey level greater than this value is set to 0, otherwise the pixel is set to 255 (fig. 3a). This process is repeated on each column for rows 181 to 360. The resulting binary image has black pixels at all of the previous brighter areas and white pixels for the darker background (fig. 3b). The threshold factor value can be estimated by the user processing a small representative sample of bruised fruit. Examination of the resulting thresholded images to determine if the bruised areas have been segmented from the surrounding unbruised tissue can be used as a measure to approximate the value of the threshold factor.

Closing of the Image

The mathematical morphological process (Haralick et al., 1987) of closing black pixel objects with a 5 × 5 structuring element eliminated details in the image that were smaller than the structuring element size and produced little change in the size of larger black pixel clusters (fig. 3c).

Find Pixel Cluster Shape From Area and Perimeter

The area and perimeter of each black pixel cluster in figure 3c is found and the cluster shape factor is found (Rehkugler et al., 1989). If the shape factor (1.0 for a circle) is greater than a user selected minimum and less than 1.5, the pixel cluster is counted as a bruise and the area is recorded; otherwise, the algorithm discounts the dark cluster as a bruise and continues. The final processed

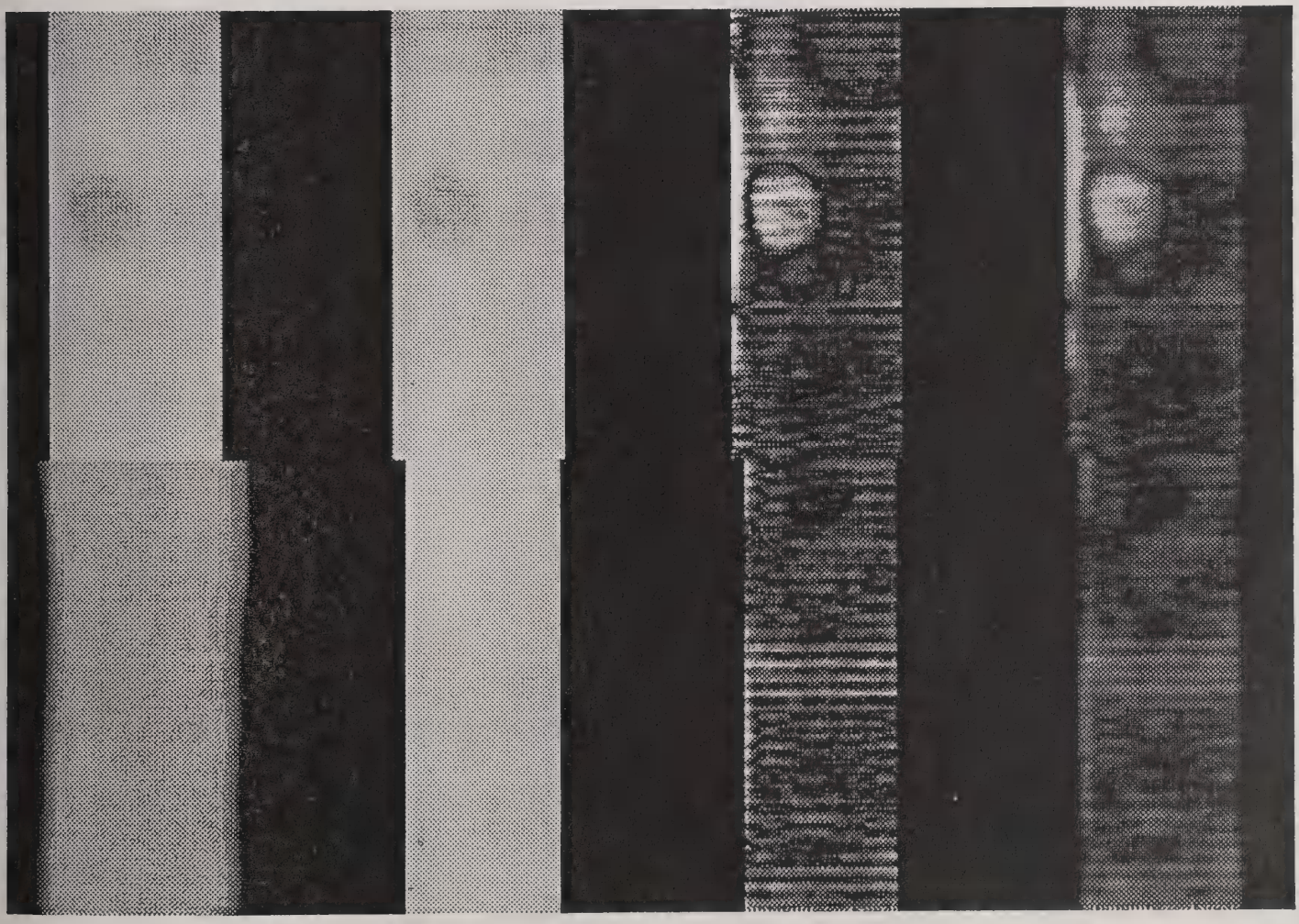

(a) (b) (c) (d)

Figure 2–Processed NIR images of an apple with a 24-h-old bruised apple: (a) background normalized to grey level equal to 200 for half of the apple surface, (b) all of background normalized to grey level 200, (c) absolute difference of normalized sphere and apple image, and (d) 5 × 5 low pass filtered image of c.

image shows that the algorithm has successfully segmented the bruised area from the unbruised areas (fig. 3d).

Load a New Apple Image and Repeat Image Process

Figure 1a is a NIR image of a 24-h-old bruise on a 'Red Delicious' apple. Figure 1b is the same apple bruise after two months in storage. Figures 4 and 5 show a sequence of images as processing occurs for the two-month-old bruise. The results are very similar to the same apple 24 h after bruising (figs. 2 and 3) except that the final processed image shows three small false clusters that were counted as bruises (fig. 5d).

Selection of Threshold and Shape Factors in the Algorithm

Eighty-seven 'Red Delicious' apples, harvested during the 1992 harvest season, were used to evaluate the algorithm. The apples were removed from cold storage in December 1992, and allowed to warm to room temperature (6 h). The apples were divided into three groups of 29 apples. Each apple of the first group was dropped 5 cm (1.97 in.) [bruise diameters = 11 to 15 mm (4.33 to 5.91 in.)], the second group was dropped 15 cm (5.91 in.) [bruise diameters = 19 to 25 mm (7.48 to 9.84 in.)], and the third group was dropped 25 cm (9.84 in.) [bruise diameters = 25 to 35 mm (9.84 to 13.77 in.)] onto a flat steel plate. Images were captured 24 h and 2 months after bruising with the apples held in cold storage between image captures.

The algorithm was used to process the three groups of 'Red Delicious' apples using three different threshold factors (1.2, 1.4, 1.6) and three different minimum shape factors (0.8, 0.9, 1.0).

Results and Discussion

A number of pixel clusters which were not bruise pixels were retained after the algorithm processed the apple images 24 h after bruising. Table 1 shows the average number of false bruise pixel clusters per apple and their average area in pixels which were included as bruised tissue for three drop heights, three minimum shape factors, and three threshold factors. For any minimum shape factor selected, as the threshold factor increased, the average number of false bruise pixel clusters decreased. Also for any threshold factor selected, as the minimum shape factor increased, the number of false bruise pixel clusters decreased.

Figure 3–Further processing of an apple with a 24-h-old bruise: (a) binary threshold of top half of image based on the product of column average and threshold factor, (b) binary threshold of bottom half of image based on the product of column average and threshold factor, (c) closed binary image, and (d) pixel cluster counted as a bruise based on shape.

A false pixel area of 198 pixels translates to an equivalent bruise diameter of 15.9 mm (0.625 in.). This is equal to the maximum bruising allowed for extra fancy fruit (USDA Agricultural Marketing Services, 1972). All false bruise clusters for a minimum shape factor of 0.8 and false bruise clusters for a minimum shape factor of 0.9 with a threshold factor of 1.2 exceed a false pixel area of 200 pixels. The value of 0.8 can be eliminated as an acceptable shape factor.

Table 2 shows the percentage of bruises that were correctly identified by the algorithm using the two remaining shape factors, three drop heights, and three threshold factors. Using a minimum shape factor of 0.9 and a threshold factor of 1.4, the greatest percentage of bruises was found regardless of drop height (bruise size). For all threshold and minimum shape factors, as the drop height (bruise size) increased, the percent of bruises located increased.

Table 3 shows the percentage of 24-h-old and 2-month-old bruises correctly located and the average number of false pixel clusters per apple using a shape factor equal to 0.9 and threshold factor equal to 1.4. The results for both bruise ages are very similar except for the largest bruise size [25 cm (9.84 in.) drop height]. The two-month-old large bruises had small pixel areas within the bruise boundaries where the reflectance had changed to equal unbruised tissue, but was not greater than unbruised tissue. This altered the bruise shape causing the algorithm to discount the large bruise. The percentage of two-month-old large bruises [25 cm (9.84 in.) drop height] correctly located was 48% compared to 93% for 24-h-old bruises.

Conclusions

An algorithm was developed that could detect both 24-h-old (NIR reflectance less than unbruised tissue) and 2-month-old bruises (NIR reflectance greater than unbruised tissue).

A minimum shape factor equal to 0.9 and threshold factor of 1.4 best separated 24-h-old and 2-month-old bruises with bruise diameters of 11 to 35 mm (0.43 to 1.38 in.). The two-month-old large bruises had small pixel areas within the bruise boundaries where the reflectance had not changed completely from darker to lighter than unbruised tissue. This patterning altered the bruise shape causing the algorithm to discount the large bruise. An average of one false bruise cluster can be expected on each apple with a 200 pixel area equivalent to 15.9 mm (0.625 in.) diameter bruise for the 0.9 minimum shape factor and the 1.4 threshold factor selected.

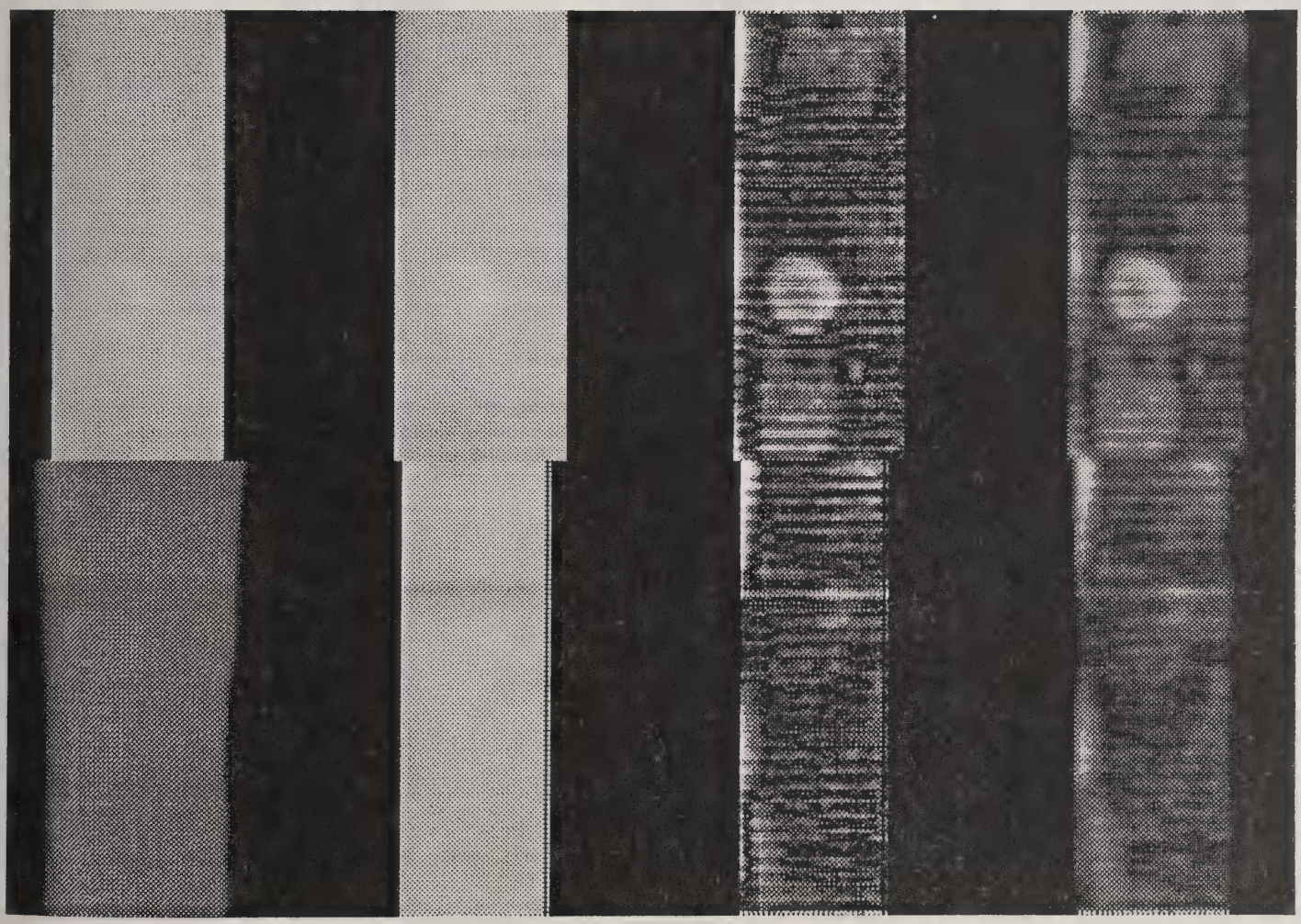

(a) (b) (c) (d)

Figure 4–Processed NIR images of an apple with a two-month-old bruise: (a) background normalized to grey level equal to 200 for half of the apple surface, (b) all of background normalized to grey level 200, (c) absolute difference of normalized sphere and apple image, and (d) 5 × 5 low pass filtered image of c.

Figure 5–Further processing of an apple with a two-month-old bruise: (a) binary threshold of top half of image based on the product of column average and threshold factor, (b) binary threshold of bottom half of image based on the product of column average and threshold factor, (c) closed binary image, and (d) pixel cluster counted as a bruise based on shape.

Table 1. Average number and area in pixels of error clusters for three threshold factors, three shape factors, and three drop heights for apples with 24-h-old bruises

	Threshold Factors					
	1.2		1.4		1.6	
Drop Height (cm)	No. Error Clusters	Area	No. Error Clusters	Area	No. Error Clusters	Area
Shape Factor = 0.8						
5	2.9	220	2.6	166	1.8	173
15	2.7	245	2.2	230	1.5	189
25	3.2	288	2.3	201	1.7	179
Shape Factor = 0.9						
5	1.7	220	1.1	157	0.6	171
15	0.9	326	0.7	188	0.6	171
25	1.7	347	1.1	184	1.0	172
Shape Factor = 1.0						
5	0.4	490	0.2	114	0.3	137
15	0.3	571	0.2	477	0.1	156
25	0.3	971	0.3	173	0.1	162

NOTE: 1 pixel = 1mm^2 (0.00155 in.^{2}).

Table 2. Average percentage of 24-h-old bruises that were correctly identified by the algorithm for two shape factors, three drop heights, and three threshold factors

Drop Height	Threshold Factors		
(cm)	1.2%	1.4%	1.6%
Shape Factor = 0.9			
5	52	52	38
15	65	69	69
25	83	93	90
Shape Factor = 1.0			
5	28	28	28
15	52	66	52
25	79	86	86

Table 3. The percent of correctly identified bruises and the number of error clusters for 24-h-old and 2-month-old bruises for three drop heights using a threshold factor of 1.4 and a shape factor of 0.9

Drop Height	24 Hour		2 Month	
(cm)	(%)	(No.)	(%)	(No.)
5	52	1.1	52	1.1
15	69	0.7	66	0.9
25	93	1.1	48	1.3

References

Graf, G. L., G. E. Rehkugler, W. F. Millier and J. A. Throop. 1981. Detection of surface flaws on apples using digital image processing. ASAE Paper No. 81-3537. St. Joseph, Mich.: ASAE.

Haralick, R. M., S. R. Sternberg and X. Zhuang. 1987. Image analysis using mathematical morphology. *IEEE Transactions on Pattern Analysis and Machine Intelligence* PAMI-9(4):532-549.

Rehkugler, G. E., W. F. Millier, R. A. Pellerin and J. A. Throop. 1976. Design criteria for apple bruise detection by infrared radiation. In *Proc. First Int. Congress on Engineering and Food*, Boston, Mass. St. Joseph, Mich.: ASAE.

Rehkugler, G. E. and J. A. Throop. 1989. Image processing algorithm for apple defect detection. *Transactions of the ASAE* 32(1):267-272.

Taylor, R. W. 1985. Automated detection of apple bruises. M.S. thesis, Cornell Univ., Ithaca, N.Y.

Throop, J. A. and G. E. Rehkugler. 1988. Image processing system for detecting bruises on fruit. U.S. Patent No. 4741042. Issued 26 April.

Throop, J. A., D. J. Aneshansely and B. L. Upchurch. 1993. Optimizing lighting and lens aperture for maximum contrast between bruised and unbruised apple tissue. ASAE Paper 93-3595. St. Joseph, Mich.: ASAE.

Upchurch, B. L. and J. A. Throop. 1992. Time effects on near-infrared imaging for detecting bruises on apples. Paper No. 1836-03. In *Proc. Optics in Agriculture and Forestry*. Bellingham, Wash.: SPIE.

USDA-Agricultural Marketing Service. 1972. United States standards for grades of apples. F. R. Doc. 64-7406, amended 1 October 1966 and 25 July 1972. Washington, D.C.: Food Safety and Quality Service.

Paper No. 956176
An ASAE Meeting Presentation

Apple Orientation on Automatic Sorting Equipment

James A. Throop, Daniel J. Aneshansley

Cornell University, Department of Agricultural and Biological Engineering, Ithaca, NY 14853

Bruce L. Upchurch

USDA-ARS Appalachian Fruit Research Station
Kearneysville, WV 25430

Written for presentation at the
1995 Annual International Meeting
sponsored by
ASAE -- The Society for engineering in agriculture, food, and biological systems

Hyatt Regency
Chicago, Illinois
June, 18 - 23, 1995

Summary: Four methods to orient apples so that their axis of rotation passes through the stem/calyx ends are presented. The time to orient unoriented apples, the time apples placed in orientation remain, and their height and width are recorded for two commercial conveyors and two experimental conveyors for 5 apple cultivars. One experimental method oriented 88% to 100% of 4 cultivars. Red Delicious oriented poorly on all devices. The difference between apple height and width, fruit shape, size, stem stiffness and length, and surface curvature appear to play a roll in apple orientation.

Keywords: Apple, Inspection, Sorting Fruit, Post-Harvest Technology

ASAE, 2950 Niles Rd., St. Joseph, MI 49085-9659 USA
Voice: 616.429.0300 FAX: 616.429.3852

Acknowledgements: The authors would like to thank Prof. W. W. Gunkel, Prof. W. F. Millier, and C. Jiang for their helpful comments and reviews of this paper. Financial support for this work was provided through a Cooperative Agreement with USDA-ARS Appalachian Fruit Research Station #58-1931-3-001 and Hatch Grants NE179 and 412.

ABSTRACT

Four methods to orient apples to place their axis of rotation through the stem and calyx were tested. Two methods used commercial bicone conveyors and two were experimental, consisting of free- to-rotate cone rollers and a powered cylindrical roller. The times to orient an unoriented apple and the time an apple placed in orientation remained in orientation were recorded.

Experimental method 1 oriented Cortlands (100%), Empires (88%), Idareds (96%) and Jonagolds (98%). If orientation occurred, it was sucessful within 10 - 13 seconds. Furthermore, once oriented, they stayed oriented at least 98% percent of the time for 20 seconds (maximum period of observation). However, method 1 was unsuccessful in orienting Red Delicious (12%) and only 60% stayed oriented for the 20 seconds.

Experimental method 2 required 4 - 5 seconds longer to orient Cortlands, Idareds, Jonagold, and Empires. As the oriented fruit rotated, they tended to wobble slightly about its axis of rotation caused by small geometric irregularities of the apple's shape. With time this motion caused the oriented apple's axis of rotation of some fruit to become unstable resulting in fruit disorientation.

Commercial methods 3 and 4 did not orient Empires, Cortlands, Idareds, or Jonagolds. In fact, the axis passing through the stem and calyx ends consistently changed to perpendicular to the axis of rotation of the bicone rollers for the 4 cultivars. However, some Red Delicious were oriented by methods 3 and 4, 68% and 60% respectively, with orientation occurring within 16 seconds. For oriented apples, less than 30% of the Empires and less than 20% of Cortlands, Idareds, or Jonagolds remained oriented while 70% of Red Delicious stayed oriented for method 3 compared to 65% for method 4.

The difference between apple height and apple width played a part in the orientation processes tested, but other factors such as fruit shape, size, stem length, stem stiffness and surface curvature appear to play a roll also.

INTRODUCTION

Considerable effort has been put into applying sensor techniques to nondestructively sense the internal and surface quality of apples. Two trains of thought regarding the handling of the fruit during this process have been taken: 1)Convey the fruit past the sensors on some form of rotating cones or rollers while using the sensor to locate the stem/calyx regions and any defect, or 2)Orient the fruit in such a manner that the locations of the stem/calyx regions are known and use the sensor to locate defects.

Yang, (1992) demonstrated a technique using structured light to differentiate the concave surfaces around the stem/calyx ends from blemishes on the rest of the convex apple surface. Yang,

(1993) carried the identification process a step further by applying neural networks. The fruit packing industry requests that apples must be sorted at rates of 6 - 10 apples per second. There is little processing time to waste on locating the stem/calyx ends. If the stem/calyx ends pass directly through the camera view, extra lighting and mirrors or cameras must be added to view the sides of the apple as it rotates on bicones.

Davenel et. al. (1988) built an automatic detection system for surface defects on apples using a commercial sorting conveying system. Their algorithm depended on the fruit turning about a horizontal axis running through the stem and calyx cavities on bicone rollers. During their study, video recordings of commercial sorters equipped with "bicone" conveyors showed that fruit did not rotate as their algorithm required.

Abbott, (1994), Armstrong and Brown, (1991), Pitts et. al., (1991), Peleg, (1993), and Chen et. al., (1993) have all attempted to measure apple firmness by a number of different techniques all requiring knowledge of where the stem/calyx regions are located. Orientation is a requirement if this type of measurement is considered.

Rehkugler and Throop (1976) demonstrated two apple orientation devices to place the stem/calyx regions in a known location. One device consisted of a combination of free-to-rotate cone rollers and a powered rotating padded cylindrical roller. Data on the ability of this system to orient apples will be reported here as the second orientation method tested in this paper. Another device consisted of a rotating inverted conical shaped transport cup with an opening at the bottom (Keesling, 1965). Through the opening a small rotating wheel contacted the fruit until the stem/calyx was positioned over the wheel causing loss of apple contact and ending apple rotation. Rehkugler and Throop (1986) presented data showing the time to orient and the number of apples correctly oriented for the inverted cone - wheel device using four apple cultivars (Figure 1). This device leaves the stem/calyx axis vertical, requiring some form of a spindling mechanism to lift the apple up out of the cup and rotate the fruit for viewing with a camera. This method of fruit handling in a conveying stream of fruit moving at a rate of 6 - 10 apples per second was impossible without causing further damage to the apples.

OBJECTIVES

1. Determine if apples can be oriented using two commercial bicone conveying systems and two experimental conveying systems.
2. If the apples are oriented, determine how long the apples will remain oriented.
3. Evaluate the effect of apple height and width on the ability of each conveying device to orient apples.

MATERIALS AND METHODS

Two groups of apples were used for testing. Group 1 contained 50 apples each of Empires, Cortlands, and Red Delicious. One month later, group 2 containing 50 apples each of Empires, Jonagold, Ida Red, and Red Delicious was selected from storage. The apples were harvested during the fall of 1994 and held in cold storage until 24 hours before testing. Each apple was numbered and height and width were recorded. By selecting group 2 one month later than group 1, two 50 apple sets of Empires and Red Delicious were available for testing which likely came from different trees. This makes it more likely that the affect of tree to tree variation in apple height and width on orientation is included for these two cultivars.

Each apple from group 1 was oriented by methods 1, 2, and 3. Each apple in group 2 was oriented by methods 1, 2, 3, and 4.

Method 1: Two plastic bicones and a cylindrical padded roller were assembled as shown in figure 2. The cylindrical padded roller rotated 96 rpm and the bicones were free to rotate independently.

Method 2: The two plastic bicones were assembled different from method 1 as shown in figure 3. The cylindrical padded roller rotated 96 rpm and the bicones were free to rotate independently.

Method 3: A commercial bicone system using four rotating molded rubber bicones turning at 96 rpm to rotate fruit while being conveyed (Figure 4).

Method 4: A different commercial bicone system using bicones slightly smaller in diameter with curved surfaces turning at 120 rpm (Figure 5).

All of the conveying assemblies were mounted on a custom laboratory device with drive belts driven by an adjustable speed drive so that the appropiate bicones or rollers were rotated during testing. The conveyor segments did not convey the fruit but were held in a stationary position while an average sized apple (70 to 75 mm diameter) rotated at speeds typical to the 60 rpm rotating speed found on moving conveying systems on commercial sorters.

Apples were placed on each system with the axis passing through the stem and calyx ends parallel to the axis of rotation of the bicones and rollers. This position was considered to be the oriented position. The time that each apple remained in this position was recorded as the time that each apple stayed oriented.

Apples were placed on each system with the axis which passes through the stem and calyx ends perpendicular to the axis of rotation of the bicones and rollers. The time for this axis to

become parallel with the axis of rotation of the rollers and bicones was recorded as the time for apple orientation.

The maximum time allowed for apples to orient or to stay oriented was 20 seconds.

Time was measured with an electronic stop watch (Model 460, Accusplit Inc., 2290A Ringwood Ave., San Jose, CA. 95131). The height and width of each apple was measured with a digital vernier caliper (Model 599-571-3, Brown and Sharpe).

RESULTS AND DISCUSSION

Figures 6 - 9 show the percentage of the fifty apples for each of 5 cultivars that were correctly oriented using one of the four previously described methods at two second intervals of time up to a total time of 20 seconds. The percentage of the fifty apples for each of 5 cultivars that stayed oriented using one of the four previously described methods of orientation is also shown at two second time intervals up to a total time of 20 seconds. All apples tested in Figures 6 - 9 came from group 2 except Cortlands. Also Cortlands were not tested in method 4 because they were no longer available from storage when the conveying device was available.

Method 1 oriented Cortlands (100%), Empires (88%), Idareds (96%) and Jonagolds (98%). If orientation occurred, it was sucessful after 10 - 13 seconds. Furthermore, once oriented, they stayed oriented at least 98% percent of the time for 20 seconds. However, method 1 was unsuccessful in orienting Red Delicious (12%) and only 60% stayed oriented for the 20 seconds (Figure 6).

Method 2 oriented Cortlands (83%), Empires (73%), Idareds (90%) and Jonagolds (95%) after a period of 16 - 18 seconds compared to 10% of the Red Delicious. Only Cortlands (96%) stayed oriented. After a period of 10 seconds, only 82% of the Jonagolds, 72% of the Idareds, 58% of the Empires, and 0% of the Red Delicous remained oriented (Figure 7). This method required 4 - 5 seconds longer to orient apples. As the oriented fruit rotated, they tended to wobble slightly about its axis of rotation caused by small geometric irregularities of the apple's shape. With time this motion caused the oriented apple's axis of rotation to become unstable resulting in fruit disorientation.

Method 3 and Method 4 could not orient Empires, Cortlands, Idareds, or Jonagolds. In fact, the axis passing through the stem and calyx ends consistently changed to perpendicular to the axis of rotation of the bicone rollers for the 4 cultivars. After 16 seconds, method 3 oriented 68% and method 4 oriented 60% of the Red Delicious. After a 14 second period, less than 30% of the Empires and less than 20% of Cortlands, Idareds, or Jonagolds stayed oriented. After 16 seconds, 70% of Red Delicious stayed oriented for method 3 compared to 65% for method 4 (Figures 8 and 9).

Orientation appears to be dependent on both cultivar and

method for achieving orientation. In fact, orientation can be dependent on apple shape factors even within a single cultivar. Red Delicious oriented better using methods 3 and 4 but with a 30% to 40% failure. The other 4 cultivars oriented best with method 1 with a 0% to 12% failure. Figure 10 compares 2 different 50 apple samples, one from group 1 and one from group 2, for the cultivars of Empires and Red Delicious using method 1. The second set of Empires (97%) oriented better than the first Empire sample (88%). The first set from group 1 of Red Delicious (60%) oriented better than the second set of Red Delicious (12%) from group 2. Except for only 60% of the second set of Red Delicious from group 2, 95% of group 1 Red Delicious and both groups of Empires stayed oriented for 20 seconds.

Figure 11 shows plots of apple height and apple width for both 50 Red Delicious apples from group 1 (top) and 2 (bottom) versus time to orient in seconds with all data points at 20 seconds representing apples which did not orient. It appears that apples that oriented had widths greater than their heights. However, at least some of the apples that matched this criteria did not orient, indicating that other features such as surface shape or curvature and apple size may be variables, as well as method, which determine if apples orient. The Red Delicious apples from group 2 have larger heights and widths than Red Delicious apples from group 1. The relationship between the spacing between the cones and also between the cones and the cylindrical roller to apple size may have been a factor which caused poorer orientation of group 2 Red Delicious. However, shape, curvature, or some other features are involved since Cortlands had larger heights and widths (Figure 12) and still oriented. Figures 12 and 13 show apple height and width versus time to orient for Empires, Cortlands, Idareds, and Jonagold using method 1. All of these cultivars had widths greater than their heights. Empires, which had the poorest record of successful orientation (88%), had the smallest difference between the height and width for each fruit. Another factor that came into play with Empire orientation is their long stiff stems which interfered with the apple rotating into the oriented position. Other cultivars tested did not have long stems.

Observation of the 4 methods of orientation found that methods 1 and 2 have three points of fruit contact compared to four points of contact for methods 3 and 4. It appears that the apples seek a position upon the contact points where the two rings of contact points about the fruit have equal circumferences and where the axis of rotation for the fruit lies through shortest dimension of the fruit, in this case the apple height. In methods 1 and 2, this is impossible to achieve equal circumferences with the wider distance (38 - 40 mm) between the cone contact points for Red Delicious apples which have the elongated pear shape, forming much different fruit diameters at the stem end compared to the calyx end, particularly when the axis of rotation of the fruit lies through the stem/calyx axis. In Northeast United States, Red Delicious have both fruit that

are elongated pear shaped and nearly round. The elongated Red Delicious can only achieve equal circumferences about the fruit when the stem/calyx axis is perpendicular to the axis of rotation of the cylindrical roller. This is the position which the unoriented fruit stayed for methods 1 and 2. The more round Red Delicious without the pear shape orient much like the other 4 cultivars which have a more symetrical shape. Method 1 oriented all of the cultivars except Red Delicious quicker and with a higher rate of success because, by turning the one cone 180° to its position in method 2, its contact point formed an edge which could aline itself with the fruit edge at the stem/calx ends providing stability to the revolving fruit once oriented. This did not work for the elongated Red Delicious when the calyx end was resting on this cone because the diameter of the fruit edge is very small compared the other 4 more symetrical cultivars.

Methods 3 and 4 had four contact points, one on each cone. The contact points were 25mm apart, narrower than for methods 1 and 2. With all 4 contact points powered and close together, apples tended to position themselves so that the fruit axis of rotation passed through the largest dimension of the apple, the apple width. For the Red Delicious elongated pear shaped fruit, this did not hold true. The stem end of this fruit has more mass than the calyx end, causing the fruit, while on the narrow spaced contact points, to topple over when in the position of the stem/calyx axis perpendicular to the axis of rotation of the bicones. Once toppled, the fruit shifted along its stem/calx axis, now the axis of rotation, with the calyx end moving further away from the contact points until rings of equal circumference are found. This motion can actually cause the calyx end of large elongated Red Delicious to extend outside of the bicones and interfere with fruit in the next lane.

Further studies need to consider apple shape and curvature and determine how these factors relate to width between cones and the width between the bicone rollers and the cylindrical roller. The angle and shape of the cone surface could also be a factor.

CONCLUSIONS

Of the four methods tested, method 1 correctly oriented the stem/calyx axis into the position of the axis of rotation of Cortland, Jonagold, Idared, and Empire apples correctly (88%-100%) in the shortest amount of time (12 seconds). For two 50 apple sets of Red Delicious, 62% and 12% were correctly oriented. The elongated pear shape of this cultivar determined if orientation occurred for all methods tested.

A difference between apple height and apple width plays a part in the orientation processes tested, but other factors such as fruit shape, size, stem length, stem stiffness and surface curvature appear to play a roll.

Present commercial bicone conveyors (methods 3 and 4) oriented 68% and 60% of the Red Delicious respectively. All fruit

of the cultivars of Cortland (not tested by method 4), Idared, Jonagold, and Empires assumed a position with the axis of rotation of the apple perpendicular to the axis of a line passing through the stem/calyx ends. The Red Delicious which failed to orient also assumed this position. It appears that the commercial orientation methods depend on an elongated pear shaped apple for orientation.

REFERENCES

1. Abbott, J. A. 1994. Firmness measurement of freshly harvested 'Delicious apples by sensory methods, sonic transmission, Magness-Taylor, and compression. *Journal of the American Society for Horticultral* Science, 119(3):510 - 515.

2. Armstrong, P. R., and G. K. Brown. 1991. Apple firmness sorting using a nondestructive acoustic technique. *ASAE* Paper 916044, 10p.

3. Chen, H., and J. Baerdemeaker. 1993. Effect of apple shape on acoustic measurements of firmness. *Journal of Agricultural Engineering Research*, 56(3):253 - 266.

4. Davenel, A., Ch. Guizard, T. Labarre, and F. Sevila. 1988. Automatic detection of surface defects on fruit by using a vision system. *Journal of Agricultural Engineering Research*, 41:1 - 9.

5. Keesling, T. B. 1965. Fruit processing method U. S. Patent No. 3225892. 15 p. Commissioner of Patents and Trademarks, Washington, D. C.

6. Peleg, K. 1993. Comparison of non-destructive and destructive measurement of apple firmness. *Journal of Agricultural Engineering Research*, 55(3):227 - 238.

7. Pitts, M. J., R. P. Cavalieri, and S. Drake. 1991. Evaluation of the PFT apple firmness sensor. *ASAE* Paper 913017, 18p.

8. Rehkugler, G. E., and J. A. Throop. 1976. Optical - mechanical bruised apple sorters. Quality detection in foods, compiled by J. J. Gaffney, ASAE, St. Joseph, Mi. pp 185-188, 192.

9. Rehkugler, G. E., and J. A. Throop. 1986. Apple sorting with machine vision. *Tranactions of the ASAE*, 29(5):pp. 1388 - 1397.

10 Yang, Q. 1992. The potential for applying machine vision to defect detection in fruit and vegetable grading. The Agricutlural Engineer Incorporating Soil and Water, Silsoe, Bedford. pp. 74 - 79.

11. Yang, Q. 1993. Classification of apple surface features using machine vision and neural networks. *Computers and Electronics in Agriculture*, 9:pp. 1 - 12, Elsevier Science Publishers B. V., Amsterdam.

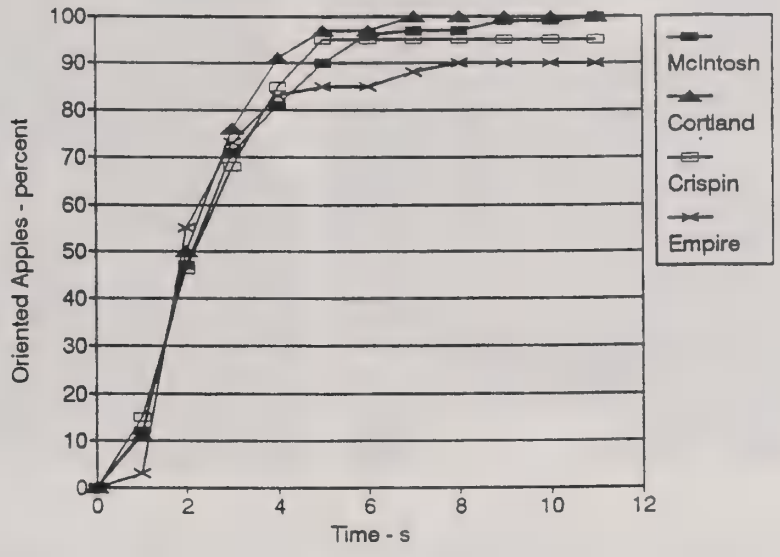

Figure 1. Time to orient and the percentage of correctly oriented fruit using the inverted cone - wheel device for four apple varieties (Rehkugler and Throop, 1986).

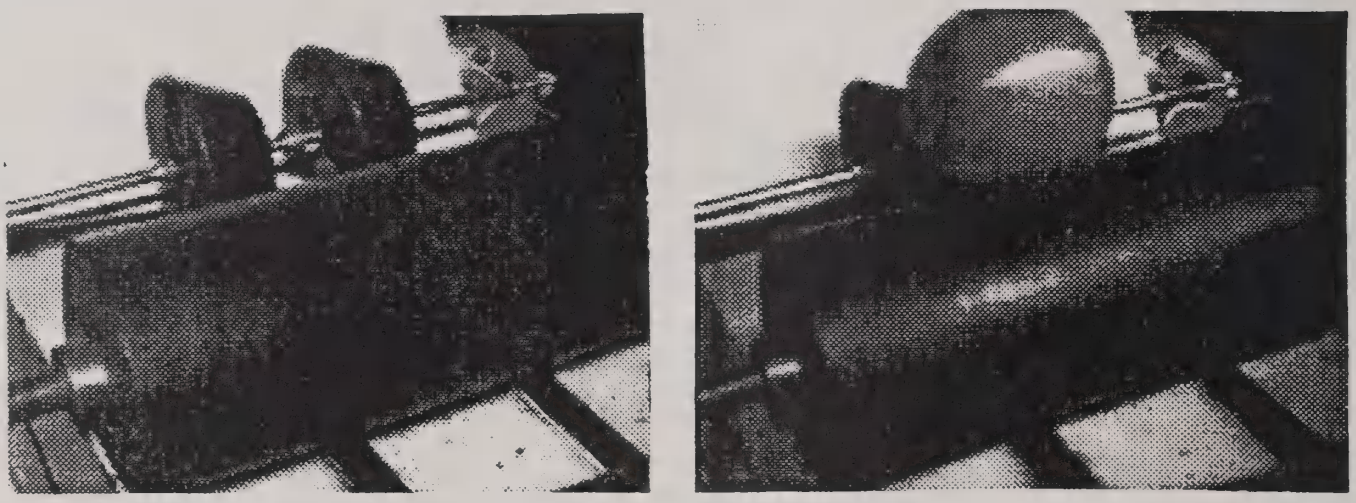

Figure 2. Picture of the experimental hardware used in method 1 for apple orientation consisting of two freely rotating cone rollers and a powered cylindrical padded roller.

Figure3. Picture of the experimental hardware used in method 2 for apple orientation consisting of two freely rotating cone rollers, one rotated 180° from its position for method 1, and a powered cylindrical padded roller.

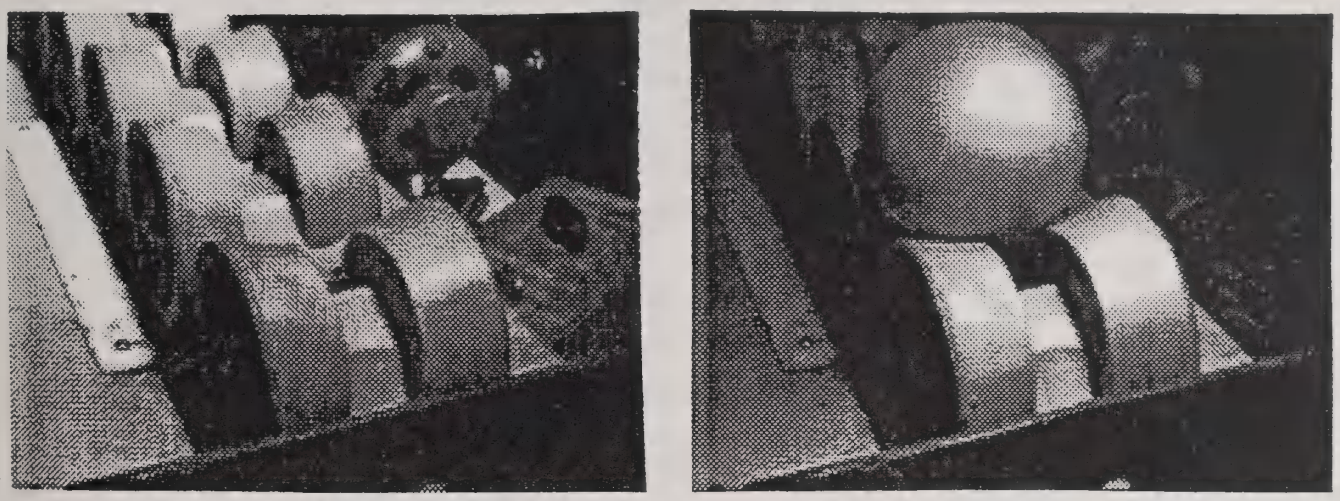

Figure 4. Picture of a commercial bicone conveyor used in method 3 for apple orientation. The bicones were rotated at normal grading machine rate but not used to convey fruit during testing.

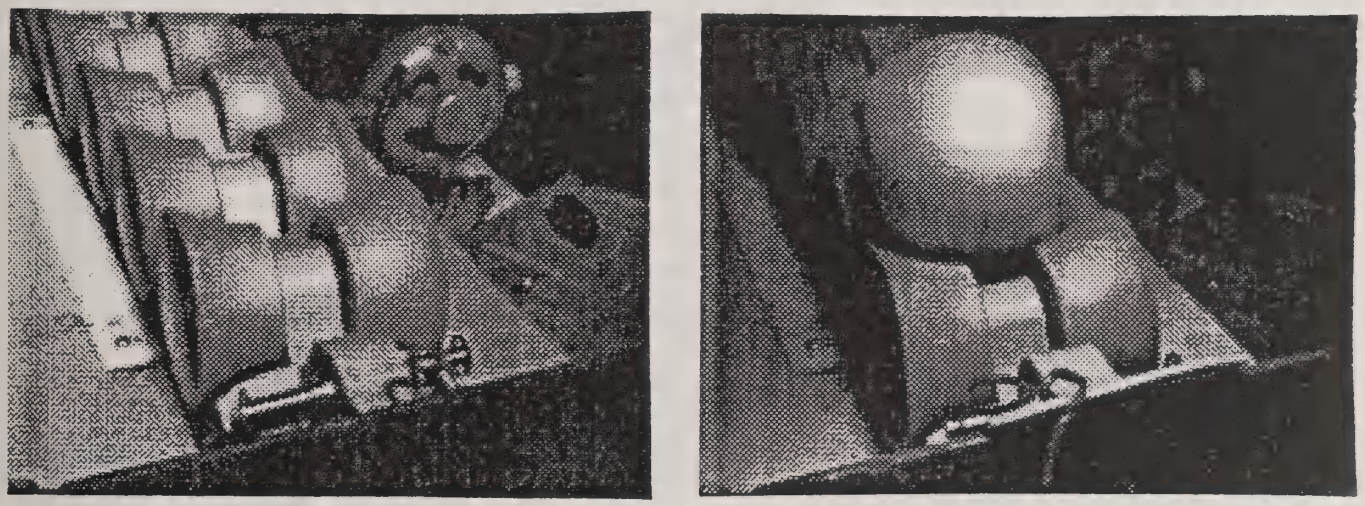

Figure 5. Picture of a commercial bicone conveyor used in method 3 for apple orientation. The bicones were rotated at normal grading machine rate but not used to convey fruit during testing.

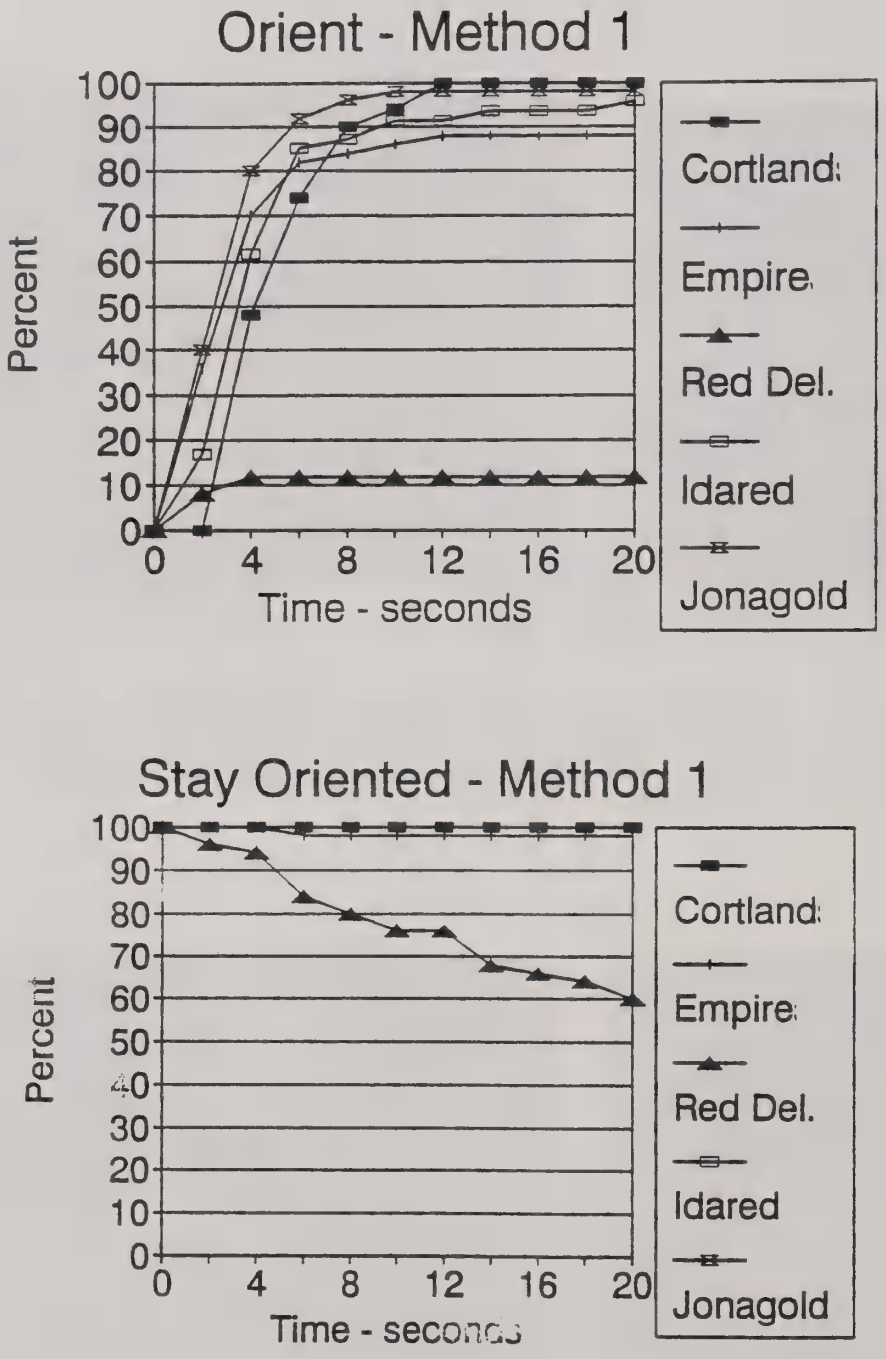

Figure 6. The percent of correctly oriented apples (top) versus time to achieve orientation and the percent of apples which remained oriented (bottom) versus time stayed oriented using method 1 is shown for 5 cultivars.

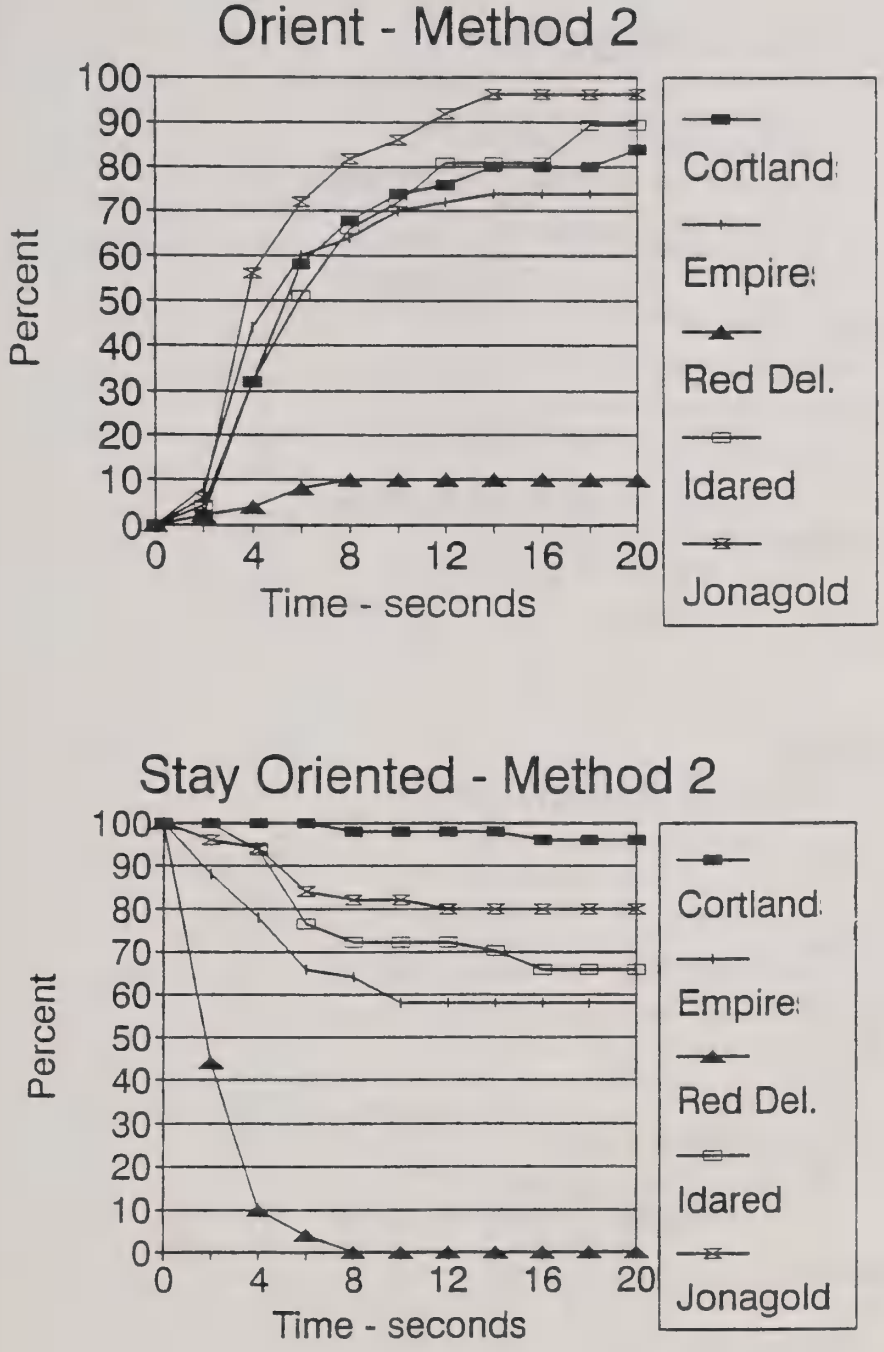

Figure 7. The percent of correctly oriented apples (top) versus time to achieve orientation and the percent of apples which remained oriented (bottom) versus time stayed oriented using method 2 is shown for 5 cultivars.

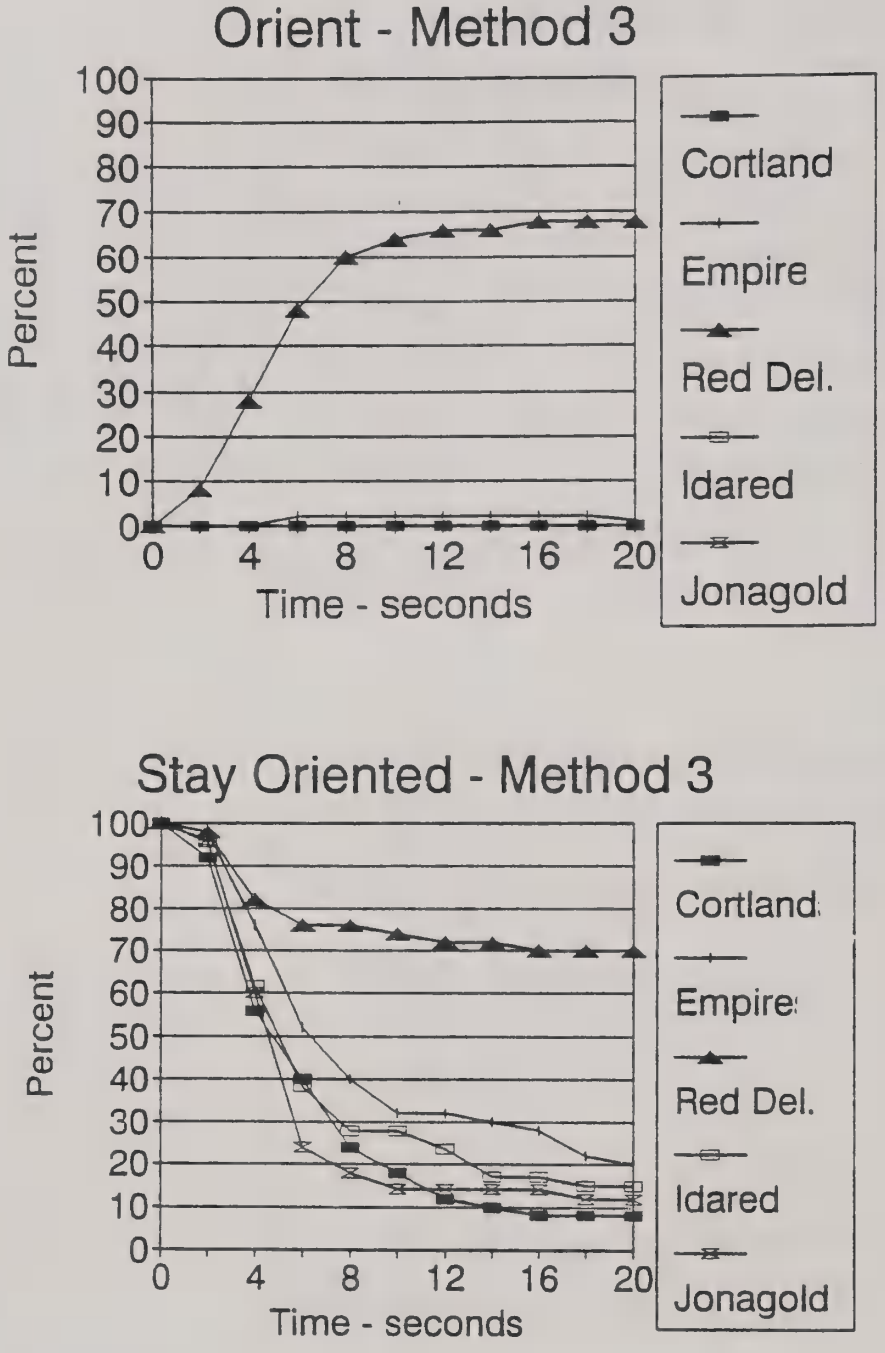

Figure 8. The percent of correctly oriented apples (top) versus time to achieve orientation and the percent of apples which remained oriented (bottom) versus time stayed oriented using method 3 is shown for 5 cultivars.

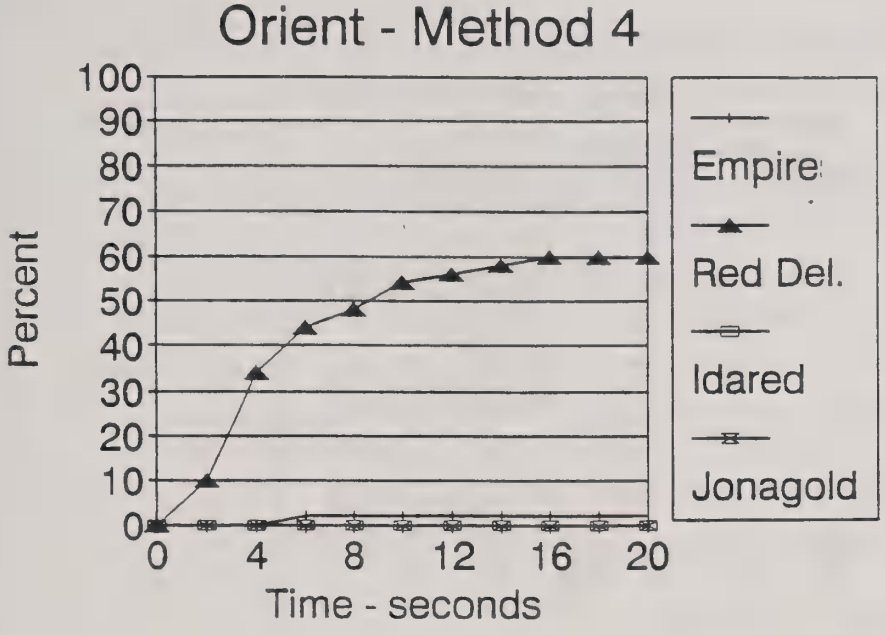

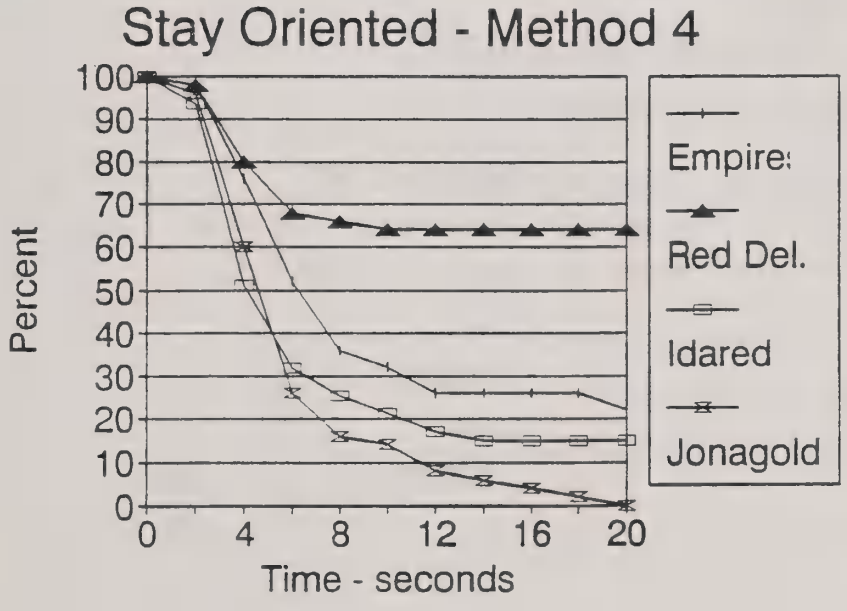

Figure 9. The percent of correctly oriented apples (top) versus time to achieve orientation and the percent of apples which remained oriented (bottom) versus time stayed oriented using method 4 is shown for 4 cultivars.

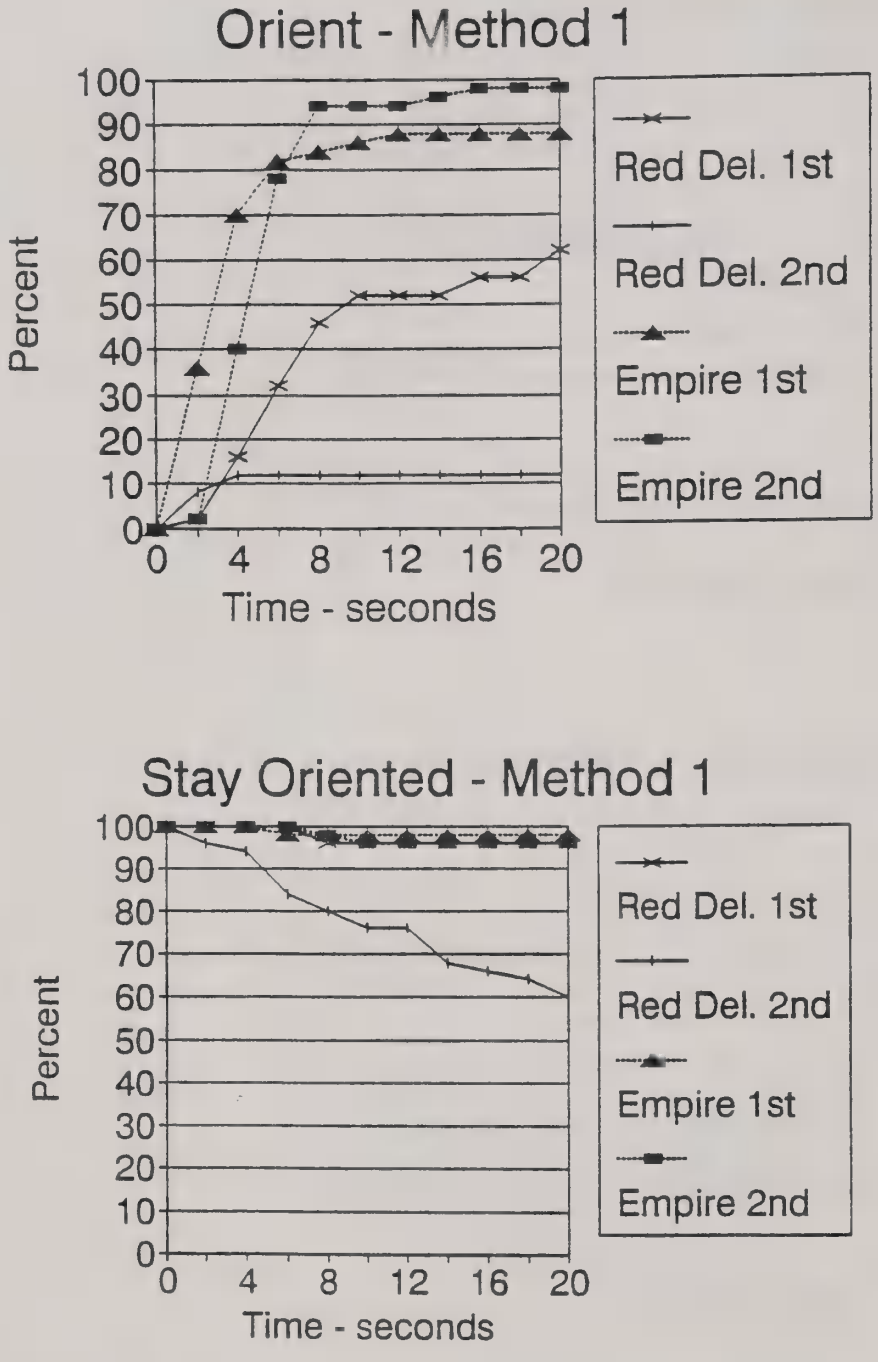

Figure 10. The percent of correctly oriented apples (top) versus time to achieve orientation and the percent of apples which remained oriented (bottom) versus time remained oriented using method 1 is shown for four 50 apple samples, two of Empires and two of Red Delicious. One month difference in storage time between sample pairs for each cultivar assured apples from different trees.

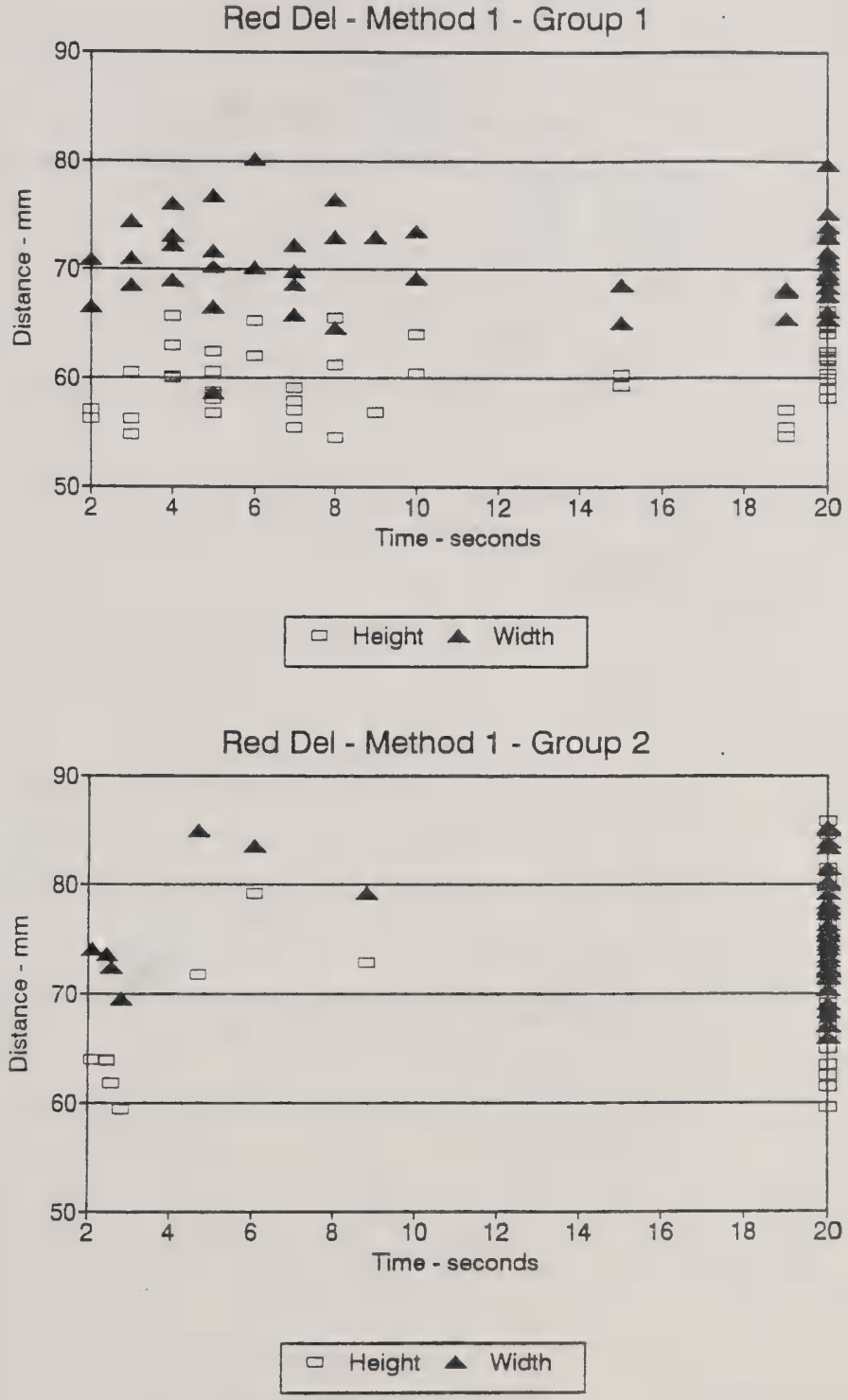

Figure 11. Apple height and width versus time to orient using method 1 for two 50 Red Delicious apple samples selected one month apart from storage. All heights and widths at a time of 20 seconds represent apples which did not orient.

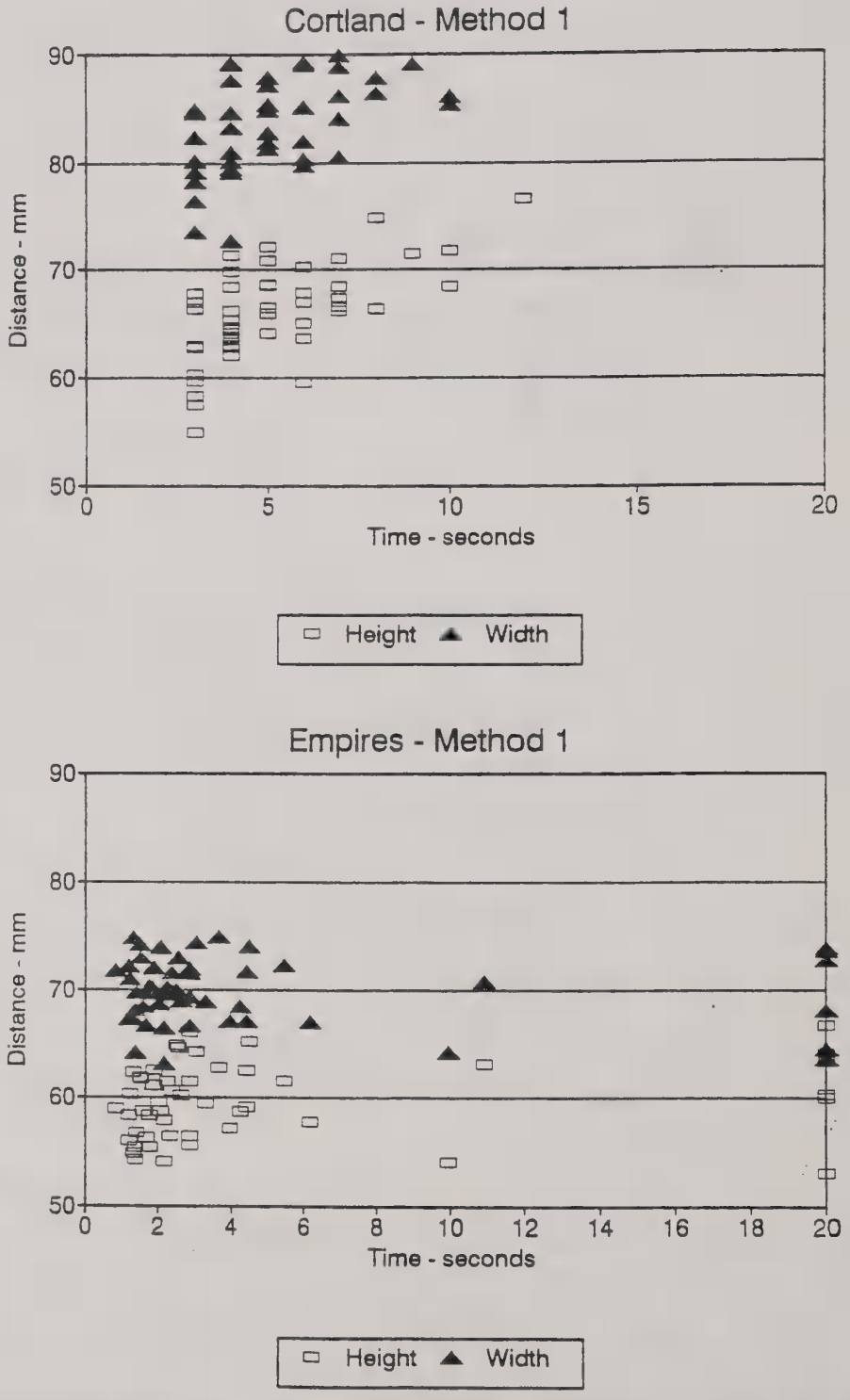

Figure 12. Apple height and width versus time to orient using method 1 for Cortlands (top) and Empires (bottom). All heights and widths at a time of 20 seconds represent apples which did not orient.

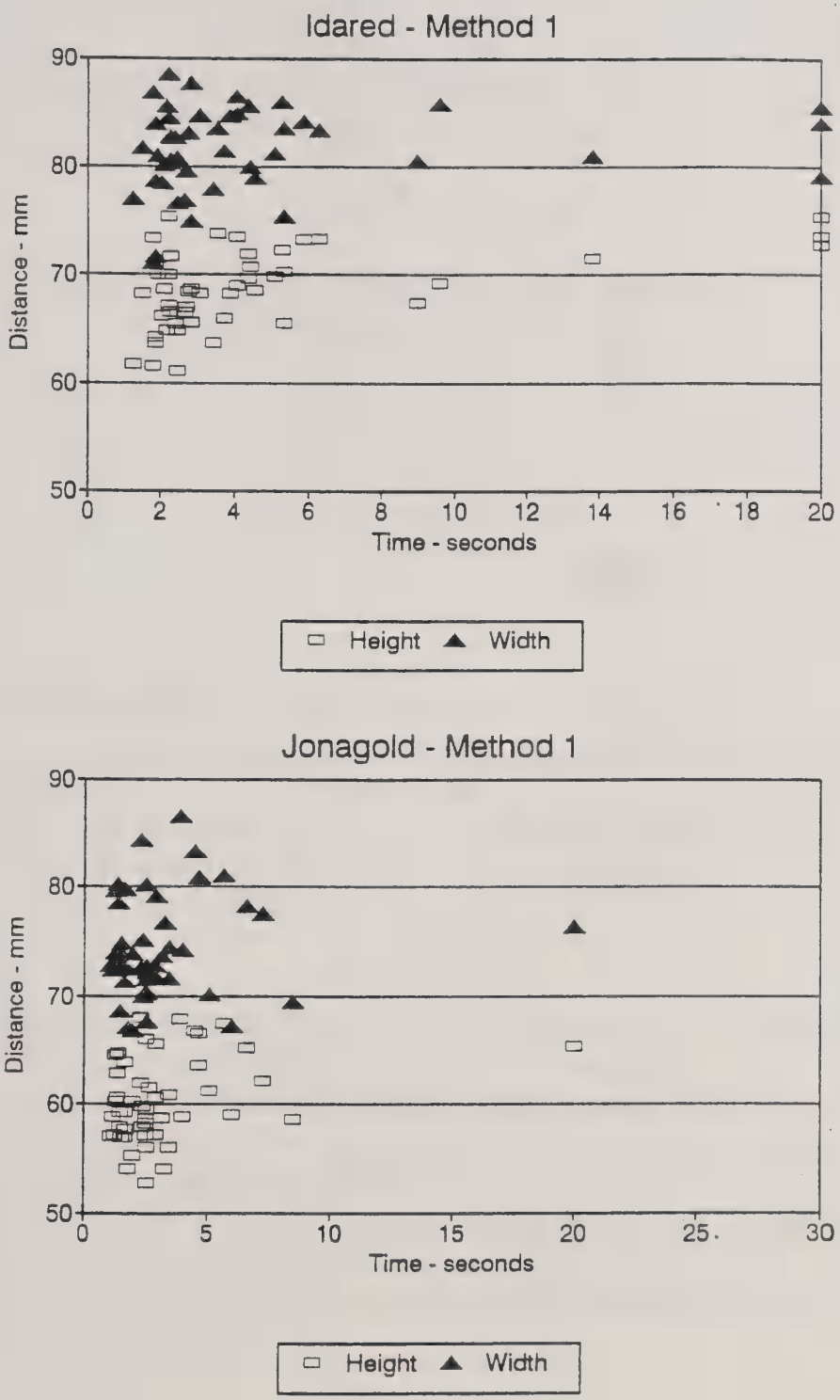

Figure 13. Apple height and width versus time to orient using method 1 for Idareds (top) and Jonagold (bottom). All heights and widths at a time of 20 seconds represent apples which did not orient.

Apple Orientation on Automatic Sorting Equipment

James A. Throop
Research Support Specialist
Department of Agricultural and Biological Engineering
Cornell University, Ithaca, NY 14853

Daniel J. Aneshansley
Associate Professor
Department of Agricultural and Biological Engineering
Cornell University, Ithaca, NY 14853

Bruce L. Upchurch
Agricultural Engineer
Formerly USDA-ARS Appalachian Fruit Research Station
Kearneysville, WV 25430

INTRODUCTION

Considerable effort has been applied to sensor techniques to nondestructively sense the internal and surface quality of apples. Two trains of thought regarding the handling of the fruit during this process have been taken: 1) Convey the fruit past the sensor on some form of rotating cones or rollers while using the sensor to locate both the stem/calyx regions and any defect, or 2) Orient the fruit in such a manner that the locations of the stem/calyx regions can be predicted and use the sensor to locate only the defects.

Structured light has been used to differentiate the concave surfaces around the stem/calyx ends from blemishes on the rest of the convex apple surface (Yang, 1992). The identification process has been carried a step further by applying neural networks to identify the altered structure of the light (Yang, 1993). The fruit packing industry requests that apples must be sorted at rates of 6 - 10 apples per second. There is little processing time to waste on locating the stem/calyx ends. If the stem/calyx ends pass directly through the camera view, extra lighting and mirrors or cameras must be added to view the sides of the apple as it rotates on bicone rollers or else this portion of the apple cheek will not be inspected. The stem/calyx could also be mistakenly identified as a defect.

An automatic detection system for surface defects on apples using a commercial sorting conveying system of bicone rollers used an algorithm dependent on the fruit rotating about a horizontal axis running through the stem and calyx cavities. During their study, video

recordings of commercial sorters equipped with "bicone" conveyors showed that fruit did not rotate as their algorithm required (Davenel et. al., 1988).

Many researchers have attempted to measure apple firmness by different techniques all requiring knowledge of where the stem/calyx regions are located. Orientation or stem/calyx identification is a requirement if this type of measurement is considered (Abbott, 1994), (Armstrong and Brown, 1991), (Pitts et. al., 1991), (Peleg, 1993), and (Chen et. al., 1993) .

Two apple orientation devices that place the stem/calyx regions in a known location have been built in the past (Rehkugler and Throop, 1976). One device consisted of a rotating inverted conical shaped transport cup with an opening at the bottom . Through the opening a small rotating wheel contacted the fruit until the surface indentation of the stem/calyx was positioned over the wheel causing loss of apple surface contact with the wheel ending apple rotation (Keesling, 1965). The time to orient and the number of apples correctly oriented for the inverted cone - wheel device using four apple cultivars was recorded (Figure 1).

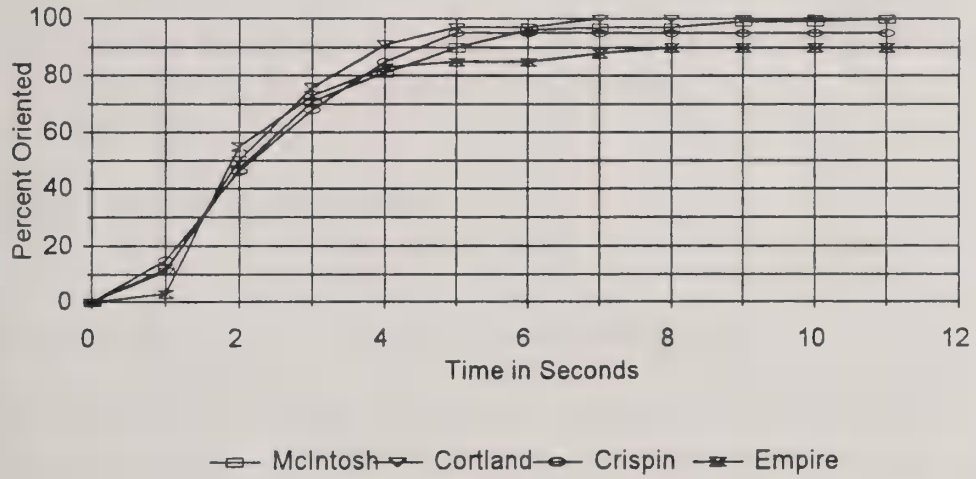

Figure 1. Time to orient and the percentage of correctly oriented fruit using the inverted cone - wheel device for four apple varieties (Rehkugler and Throop, 1986).

This device leaves the stem/calyx axis vertical, requiring some form of a spindling mechanism to lift the apple up out of the cup and to rotate the fruit for viewing the whole apple surface with a camera. A conveying stream of fruit moving at a rate of 6 - 10 apples per second was impossible by this device without causing further damage to the fruit.

A second device consisted of a combination of free-to-rotate opposing cone rollers on one shaft and a powered rotating padded cylindrical roller on a second shaft. After orientation to an axis of rotation about an axis passing through the stem/calyx ends, some fruit tended to wobble. One of the cones was changed to a vertical disk which tended to engage the shoulder formed

between the concave and convex surfaces that intersect at the stem/calyx ends resulting in less wobble. This device correctly oriented 88% - 100% of Empires, Cortlands, Jonagolds, and Idareds (Throop et. al., 1995). The fruit was not grouped by size for this study.

Further modifications were made to the cone shaped roller changing the flat angular surface to a concave surface. The vertical disk and cone shaped roller were spring loaded towards each other allowing lateral movement along the common shaft about which they rotate. This allowed a greater range of fruit sizes to be oriented. Testing was carried out with the following objectives in mind.

OBJECTIVES

1. Determine which apple cultivars can be oriented using two commercial bicone conveying systems and one experimental conveying system.
2. If the apples are oriented, determine how long the orientation process takes and how long the apples will remain oriented.
3. Determine if the new device can handle a range of large and small fruit without altering the geometry between the disk/cone and cylindrical roller.

MATERIALS AND METHODS

Apples were harvested and placed in cold storage during the Fall of 1995. They were removed from storage during November 1995 and sized into two groups, 88's and 128's (88 and 128 apples per standard container consisting of 4 tray packs) before testing (Omni Sort, Durland-Wayland, Lagrange , GA). The typical sample size was 44 apples except when to few apples of a size catergory for a particular cultivar could be found (Table 1).

Three conveying and orienting devices were tested.

Experimental Device: Consisted of a plastic bicone with a concave surface and a flat vertical disk assembled on one shaft parallel to a cylindrical padded roller on a second shaft (Figure 2). Both the flat disk and bicone were spring loaded with compression springs toward each other allowing them to move horizontally along their common shaft compensating for different sized fruit. The cylindrical padded roller rotated 96 rpm producing an apple rotational speed of about 60 RPM. The bicone and disk rotated independently of each other and dependently on their contact with the fruit surface.

Table 1. The number of apples and size for each cultivar tested for orientation.

Cultivar	Size 128	Size 88
Golden Delicious	44	44
McIntosh	10	44
Fuji	41	44
Rome	44	43
Gala	5	44
Jonagold	14	44
Crispin	25	44
Cortland	22	44
Empires	44	18
Granny Smith	22	44
Red Delicious (East)	44	44
Red Delicious (Wash)	44	44

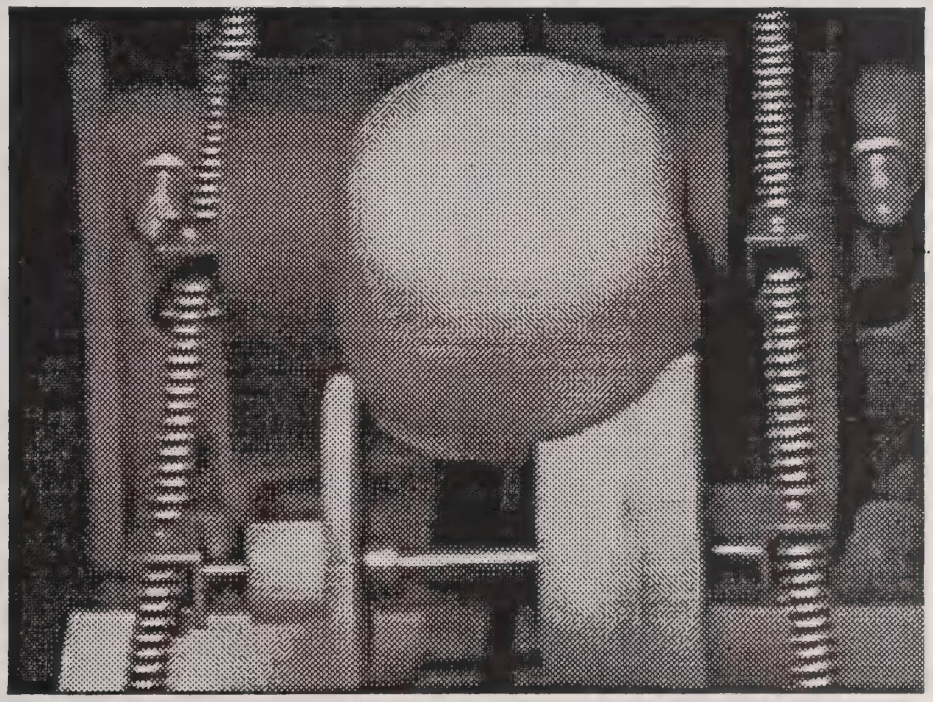

Figure 2. Picture of experimental conveying device after apple orientation.

Commercial Device 1: A commercial bicone system consisting of two pairs of powered molded rubber bicones rotating on two separate parallel shafts with their angular flat surfaces facing towards each other turning at 96 rpm. Contact with the apple surface produced apple rotation of about 60 RPM (Figure 3).

Commercial Device 2: A commercial bicone system consisting of two pairs of powered molded rubber bicones slightly smaller in diameter rotating on two separate parallel shafts with their angular concave surfaces facing towards each other turning at 120 rpm. Contact with the apple surface produced apple rotation of about 60 RPM (Figure 4).

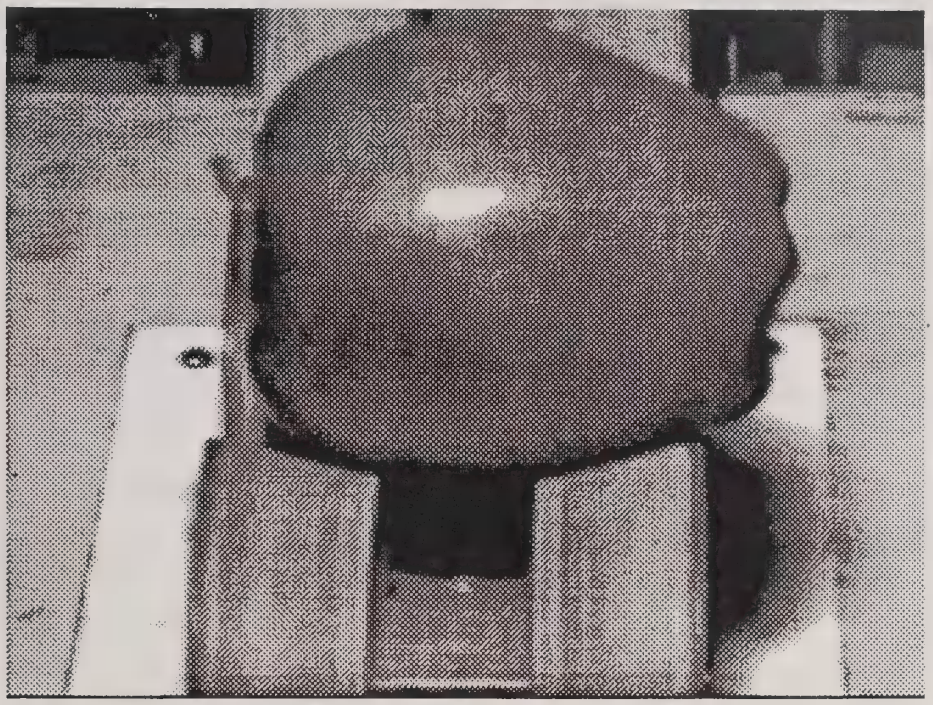

Figure 3. Picture of a commercial bicone conveyor after apple orientation.

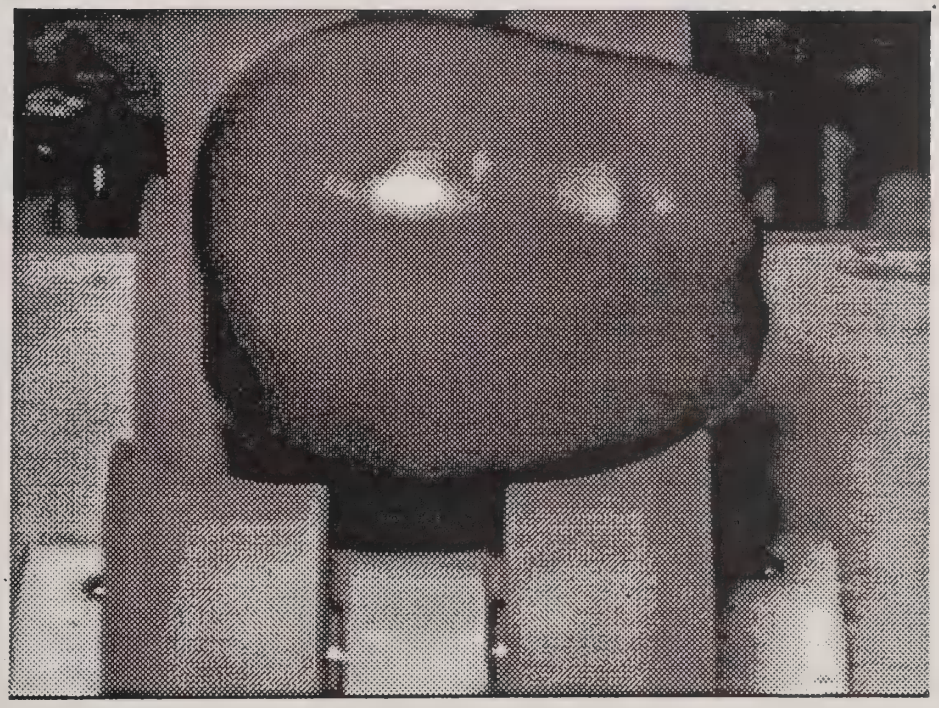

Figure 4. Picture of a second commercial bicone conveying device after orientation.

The conveying assemblies were mounted on a custom laboratory device with drive belts driven by an adjustable speed drive providing power to the appropiate bicones or rollers during testing. The conveyor segments did not convey the fruit but were held in a stationary position. Contact with the surface of an average sized apple (70 to 75 mm diameter) resulted in rotational speeds of about 60 rpm, typical of the apple rotational speed of moving conveying systems on commercial sorters.

The first experiment, placed apples on each system so that the axis passing through the stem/calyx ends was parallel to the axis of rotation of the bicones and rollers. This position was considered to be the oriented position. The time that each apple remained in this position was recorded as the time that each apple stayed oriented.

In the second experiment apples were placed on each system so that the axis which passes through the stem/calyx ends was perpendicular to the axis of rotation of the bicones and rollers. The time for the stem/calyx axis to become parallel with the axis of rotation of the rollers and bicones was recorded as the time for apple orientation.

The maximum time allowed for apples to orient or to stay oriented was 0.3 minutes. Time was measured with an electronic stop watch (Model 460, Accusplit Inc., 2290A Ringwood Ave., San Jose, CA. 95131).

RESULTS AND DISCUSSION

Condition 1: Apples placed on experimental conveying device (Experimental Device) with the axis of rotation perpendicular to the stem/calyx axis.

After 0.2 minutes, Cortland, Empire, Fuji, Jonagold, McIntosh, and Rome apples oriented so that their axis of rotation coincided with an axis passing through the stem and calyx with a 95% to 100% accuracy. The exception was the large Fuji which oriented only 82% correctly (Figure 5). The same cultivars remained oriented longer than 0.2 minutes 97% to 100% of the time when they were placed on the device so that their stem/calyx was parallel to the axis of rotation of the cone/disk and the roller. If the apple rotational speed for the same 6 cultivars was increased from 60 RPM to a rotational speed of 90 RPM, some of the fruit oriented correctly in a shorter length of time as indicated by a greater slope of curves between times 0 minutes and 0.05 minutes. However, the apples that required the most time to orient for 60 RPM required more time to orient for 90 RPM. This reduced successful orientation for small Empires from 94% to only 83%, large Jonagolds from 97% to 87% , and increased successful orientation of large Fujis from 82% to 88% after a time of 0.2 minutes (Figure 6).

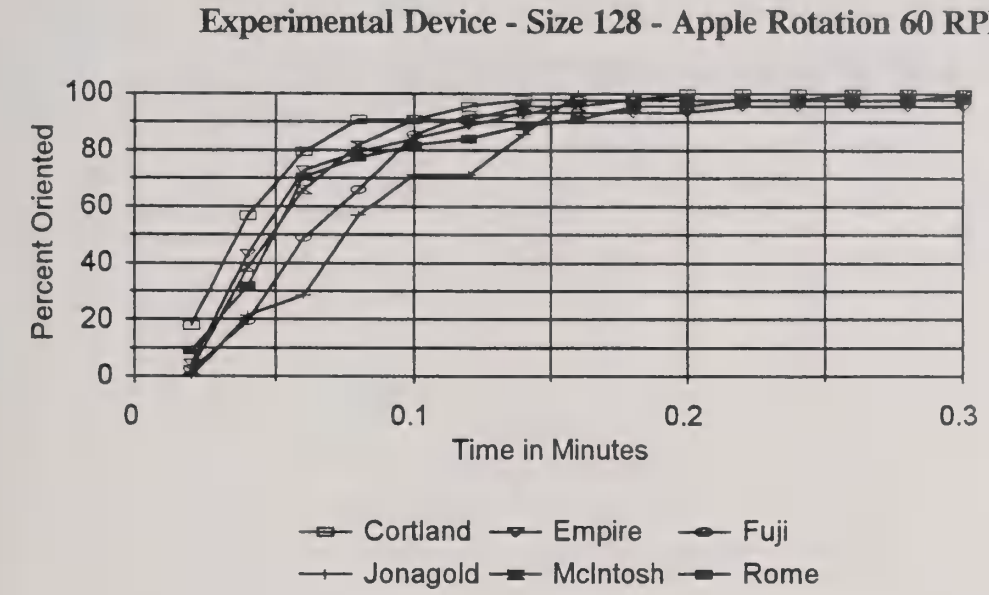

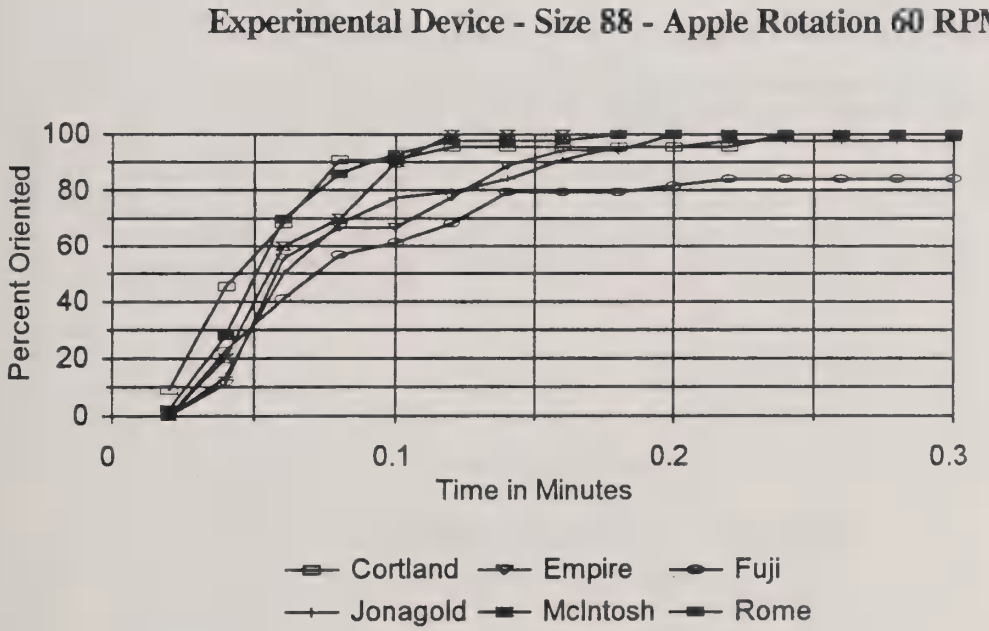

Figure 5. Percent of apples rotating at 60 RPM of size 128 (top) and size 88 (bottom) which changed their axis of rotation from perpendicular to the stem/calyx axis to the same as the stem/calyx axis using the experimental device.

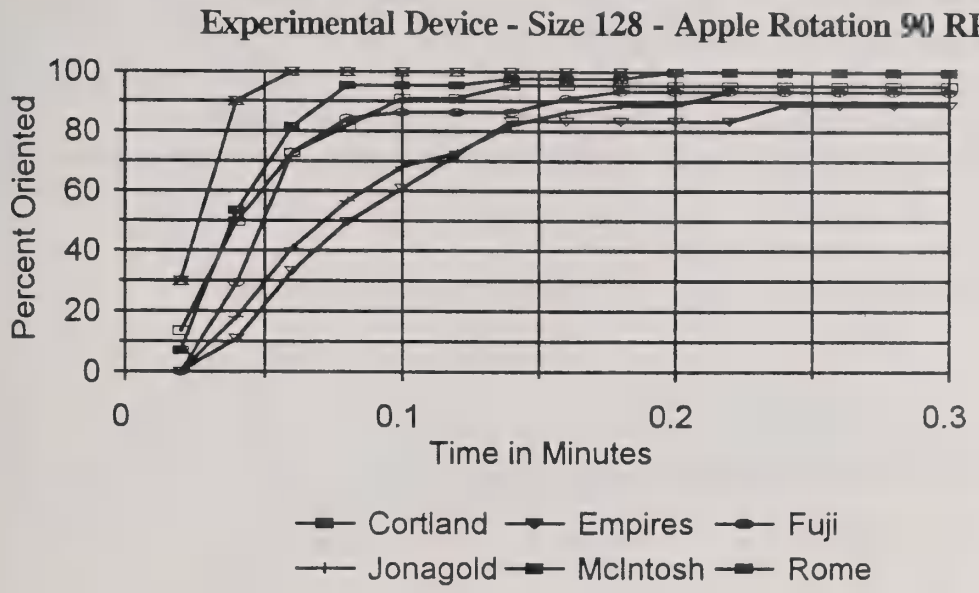

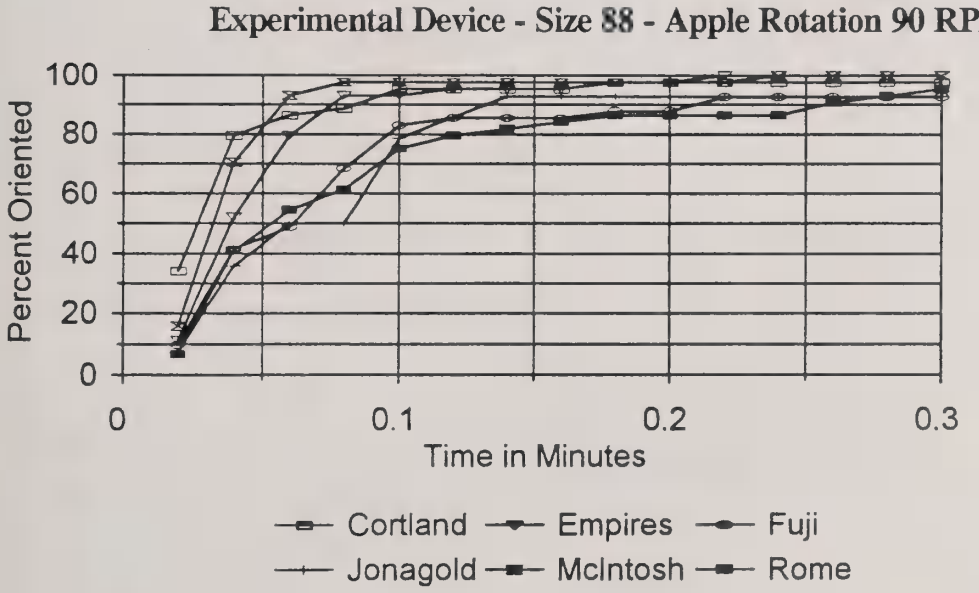

Figure 6. Percent of correctly oriented apples using an apple rotational speed of 90 RPM for size 128 (top) and size 88 (bottom) apples. The axis of rotation was changed from perpendicular to the stem.calyx axis to about the stem/calyx axis using the experimental device.

Golden Delicious, Granny Smith, Crispin, Red Delicious, and Gala (unable to find 88 size) have a greater variation in overall shape causing difficulty in orientation by any device. In some cases the apple shape approaches that of a sphere (height and width equal) which has no

geometrical bias favoring a specific orientation. With the exception of large Granny Smith (57%) and large Crispin (52%), successful orientation to a rotational axis about the stem/calyx axis was achieved 60% to 82% of the time while using the experimental conveying device (Figure 7). Controlling the maximum size as well as the minimum size for the 88 sized fruit would improve the success rate of the large Granny Smith and Crispin cultivars as some of the

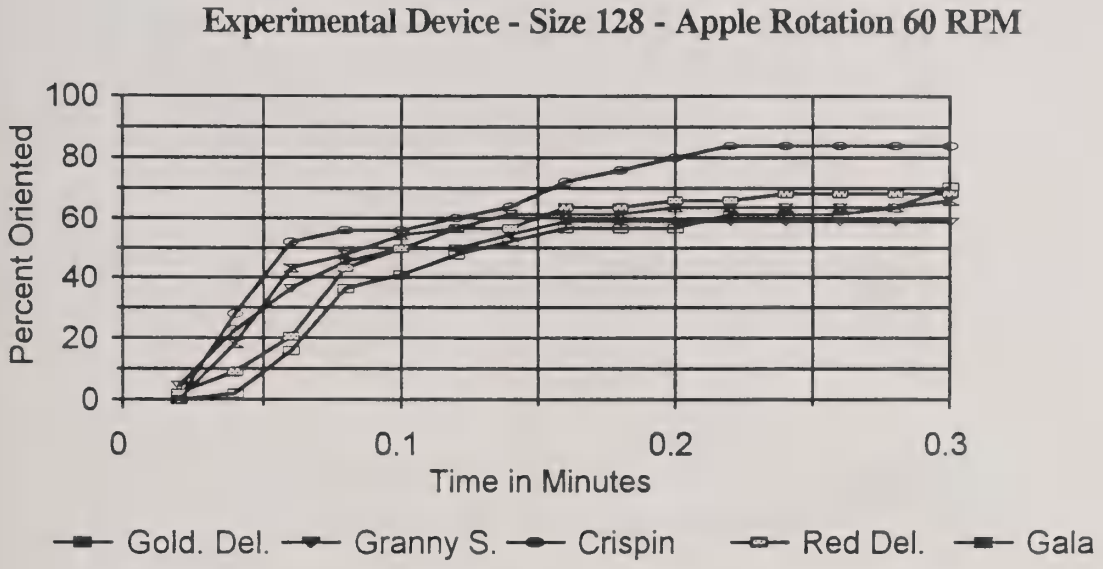

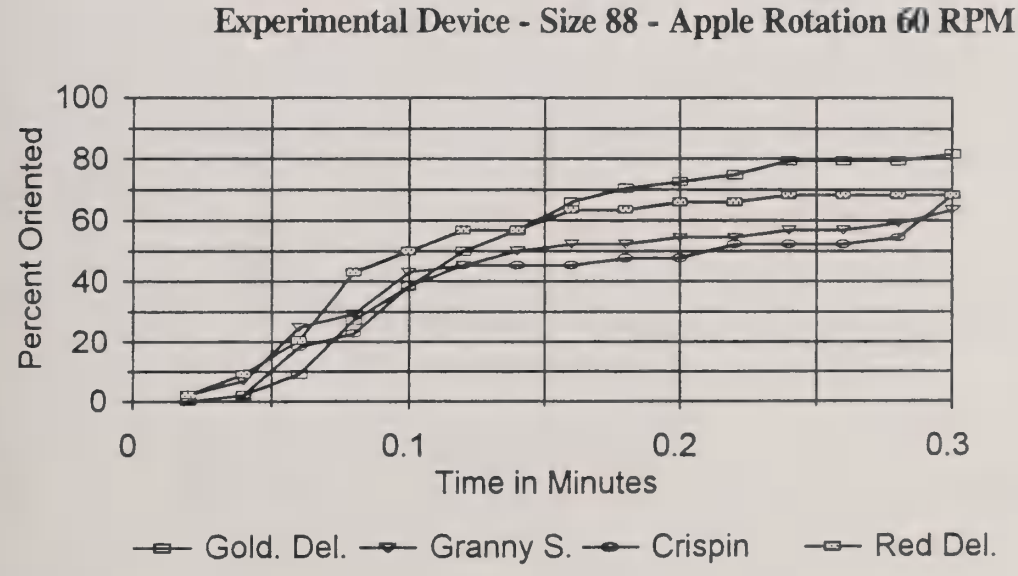

Figure 7. Percent of apples rotating at 60 RPM of size 128 (top) and size 88 (bottom) which oriented from an axis of rotation perpendicular to the stem/calyx axis to an axis of rotation about the stem/calyx axis using the experimental device.

fruit were just to large for the conveying device. If the 5 cultivars were placed on the device in an oriented position, 70% or more of the fruit stayed oriented in this position of rotating about the stem/calx axis for 0.2 minutes.

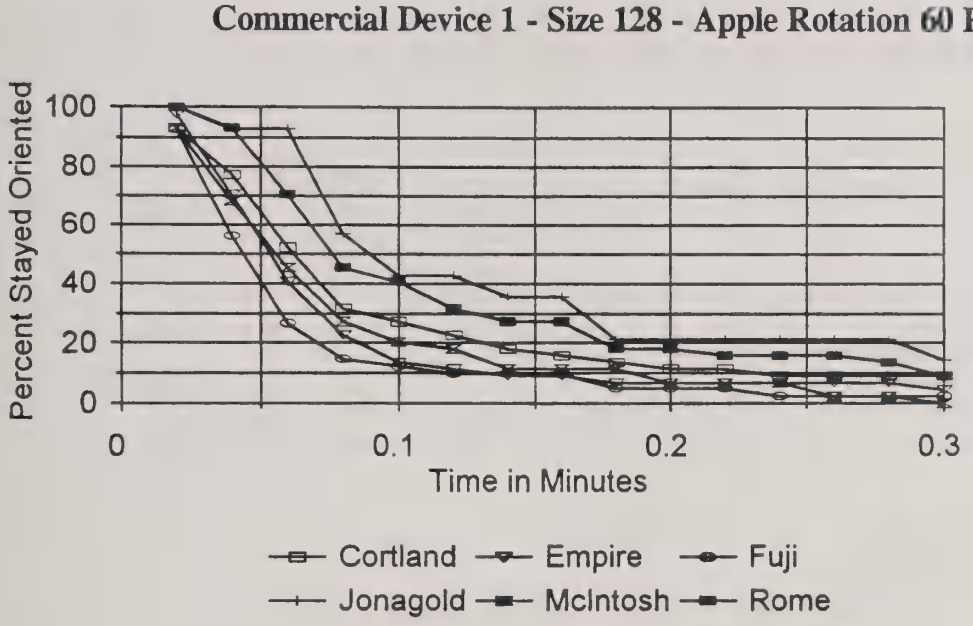

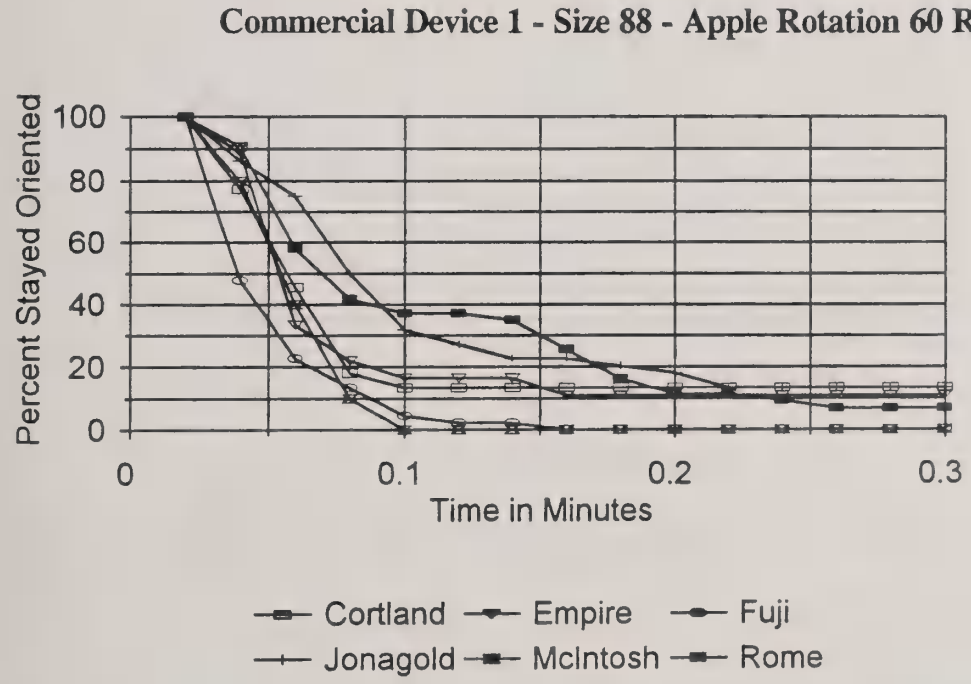

Figure 8. Percent of apples of size 128 (top) and size 88 (bottom) which continued rotating about the stem/calyx axis using a commercial bicone conveying device described in method 2.

Condition 2: Apples placed on a commercial bicone conveying device (Commercial Device 1) with the axis of rotation about the stem/calyx axis.

When Cortland, Empire, Fuji, Jonagold, McIntosh and Rome apples were placed on the commercial conveying device with their axis of rotation about the stem/calyx axis, 60% of the

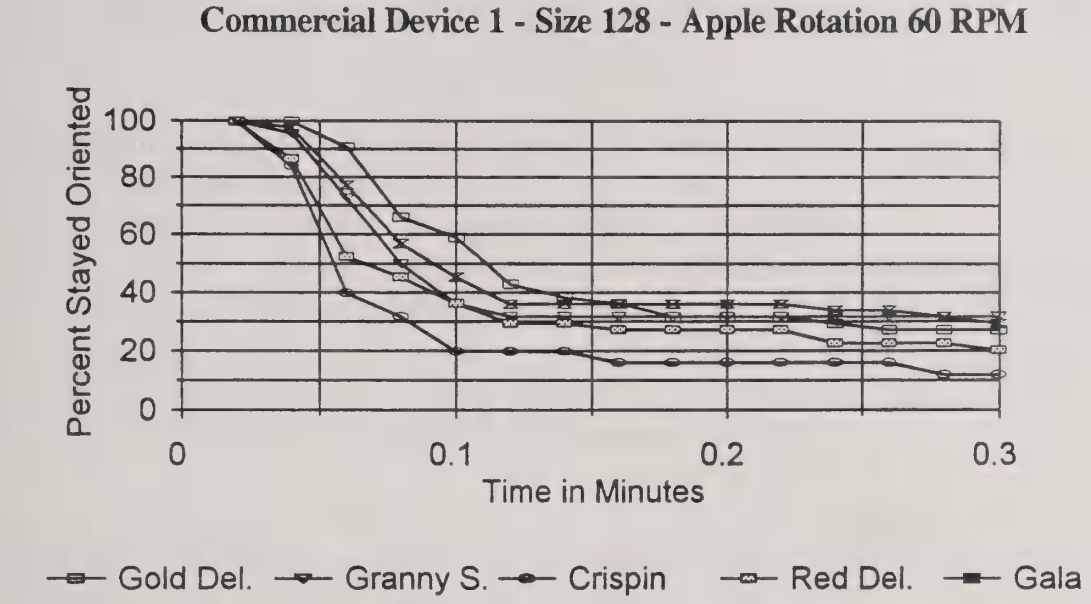

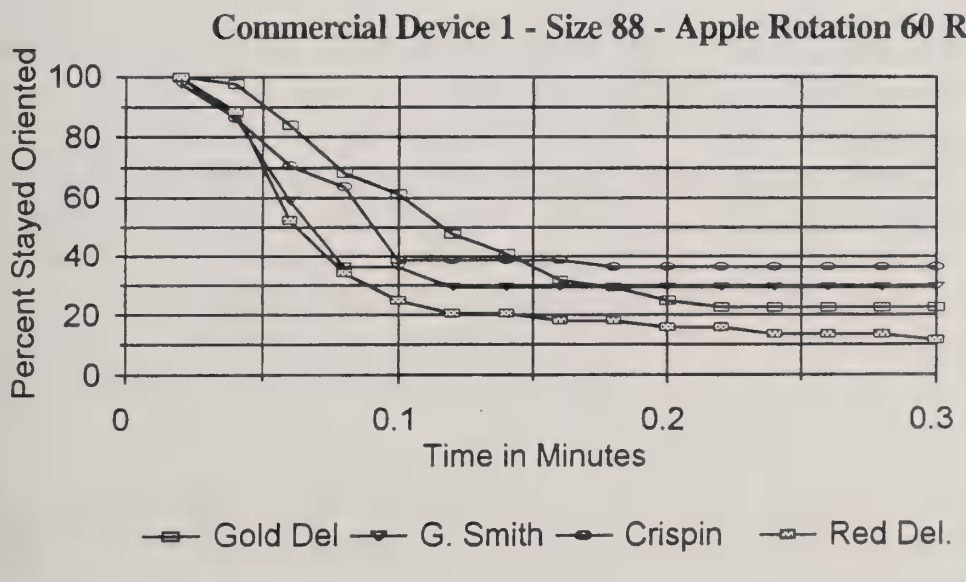

Figure 9. Percent of apples of size 128 (top) and size 88 (bottom) which continued rotating about the stem/calyx axis while using a commercial device 1.

fruit regardless of size assumed a new axis of rotation perpendicular to the stem/calyx axis after a period of time of 0.10 minutes (Figure 8). After 0.20 minutes, 80% or more of the fruit had made this axis of rotation shift. For this particular axis of rotation, the stem/calyx ends would rotate directly through the center of the field of view of an overhead camera. A large portion of the surface area composing of the apple cheek would not be in the camera field of view and would not be inspected. This orientation response was typical for these 6 cultivars regardless of the commercial bicone conveying device used, commercial device 1 or 2.

After a period of 0.10 minutes, 40% or more of Golden Delicious, Granny Smith, Crispin, Red Delicious, and Gala changed from an axis of rotation about the stem/calyx to one of rotating about an axis perpendicular to the stem/calyx axis. This increased to 65% after 0.20 minutes (Figure 9). Many of the apples of these 5 cultivars approached the shape of a sphere (height and width equal) which has no geometrical bias favoring a specific orientation thus fewer apples compared to the other 6 cultivars tested changed orientation but still a significant number did shift axis of rotation to that of perpendicular to the stem/calyx axis. Similar results were obtained for both commercial device 1 and commercial device 2.

Condition 3: Red Delicious apples from Washington State placed on the experimental device rotating about the stem/calyx axis and placed on the bicone conveyors (commercial devices 1 and 2) rotating about an axis perpendicular to the stem/calyx axis.

It was observed that the bicone conveying devices tended to orient apples which had a height (distance between the stem and calyx ends) greater than the maximum diameter measured measured perpendicular to the stem/calyx axis. Only a few apples from the 11 cultivars grown in the eastern United States grew with this characteristic shape. Red Delicious apples grown in the State of Washington typically grow with this characteristic elongated shape with a height greater than their maximum diameter. Apples of the 88 and 128 size were obtained from the State of Washington and tested. Regardless of size, most of the apples changed from an axis of rotation about the stem/calyx axis to an axis of rotation perpendicular to the stem/calyx axis when using the experimental device (Figure 10).

The commercial devices 1 and 2 oriented 88% to 96% of the fruit from an axis of rotation perpendicular to the stem/calyx axis to an axis of rotation about the stem/calyx axis (Figure 10).

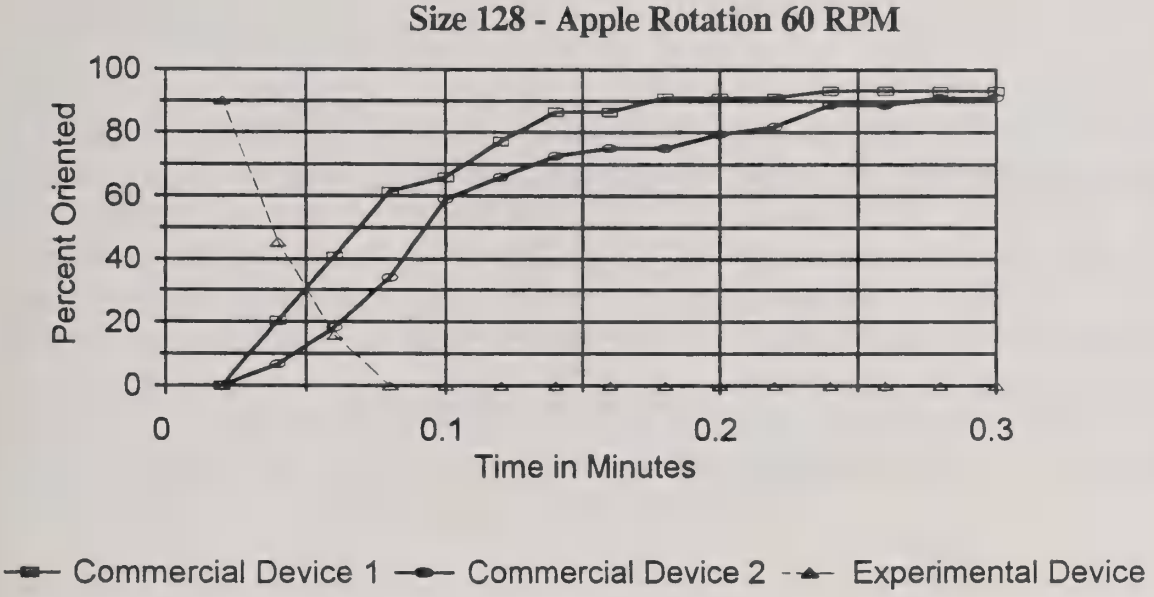

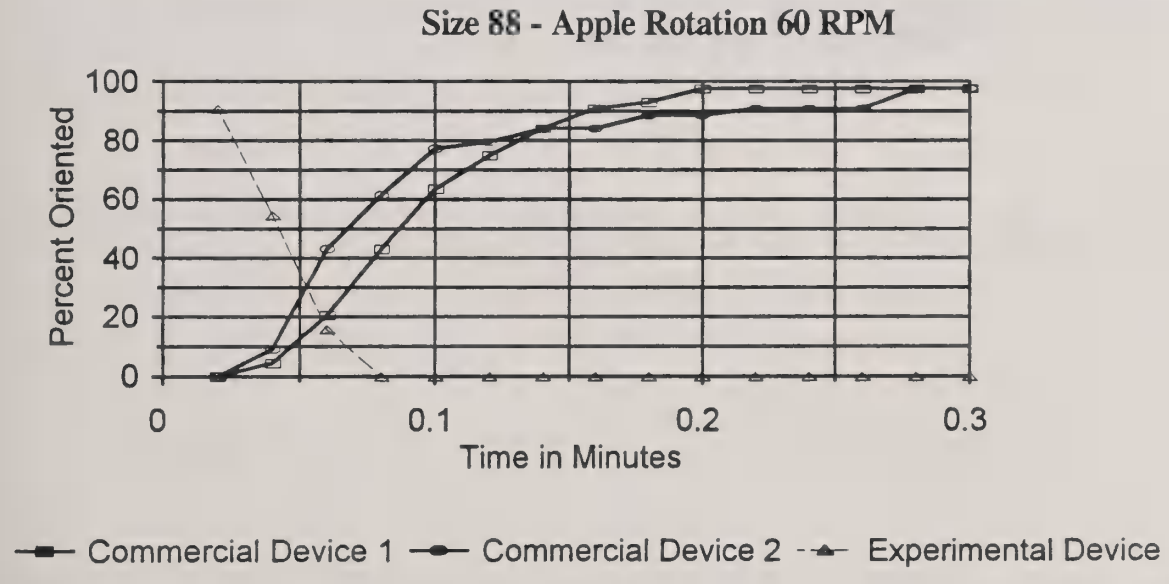

Figure 10. The percentage of Red Delicious apples harvested from Washington State of size 128 (top) and size 88 (bottom) that stayed oriented using the experimental conveying device and correctly changed orientation to rotate about the stem/calyx axis while using bicone roller conveyors (commercial devices 1 and 2).

CONCLUSIONS

It is clear that the commercial bicone roller conveyors (commercial devices 1 and 2) presently used on sorting machines today orient primarily one shape, that of an apple elongated so that the height measured as the distance between the stem/calyx ends is greater than a maximum diameter measured perpendicular to this height. On the commercial bicone rollers, Washington State Red Delicious apples oriented to a rotational axis about the stem/calyx axis with a 88% to 96% success rate. When 11 other cultivars grown in Eastern United States were placed on this device, 60% to 100% of the fruit assumed an axis of rotation about an axis perpendicular to the stem/calyx axis. When considering automatic fruit inspection for these 11 cultivars, this places a large portion of the surface area composing of the apple cheek out of an overhead camera's field of view and these hidden areas would not be inspected.

The experimental device oriented 95% to 100% of Cortland, Empire, Jonagold, McIntosh, Rome, small Fuji apples and 82% of large Fuji apples so that fruit rotation was about the stem/calyx axis. With the exception of large Granny Smith (57%) and large Crispin (52%), successful orientation was achieved 60% to 82% of the time for Golden Delicious, small Granny Smith, small Crispin, Red Delicious, and small Gala apples. All of the Washington State Red Delicious apples assumed an axis of rotation perpendicular to the stem/calyx.

The lateral movement of the disk and angular concave surfaced cone for the experimental device allowed comparitive success of orientation of both fruit sizes. With the exception of very large Granny Smith and Crispin (reduced 5% to 10 %), little difference was found for successful orientation between fruit sizes for most cultivars.

REFERENCES

Abbott, J. A. 1994. "Firmness Measurement of Freshly Harvested 'Delicious Apples by Sensory Methods, Sonic Transmission, Magness-Taylor, and Compression". *Journal of the American Society for Horticultral Science*, 119(3):510 - 515.

Armstrong, P. R., and G. K. Brown. 1991. "Apple Firmness Sorting Using a Nondestructive Acoustic Technique". ASAE Paper 916044, 10p.

Chen, H., and J. Baerdemeaker. 1993. "Effect of Apple Shape on Acoustic Measurements of Firmness". *Journal of Agricultural Engineering Research*, 56(3):253 - 266.

Davenel, A., Ch. Guizard, T. Labarre, and F. Sevila. 1988. "Automatic Detection of Surface Defects on Fruit by Using a Vision System". *Journal of Agricultural Engineering Research*, 41:1 - 9.

Keesling, T. B. 1965. "Fruit Processing Method" *U. S. Patent No. 3225892*. 15 p. Commissioner of Patents and Trademarks, Washington, D. C.

Peleg, K. 1993. "Comparison of Non-destructive and Destructive Measurement of Apple Firmness". *Journal of Agricultural Engineering Research*, 55(3):227 - 238.

Pitts, M. J., R. P. Cavalieri, and S. Drake. 1991. "Evaluation of the PFT Apple Firmness Sensor". ASAE Paper 913017, 18p.

Rehkugler, G. E., and J. A. Throop. 1976. "Optical - Mechanical Bruised Apple Sorters". *Quality Detection in Foods*, compiled by J. J. Gaffney, ASAE, St. Joseph, Mi. pp 185-188, 192.

Rehkugler, G. E., and J. A. Throop. 1986. "Apple Sorting with Machine Vision". *Tranactions of the ASAE*, 29(5):pp. 1388 - 1397.

Throop, J. A., D. J. Aneshansley, and B. L. Upchurch. 1995. "Apple Orientation on Automatic Sorting Equipment". ASAE Paper 956176, 20p.

Throop, J. A., D. J. Aneshansley, and B. L. Upchurch. 1995. "Fruit Orienting Device". *Patent Application CRF D-1791*, U. S. Patent Office, Washington, DC.

Yang, Q. 1992. "The Potential for Applying Machine Vision to Defect Detection in Fruit and Vegetable Grading". *The Agricutlural Engineer Incorporating Soil and Water*, Silsoe, Bedford. pp. 74 - 79.

Yang, Q. 1993. "Classification of Apple Surface Features Using Machine Vision and Neural Networks". *Computers and Electronics in Agriculture* , 9:pp. 1 - 12, Elsevier Science Publishers B. V., Amsterdam.

Paper No. 973079
An ASAE Meeting Presentation

APPLE STEM AND CALYX IDENTIFICATION FOR AUTOMATIC SORTING

Jose Campins, James A. Throop, Daniel J. Aneshansley

Cornell University, Department of Agricultural and Biological Engineering, Ithaca, NY 14853

Written for presentation at the
1997 ASAE Annual International Meeting
Sponsored by ASAE

Minneapolis Convention Center
Minneapolis, Minnesota
August 10-14, 1997

Summary:

A computer vision algorithm was developed to identify stem and calyx of rotating apples. The algorithm uses structured light for the identification. Representative samples of all possible orientations of the apple where considered in the evaluation of the algorithm. The algorithm considers implementation problems such as the elimination of background from the image. Results show that structured lighting is a feasible solution to detecting the stem and calyx of apples. Further research is required to optimize some parameters of the algorithm.

Keywords:

Automated inspection, Apples, Grading, Stem, Structured light, Detection

ASAE, 2950 Niles Rd., St. Joseph, MI 49085-9659 USA
Voice: 616.429.0300 FAX: 616.429.3852 E-Mail: <hq@asae.org>

Abstract:
An algorithm that uses three-dimensional information of the apple skin was developed to identify stem and calyx of apples. A structured lighting system was used to obtain the three dimensional information of the apple surface. The setup used to capture image data was a replica of the one that would be used in an industrial environment. The location of the stem and calyx were estimated by analyzing the geometry of the reflected light pattern. The parameters used to estimate the location of the stem and calyx were the rate of change in the slope of the projection lines and the pattern of the discontinuities of the light patterns. The analysis of the light pattern was based on the assumption of spherical apples. A sampling methodology was implemented to ensure that representative samples of all possible apple orientations were used. The algorithm was evaluated based on the difference between the actual location of the calyx/stem and the algorithm's estimate of location. The apple variety used for the algorithm evaluation was Red Delicious. This variety has very irregular geometry and presented a worst case scenario for the algorithm evaluation. The results obtained indicate that the algorithm used is adequate to locate the stem and calyx of the apples, especially when the stem/calyx are located near the center of the apple silhouette. Further research needs to be done to observe the effect of the setup geometry on the algorithm performance. It was also recommended to investigate the possibility of detecting the calyx/stem using a pattern classifier, since this would simplify the overall grading system.

Objectives:
The objective of this work was to identify a feasible computer vision solution to identify the stem and calyx of Red Delicious apples when they appear in the field of view of the camera for the possible orientations at which the stem and calyx could be observed by the camera used for inspection. Develop the image enhancements required to successfully implement the technique used. Analyze the expected error in estimating stem or calyx location at each possible orientation of the apple. Examine other possible techniques that could be used to identify the stem and calyx of the apples. Suggest future work that should be done including considerations of other techniques for identifying the stem and calyx as well as optimizations for the algorithm developed.

Introduction:
Currently one of the limitations in implementing an automated apple grading system is that it is not possibly to mechanically orient all apples (Throop et al., 1997). The knowledge of apple orientation during the inspection process has been recognized to be important for automated grading (Rehukugler et al., 1986) (Throop et al., 1988). Throop et al. (1997) compared the performance of two orienting devices. The goal of the orienting device was to rotate all apple varieties along the stem/calyx axes. This would expose the cheek of the apple for inspection and avoid the appearance of the stem and calyx in the field of view of the camera. The results showed that the varieties that were successfully oriented with one system would not orient using the other device.

Another problem related to the uncertainty of the apple orientation is that the stem and calyx could be misclassified as blemishes (Yang, 1993) (Throop, 1997). One of the approaches followed in the research is to use the spectral reflectance from the apple surface at various wavelengths. Aneshanley et al. (1997) completed a reflectance spectra analysis of several surface defects on various apple varieties. The study concluded that some other features besides reflectance information would be needed to identify all possible defects present on the apple's surface. In addition, it seems not possible to use reflectance information to distinguish the stem and calyx of the apple from skin defects (Personal Communication. Throop, 1997). This will lead to erroneous classification of all apples not oriented at time of evaluation by the system.

Yang (1993 and 1996) used structured lighting to identify the stem and calyx of apples. The method used two images: one image using diffuse lighting and a second image using the structured light source. The criteria to distinguish the stem and/or calyx from other defects was based on curvature of the laser lines, and this parameter is heavily dependent on the apples being spherical. This model is accurate for most varieties, but it is clearly not an accurate representation of varieties such as Red Delicious. No information is provided regarding the conditions on which the algorithm fails to identify the stem and calyx. In addition, the procedure to ensure that all angles of view were covered and the effect of orientation were not clear from either of Yang's papers. The study presented here, implements an algorithm similar to that developed

by Yang (1993) and examines the performance of the technique at all possible locations of the stem and calyx, as well as the effect of using non-spherical apples. The algorithm developed in this work also considers the pattern of broken line projections in the image.

System Setup Overview:

The stem and calyx identification was achieved by means of a structured lighting setup. The structured light source was a 1-mW diode laser (SNF-533L-685-20-5-038. Lasiris, Inc.). This laser was provided with lenses that produced a pattern of parallel lines. The fan angle of the laser stripes was 5° and the interbeam angle was 0.38°. The maximum number of laser stripes that could be projected onto the apple was 7 to 9 lines, depending on the size and orientation of the fruit. The lines were projected parallel to the axis of rotation (see Figure 1). The angle between the focal camera axis and the laser light beam was set to 20°. The projections of the laser light into the scene were recorded using a B/W CCD solid state camera (model: 4815-5000/0000. Cohu). The lens used during the experiment had a focal distance of 15mm. The resolution of the image was set to 256x256 pixels, and the area of the field of view was set to 5"x5" (12.7x12.7 cm). The frame grabber used to digitize the image was a Raptor-1M (RAP-PCI-VS-1, BitFlow, Inc., Woburn, MA). The software used to capture the images was Quantim (Zedec Technologies, Inc., Burlington, NC).

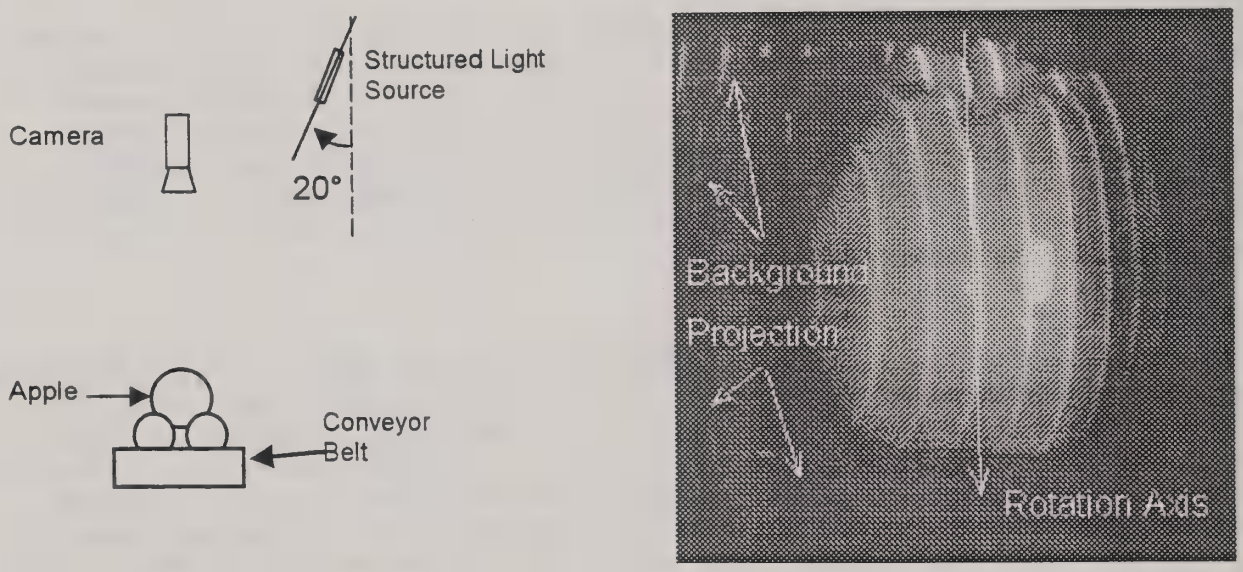

Figure 1. A Red Delicious apple with eight line of structured light parallel to the axis of rotation.

This work was to determine the error associated with the estimation of the calyx and stem location, on the image, at each possible orientation of the apple. To achieve this, the apples were manually oriented on the still belt to ensure that all possible orientations of the apple were considered in the analysis. The consideration of all possible apple orientations was achieved by superimposing a grid onto a monitor while viewing the apple with the camera. The calyx and the stem were manually positioned at the center of each square of the grid. The grid had 64 squares, each of which was 32x32 pixels and covered an area of 0.625"x0.625" (1.6cmx1.6cm). All feasible orientations were considered for both the stem and calyx. For a large size Red Delicious apple, this technique yielded approximately 40 to 55 orientations.

The evaluation of the algorithm required the acquisition of three images for each possible apple orientation: no ambient light, some ambient light, and saturated apple silhouette. The image with some ambient lighting was used for display purposes and for verification of calyx and stem location. This image was captured by using a 60-W incandescent lamp located above the camera. The saturated apple silhouette was formed by illuminating the scene with incandescent light from the sides of the image. The positioning of the lamp for ambient and saturated conditions was not critical. The laser light source was turned off during the positioning of the apple to ensure that there was no bias in the final setup of the image. The image with background light was used to display the results and to ensure that the calyx was positioned correctly. The image with no background light was used to analyze the laser light pattern and to estimate the location of the calyx or stem. The last image, the saturated apple silhouette, was required to find the center of mass of

the apple and to normalize the apple size. All three images were taken without relocating the apple, ensuring that the images had a perfect pixel to pixel correspondence. The operation of the algorithm only requires the image with no ambient light.

The algorithm was developed and tested using images from three different groups of apples. Images from the first group were captured using laser line projections and no background light. This set of images used four apples and a total of over 160 images, slightly over 40 orientations per apple. These images were used only for initial developing and debugging of the algorithm. A second set of images was taken using two different apples. The three image setups described above were taken for each of the possible orientations of the apples. These images were used to train the algorithm. A third set of images was used to evaluate the performance of the algorithm. The performance of the algorithm was measured as the Euclidean distance from the actual to the estimated location of the stem or calyx. All three images were taken for each of the apple orientations. Seven apples were used in this test, yielding over 350 views (1050 images).

Algorithm Description:

The algorithm developed for the stem and calyx identification consists of image preprocessing and hypothesis forming. The preprocessing part of the algorithm reduces the original image to a form of information that can be readily used to estimate the location of the stem and calyx. The preprocessing included: structured light thresholding, thinning, labeling, background projection removal, contour smoothing, determining slope and rate of slope change and connecting line segments. The hypothesis forming used the values of the slope, rate of change in slope and information about the connectivity of the line segments. The algorithm is shown schematically in Figure 2.

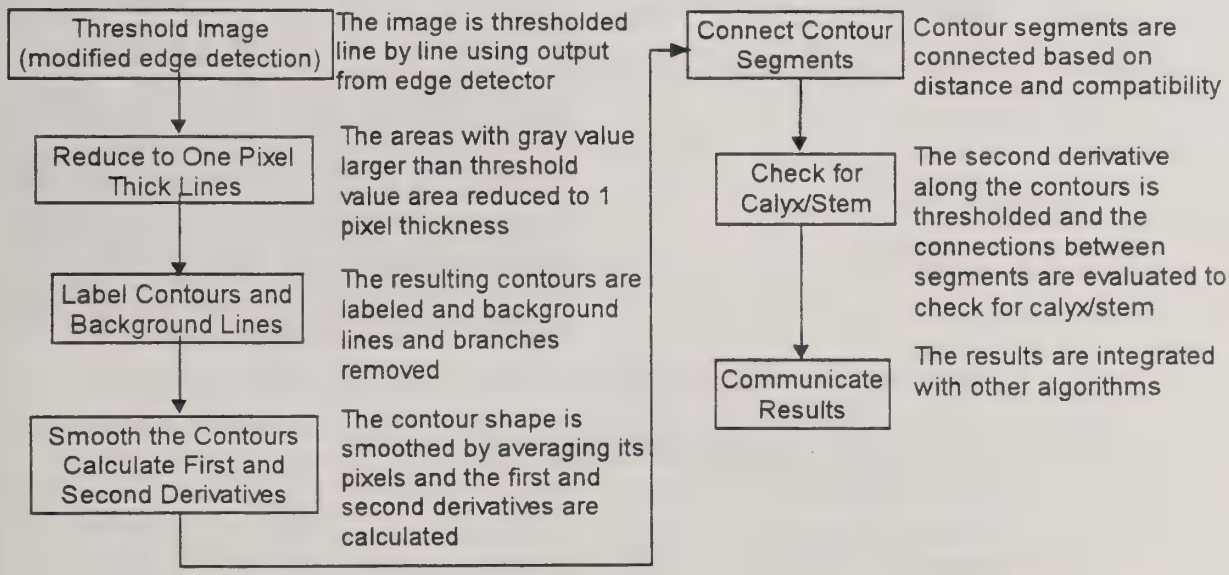

Figure 2. Schematic Representation of the Algorithm

Identification and Thinning of the Laser Line Projections:

The first goal of the algorithm is to identify all the pixels that correspond to laser projections. The laser line projections are identified using a modified Sobel edge detector (Jain et al., 1995). The filter mask used was defined by the convolution of a 3x1 step edge and a 3x1 mean filter. The filter mask resulting from the convolution was [-1 -1 0 1 1]. There was no need to use a mask larger than a row vector because most of the edge information is in the vertical axis of the image (laser lines are projected parallel to the vertical axis of the image, see Figure 1). This size of filter proved to be adequate for the profile of the lines to be identified. A structured line projection was defined as the region of the original image between a local maximum and minimum response of the edge detectors. These regions were left unchanged on the original image, while the rest of the image was set to zero. The thinning was achieved by detecting the maximum gray value inside each of the unchanged regions of the image along each horizontal line of the image.

Labeling:
It is important to identify the laser line to which each pixel belongs. This simplifies the implementation of the following sections of the algorithm. Two pixels were considered to belong to the same contour, if they were within a 5x5 pixel window. This is necessary because the output from the contour detection section often yields broken line segments. This is due to the fact that, the algorithm used to perform the thinning is restricted to identify one pixel per horizontal line of the image. Therefore, the smallest slope that a line can have without being broken is plus or minus one (±45°).

Removing Background:
The method used to determine which pixels to erase is shown graphically in Figure 3. Figure 3 shows a typical image with three laser lines projecting on the background as well as the apple. It was impossible to remove the background lines by means of fitting a simple line. Due to this, it was necessary to use a maximum and minimum allowable slope and the origin of the fitted line. The expected origin of the line was set to the first and/or last pixel of each line segment, depending on the location of the segment. However, it was necessary to have +/- 2 pixels on the origin. The start of the background lines was fixed in the image due to the geometry of the conveyor belt. The dimensions of the conveyor belt do not change with time, this ensures that the background projections would begin and end at the same points (unless the line projects onto the apple). Therefore, only those segments that begin within the areas labeled Search Area in Figure 3 were considered for removal. The areas are given by the location of the bicone rollers on the belt and the width of the laser lines. The area delimited by the dashed lines, in Figure 3, is the region in which the pixels belonging to the segment would be erased. Note that only a small number of pixels are lost for those segments corresponding to the apple projections.

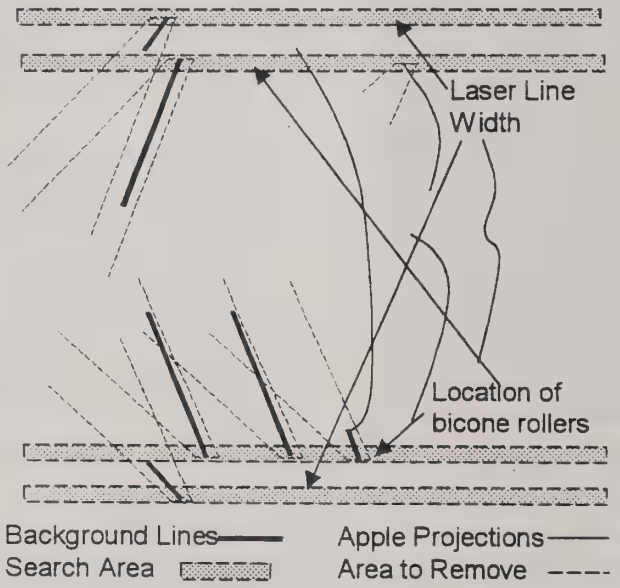

Figure 3. Background Elimination

Smooth the Contours:
The contours obtained from the thresholding and thinning algorithm are too noisy due to the imperfections in thinning algorithm and to the digitalization of the image. To minimize the effect of this noise, the contours were smoothed using a linear mean filter of five pixels length. The smoothing filter was applied along the length of each contour. The sum of the x and y coordinates of each group of four pixels was used to calculate the slope and the change in slope from point to point (i.e. the first and second derivatives of the contours).

Connect Line Segments after Background Lines Removed:
Each laser lines projected by the structured light source often yields more than one line segment on the image. This is usually due to the calyx or stem appearing on the field of view. However, the contours could be broken due to changes in the reflectance properties of the apple surface and/or other abrupt changes in the geometry of the fruit. In order to evaluate the source of the discontinuities, it is necessary to identify all

the segments that belong to the same laser line projection. The lines were identified based on the number of neighbors that each line projection had and the classification of its neighbors. Sometimes there was more than one possible (i.e. compatible, based on the above discussion) connection for each of the segments. The most likely connection between segments is defined as the connection that minimizes the distance between compatible connecting ends of the contours. The operation of connecting line segments could be highly simplified using a coding technique for the structured lighting (Jain et al.,1995; Boyer and Kak, 1987).

Calyx/Stem Detection:
The detection of the calyx/stem was divided into two sections. The first dealt with the possibility of having a calyx or stem appearing in the image but not breaking the laser lines. The second case deals with the case where the laser lines are broken. The criteria selected to indicate the existence of the calyx or stem on a continuous contour was the second derivative of the laser line projections. A point was defined to be a calyx if its second derivative was larger or smaller than predefined threshold values. The threshold values were determined by trial and error. The threshold values corresponded to the two possible curvatures that can be present on any image. A different threshold was used for the maximum and minimum change in slope.

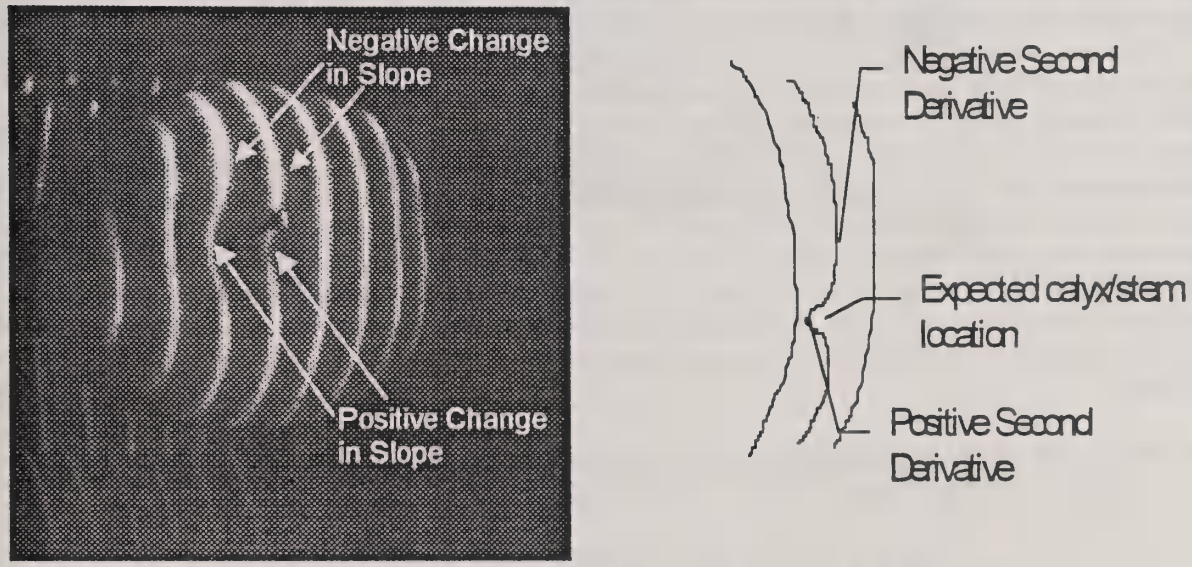

Figure 4. Graphical Representation of First and Second Derivative

In the case of discontinuous segments, it was necessary to fit a line that would fit the model surface. This is very difficult to do for varieties such as Red Delicious, because their shape is very irregular and there is no line model that will always fit the surface, with the information given. The best approach was to fit a circumference between connecting ends. The circumference was defined by the two ends of the segments and the slope of one of them. A calyx/stem was said to occur when the difference between the slopes of the fitted circumference and the slope of the segment were different by a predetermined value. This approach could not be used when the connecting points were too close. This was because the fitted circumference is highly sensitive to the estimate of the location of the connecting points. In this case, the likelihood of stem/calyx was determined based on the differences among the slopes at points A and B, and the slope of the line connecting the two points.

Results and Discussion:

The algorithm usually yielded more than one estimate of calyx/stem location. It was very difficult to take into account each estimate in the evaluation of the algorithm. Therefore, the actual location estimated was defined to be the average of all the estimates generated by the algorithm. The algorithm performance was evaluated based on the distance between the actual location of the stem/calyx and the estimated location provided by the algorithm.

The performance of the algorithm was controlled by many parameters. The optimal value of most parameters could be determine by examining the results obtained from a few images, since the results were very sensitive to the values of these parameters. This was the case for the selection of the threshold for the filter mask output, the window size used to label the structured light projections and the number of pixels considered to estimate the slope of the line segments. However, there are other parameters that have an impact on the performance of the algorithm, whose optimum values are not easily determined. These parameters are the thresholds values used by the algorithm to estimate the location of the stem or calyx. The optimum value for these constants was estimated by running the algorithm multiple times at different settings and manually deciding which combination performed best. The best set of parameters was the one that minimized the average error between the actual calyx/stem and its predicted location. In addition, it was important to choose the combination of parameters that minimized the number of unidentified calyx/stem.

The results also show that the average error and the number of missed stem/calyx locations do not change in the same direction as the values of the parameters are changed. That is, changing one parameter often caused an increase in one measure of error and a decrease in the other. The accuracy of the algorithm is increased by relaxing the threshold values. This means that the system will only detect those features that are obvious to the algorithm. It also implies that fewer features would be detected, increasing the number of non-detected stem or calyx. Increasing the sensitivity (tightening the threshold values) of the algorithm triggers many false detection's that are due to the changes in skin geometry of the Red Delicious. This leads to less accurate estimates on the location of the stem and calyx, but it also ensures that more less obvious calyxes/stems are detected. These observations indicate that the selection of the parameters should be based on the priority of the algorithm: accuracy or detection ability. However, the effect of parameter selection should not be as pronounced as in Red Delicious, since the parameters used to estimate the likelihood of stem or calyx are based on a spherical model of the apples.

This set of parameters was used to analyzed images from seven different apples. The apples chosen had different geometry's and sizes. Table 1 summarizes the geometry of the apples used.

Table 1. Apple Geometry's

Apple	Height (in)	Diameter (in)	Roundness
1	3.30	3.10	Irregular(3)
2	3.25	3.11	Irregular(2)
3	3.20	2.75	Irregular (1)
4	3.20	3.13	Irregular(4)
5	2.88	2.95	Irregular(5)
6	2.60	2.53	Irregular(5)
7	2.55	2.50	Irregular(5)

*Irregular(1) stands for the most irregular apple and Irregular(5) the most spherical apples.

The results show that the algorithm yields good results close to the center of the image. This is expected, since the image is more sensitive to changes in surface geometry of the apple at the center of the image. An unexpected result is that the accuracy of the algorithm seems to be largely independent of the radius at which the calyx/stem is located (the radius is the distance from the center of gravity of the apple to the location of the stem/calyx). However, the results show that with an increase in the radius the number of non-identified calyx/stem increases. The local coordinates are calculated with respect to the center of gravity of the apple. The center of gravity was determined by thresholding the apple silhouette. Any background on the image was removed using morphological opening (Jain et al., 1995). The center of gravity was determined using the first order moments of the image (Jain et al., 1995). The radius of the apple silhouette was defined as the radius of the circle with the same area as the apple

silhouette. Note that this is an underestimate of the radius, since some of the apple views had elongated silhouettes. Therefore, normalized errors are slightly overestimated, since the errors are normalized with respect to the radius the. The normalized results obtained from the algorithm as a function of the distance between the center of gravity and the actual location of stem/calyx are shown in Figure 5. A zero error corresponds to non-detected stem/calyx. The error magnitude is fairly constant for all locations, except for those where the calyx/stem was located close to the outside radius of the apple (when viewed from the top). Close to the outside radius, there are significantly more non-detected cases and larger errors. The effect of the angular location of the stem or calyx in the image is shown in Figure 6. The angle was defined in degrees, with the origin at the center of gravity, positive clockwise, and zero degrees in the direction of the laser source. The graph shows no clear trend. It could be argued that the algorithm is slightly more accurate in the region close to 0 degrees.

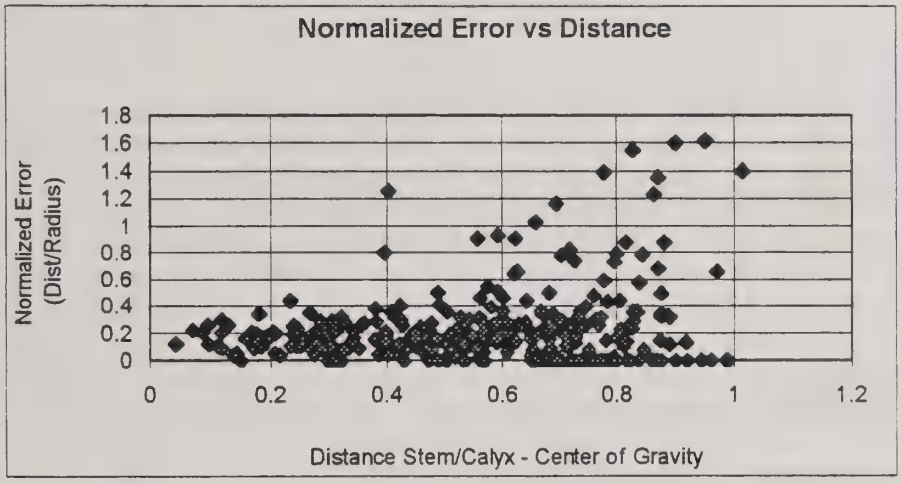

Figure 5. Normalized Error vs. Distance from C.G.

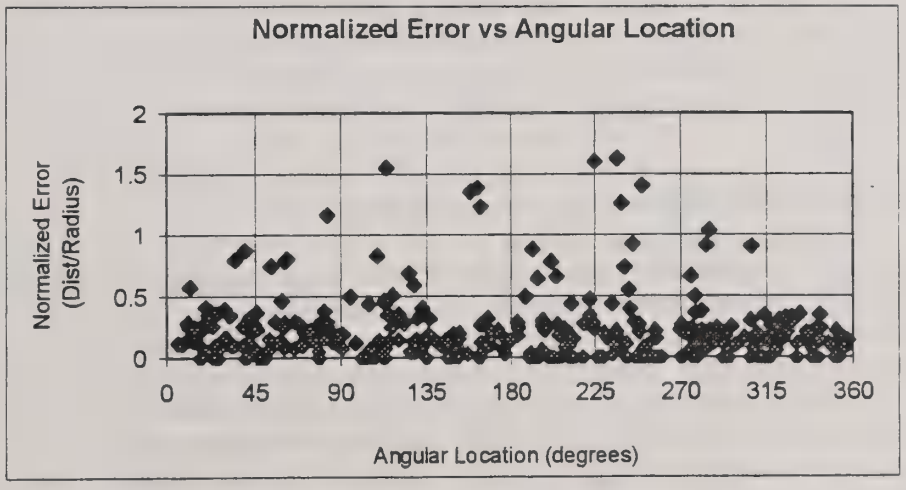

Figure 6. Normalized Error vs. Angular Location

The histogram of the errors obtained by the algorithm are shown in Figure 7. The error is clearly not normally distributed. Most of the errors in the location estimation are located around 20. This is approximately the spacing between laser lines in the image. Therefore, it seems that there is a clear influence of the resolution of the structured lighting on the performance of the algorithm. The structured light pattern projected onto the apples in this work was set by the laser lenses. Therefore, it was not possible to verify this conclusion. The effect of structured light resolution on the performance of the algorithm is left for future work. It is important to note that the processing time of the algorithm would be highly increased by adding more

projections in the image. Therefore, there will be a trade off between accuracy and speed of the algorithm.

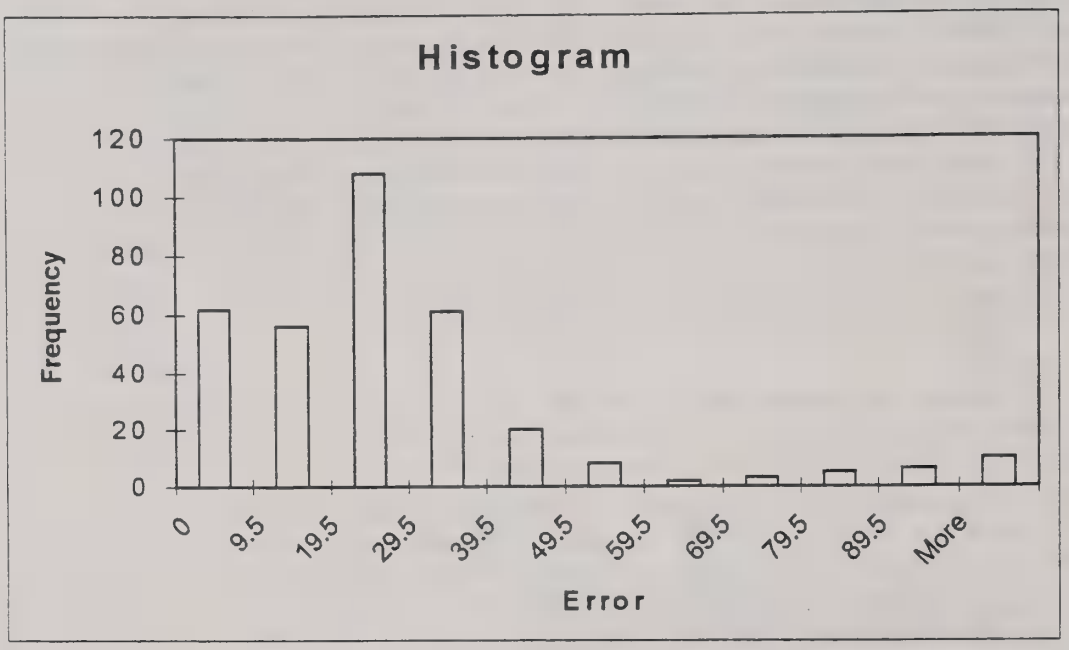

Figure 7. Error Histogram

***62 non detected images are not shown on the histogram.**

The performance measure was the distance between the actual stem/calyx location and the location estimated by the algorithm. Therefore, it is important to examine the error associated with the actual stem/calyx location. The first possible error to note is that the calyx and stem were considered to be point locations in the image, while in practice they are wider than one pixel. The error associated with this assumption is difficult to quantify. A second source of error in the determination of the actual location of the stem or calyx is that, it is not possible to precisely locate the stem or calyx at the center of each location required. The error associated with manual orientation of the apple could range anywhere from 0 to 10 pixels. Therefore, it is important to note that there is not improvement for errors of 10 to an error of 15.

A total of 342 images were collected to test the algorithm. These images were representative samples of all possible orientations that the apples can achieve in the prototype transport system. There was a total of 62 non-detected apples. From this set,180 images corresponded to images with the calyx/stem located within the center part of the apple image (interior circle with diameter 40% percent smaller than the original apple). In this region only 14 stems or calyxes were not identified. The mean error in the location of the stem and calyx was 20% of the radius of the apple, and the standard deviation 12.2% (μ=17 pixels, s=10 pixels). Most of the errors on the outside area were also in this range. However, the number of outliers (large errors) and non-detected stems/calyxes increased considerably.

Conclusion and Future Work:

Conclusion:

A setup using structured lighting and a computer vision algorithm was developed to automatically identify the stem and the calyx on rotating apples. The setup was designed considering the environment in which the system would be expected to operate. For this purpose, the images used for the analysis were captured using a prototype transport system similar to the ones used in apple packing plants. The algorithm described includes the image processing steps required to identify the stem and calyx under this setup.

The algorithm seems to be accurate enough with the setup used. However, the accuracy of the system is likely to improve by projecting a larger number of lines onto the apples. There were approximately nine laser lines projected on the surface of the apple. Therefore, The spacing between them was larger, approximately 0.1% of the radius. This resolution seems to be very close to the mean value of the error in the algorithm's estimates. Therefore, it would be expected that the accuracy of the system would improve if more lines were projected onto each apple.

Defects on the apple skin are usually present on the cheeks of the fruit. It is expected that most of the time there will be a significant separation between the stem or calyx and any possible defect. Therefore, an error of 20% of the radius of the apple might be sufficient to avoid the misclassification of the stem and calyx. Otherwise, a grid with higher resolution should be used.

Future Work:
The work presented here did not do any optimization of the physical parameters of the system. These parameters are the angle between the structure light source and the focal axis of the camera, number of lines projected onto the apple and the resolution of the camera. The former parameter has a direct effect on the performance of the algorithm, since it effects the sensitivity of the laser projections to changes in surface geometry. The number of lines projected onto the apple, and the camera resolution have an effect on the overall performance of the algorithm and computation requirements on the algorithm. Therefore, it will be necessary to identify the optimum values for these parameters prior to implementing the system. Note that the values used for some of the internal parameters of the algorithm will need to be changed if the setup is modified. The addition of a hypothesis verification section would add more reliability to the algorithm. A second advantage is that the thresholds of some parameters could be tightened to ensure that all calyxes and stems are detected. False identification could be removed in the hypothesis verification, reducing the number of non-detected stems or calyxes.

This work used Red Delicious apples to evaluate the performance of the algorithm. This was done because this variety is the one that most severely tests the assumption of the apples being spherical. Therefore, it is expected that the system performance will improve for more spherical varieties. Although, the system parameters might need to be changed for the each varieties.

The technique used to segment most of the defects is a pattern classifier based on reflectance at different wavelengths. Therefore, the next focus of the research should be to study the possibility of identifying stem and calyx using a pattern classifier. In the introduction and literature review sections, it was pointed out that it seems not possible to successfully identify all types of defects based using only the surface illuminance levels. However, it might be possible to develop a pattern classifier based on other parameters besides gray levels. Some other parameters that could be used as input variables for a pattern recognition algorithm could be: defect shape, texture, number of blobs, etc. Note that an important consideration to selecting the input parameter for the classifier is that these parameters have to be normalized, since the shape and size of the defects is not constant.

References

D. J. Aneshansley, J. A. Throop and B. L. Upchurch. Reflectance Spectra of Surface Defects on Apples. Proceedings from the Sensors for Nondestructive Testing International Conference, pp 143-160, 1997. NRAES, Ithaca, NY.

K. L. Boyer and A. C. Kak. Color-Encoded Structured Light for Rapid Active Ranging. IEEE transactions on Pattern Analysis and Machine Intelligence, vol. 9, no. 1, 1987.

J. A. Jalkio, R. C. Kim and S. K. Case. Three Dimensional Inspection Using Multistripe Structured Light. Optical Engineering, vol. 24(6), 1985.

R. Jain, R. Kasturi and B. G. Schunck. Machine Vision. McGraw-Hill, New York, 1995.

G.E. Rehkugler and J.A. Throop. 1986. Apple Sorting with Machine Vision. Transactions of the ASAE 29(5):1388-1397.

J. Schürmann. Pattern Classification: a Unified View of Statistical and Neural Approaches. Wiley-Interscience, New York, pp. 73-73, 1996.

J.A. Throop and G. E. Rehkugler. 1988. Image Processing for detecting Bruises on Fruit. U. S. Patent No. 4741042, Issued Apr. 26, 1988.

J. A. Throooop, D. J. Aneshansley and B. L. Upchurch. Apple Orientation on Automatic Sorting Equipment. Proceedings from the Sensors for Nondestructive Testing International Conference, pp 328-342, 1997. NRAES, Ithaca, NY.

J. A. Throop and D. J. Aneshansley. Personal Communication. 1997.

Q. Yang. Finding Stalk and Calyx of Apples using Structured Lighting. Computers and electronics in Agriculture, vol(8), pp. 31-42. 1993.

Q. Yang. Classification of Apple Surface Features using Machine Vision and Neural Networks. Computers and electronics in Agriculture, vol(8), pp. 1-12, 1993.

Q. Yang. Apple Tem and Calyx Identification with Machine Vision. Journal of Agricultural Engineering Research, vol(63),229-236, 1996.

Reflectance Spectra of Surface Defects on Apples

Daniel J. Aneshansley
Associate Professor
Department of Agricultural and Biological Engineering
Cornell University, Ithaca, NY 14853

James A. Throop
Research Support Specialist
Department of Agricultural and Biological Engineering
Cornell University, Ithaca, NY 14853

Bruce L. Upchurch
Agricultural Engineer
Formerly USDA-ARS Appalachian Fruit Research Station
Kearneysville, WV 25430

BACKGROUND

Using spectral reflectance to assess fruit quality, both for maturity and for defects, dates back to the early 1940's (Lott, 1943). The earliest work used reflectance spectra to measure fruit maturity (Bittner, et.al.1968). Bruised apple pulp consistently had a lower reflectance at 600 nanometers (Ingle and Hyde, 1968). It was reported that when water replaced air in the intercellular air spaces in plant tissue, the near-infrared reflectance decreased (Woolley, 1971). Later, it was recognized that apple bruising ruptured cells releasing cell fluid filling the intercellular spaces under the apple skin resulting in a reduction of the near-infrared reflectance from the apple surface (Brown et. al, 1974). It was further suggested that for processed apples, different wavelengths (wavelenghts is used to indicate bands of wavelengths centered about a specific wavelength) could be used to discriminate between apple defects, flesh, skin, stem or calyx ends. Further study of the mechanics of the trimming and orientation mechanisms was indicated to make sensing feasible (Reid, 1976).

The examination of more than one wavelength provided improvements. A regression model found that two selected wavelengths between 350nm - 750nm performed better than a single wavelength at classifying bruised and unbruised tissue. Further study found that a two wavelength derivative model worked the best (Fuzzen, 1981). Recognizing that not all apple flesh browned equally, the optical reflectance of bruised and unbruised apple flesh using 16 wavelengths (350nm - 700nm) was measured for five different peeled processing varieties (McIntosh, Greening, Spartan, Red Delicious, and Northern Spy). The resulting classifier was reduced from 16 to 5 wavelengths and still classified 100% of peeled

Northern Spy bruised tissue from unbruised tissue (Pen et. al., 1985). A spectrophotometric study of diffuse reflectance between 400nm and 1000nm wavelengths compared a single wavelength, two wavelength ratio, two wavelength difference, normalized two wavelength difference, and reflectance derivative models to classify bruised from unbruised apple tissue (Upchurch et. al., 1990). This study was carried further to include early frost damage and red/green areas on the surface of Empires. The ratio, normalized difference, and deriative models using more than one wavelength classified color and damage better than a single wavelength (Upchurch et. al., 1991). All of the above work was performed on labratory spectrophotometers with no attempt to apply the techniques to a processing or sorting line.

Digital images of apples, captured using a video matrix camera and near-infrared (NIR) light, were used to compute a linear discriminant classifier capable of detecting bruises on Red Delicious apples as accurately as a human inspector (Graf, 1982). An attempt to apply a quadratic discriminant classifier to NIR images, captured with a line scan camera, failed to handle the variability of the data (Taylor, et. al. 1985). Conversion of Taylor's algorithm from a quadratic to a linear classifier did not improve the performance. A nonstatistical threshold-thinness ratio image processing algorithm had a lower grade-by-grade classification error than Graf's algorithm. Apple orientation is important, as part of the inspection process (Rehkugler et. al., 1986) (Throop et. al., 1988). Processing of NIR images of defects other than bruising segmented some defects successfully (Rehkugler et. al., 1989). An attempt to apply the two wavelength models using a camera and two bandpass filters instead of a spectrophotometer did not perform the same way as with a spectrophotometer . It was observed that reflectance characteristics captured through a camera/lens/filter system produced different results than those achieved with the spectrophotometer (Upchurch et al, 1990).

Electronic inspection of apples will be dependent on electronically capturing images, and based on reflectance spectral data, quickly surface and subsurface damage by type and as difference from undamaged tissue. The reflectance characteristics of a few defects that damage apple tisssue have been fully investigated. This study was designed to further advance electronic inspection of apples by using a lens/camera system to look at reflectance spectral characteristics of many different types of damaged tissue.

OBJECTIVES

The objectives of this study were to gather detailed visible and NIR spectral reflectance data for a large number of defects found in five varieties of apples and to analyze these data. The data were to be captured with imaging system that could be used in an inspection station; a matrix camera equipped with lens and optical filters. A classifier was to be

developed that would determined which wavelengths of light best separate defects and good apple tissue based on the computed Mahalanobis distance and the classification error.

MATERIALS AND METHODS

During the 1995 harvest season, different apple cultivars with defects were gathered from the experimental orchards at the Geneva Experiment Station, Geneva, NY and at the Appalachian Fruit Research Station, Kearneysville, WV (Table 1). The apples were held in cold storage until 24 hours before image capture.

Table 1. A list of defects and cultivars from which reflectance spectra was gathered.

Defect	Red Delicious	Golden Delicious	Crispin	McIntosh	Empire
Bitter Pit		X			
Blister Spot			X		
Bruise	X	X			
Codling Moth	X		X		
Corking	X				
Fly Speck	X	X			
Hail Damage	X				
Powdery Mildew	X			X	
Leaf Roller	X	X			
Puncture(New)	X	X	X		
Puncture(Old)				X	
Rot	X				
Russet	X	X			
Scab	X			X	
Scald	X				
Sting	X	X	X		
Sunburn	X				
Sooty Blotch		X			X

Two camera/lens/adjustable filter combinations were used. System 1 consisted of a CCD monochrome camera (Model 4900, Cohu Electronics, San Diego, CA) with its gain adjusted to full and equipped with a 25mm lens with the aperture set at f1.4. A tunable filter system (Model:VS-VIS3-20-MC-20-SQ, Cambridge Research & Instrumentation Inc., Cambridge, MA) was placed in front of the camera lens. The filter had variable attenuation control and was adjusted for 29 different wavelengths between 460nm to

750nm, both of which were controlled from the serial port of the image capture computer. For each wavelength selected the filter had a 20nm bandpass and a 20nm aperture diameter. System 2 consisted of a CCD monochrome camera (Model 4800, Cohu Electronics, San Diego, CA) equipped with a 25 mm lens with the aperture set at f1.4. A tunable filter system (Model:VS-NIR1-35-MC-20-RN, Cambridge Research & Instrumentation Inc., Cambridge, MA) was placed in front of the camera lens. The filter had variable attenuation control and was adjusted for 29 different wavelengths between 750nm to 1030nm, both of which were controlled from the serial port of the image capture computer. For each wavelength selected the filter had a 35nm bandpass and a 20nm aperture diameter. A white teflon cylinder 76 mm diameter by 76mm high was placed in the field of view of both systems. For each wavelength tested, the correct attenuation setting for the neutral density portion of the variable filter allowing a camera output of 175 out 255 grey levels was recorded in a look up table. This assured that the camera output was normalized to a standard output grey level while viewing the teflon cylinder regardless of changes in camera response due to wavelength or of changes in the transmission characteristics of the variable filter. System 1 and system 2 were each controlled by different PCI bus Alpha 275 MHz processor equipped computers (Model SYS-AXP275AN, BTG Micro Systems, Fairfax, VA and Model Cobra Cab 275, Carrera Computers Inc., Laguna Hills, CA) with frame grabber cards (Raptor-PCI, BitFlow, Woburn, MA) installed for image capture. Filter control was through the serial port via a subroutine running under image capture and processing software (Quantim, ZEDEC Technologies Inc., Burlington, NC). For every apple tested, this combination provided sequential filter adjustment and image capture for 58 images continuously for each of the different wavelengths tested. A total of 10,200 images 256 pixels high by 256 pixels wide were captured in this study. Images were stored on a rewriteable 650 MB/disk PD/CD-ROM drive (Model:LF-1004AB, Panasonic Communications & Systems Co., Secaucus, NJ).

Diffuse lighting was produced by placing the apples inside of a 222mm diameter cylindrical white acrylic diffuser 406mm high with four tungsten lamps placed around the outside. The 40 watt lamps (model 40A, 40W, General Electric, Cleveland, Ohio) were placed in a 305mm per side square centered about the outside of the diffuser at a height of 184mm (Figure 1). To minimize 60 Hz fluctuations, the adjustable 120 VAC to the lamps was converted to adjustable 160 VDC (4V pk-pk ripple) by using a 10A bridge rectifier (GBPC-1004, General Instruments) and a capacitor filter (80 uf 450 VDC, 36DX-800F450DC, Sprague).

The average grey level intensity of undamaged and damaged areas 4 pixels wide by 4 pixels high were interactively found on the apple images. This average grey level was divided by an average grey level of a corresponding spatial area from the teflon cylinder image for each wavelength tested with the resulting quotient considered as a measure of reflectance. Thus, the reflectance of teflon was considered to have a value of 1.

Although only 3 - 4 apple images were captured, many different areas of damage were present within an image such at 10 to 30 of defects were observed in the 3-4 apples. Discriminant analysis of the two classes of tissue (damaged and undamaged) was performed (Minitab 9.0, Minitab Inc., State College, PA). The classification error in percent and Mahalanobis distance between class means was recorded for each 10nm change in wavelength between 460nm and 1030nm. Whenever the classification error was the smallest for both classes, the Mahalanobis distance was the greatest indicating the greatest reflectance difference between damaged and undamaged tissue.

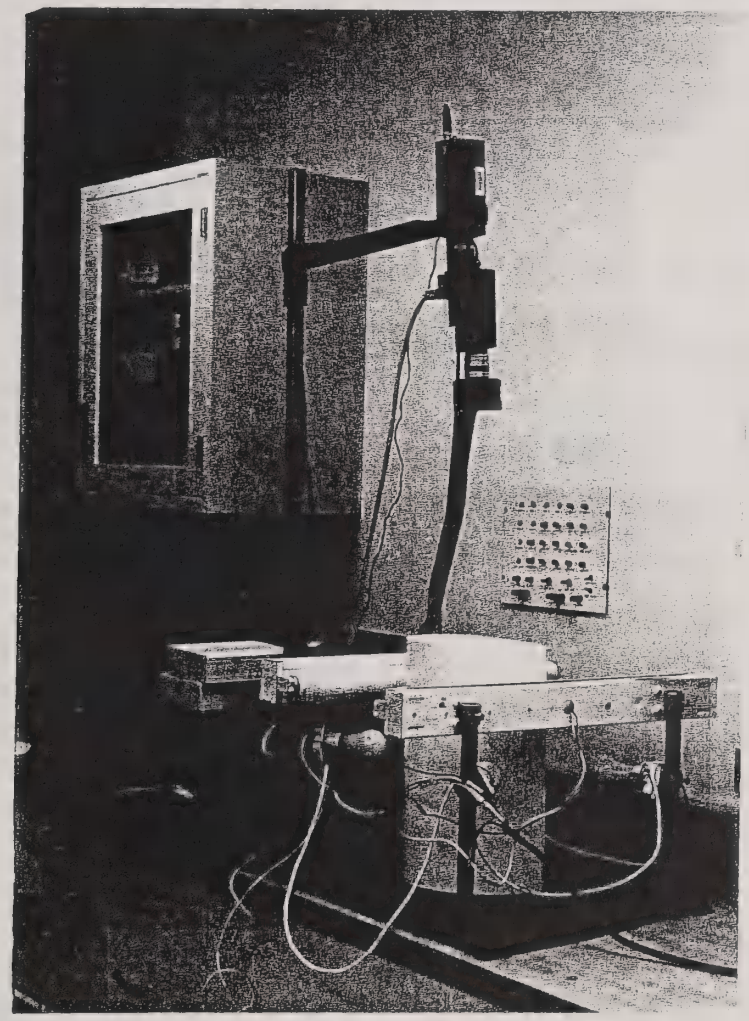

Figure 1. Picture of the camera/filter, diffuser, and lamps used to capture images.

RESULTS AND DISCUSSION

Bitter Pit

Bitter pit starts as an internal disorder and later causes external blemishes. Its cause is related to the competition between fruits and leaves for water and nutrients. Before harvest small areas of cortical tissue at the terminals of branched vascular bundles near the skin

appear water soaked. Later the spots can take on a deep-red color or bright green color. After harvest the affected cells die and lose moisture causing the skin to sink. The skin over the area becomes gray, brown, or black. If the skin is peeled, small brown dry spongy tissue is found (Pierson et. al., 1971). The reflectance curves show both the color change of the skin as a decrease in reflectance, a decrease in reflectance for 700nm - 830nm due to scattering caused by the damaged cells, and the cellular dehydration for damaged with respect to undamaged tissue as an increase in reflectance particularly near the water absorption band at 970nm (Figure 2).

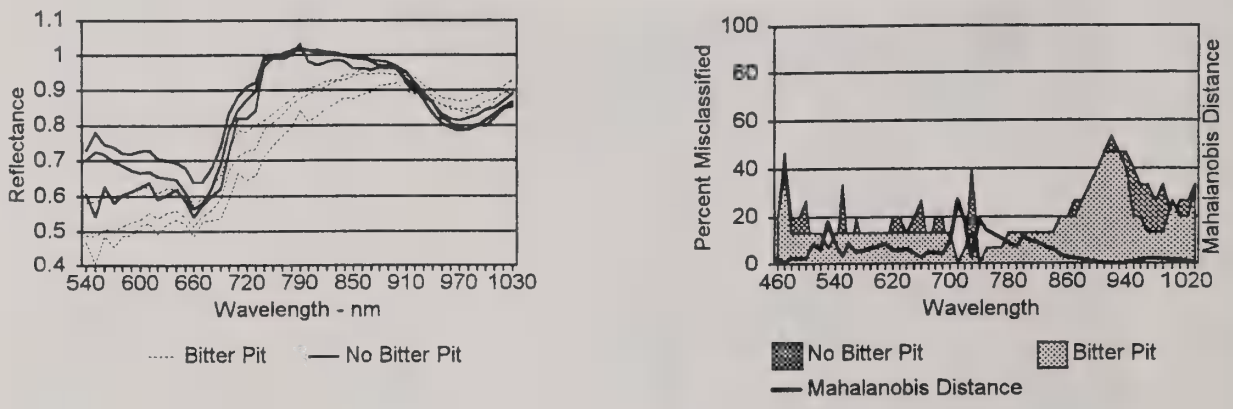

Figure 2. Reflectance of bitter pit damaged and undamaged Golden Delicious tissue (left) and the results of the discriminant analysis comparing the two classes of tissue (right).

The greatest reductions in reflectance occurred at 540nm (green) and 760nm. Correspondingly the discriminate analysis had the lowest classification error at these wavelengths and the greatest separation between the two classes of tissue as indicated by the greatest Mahalanobis distance. There is a good possibility that this defect would show up early in the harvest season before storage as a reduced reflectance at 970nm even before it became visible on the skin because of the excess moisture present.

Blister Spot

Blister spot is caused by *pseudomonas syringae pv. papulans* bacteria which is present on both the leaves and fruit during the growing season. Primarily damage is found on the surface of Crispin apples where the spots on the skin begin to show up in late July or early August. The spots originate at the lenticels and turn brown as affected cells die. The reflectance curves show this change in color as well as the light scattering affect for NIR caused by the dead cells with the resulting reduction in surface reflectance (Figure 3). From the discriminant analysis we see that when undamaged tissue reflectance decreased, there was a corresponding decrease in reflectance for blister spot damaged tissue as indicated by the uniform Mahalanobis distances between classes for wavelengths of 500nm-760nm. For wavelengths above 800nm, blister spots gradually faded until they appeared the same as undamaged tissue making classification impossible.

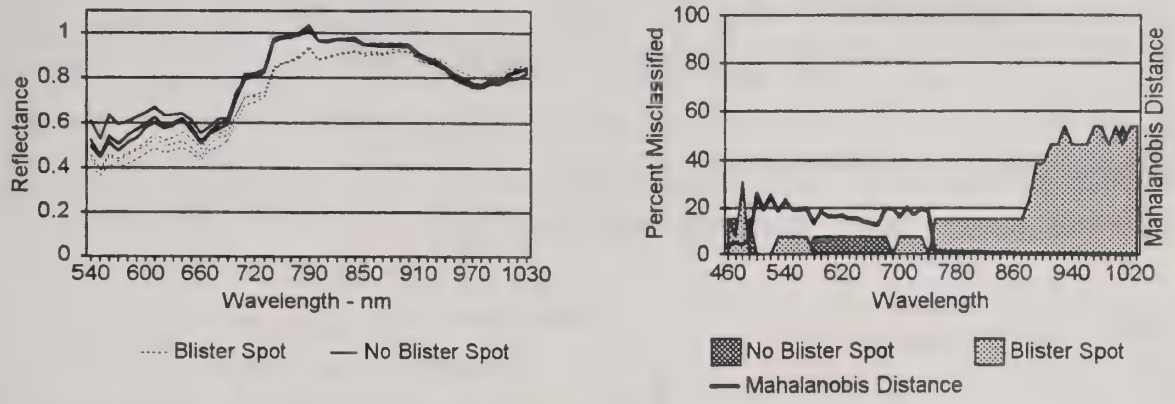

Figure 3. Reflectance of blister spot damaged and undamaged Crispin tissue (left) and the results of the discriminant analysis comparing the two classes of tissue (right).

Hail

Apples tend to outgrow hail damage early in the season with a tendency to become slightly misshapen. Late in the growing season, internal bruising can occur resulting in slightly sunken spots in the skin with bruised tissue underneath which is usually brown in color and sometimes spongy in texture as dehydration occurs. This condition can be confused with cork spot, but usually in cork spot the brown spongy tissue is deeper into the flesh. No difference in reflectance between hail damaged and undamaged tissue was found for the visible wavelengths. From 690nm - 720nm the greatest reduction in reflectance occurs as scattering increases due to the damaged cells. As the wavelength increases past 900nm, reflectance from some hail damaged areas equals or exceeds that of undamaged tissue due to partial dehydration (Figure 4). The discriminant analysis had large classification errors for the visible wavelengths resulting from small reflectance differences compared to the typical reflectance variations for all tissue classes. Large classification errors for the NIR

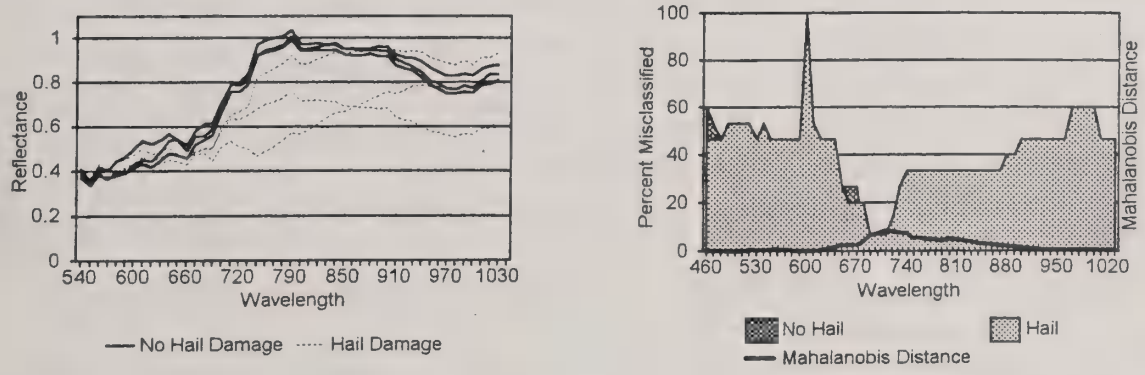

Figure 4. Reflectance of hail damaged and undamaged Red Delicious tissue (left) and the results of the discriminant analysis comparing the two classes of tissue (right).

wavelengths above 760nm occurred because of the wide variation in depth of damage in combination with variable amounts of dehydration. Dehydration is dependent on the length

of time after damage and the depth of damaged cells. The Mahalanobis distance was the greatest for wavelengths 690nm - 740nm with the lowest classification error indicating the largest separation between damaged and undamaged classes (Figure 4).

Cork Spot

The apples may develop one or more spots slightly sunken with a surface that is never brown or black. The corky areas are usually larger than bitter pit and may lie just below

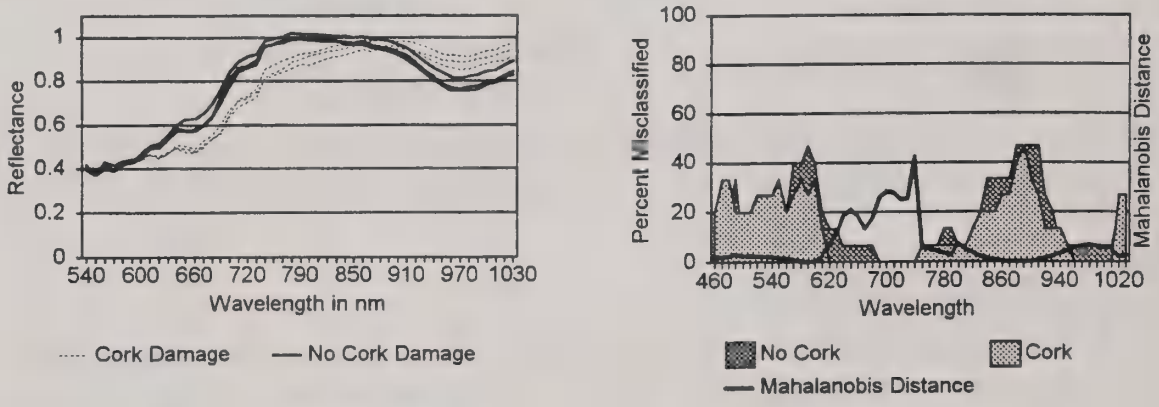

Figure 5. Reflectance of cork damaged and undamaged Red Delicious tissue (left) and the results of the discriminant analysis comparing the two classes of tissue (right).

the skin or halfway to the core. The underlying tissue is brown and spongy showing loss of moisture. Although there is uncertainity to the cause of this damage, an imbalance of boron and calcium may disturb the permeability of the cell walls resulting in the death of certain cells influencing development of cork spot. Reflectance of cork spot on Red Delicious apples decreases in reflectance at 630nm - 820nm. At 860nm the reflectance of cork tissue equals that of undamaged tissue. Above 920nm cork damage has a reflectance greater than undamaged tissue due to the loss of moisture within the cells (Figure 5). Cork spot damage is very similar to hail damage with the exception that the depth of injured cells tends to be consistantly greater in depth. This is verified in the discriminant analysis where the classification error is lower for most wavelengths. Similar to hail damage, the Mahalanobis distance is greatest for the 690nm - 740nm wavelengths but larger in magnitude (Figure 5). The camera system used in this study is not sensitive enough to measure cork damage located deeper in the fruit.

Flyspeck

Flyspeck are superficial specks of fungal growths occurring in groups of 8 to 50 specks or more. The causal fungus, *microthyriella rubi* which is active in cool humid weather develops on mature fruits. The specks can be scrapped off easily although cleaning the total apple surface with automatic equipment successfully can be difficult. The reflectance of fly speck damage decreased for all NIR wavelengths. For both Red and Golden Delicious (not shown), the greatest Mahalanobis distance occurs at 740nm, corresponding with a

classification error of 0 percent for both damaged and undamaged tissue (Figure 6). Golden Delicious exihibited a second Mahalanobis distance peak for wavelengths between 500nm-520nm with a classification error of 0 percent. The classification error above 800nm was higher for Golden Delicious compared to Red Delicious, indicating that the selection of images of reflectance of 740nm would be best for classification of flyspeck damage on both Red and Golden Delicious.

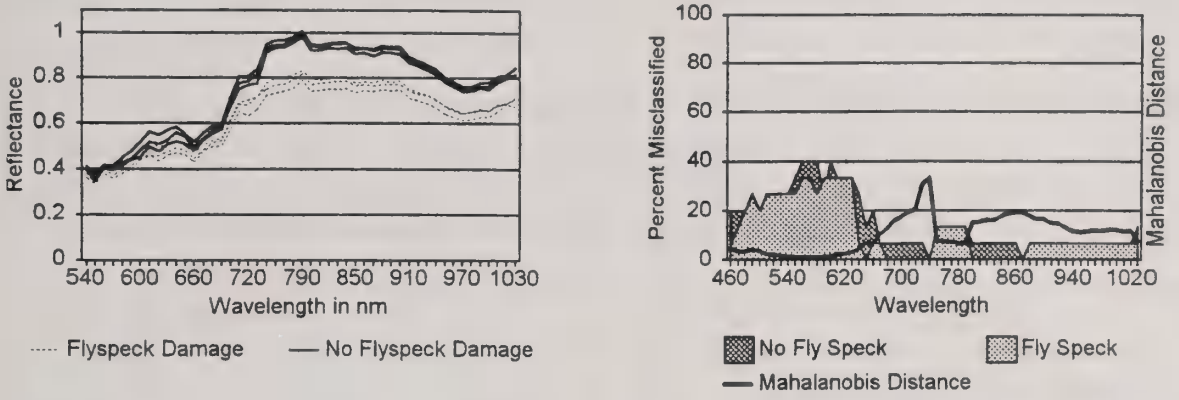

Figure 6. Reflectance of flyspeck damaged and undamaged Red Delicious tissue (left) and the results of the discriminant analysis comparing the two classes of tissue (right).

Brown Rot

Brown rot caused by the fungus *Monilinia fructicola* enters the fruit through either the stem/calyx ends, wounds, cracks, or insect-feeding injuries. It produces circular medium brown spots into the apple flesh that are soft but not mushy. This fungus can be controlled by low temperatures in refrigerated storage unless it has become well established. Once established, large areas can become affected over time. The reflectance is reduced for rot

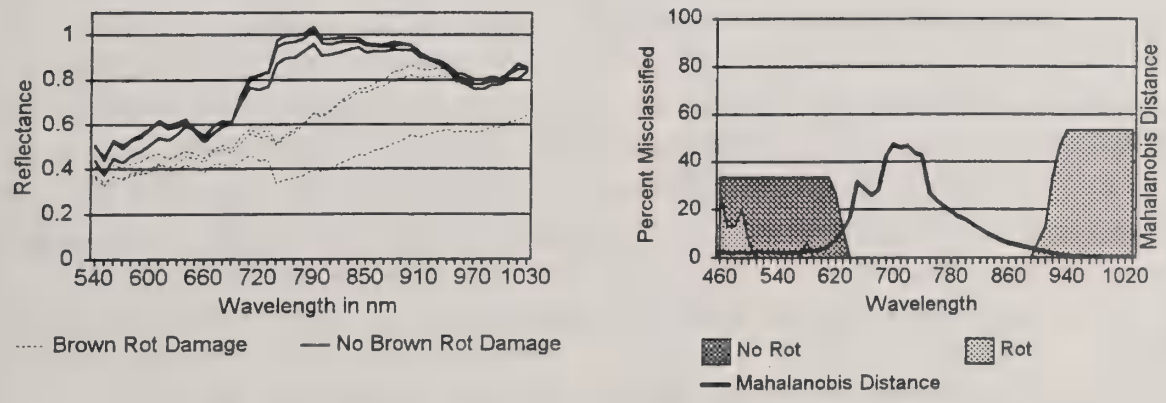

Figure 7. Reflectance of brown rot damaged and undamaged Red Delicious tissue (left) and the results of the discriminant analysis comparing the two classes of tissue (right).

damaged tissue for all of the visible and near-infrared wavelengths tested with the greatest reduction occurring between wavelengths 700nm - 800nm. This corresponds with the greatest distance between between the two classes, damaged and undamaged tissue, as indicated by the largest mahalanobis distances and lowest classification errors for this range of wavelengths (Figure 7). As the wavelength increased beyond 930nm, some rot damaged tissue looked identical to undamaged tissue while in other cases the damage was severe enough to cause release of cellular fliud further decreasing reflectance.

Scab

Infections of the fungus *venturia inaequalis* is spread to new fruit and leaves during rainy periods in the spring. Cool moist weather conditions can further infect fruit any time in the growing season. Irregularly circular scab lesions first appear and become larger turning an olive green or brown in color. Highly infected apples can become misshapen. Scab injury

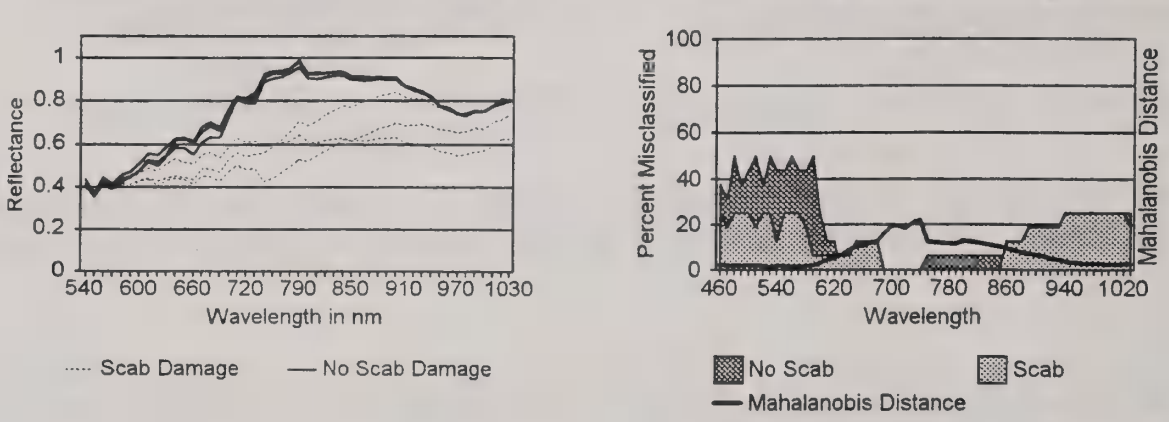

Figure 8. Reflectance of scab damaged and undamaged Red Delicious tissue (left) and the results of the discriminant analysis comparing the two classes of tissue (right).

reduced reflectance from 600nm to 930nm. The greatest class separation occurred between 700nm-750nm as indicated by the greatest values of Mahalanobis distance and with classification errors of 0 percent (Figure 8). Some of the scab areas on the Red Delicious disappeared above 940nm and could not be discerned from undamaged tissue. Reflectance of more severe scab damage on McIntosh (not shown) had a much higher Mahalanobis distance value of 65 but still peaking at 740nm. Unlike Red Delicious, all increasing wavelengths tested for McIntosh had a 0 percent classification error.

Sooty Blotch

Late-summer rains combined with cooler temperatures are conducive for the fungus, *gloeodes pomigena*, to produce dark granular irregular spots with indefinite outlines varying greatly in size on the skin surface. The blotches are thin fungal crusts which can be removed with scraping or rubbing. In severe cases moisture loss can occur and the spots can become sunken in storage. Reflectance of sooty blotch damage general lowered the reflectance for all wavelengths tested on Golden Delicious apples. However, the largest

Mahalanobis distances between classes occurred for NIR wavelengths of 700nm to880nm. A minimum classification error of 7 percent occurred for these same wavelengths which increased to nearly 30 percent for wavelengths between 920nm and 970nm. The greater classification error for 920nm-970nm may be caused by some spots where moisture loss has occurred increasing the reflectance for these areas back to that of undamaged tissue. The presence overall of a general classification error of 7 to 10 percent can be due to the variable thickness and discoloration of the surface spots (Figure 9). Simular results of reflectance for sooty blotch damaged Empire apples (not shown) also had the largest Mahalanobis distances between classes for 700nm-880nm wavelengths but with 0 percent classification error.

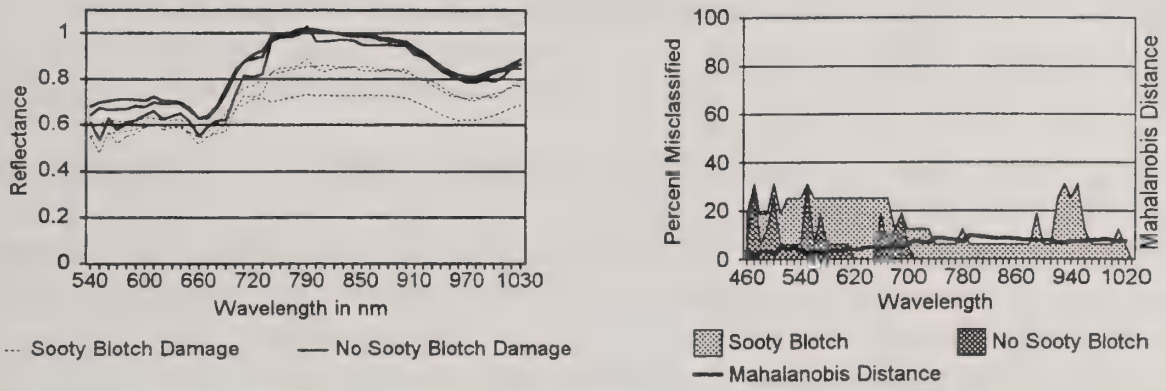

Figure 9. Reflectance of sooty blotch damaged and undamaged Golden Delicious tissue (left) and the results of the discriminant analysis comparing the two classes of tissue (right).

Scald

Scald is a physiological disorder where apples develop superficial browning and death of the skin during and after removal from cold storage. For some varieties the underlying tissue can also be affected. The severity of damage varies from year to year. Reflectance from scald damaged regions on Red Delicious was typically less than undamaged tissue for all wavelengths tested above 600nm. The greatest difference between classes occurrs beyond 880nm at which time the classification error becomes 0 percent. There is a corresponding large increase in the Mahalanobis distance. The wavelengths for this large class difference tends to coincide with the maximum water absorption band at a wavelength of 960nm indicating that the tissue break down may release cellular fluids under the skin (Figure 10).

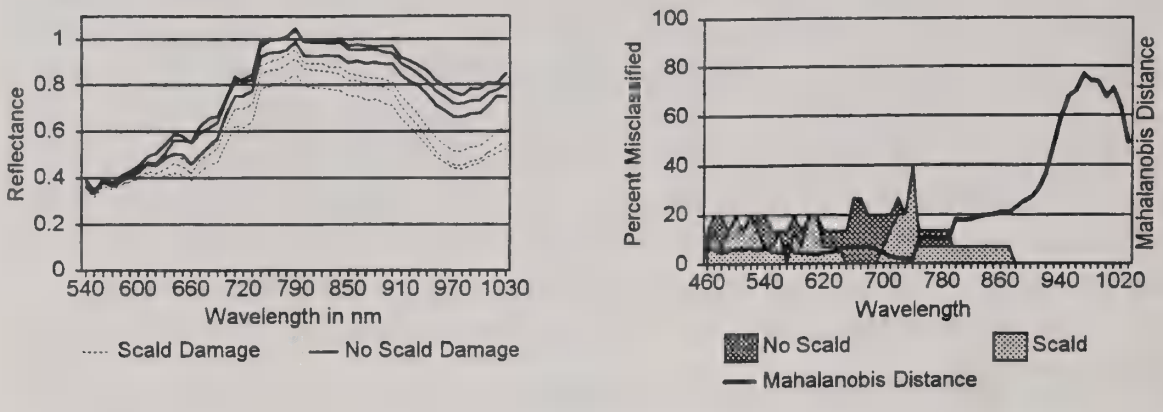

Figure 10. Reflectance of scald damaged and undamaged Red Delicious tissue (left) and the results of the discriminant analysis comparing the two classes of tissue (right).

Bruise

Skin covering bruised areas is normal or slightly discolored but under this skin are raptured cells where the surrounding tissue turns a light brown and is filled with the fluid from the broken cells. If placed in storage, this fluid eventually evaporates through the skin causing the bruised tissue to become dry and spongy. This study looked at fresh bruises that were 24 hours old. The reflectance of bruised tissue was lower than undamaged tissue for all wavelengths tested above 680nm. The classification error was 5 percent or less for all wavelengths above 800nm for Red Delicious (shown) and 850nm for Golden Delicious (not shown). The lowest classification error and greatest Mahalanobis distances occurred at 970nm, similar to scald. This wavelengths again coincide with the maximum water absorption band at 970nm indicating light absorption by the released cellular fluids under the skin (Figure 11).

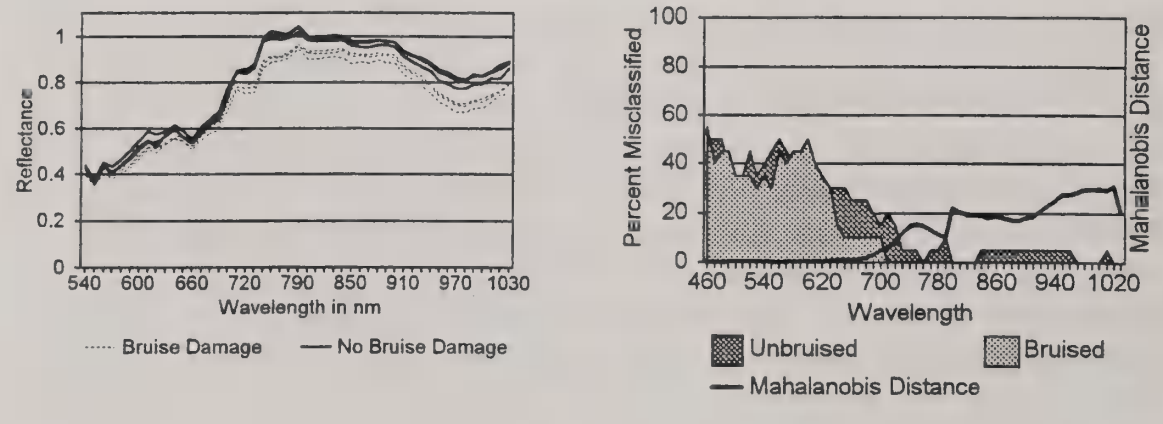

Figure 11. Reflectance of bruise damaged and undamaged Red Delicious tissue (left) and the results of the discriminant analysis comparing the two classes of tissue (right).

Leaf Roller and Codling Moth

The larvae of the red-banded leaf roller consume areas of skin and outer flesh. This results in areas of dark colored dead cells which usually have dryed out. Although codling moth larvae can bore directly into the apple core causing severe damage, usually they eat some skin and outer flesh before they consume a lethal dose of poison and die. The codling moth spots are smaller but more numerous than leaf roller injury. They both have similar reflectance properties and are reported together. The reflectance of leaf roller damage on Golden Delicious (shown) look identical to the codling moth injury on Crispin (not shown). The reflectance is reduced over the visible regions of green to red as well as wavelengths between 700nm - 880nm. The reflectance than increases to that of undamaged tissue and in cases where drying has occurred exceeds undamaged tissue reflectance above the water absorption wavelength of 970nm. Reflectance from damage on Red Delicous (not shown) does not have a usable decrease in reflectance in the visible wavelengths but has very similar reflectance characteristics for NIR. The discriminant analysis showed corresponding large values of Mahalanobis distances and 0 percent classification error for the wavelengths where the reflectance for damaged areas was the lowest (Figure 12).

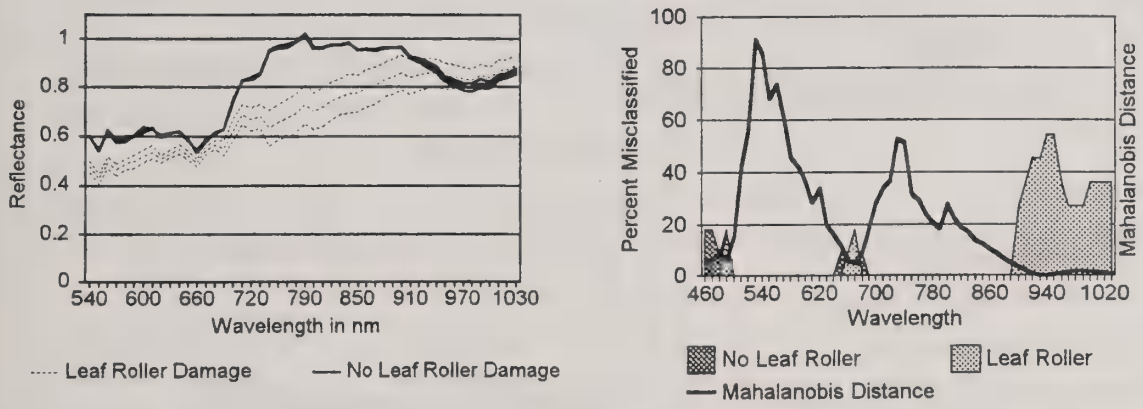

Figure 12. Reflectance of leaf roller damaged and undamaged Golden Delicious tissue (left) and the results of the discriminant analysis comparing the two classes of tissue (right).

Russet

Russeting is a skin damage where areas become light tan in color with a slightly rough texture. It is caused by virus infection, insect stings, early frost damage at time of blossom, and by the fungus commonly refered to as powdery mildew. The damage is usually only skin deep affecting only the appearance and does not affect the eating quality of the fruit. The reflectance from russet damaged Red Delicious tissue increases for wavelengths around 540nm and decrease for wavelengths between 680nm to 740nm. However, the differences are small compared to the apple-to-apple variability resulting in very small

Mahalanobis distances with a large classification error for all wavelengths (Figure 13).The

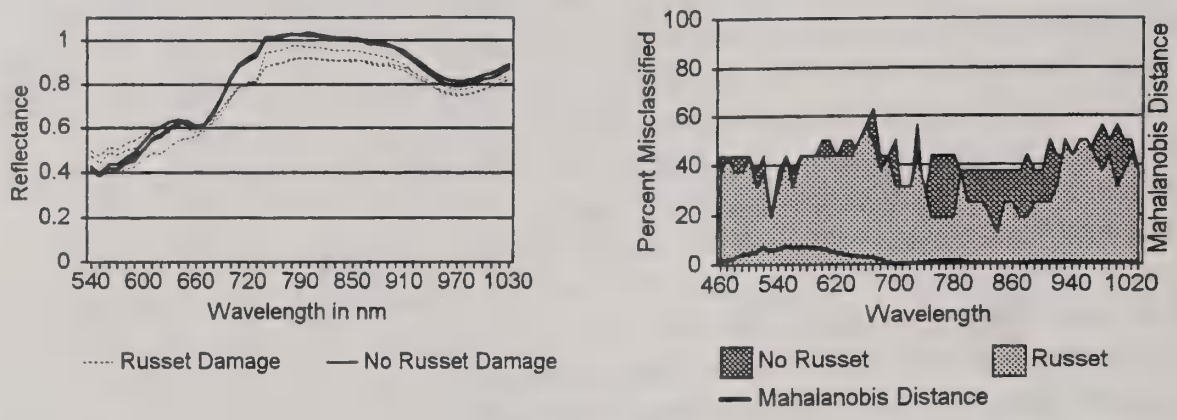

Figure 13. Reflectance of russet damaged and undamaged Red Delicious tissue (left) and the results of the discriminant analysis comparing the two classes of tissue (right).

reflectance from russet damaged Golden Delicious tissue decreases for wavelengths around 540nm and for wavelengths between 680nm to 740nm. Again, the differences are small compared to the apple-to-apple variability resulting in very small Mahalanobis distances with a large classification error for all wavelengths (Figure 14).

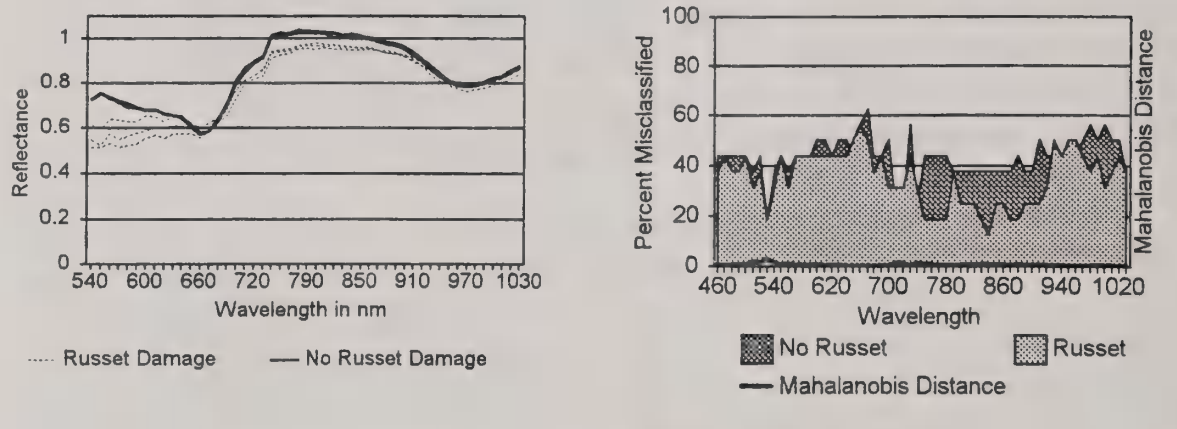

Figure 14. Reflectance of russet damaged and undamaged Golden Delicious tissue (left) and the results of the discriminant analysis comparing the two classes of tissue (right).

If the reflectance for a wavelength of 540nm is used to segment russet, it will require a different algorithm for green/yellow apples versus solid red apples. At 540nm it will be difficult to segment russet damage on green/red cultivars such as Empires or McIntosh because russet damage on solid red apples has a greater reflectance than undamaged tissue compared to solid green/yellow apples where russet damage reflectance is less than undamaged tissue.

Sunburn

Sunburn is a gold or bronze coloring of the skin as a result to exposure to long periods of intense sunlight. None of the cells in the skin are killed and the flesh underneath, if anything, becomes slightly firmer. Apples with this type of injury can rapidly soften in affected areas upon removal from cold storage. Little variation in reflectance is apparent with only minor color variations for the green through red wavelengths. Based on the Mahalanobis distance and classification error, only some areas of sunburn where the red color of the Red Delicious is altered holds any hope for segmentation and detection (Figure 15).

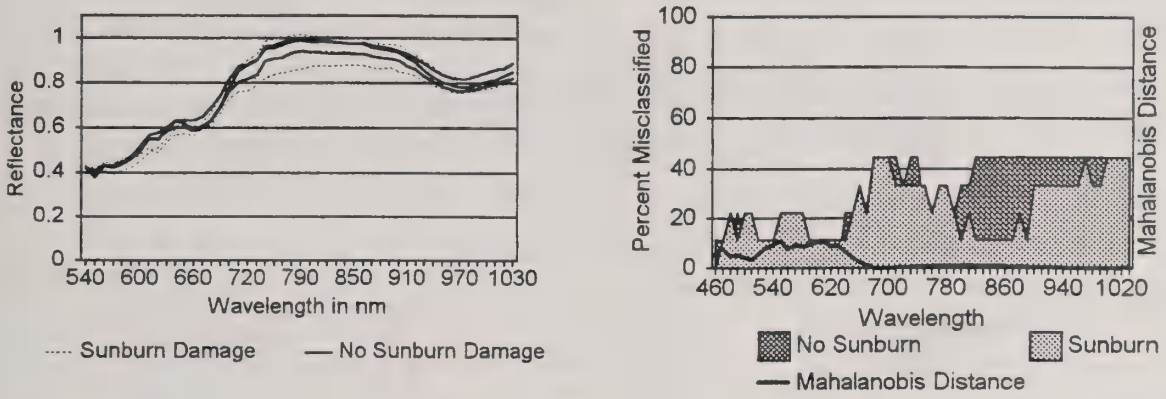

Figure 15. Reflectance of sunburn damaged and undamaged Red Delicious tissue (left) and the results of the discriminant analysis comparing the two classes of tissue (right).

Sting

The reflectance of damage from stinging insects on apples, in this case Red Delicious, is highly dependent on the length of time before harvest that the damage occurred. If early in the growing season, the area takes on a russet like appearance with healing underneath. Later in the season, the affected cells die and dehydrate much like coddling moth or leaf-roller damage. The reflectance for all types of sting damage is reduced between 700nm-790nm. The reflectance beyond 860nm for early russet like damage appears equal to undamaged tissue. Late season damage dehydrates and increases in reflectance beyond 920nm (Figure 16). For wavelengths of 740nm-760nm, classification error was 0 percent and the largest Mahalanobis distance occurred regardless of early or late season damage.

Puncture (new)

Punctures, particularly those caused by stems, are a common form of damage. The breakage of the skin allows bacteria and fungus to enter the fleshy portion of the apple causing rapid decay. Reflectance for all NIR wavelengths decreased for punctured areas caused by stems (Figure 17). A large Mahalanobis distance between classes with a corresponding 0 percent classification error indicates that all that is required for puncture segmentation in NIR is the correct pixel resolution for the small damage size.

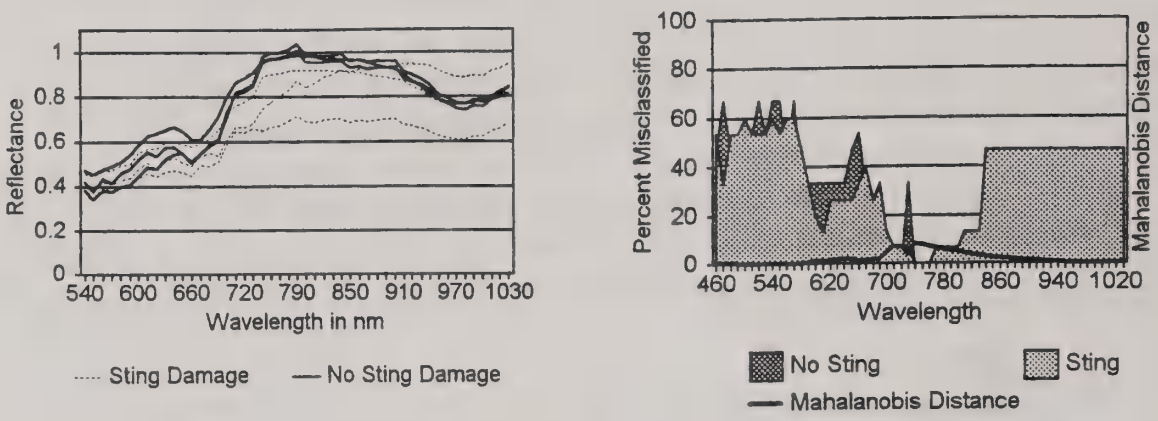

Figure 16. Reflectance of insect sting damaged and undamaged Red Delicious tissue (left) and the results of the discriminant analysis comparing the two classes of tissue (right).

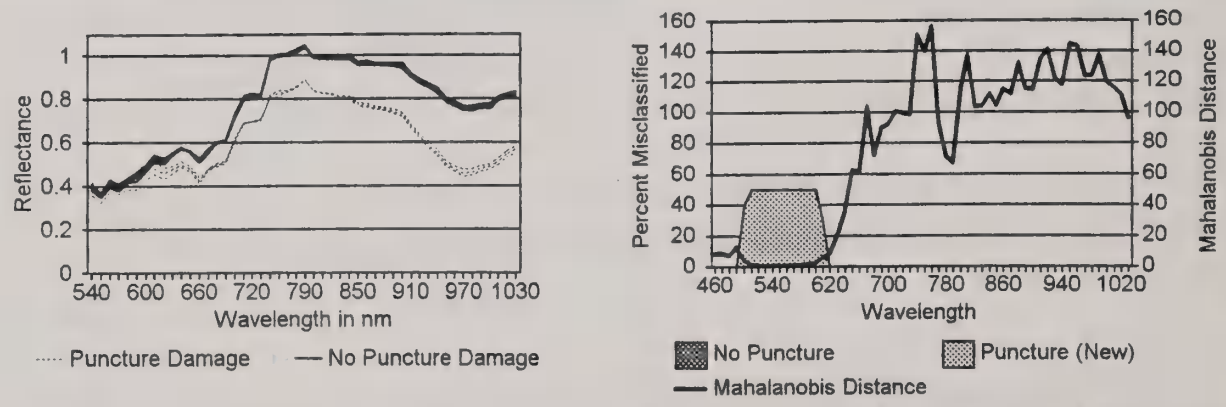

Figure 17. Reflectance of newly puncture damaged and undamaged Red Delicious tissue (left) and the results of the discriminant analysis comparing the two classes of tissue (right).

CONCLUSIONS

For the eighteen defects reported, reflectance images at 4 wavelengths give the greatest contrast between damaged and undamaged tissue. Russet, sunburn, early sting, and blister spot damage showed the greatest Mahalanobis distances for 540nm wavelengths and a low classification error. These types of damage are typically limited to the skin and usually alter color only. The change in reflectance for sunburn and russet where very small and will be difficult to differentiate from undamaged tissue regardless of the wavelength used. Bitter pit, blister spot, hail, cork, fly speck, brown rot, scab, sooty blotch, leaf roller and codling moth damage showed the greatest contrast between damaged and undamaged tissue for reflectance images of 750nm. The defects which showed reflectance responses of greater than undamaged tissue such as cork, bitter pit, leaf roller, stored bruises (not

shown), codling moth, and some early season insect stings occurred for 1030nm reflectance images. This wavelength is an absorption band for water thus if different moisture conditions appear in the damaged area compared to moisture conditions for undamaged tissue, it would be a useful wavelength for defect segmentation. Finally, scald and new bruising had greatly reduced reflectance for damaged compared to undamaged areas at 970nm. This is due to a combination of scattering due to the ruptured cells in combination with the absorption due to the fluid released from the ruptured cells.

Specific narrow and broad bands of wavelengths of light have been defined by discriminant analysis where the greatest contrast between classes of tissue in apple images can be expected for a number of different types of damage and different cultivars. However, this is only part of the information required for developing an electronic sorting system capable of detecting many kinds of damage and identifying each one from each other. This process of identification will require inclusion of pattern recognition as well as reflectance information and an algorithm approach allowing training to handle the wide range of defect types all on many different cultivars. The data presented in this report represents only the first part of the process.

REFERENCES

Bittner, D. R. and K. H. Norris. 1968. "Optical Properties of Selected Fruit vs Maturity". *Transactions of the ASAE* 11(4):534-536.

Brown, G. K., L. J. Segerlind and R. Summit. 1974. "Near-Infrared Reflectance of Bruised Apples". *Transactions of the ASAE* 17(1):17-19.

Graf, G. L. 1982. "Automatic Detection of Surface Blemishes on Apples Using Digital Image Processing". *Ph. D. thesis*. Cornell University, Ithaca, NY 267p.

Fuzzen, D. R. 1981. "Parameters for Automatic Bruise Detection in Apples". *M. S. Thesis*, University of Guelph.

Ingle, M. and J. F. Hyde. 1968. "The Effect of Bruising on Discoloration and Concentration of Phenolic Compounds in Apple Tissue". *Proc. Amer. Soc. Hort. Sci.* 93:738-745.

Lott, Richard V. 1943. "Some Spectral Curves of Maturing Apples". *Proc. Amer. Soc. Hort. Sci.* 43:59-62.

Pen, C. L., W. K. Bilanski and D. R. Fuzzen. 1985. "Classification Analysis of Good and Bruised Peeled Apple Tissue Using Optical Reflectance". *Transactions of the ASAE* 18:(1):326-330.

Pierson, C. F., M. J. Ceponis, and L. P. McColloch, 1971. *Marketing Diseases of Apples, Pears, and Quinces*, Agricultural Handbook No. 376, Agricultural Research Service, United States Department of Agriculture, Washington, D.C.

Reid, W. S. 1976. "Optical Detection for Skin, Bruise Flesh, Stem, Calyx". *Journal of Agric. Engng. Res.* 21(3):291-295.

Rehkugler, G. E. and J. A. Throop. 1986. "Apple Sorting with Machine Vision". *Transactions of the ASAE* 29(5):1388-1397.

Rehkugler, G. E. and J. A. Throop. 1989. "Image Processing Algorithm for Apple Defect Detection". *Transactions of the ASAE* 32(1):267-272.

Taylor, R. W. 1985. Automated detection of apple bruises. *M. S. thesis*, Cornell University, Ithaca, NY.

Throop, J. A. and G. E. Rehkugler. 1988. "Image Processing System for Detecting Bruises on Fruit". *U. S. Patent No. 4741042*, Issued Apr. 26, 1988.

Upchurch, B. L., H. A. Affeldt, W. R. Hruschka, K. H. Norris, and J. A. Throop. 1990. "Spectrophotometric Study of Bruises on Whole Red Delicious Apples". *Transactions of the ASAE* 33(2):585-589.

Upchurch, B. L., H. A. Affeldt, W. R. Hruschka, K. H. Norris, and J. A. Throop. 1991. "Optical Detection of Bruises and Early Frost Damage on Apples". *Transactions of the ASAE* 34(3):1004-1009.

Woolley, J. T. 1971. "Reflectance and Transmittance of Light by Leaves". *Plant Physiol.* 47:656-662.

ELSEVIER

Postharvest Biology and Technology 14 (1998) 11–20

Postharvest Biology and Technology

Pattern recognition models for spectral reflectance evaluation of apple blemishes

W.M. Miller [a,*], J.A. Throop [b], B.L. Upchurch [c]

[a] *University of Florida, IFAS, Citrus Research and Education Center, 700 Experiment Station Road, Lake Alfred, FL 33850-2299, USA*

[b] *Cornell University, Room 79, Riley-Robb Hall, Ithaca, NY 14853, USA*

[c] *Union Camp, PO Box 1391, Savannah, GA 31402, USA*

Received 16 December 1997; accepted 25 April 1998

Abstract

Surface blemishes of various apple varieties were analyzed by their reflectance characteristics between 460 and 1130 nm. Normalized reflectance data were collected at 10 nm increments with liquid crystal tunable filters. Data were utilized as input values for various pattern recognition models specifically multi-layer back propagation, unimodal Gaussian, K-nearest neighbor and nearest cluster algorithms. Partitioning data into 50:50 training and test sets, correct classification in separating unflawed versus blemished areas ranged from 62 to 96% (Year I) and from 73 to 85% (Year II). The algorithm which yielded the highest correct classification was the multi-layer back propagation but minor variation was found for number of hidden nodes or neural net architecture.

Keywords: Artificial intelligence; Grading; Neural network

1. Introduction

For fresh fruits and vegetables, surfaces blemishes are considered grade-lowering characteristics under USDA grade standards. Such defects may be the result of environmental conditions, insects, pathogens or physiological disorders. In some cases such defects actually may degrade internal quality while, in other instances, the blemished portion is only a cosmetic flaw. For eastern United States apples, four grades are defined ranging from US Extra Fancy to US Utility (USDA, 1976). Some defects, such as russet and sunburn, are observed readily in manual grading, while others, e.g. bruising, are not easily discerned. To eliminate the arduous task of grading and provide a more uniform product, automated

* Corresponding author. Tel.: +1 941 9561151; fax: +1 941 9564631.

0925-5214/98/ - see front matter
PII S0925-5214(98)00023-4

Table 1

Application	MLBP	Bayes	KNN	NC	RBF	DA	MLBP(H)
Target recognition[a]	90.7	92.5	92.7	—	—	—	—
Map feature[b] data	91.2	89.3	91.9	—	—	—	89.3
Handwriting[c]	94.8	—	94.8	—	95.2	—	—
Carrot defect[d]	89.0	81.3	—	—	—	—	—
Potato defect[e]	67.8	—	—	—	—	71.6	—

Bayes, unimodal Gaussian; MLBP(H), Multilayer back propagation (hardware); KNN, k nearest.
[a] Ruck et al. (1989); [b] Daud et al. (1995); [c] Lee (1991); [d] Howarth and Searcy (1991); [e] Deck et al. (1995).

grading via solid-state camera sensing has been advanced (Rehkugler and Throop, 1986; Upchurch et al., 1994; Tao et al., 1995; Guedalia, 1997). Also, other sensors such as X-ray (Schatzki et al., 1997; Shahin and Tollner, 1997) and infrared sensing (Moons et al., 1997) have been proposed for detection of surface flaws and internal quality.

In conjunction with sensor technologies, classification strategies have been advanced. An early treatise on the subject was presented by Duda and Hart (1973). Their work centered on Bayesian decision theory and non-parametric techniques such as Parzen windows. More recently, techniques such as neural networks (Rogers and Kabrinsky, 1991; Schalkoff, 1992; Lawrence, 1994) have been proposed and applied to fresh fruit and vegetable machine-based grading (Miller, 1992; Deck et al., 1995; Guedalia, 1997; Heinemann et al., 1997; Miller and Drouillard, 1997). The neural network approaches have been cited for the advantages of knowledge plasticity to changing inputs and outputs, fault tolerance, noise immunity and interpolation/extrapolation capabilities. Comparison of statistical classifiers and neural networks has been undertaken for numerous application as compiled in Table 1. As exhibited in this table, such pattern recognition comparison has been inconclusive in identifying a single technique that exhibits robust superiority with respect to correct classification of multi-feature data sets.

With no clear superiority among classification techniques, software products have been developed to implement various pattern recognition approaches for comparison. Based on reflectance levels at various wavelengths, various pattern recognition models were tested for their capability to segregate surface flaws of apples. Specific objectives were:

1. To develop baseline reflectance data, 460–1130 nm, for typical surface defects found on apples grown in the eastern United States for fresh market consumption;
2. To compare pattern recognition techniques that could be implemented for categorizing specific defects and segregating sound versus defective apples; and
3. To establish optimal wavelength(s) for specific and general defect determination.

2. Materials and methods

During the Fall harvest seasons of 1995 and 1996, various apple varieties were collected from trees at the USDA Appalachian Fruit Research Station, the WVU Kearneysville experimental farm, and from commercial packers. Varieties included in one or both years were: 'Empire', 'Gala', 'Golden Delicious', 'Granny Smith', 'Red Delicious', 'Rome', 'Red Stayman' and 'York'. The defects encountered were: bitter pit, blister, bruise, cork, fly spec, hail damage, insect damage, punctures, rots (reds), russet (reds), scab, scald and sooty blotch. For a given defect, five to ten different areas were scanned as well as an equal number of corresponding unflawed areas. Stem and calyx areas were scanned also since their geometry and resultant shadowing can be interpreted as defects in machine vision analysis (Crowe and Delwiche, 1996).

The two camera/lens and adjustable filter arrangement used to acquire the spectral data has been described by Aneshansley et al. (1997). Two electronic tunable filter systems were used to span the visible, 460–750 nm, and near infra-red spectra, 750–1030 nm. The bandwidth of the visible filter was 20 nm while the near infra-red bandwidth was 35 nm. Utilizing 10 nm steps, 58 selectively filtered images were acquired for each scanned area. All reflectance data were first normalized based on a standard reflectance from either a Teflon sphere or cylinder which exhibited minimal absorption bands over the selected spectra. The 58 normalized reflectance values for a given defect or unblemished area constituted an input data set. All data sets were then normalized by: $\text{Value}_{\text{norm}} = (\text{Value} - \text{Value}_{\text{min}})/(\text{Value}_{\text{max}} - \text{Value}_{\text{min}})$.

The pattern classification was conducted on the normalized data using two software packages (PRW Vers. 2.1; Unica Technologies, Brighton, MA, and NeuroShell2; Ward Systems Group, Frederick, MD). Data were split into training and test sets of equal size. The PRW software offered the versatility of comparing models other than multi-layer back propagation (MLBP) methods and included the unimodal Gaussian (UG), K-nearest neighbor (KNN), and nearest cluster (NC) techniques. For the NeuroShell2 software, testing was extended on classification success to more complex neural network configurations of multiple hidden slabs and a three-layer jump model.

The data were analyzed separately for each season with all defects included, i.e. two category results of either sound or defect classification. Nine-hundred and eighty-two, and 1316 scanned spectra were available for the first and second seasons, respectively. Further analysis of the data was performed to classify each defect by its discrete reflectance signature. Also, contribution factors were extracted to compare with a separate assessment via discriminant analysis (Aneshansley et al., 1997). For pattern recognition technique comparison of the overall data, the following test conditions were selected: multi-layer back propagation (MLBP @ 10, 20, 30, 40 and 50 hidden nodes), nearest cluster (NC @ 1, 5, 10, 25 and 50 clusters), and K-nearest neighbor (KNN @ 1, 2, 5, 10 and 25 neighbors). For comparison to more traditional Bayesian modeling, an UG was included. General protocol in selection of numbered clusters, nearest neighbors, etc., and their interactions with other model variables, is detailed by Kennedy et al., 1995. Typical epoch process time on a 75-MHZ Pentium™ computer was approximately 1.1 s for the 50 hidden node model coupled to 58 inputs, two outputs for the MLBP. The contribution factors or weights, were extracted for each of the MLBP models. A cross correlation was performed among the contribution factors for each season's MLBP models.

3. Results and discussion

The train and test approach is commonly implemented in classification assessment. Some researchers have suggested a third evaluation through a validation set to overcome bias and over-learning (Kennedy et al., 1995). However, as this study was directed at model comparisons, it was decided that a test/train breakdown was adequate. All data were normalized twice; first in instrumentation calibration and then in model preprocessing.

In an overall approach, all defects, including bruising, were categorized together. Therefore, the neural network outputs were binary with 0 for sound or 1 as defect. Fifty-eight inputs, representing the reflectance data, were used for both the 1995 and 1996 apple data. Random number generation was used to develop the test and train data sets. Default transfer functions for MLBP were hyperbolic for PRW and logistic for NeuroShell2. Tables 1 and 2 present the data for the two seasons. Both training and test data were tabulated with respect to percent correct classification. Correctly classified objects were denoted as either acceptable as acceptable (A/A) or reject as reject (R/R). Error types, i.e. (A/R) acceptable as reject (true state) or (R/A) reject as acceptable (true state), were extracted. It would be anticipated that a singular NC model would degenerate to 50% and that the KNN (1) model would yield 100% in training. The first constitutes an equal probability selection, the latter self identification.

Table 2
Test results of pattern recognition models, 1995 apple data

Technique	Variable	Overall training		Overall test		Training				Test				% Change Trn-Tst
		% Correct avg.	% Correct std. dev.	% Correct avg.[a]	% Correct std. dev.	A/A[b] % correct	R/R[b] % correct	R/A[b] % error	A/R[b] % error	A/A % correct	R/R % correct	R/A % error	A/R % error	
MLBP	10	97.0	1.7	96.2[a]	0.6	97.8	96.1	2.2	3.9	97.8	94.5	2.2	5.5	0.8
MLBP	20	96.2	1.0	95.5[a]	0.5	98.0	94.5	2.0	5.5	97.9	93.1	2.1	6.9	0.7
MLBP	30	95.8	1.8	94.2[a]	1.0	97.7	94.0	2.3	6.0	95.7	92.6	4.3	7.4	1.7
MLBP	40	95.0	1.2	94.5[a]	0.9	98.8	91.2	1.2	8.8	98.1	90.7	1.9	9.3	0.5
MLBP	50	96.7	0.4	95.2[a]	0.8	98.7	94.7	1.3	5.3	97.6	92.6	2.4	7.4	1.5
UG	—	91.0	0.4	91.7[a]	0.5	99.6	82.6	0.4	17.4	99.4	83.7	0.6	16.3	−0.8
NC	1	50.9	0.6	49.1[c]	0.8	33.3	66.7	66.7	33.3	33.3	66.7	66.7	33.3	3.5
NC	5	78.7	0.8	78.5[b]	0.8	99.7	58.2	0.3	41.8	99.9	56.4	0.1	43.6	0.2
NC	10	62.9	16.6	61.6[c]	18.4	30.4	93.9	69.6	6.1	30.9	94.2	69.1	5.8	2.0
NC	25	89.2	1.9	88.1[a,b]	3.3	96.0	82.6	4.0	17.4	95.0	81.0	5.0	19.0	1.3
NC	50	92.1	1.2	89.3[a]	1.5	95.2	88.9	4.8	11.1	93.9	84.6	6.1	15.4	3.0
KNN	1	100.0	0.0	95.7[a]	0.7	100.0	100.0	0.0	0.0	96.1	95.2	3.9	4.8	4.3
KNN	2	97.8	0.4	93.8[a]	1.0	100.0	95.7	0.0	4.3	97.9	89.6	2.1	10.4	4.1
KNN	5	97.2	0.8	95.0[a]	0.9	98.0	96.5	2.0	3.5	95.7	94.3	4.3	5.7	2.3
KNN	10	94.0	0.8	93.6[a]	0.5	98.3	89.9	1.7	10.1	97.9	89.2	2.1	10.8	0.4
KNN	25	92.1	1.0	91.9[a]	0.2	99.1	85.3	0.9	14.7	99.0	84.5	1.0	15.5	0.2

A/A, acceptable as acceptable; R/R, reject as reject; R/A, reject as acceptable (true state); A/R, acceptable as reject (true state).
[a] Means with same letter are not significantly different at 5% level, Duncan's test. NC (1) not included.

Table 3
Test results of pattern recognition models, 1996 apple data

Technique	Variable	Overall training		Overall test		Training				Test				% Change Trn-Tst
		% Correct avg.	% Correct std. dev.	% Correct avg.[a]	% Correct std. dev.	A/A[b] % correct	R/R[b] % correct	R/A[b] % error	A/R[b] % error	A/A % correct	R/R % correct	R/A % error	A/R % error	
MLBP	10	85.9	0.2	83.6[a,b]	1.6	93.2	78.5	6.8	21.5	92.5	75.1	7.5	24.9	2.7
MLBP	20	86.8	1.8	85.1[a]	1.7	92.3	81.2	7.7	18.8	91.6	78.8	8.4	21.2	1.9
MLBP	30	87.0	1.2	83.8[a,b]	0.5	92.4	81.5	7.6	18.5	91.1	76.9	8.9	23.1	3.7
MLBP	40	86.4	2.8	83.9[a,b]	0.1	90.9	81.8	9.1	18.2	91.4	76.8	8.6	23.2	2.9
MLBP	50	84.8	1.1	83.3[a,b]	0.6	91.7	77.8	8.3	22.2	92.2	74.8	7.8	25.2	1.7
UG	—	78.7	1.3	77.9[c,d]	2.3	95.9	61.1	4.1	38.9	97.5	58.9	2.5	41.1	1.1
NC	1	51.4	0.4	48.6	0.4	66.7	33.3	33.3	66.7	66.7	33.3	33.3	66.7	5.5
NC	5	74.1	1.3	73.0[c]	1.5	97.6	50.1	2.4	49.9	98.3	48.4	1.7	51.6	1.4
NC	10	74.9	1.3	73.5[c]	1.1	91.5	57.8	8.5	42.2	91.5	56.2	8.5	43.8	1.9
NC	25	76.6	0.5	74.5[d,e]	2.1	90.0	62.6	10.0	37.4	89.5	60.1	10.5	39.9	2.8
NC	50	78.1	1.9	75.0[d,e]	0.6	90.1	65.6	9.9	34.4	89.9	60.6	10.1	39.4	3.8
KNN	1	100.0	0.0	81.7[a,b]	1.6	100.0	100.0	0.0	0.0	85.4	78.3	14.6	21.7	18.3
KNN	2	90.2	1.6	80.5[b,c]	2.0	100.0	80.2	0.0	19.8	94.8	66.7	5.2	33.3	10.7
KNN	5	89.5	1.0	83.1[a,b]	2.0	93.4	85.4	6.6	14.6	90.0	76.6	10.0	23.4	7.1
KNN	10	86.1	1.2	81.5[a,b,c]	2.9	95.2	76.8	4.8	23.2	93.4	70.1	6.6	29.9	5.3
KNN	25	83.7	1.1	80.1[b,c]	1.8	94.2	72.8	5.8	27.2	92.7	68.1	7.3	31.9	4.2

A/A, acceptable as acceptable; R/R, reject as reject; R/A, reject as acceptable (true state); A/R, acceptable as reject (true state).
[a] Means with same letter are not significantly different at 5% level, Duncan's test. NC (1) not included.

Table 4
Percent correct classification levels when classified for specific defect

Model	1995 test						1996 test					
	Training			Test			Training			Test		
	A/A	R/R	CR	A/A	R/R	CR	A/A	R/R	CR	A/A	R/R	CR
MLBP (10)	98.8	95.9	70.9	95.4	94.1	62.1	98.3	78.2	41.6	96.8	75.5	29.6
NC (10)	92.9	60.5	21.5	91.9	68.0	21.9	98.3	64.6	17.7	96.4	63.4	11.6
KNN (10)	98.8	95.9	70.9	98.3	81.3	42.0	97.0	70.0	30.5	96.8	69.4	25.0
UG	91.2	92.4	69.2	93.1	91.1	68.3	98.3	71.2	42.0	98.0	76.5	35.2

A/A, Acceptable as acceptable; CR, Correct category within reject; R/R, Reject as reject.

Since the singular NC model provides no training potential, it was not included in statistical comparisons that follow.

3.1. 1995 apple data

Means from the test averages were compared through a Duncan's multiple range analysis tests with significant difference among test means indicated in Table 2. The NC models with five and ten clusters did not perform as well as the other pattern recognition models. With these NC models of lower performance, it was not clear why the error rates were higher since the type of errors, R/A and A/R, were reversed between these two NC model results. The degradation from training to test results, noted as % change of the last column, was small with values greater than 4% for only two of the KNN models.

Input data were also presented with each defect representing a separate class. Each type of model was tested in this approach (Table 4). Percent of fruit in the correct reject class (CR) was identified. The highest CR value was 68.3% for the UG model. However, other than the NC (10) model, a high percent of the fruit was still segregated correctly with respect to a two-category criteria of accept/reject.

3.2. 1996 apple data

Means from the test averages were compared again through a Duncan's multiple range analysis and differences between means indicated superior performance of all MLBP models and KNN models of one, five and ten nearest neighbors (Table 3). The degradation levels between training and test results were higher than in the 1995 analysis. These % change degradation figures provide some indication of model robustness. Percent change in KNN of one and two nearest neighbor was greater than 10% while the MLBP, NC and UG models had the smallest degradation ranging from 1.1 to 5.5%. In general, all models showed poorer performance in the second season and may be attributed to a larger data set with more diverse defects included. The CR analysis (Table 4) indicated a drop in correct identification of specific defects. CR levels were less than 60% in all cases and were approximately 50% of those obtained in the 1995 test model results. Overall correct classification remained high, as with the 1995 data, with A/A values ranging from 96.4 to 98.0% and R/R values were from 63.4 to 76.5%.

3.3. Neural network comparisons

An area of current research interest is the configuration, i.e. structural interconnection, of the neural network for back propagation. Architectures with advanced feedback or feedforward elements include the Jordan Elman and jump connection models as well as multiple hidden layers with varied transfer functions. In this research, the jump step approach and the MLBP with different transfer functions in the hidden layer were assessed. In the latter, three hidden slabs were structured with either 7 or 17 nodes per

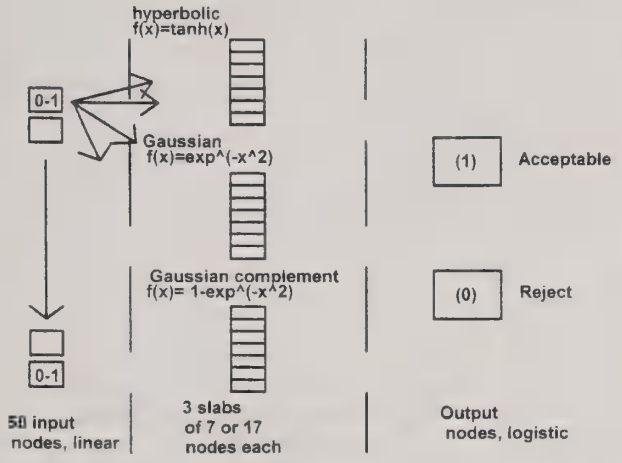

Fig. 1. General configuration for MLBP with three transfer function in hidden node layer.

slab. Transfer functions were hyperbolic tangent, Gaussian and Gaussian complement (Fig. 1). In the jump step configuration, the inputs were passed both to the hidden layer and to the output layer (Fig. 2). The comparative results based on the 1995 and 1996 apple data are presented in Table 5. No superiority was found for the more complex models evaluated. A statistically significant difference, at the 5% level, was found between years and the standard MLBP neural net models. The latter occurred even though the learning rate and momentum variables were identical. Overall correct classification in testing ranged from 92.3 to 96.2% (1995 data) and from

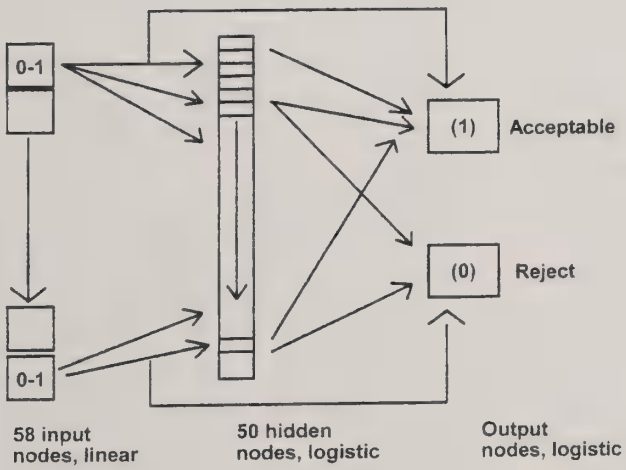

Fig. 2. General configuration for MLBP set for a jump step connection.

Table 5
Test comparison results for various MLBP models

Technique	Variable	1995	1996
MLBP (PRW)	10	96.2	83.6
	20	95.5	85.1
	30	94.2	83.8
	40	94.5	83.9
	50	95.2	83.3
MLBP (WARD)	10	93.0	82.5
	20	93.0	83.7
	30	92.8	83.6
	40	92.6	82.7
	50	92.3	83.6
MLBP[a] (variable transfer function)	3@7	93.2	89.4
	3@17	94.0	88.4
MLBP[a] (jump)	50		88.8

[a] Ward Systems software.

82.5 to 89.4% (1996 data) among the MLBP standard and advanced models.

3.4. Contribution factors

An important aspect of this study was to ascertain if certain wavelengths could be selected for bruise and blemish defect of apple. An obvious value to extract for that analysis would be contribution weights associated with the input values. These factors represent a normalized contribution with respect to the input variables. In this study, the inputs were the 58 reflectance values taken at 10 nm increments. These factors using minimum, maximum, and smoothed average results for the seven neural net models versus scanned spectra were plotted in Figs. 3 and 4 for the apple data of 1995 and 1996. Peaks occurred at 740, 600 and 530 for the first season, and 710 and 460 in the second season. The bandpass from 690 to 750 provided the largest contribution factors. This spectral segment was in the overlap between visible and near infra-red, and indicated the importance of scanning beyond the visible spectrum. A cross correlation between the models indicated the contribution factors was consistent between the models for each year (Table 6). Values for r ranged from 0.78 to 0.96. An overall cross corre-

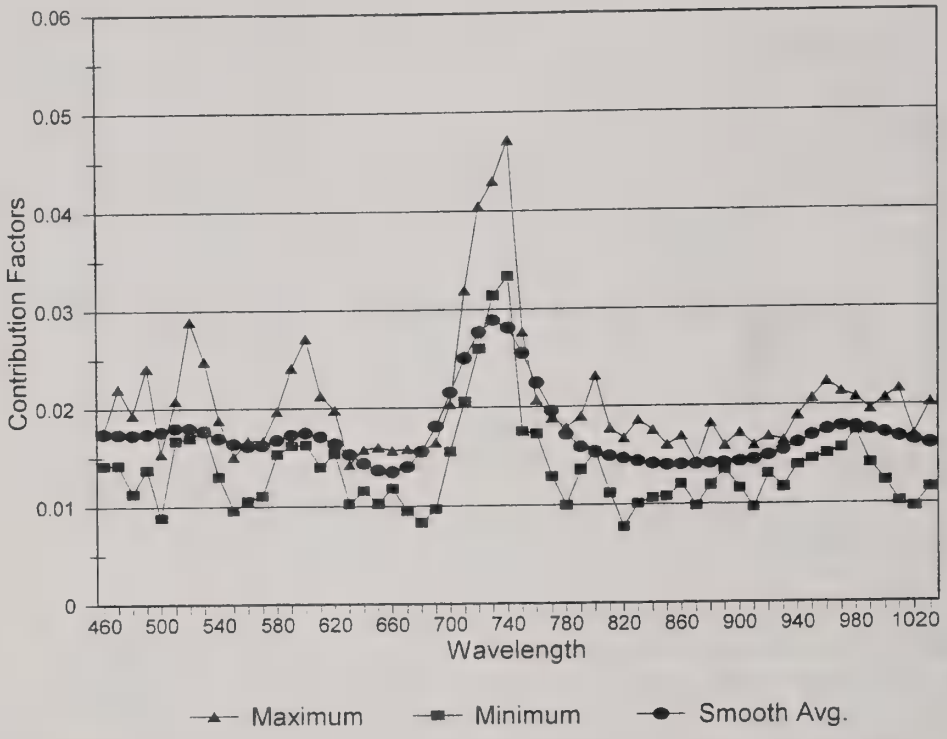

Fig. 3. Contribution factors for each input value for various MLBP models, 1995 data.

lation for both years was statistically significant but not as high, $r = 0.59$.

3.5. Comparative analysis

Utilizing another data analysis procedure, discriminant analysis (Aneshansley et al., 1997), a comparison was made for specific defect results of the neural network models. For an individual defect, contribution factors were determined and compared the Mahalanobis distance of the discriminant approach. Again, a smoothing function was applied to the contribution factors versus wavelength data. The apple scald defect was selected for analysis as it's peak Mahalanobis distance was greater than 900 nm, beyond the principal peak at 690–750 nm found for most apple defects (Figs. 3 and 4). The correlation value between a smoothed contribution factor and the Mahalanobis distance associated with each wavelength was 0.92. This high correlation indicated the need for either data smoothing or bootstrap implementation as individual neural network analyses, at 10–50 hidden nodes, had much lower values ranging from 0.16 to 0.45. The high correlation coefficient provided confidence that the neural networks could function on the more limited data sets of an individual defect.

4. Conclusion

The optical analysis system, configured by using two CCD black and white cameras with electrically tunable filters to scan visible and near infrared, provided discrete reflectance curves to analyze defects found in eastern United States apples. It was necessary to normalize the reflectance values of the apples based on a Teflon standard. Utilizing both sound and defect areas from various grade lowering defects, a database of reflectance values was developed at 10 nm increments from 460 to 1130 nm. These reflectance values were used in pattern recognition models based on MLBP, NC, KNN and UG models. With a more limited data set, all models exhibited higher success rates in classification of the 1995 season's data. Overall, the MLBP pro-

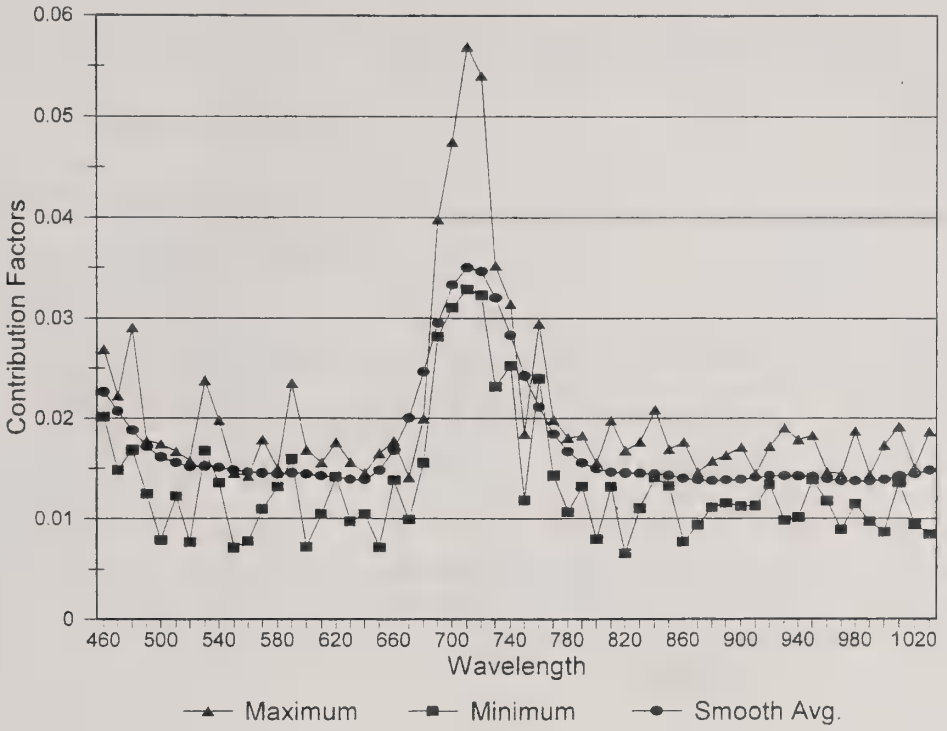

Fig. 4. Contribution factors for each input value for various MLBP models, 1996 data.

vided the highest correct classification rates, ranging from 83 to 85% for the 1996 data and from 94 to 96% for the 1995 data. The more complex neural network models of jump connections and multiple transfer functions in the hidden layer did not provide higher success rates. Contribution

Table 6
Cross correlation value (r) for contribution factors based on seven MLBP models, 460–1030 wavelength

Model	MLBP (10)	MLBP (20)	MLBP (30)	MLBP (40)	MLBP (50)	MLBP (3@7)	MLBP (3@17)
Apple95 data							
MLBP (10)	1.00						
MLBP (20)	0.89	1.00					
MLBP (30)	0.82	0.83	1.00				
MLBP (40)	0.89	0.91	0.81	1.00			
MLBP (50)	0.86	0.89	0.78	0.91	1.00		
MLBP (3@7)	0.81	0.79	0.83	0.87	0.83	1.00	
MLBP (3@17)	0.84	0.87	0.81	0.88	0.85	0.84	1.00
Apple96 data							
MLBP (10)	1.00						
MLBP (20)	0.95	1.00					
MLBP (30)	0.92	0.94	1.00				
MLBP (40)	0.95	0.96	0.93	1.00			
MLBP (50)	0.92	0.94	0.90	0.96	1.00		
MLBP (3@7)	0.88	0.91	0.91	0.92	0.90	1.00	
MLBP (3@17)	0.91	0.93	0.91	0.94	0.93	0.89	1.00

Overall cross correlation results of the averages of Apple95 and Apple96 data: 0.59.

factors, established from the MLBP models, indicated the most significant wavelengths were in the 690–750 nm range and 530 nm when considering data from both seasons.

Acknowledgements

W.M. Miller would like to recognize the financial support from the University of Florida's Faculty Development Program and the USDA-ARS to undertake this study. William Anger, Engineering Technician, USDA-AFRS, contributed significantly to the instrumentation and data acquisition portions of the program. Greg Drouillard, Sr. Engr. Tech., University of Florida is acknowledged for his computer work in data reduction and analysis. Florida Agricultural Experiment Station Journal Series No. A-00384.

References

Aneshansley, D.J., Throop, J.A., Upchurch, B.L., 1997. Reflectance spectra of surface defects for apples. In: M. Salius (Ed.), Sensors for Nondestructive Testing, measuring the Quality of Fresh Fruits and Vegetables. NRAES-97. NRAES, Ithaca, NY, pp. 143–160.

Crowe, T.G., Delwiche, M.J., 1996. Real-time defect detection in fruit-part II: an algorithm and performance of a prototype system. Trans. ASAE 39 (6), 2309–2317.

Daud, T., Duong, T., Tran, M., Langenbacher, H., Thakoor, A., 1995. High resolution synaptic weights and hardware-in-the-loop learning. Vol. 2424. SPIE—International Society for Optical Engineering; Bellingham, WA. pp. 489–500.

Deck, S.H., Morrow, C.T., Heinemann, P.H., Sommer, H.J., 1995. Comparison of a neural network and traditional classifier for machine vision inspection of potatoes. Appl. Engr. Agric. 11 (2), 319–326.

Duda, R.O., Hart, P.E., 1973. Pattern Classification and Scene Analysis. Wiley, New York.

Guedalia, I.A., 1997. Visual based quality sorting of fruit. In: M. Salius (Ed.), Sensors for Nondestructive Testing, Measuring the Quality of Fresh Fruits and Vegetables. NRAES-97. NRAES, Ithaca, NY, pp. 232–238.

Heinemann, P.H., Sommer, H.J., Morrow, C.T., Marrazzo, W.N., Crassweller, R.M., He, B., 1997. Machine vision based station for grading of "Golden Delicious" apples. In: Sensors for Nondestructive Testing, Measuring the Quality of Fresh Fruits and Vegetables. NRAES-97. NRAES, Ithaca, NY, pp. 239–248.

Howarth, M.S., Searcy, S.W., 1991. Comparison of Bayesian and Neural Network Classifiers for Grading Carrots. ASAE Publ. 7012-91. ASAE, St. Joseph, MI.

Kennedy, R., Lee, Y., Reed, C., Roy, B.V., 1995. Solving Pattern Recognition Problems. Unica Technologies, Brighton, MA.

Lawrence, J., 1994. Introduction to Neural Networks Design, Theory and Applications. California Scientific Software, Nevada City, CA.

Lee, Y., 1991. Handwritten digit recognition using K nearest-neighbor, radial-basis function, and backpropagation neural networks. Massachusetts Institute of Technology. Neural Computation 3, 440–449.

Miller, W.M., 1992. Classification analysis of Florida grapefruit based on shape parameters. In: G.K. Brown and Y. Sarig (Eds.), Food Processing Automation II. ASAE Publ. 02-92. ASAE, St. Joseph, MI, pp. 339–347.

Miller, W.M., Drouillard, G.P., 1997. On-line blemish, color, and shape analysis for Florida citrus. In: M. Salius (Ed.), Sensors for Nondestructive Testing, Measuring the Quality of Fresh Fruits and Vegetables. NRAES-97. NRAES, Ithaca, NY, pp. 249–260.

Moons, E., Dardenne, P., Dubois, A., Sindic, M., 1997. Nondestructive visible and NIR spectroscopy for the determination of internal quality in apple. In: M. Salius (Ed.), Sensors for Nondestructive Testing, Measuring the Quality of Fresh Fruits and Vegetables. NRAES-97. NRAES, Ithaca, NY, pp. 122–132.

Rehkugler, G.E., Throop, J.A., 1986. Apple sorting with machine vision. Trans. ASAE 29 (5), 1388–1397.

Rogers, S.K., Kabrinsky, M., 1991. An Introduction to Biological and Artificial Neural Networks for Pattern Recognition. SPIE, Bellingham, WA.

Ruck, D.W., Rogers, S.K., Kabrinsky, M., 1989. Feature Selection Using a Multilayer Perception. Report of Air Force Inst. Of Technology. Wright–Patterson AFB, OH.

Schalkoff, R.J., 1992. Pattern Recognition: Statistical, Structural and Neural Approaches. Wiley, New York.

Schatzki, T.F., Haff, R.P., Young, R., Can, I., Le, L.-C., Toyofuku, N., 1997. Defect detection in apples by means of x-ray imaging. In: M. Salius (Ed.), Sensors for Nondestructive Testing, Measuring the Quality of Fresh Fruits and Vegetables. NRAES-97. NRAES, Ithaca, NY, pp. 161–171.

Shahin, M.A., Tollner, E.W., 1997. Detection of watercore in apples using x-ray line scans feature extraction and classification. In: Sensors for Nondestructive Testing, Measuring the Quality of Fresh Fruits and Vegetables. NRAES-97. NRAES, Ithaca, NY, pp. 389–400.

Tao, Y., Chance, L., Liu, B., 1995. Full scale fruit vision sorting system design-factors and considerations. In: R. Lacey (Ed.), Food Processing Automation IV. ASAE Publ. 14-95. ASAE, St. Joseph, MI, pp. 14–22.

Upchurch, B.L., Throop, J.A., Aneshansley, D.J., 1994. Influence of time, bruise-type and severity on near-infrared reflectance from apple surfaces for automatic bruise detection. Trans. ASAE 37 (5), 1571–1575.

USDA, 1976. United States Standards for Grades of Apples. US-GPO:1987-201-037:60201/AMS.

Paper No. 976044
An ASAE Meeting Presentation

Inspection of Processed Fruit Before and After Peeling

James A. Throop, Daniel J. Aneshansley

Cornell University, Department of Agricultural and Biological Engineering, Ithaca. NY 14853

Written for presentation at the
1997 ASAE Annual International Meeting
Sponsored by ASAE

Minneapolis Convention Center
Minneapolis. Minnesota
August 10-14. 1997

Summary: Reflectance spectra from apple images with rot. bruise, cracks, codling moth. leaf roller, scab. hail, corking, and bitter pit typical of the type of damage found on apples entering a processing plant were captured every 10nm for wavelengths between 460nm - 1030nm. The Mahalanobis distance was used to identify three wavelength bands (540nm. 740nm. and 1010nm) for segmentation of defects on apples which would normally result in trim waste. Defects segmentation was possible by simple image subtraction.and thresholding. This technique could be used for the inspection of apples entering a processing plant..

Keywords: Apples. Apple Quality, Defects. Defect Detection, Inspection. Image Analysis. Image Processing,

ASAE. 2950 Niles Rd.. St. Joseph. MI 49085-9659 USA
Voice: 616.429.0300 FAX: 616.429.3852 E-Mail: <hq@asae.org>

Acknowledgments: This project is supported in part by USDA Cooperative Agreement 58-1931-5-019 with the ARS-USDA Appalachian Fruit Research Station, Kearneysville, WV, and by the Agricultural Experiment Station at Cornell University with Hatch Regional Project NE179 and Hatch Project 412. We would also like to acknowledge the continued assistance and expertise of Mr. Bill Anger of ARS-USDA Appalachian Fruit Research Station in this project.

Abstract:

Three cultivars of cull apples from a processing plant were examined before and after peeling. Reflectance spectra were measured from images captured every 10nm for wavelengths between 460nm and 1030nm. Typically the cull apples were rotting and little could be determined about the reflectance spectra of other types of damage. By visual inspection of the fruit at the processing plant, 9 typical defects were found which cause trim waste. There defects were bitter pit, bruising, codling moth, corking, cracks, hail, leaf roller, rot, and scab. Hand-picked apples with these types of damage were used to find the reflectance spectra for each individual kind of defect. Eight cultivars were included. Discriminant analysis was used to classify damaged from undamaged tissue. The magnitude of the Mahalanobis distance was used to identify the wavelengths of reflected light from the apple surface with the lowest and greatest contrast between damaged and undamaged tissue. Three wavelengths, (540nm, 740nm, and 1010nm), were identified which produced apple images that either had a reflectance nearly equal to undamaged areas or a reflectance much different than undamaged areas. The image at the wavelength with the greatest reflectance change for damaged tissue was subtracted from the image at the wavelength with the least reflectance change. Thresholding the resultant image segmented the damaged areas.

Background:

Unlike fresh-market apples where color, crispness, and flavor are the main factors for consumer acceptance, processing apples are valued for cultivar, fruit size, and quality characteristics that result in reduced trim waste. Ladd and Martin (1976) proposed that researchers use product characteristics for differentiating processed apples by cultivar, size and grade. This view of the product as a collection of characteristics was first proposed by Lancaster (1971). This view values processed apples for their utility - bearing characteristics where prices paid for the raw product depend on the amount of each characteristic contained in the product (Lucas, 1975). This has resulted in the development of pricing models through the estimation of hedonic price functions, which are regressions of price received as a function of the product's quality attributes (Lucas, 1975). Tronstad et. al. (1992) developed a hedonic price model for fresh - market apples using characteristics of location, time, cultivar, size, grade, and storage method as they relate to retail market pricing.

Harper et. al., (1992) developed a model based on production - related quality attributes for processing apples. Three varieties of processing apples (York Imperial, Rome Beauty, and Golden Delicious) were assessed for size and nine quality defects including trim bruise, misshapen fruit, bitter pit, decay, internal breakdown, scab, hail damage, insect damage, and York spot. Price discounts in the sample were statistically significant for fruit size, bruising, bitter pit, decay, misshapen fruit, and internal breakdown. Insect damage, hail damage, apple scab and York spot did not cause significant price discounts because of the small amount of damage present. This study demonstrated that further expenditure to reduce the quality defects was uneconomical to the grower due to the small discount of apple price. It is obvious that (1) all defects can not economically be completely eliminated and (2) the processor cannot afford to ignore these quality defects because of the large volume of fruit purchased. Price

discounts for cultivar and size differences were 10 to 30 times greater than any discounts for the nine quality defects tested.

At present, apples entering the processing plant are random sampled and inspected for fruit that are undersized and/or have defects affecting quality similar to those described above. The report presently returned to the producer has very limited information useful for orchard management that would improve apple quality. Automatic defect identification during the inspection process would be useful to return specific information to the producer so that orchard management changes could be implemented to correct for deficiencies during harvest and transporting to the plant. Automatic sorting would be more consistent than present human inspectors who gradually tire and vary in level of expertise. Aneshansley et. al.(1997) has shown that specific narrow and broad bands of wavelengths of light have been identified by discriminant analysis to provide the greatest contrast in reflectance between damaged and undamaged tissue. These same techniques will be used to demonstrate that defects in processing apples that cause trim-waste can easily be segmented by simple fast image processing methods such as image subtraction and thresholding.

Objectives:

The objectives of this study were:

1) to obtain reflectance spectra between 460nm and 1030nm at 10 nm intervals for processing apples with damage from rot, bruising, cracks, codling moth, leaf roller, scab, hail, corking, and bitter pit which require excessive trimming after peeling.

2) determine if the difference in reflectance spectra of damaged areas on apples can be used to segment defects by selecting specific wavelength bands that produce the high and low contrast in the captured images between damaged and undamaged tissue.

3) show that segmentation of damaged areas for automatic apple inspection of fruit entering the processing plant can be done quickly by subtracting the image with high contrast from the image with low contrast and simple thresholding.

Materials and Methods:

During the 1996 harvest season, a total of 25 cull apples from 3 cultivars (Red Delicious, York, and Rome Beauty) were removed from bulk apple bins in the storage yard of National Fruit Products, Winchester, VA. Because the cull apples with different defects from the processor also typically were rotting, little could be determined about the reflectance spectra for each different kind of damage. By visual inspection of the fruit at the processing plant, 9 typical trim-waste causing defects were found including bitter pit, bruising, codling moth, corking, cracks, hail, leaf roller, rot, and scab. Apples were then gathered from the orchard with these specific defects to determine the spectral characteristics useful for segmentation of each individual kind of defect from apple images for easy image processing.

During the 1995 and 1996 season, 18 - 22 damaged apples for each defect and including 8 cultivars (York, Golden Delicious, Red Delicious, Stayman, Gala, Empire, Granny Smith, and

Rome Beauty) were hand harvested from orchards near the USDA Appalachian Fruit Research Station, Kearneysville, WV. The apples were placed in common cold storage until 24 hours before images were captured.

The description of image capture, light filtering, and fruit lighting can be found in Throop and Aneshansley, 1997. Each cull apple from the processor was imaged and then peeled (White Mountain Apple Parer and Corer, Winchendon, MA) and imaged again.

The average grey level intensity of undamaged and damaged areas 4 pixels wide by 4 pixels high were interactively located and recorded from the apple images. Discriminant analysis of the two classes of tissue (damaged and undamaged) was performed (Minitab 11.0, Minitab Inc., State College, PA). The classification error and Mahalanobis distance between class means was recorded for each 10nm change in wavelength between 460nm and 1030nm. Whenever the classification error was the smallest for both classes, the Mahalanobis distance was the greatest indicating the greatest reflectance difference between damaged and undamaged tissue.

Results and Discussion:

Figures 1 shows the Mahanlanobis distance for unpeeled York, Rome, and Red Delicious apples computed from images of cull fruit from the processing plant. The apples were being stored outside the processing plant waiting to be processed. Consequently almost every cull fruit had rot damage in addition to some other defect such as bitter pit, scab, bruising, cracks, and gashes. As evidenced by the greater Mahalanobis distance, the damaged tissue on the cull fruit showed the greatest difference from undamaged tissue for a wavelength band between 700nm and 760nm. After the same cull apples were peeled, they showed a greatest contrast between damaged and undamaged tissue for a visible wavelength band between 500nm and 640nm and a near - infrared (NIR) band between 960nm and 1000nm (Figure 2). This shift of the reflectance spectra to the visible region is a direct result of the removal of the skin as indicated by a shift in magnitude of the Mahalanobis distance for the visible wavelengths.

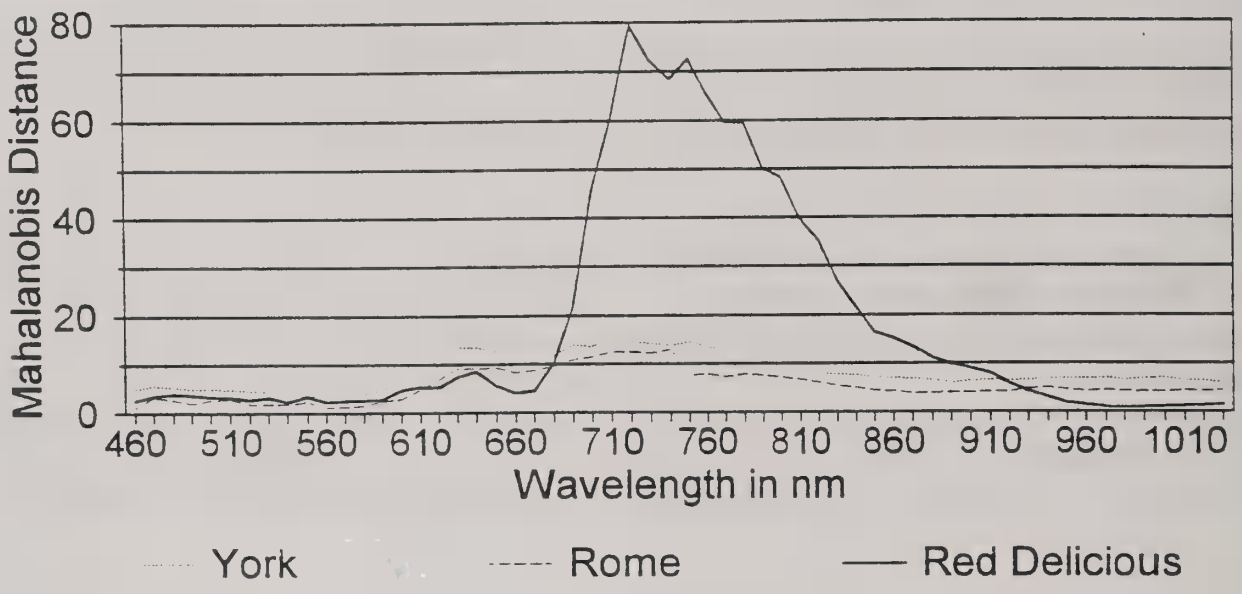

Figure 1. Plot of Mahalanobis Distance and Wavelength for Three Cultivars of Unpeeled Cull Processed Apples.

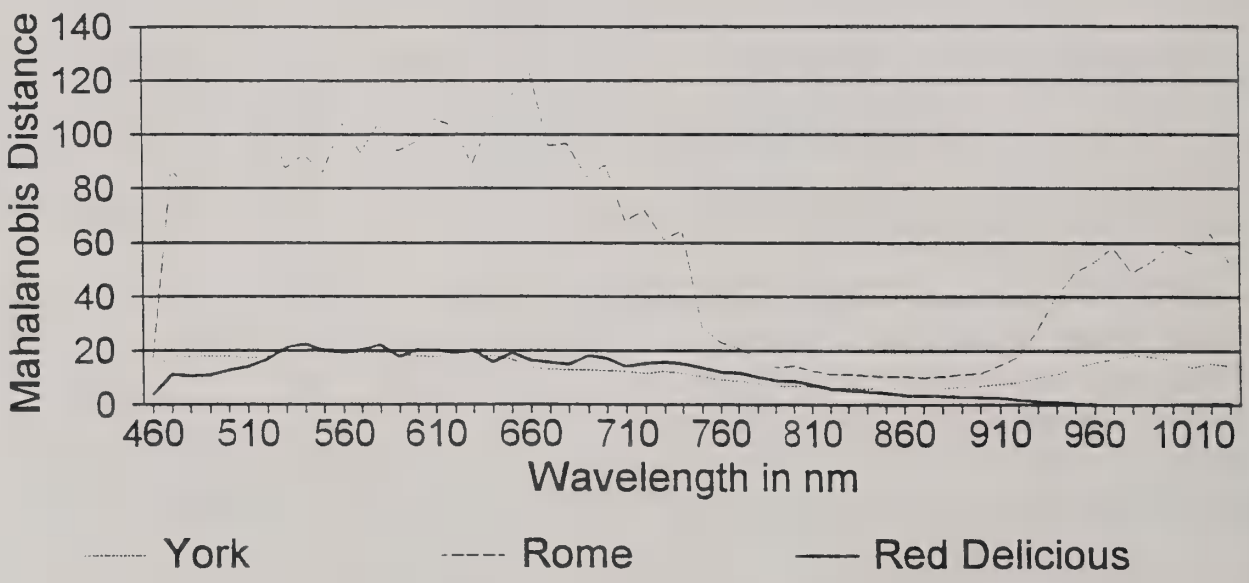

Figure 2. Plot of Mahalanobis Distance and Wavelength for Three Cultivars of Peeled Cull Processed Apples.

An unpeeled York apple with a crack surrounded by rot and a large bruised area is shown in Figure 3. The apple image captured at 730nm (B) has a greater contrast between damaged and undamaged tissue compared for images at the other wavelengths shown (540nm and 1010nm).

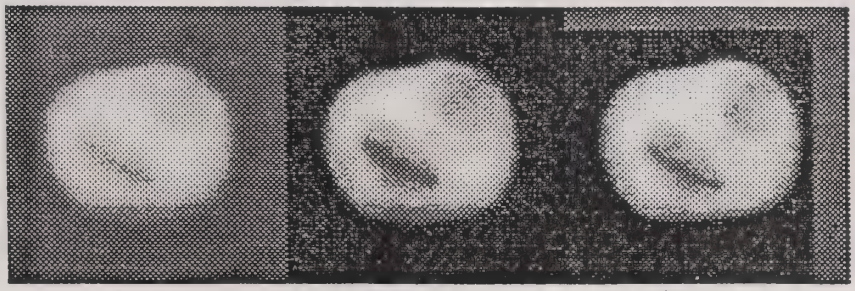

(A) (B) (C)

Figure 3. Image of an Unpeeled York Apple From a Bin at the Processing Plant Captured at Wavelengths of 540nm (A), 730nm (B), and 1010nm (C) and All Normalized to a Grey Level of 255.

Consistent with the magnitude of the Mahalanobis distance from the discriminant analysis, the York apple after peeling had a greater contrast between damaged and undamaged tissue for wavelengths of 540nm compared to the image captured at 860nm. These differences can be used to segment the damaged areas by simple image subtraction and thresholding (Figure 4).

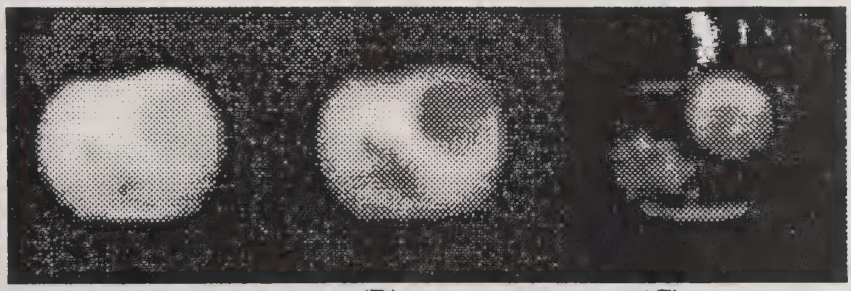

(A) (B) (C)

Figure 4. Image of the York Apple After Peeling Captured and Normalized at 860nm (A), 540nm (B), and Subtracting B From A and Thresholding (C).

Bitter Pit

The discriminant analysis of 2 groups of Golden Delicious apples with bitter pit produced Mahalanobis distances for each tested wavelength as shown in Figure 5. Bitter pit is a physiological disease where small areas of cortical tissue at the terminals of branched vascular bundles near the skin surface is altered to cause death of the affected cells. As the cells die, moisture is lost and the spots become slightly sunken and change color from a dark green to a

deep red color. As time passes the spots become dark gray or brown. The Mahalanobis

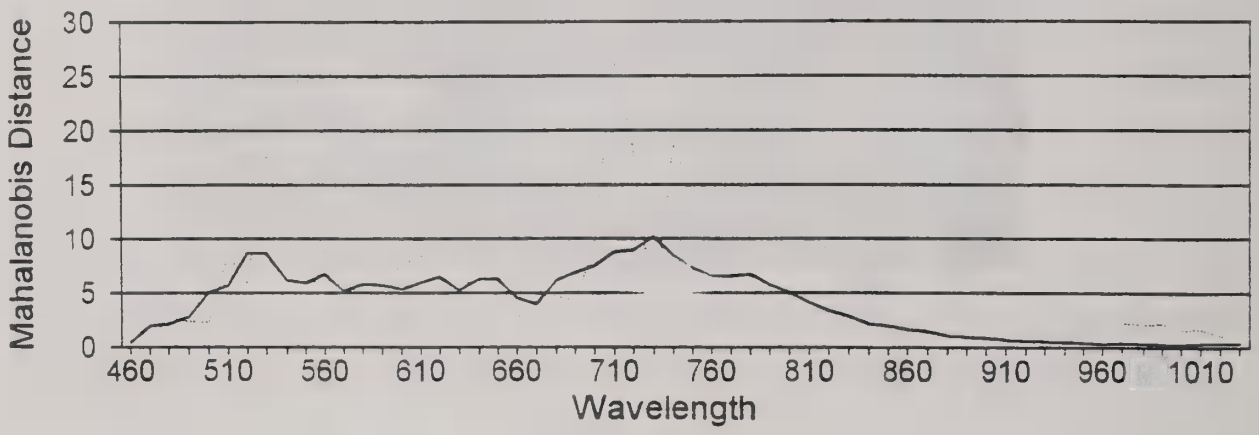

Figure 5. Mahalanobis Distance for Wavelengths Tested for Two Different Groups of Golden Delicious Apples with Bitter Pit Damage.

distance for the Golden Delicious apples was the greatest for wavelengths between 700nm and 740nm. This occurred when the NIR reflectance for damaged tissue was lowest compared to undamaged tissue. For wavelengths greater than 900nm, the reflectance for damaged tissue was equal to or slightly higher than undamaged tissue. For wavelengths above 960nm the reflectance sometimes increased for damaged tissue with respect to undamaged tissue due to the drying of the affected cells.

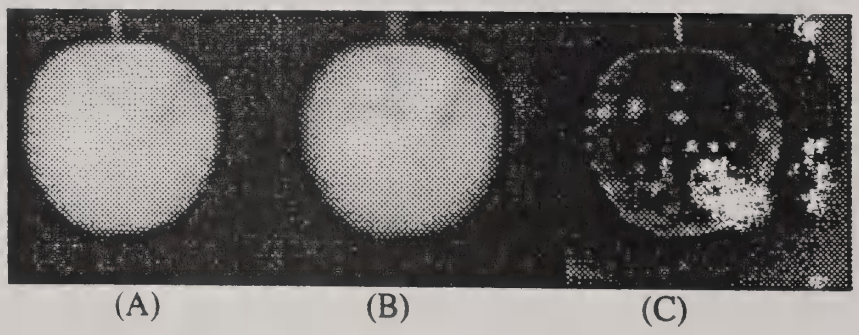

Figure 6. Images of a Golden Delicious Apple with Bitter Pit Captured at 1010nm (A), 740nm (B), and the Resulting Image by Subtracting B from A Showing the Damage Segmented (C).

By subtracting two normalized images, the first taken at a center wavelength of 1010nm minus the second taken with a center wavelength of 740nm, it is easy to segment bitter pit damage from undamaged tissue on unpeeled Golden Delicious apples by simple thresholding of the resulting image (Figure 6).

Bruising

Impact bruising severe enough to cause trim-waste was produced on Red and Golden Delicious apples by dropping from a height of 15 cm onto concrete. Images were captured 24 hours after dropping. The greatest Mahalanobis distance was for wavelengths greater than 940nm indicating the decrease in reflectance due to the 970nm water absorption band indicating the presence of fluid released from the crushed cells under the skin (Figure 7).

Bruising was segmented from unbruised tissue by subtracting a normalized image with a center wavelength of 1010nm from a reference normalized image generated from a teflon

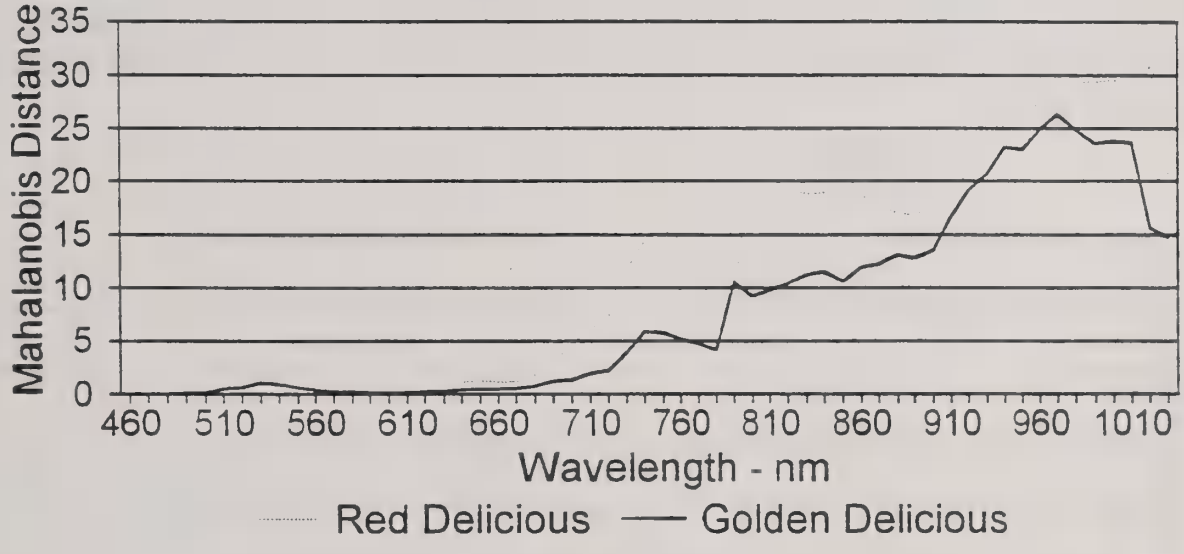

Figure 7. Mahalanobis Distance Versus Wavelength for Red and Golden Delicious Apples Bruised by a 15cm Drop onto Concrete.

standard which was logically ANDED with a normalized image of the same apple with a center wavelength of 540nm (Figure 8). When the subtraction is completed, the pixels representing the bruise are visible after simple thresholding.

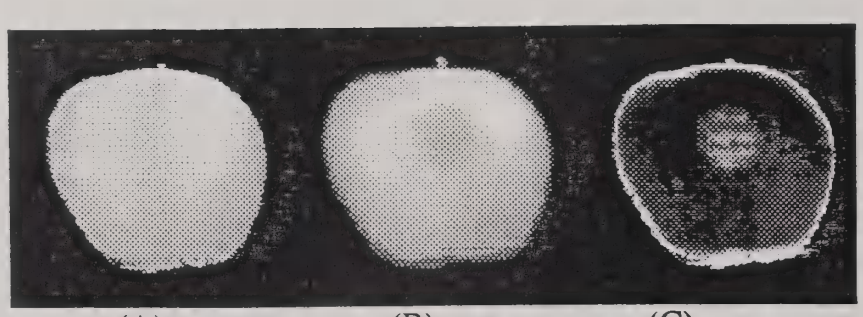

Figure 8. Logically ANDED image of teflon reference and 540nm image of Red Delicious bruised apple (A), 1010nm image, and the resulting image after subtraction of B from A showing the segmented bruise (C) after thresholding.

Codling Moth

Codling moth damage had the greatest Mahalanobis distance for images captured using wavelengths between 700nm and 750nm for the 3 cultivars tested, Empire, Golden Delicious, and Stayman (Figure 9).

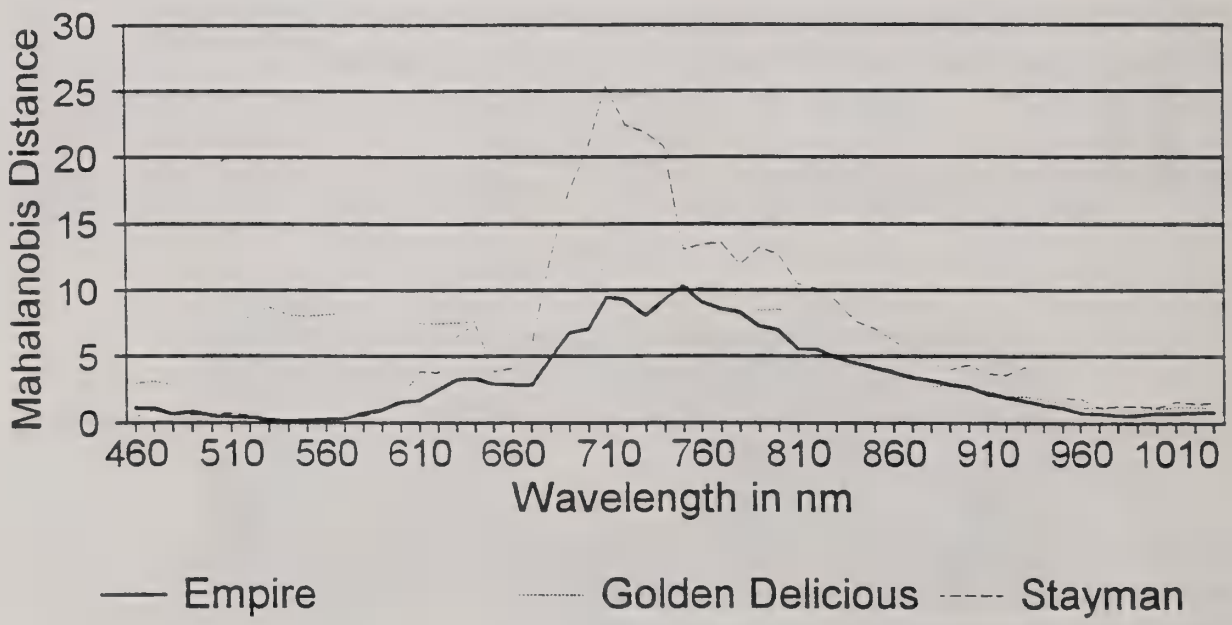

Figure 9. Mahalanobis Distance Versus Wavelength for Golden Delicious, Empire, and Stayman Apples with Codling Moth Damage.

By subtracting two normalized images, the first taken at a center wavelength of 1010nm minus the second taken with a center wavelength of 740nm, codling moth damage can be segmented from undamaged tissue on the 3 cultivars tested by simple thresholding (Figure 10).

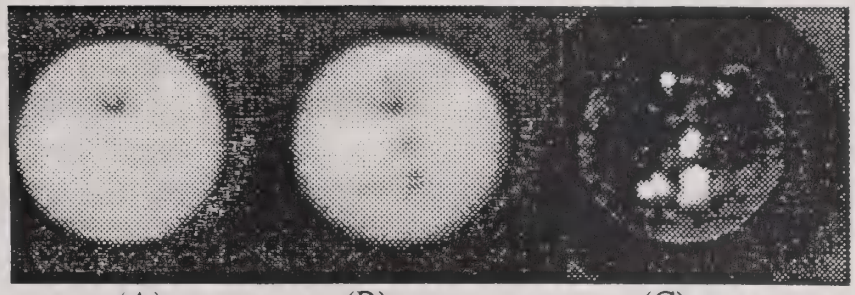

(A) (B) (C)

Figure 10. A Stayman apple with codling moth damage captured at 1010nm (A), 740nm (B), and the resulting image after subtracting B from A showing the segmented codling moth damage (C).

Cork Spot

Cork spot, sometimes called York spot is suspected to be caused by a nutritional problem related to an imbalance of calcium and boron. The resulting damage of spots of dead cells show the greatest Mahalanobis distances for wavelengths between 690nm and 740nm for Stayman and Red Delicious and 600nm and 640nm for York apples (Figure 11).

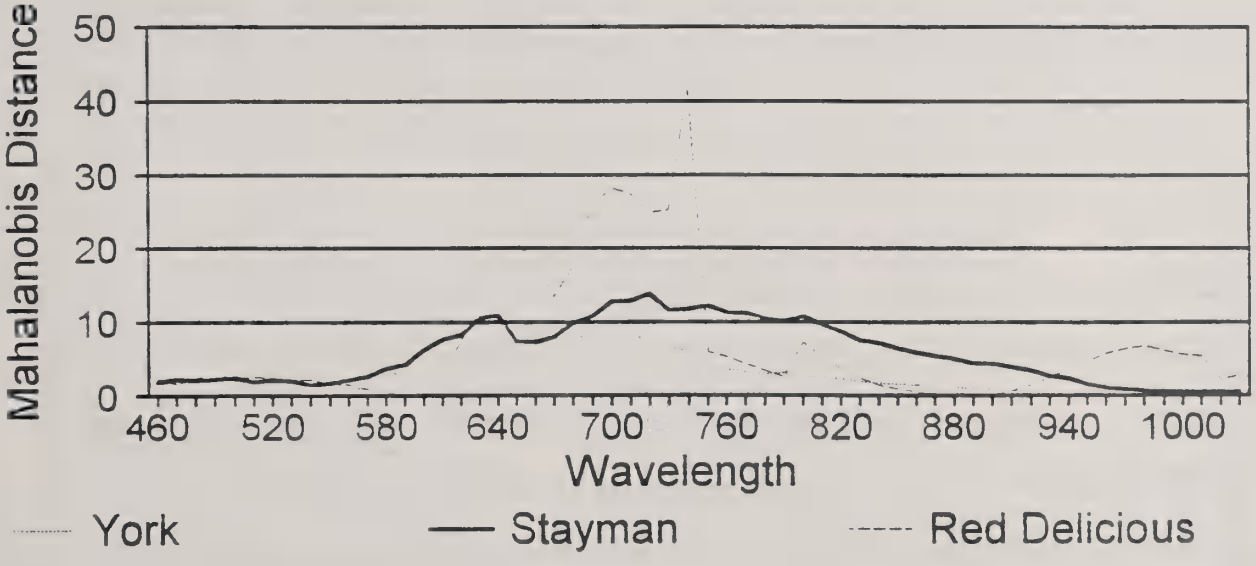

Figure 11. Mahalanobis Distance Versus Wavelength for Red Delicious, York, and Stayman Apples with Cork Spot (York Spot) Damage.

By subtracting two normalized images, the first captured at a center wavelength of 1010nm minus the second captured with a center wavelength of 740nm, cork spot damage can be

segmented from undamaged tissue on Stayman and Red Delicious apples by simple thresholding (Figure 12). As indicated by the lower Mahalanobis distances for York apples, cork spot damage segmentation for some York apples was not always successful at 740nm. The Mahalanobis distance measured indicates that a wavelength band with a center wavelength of 640nm should work better (Figure 11).

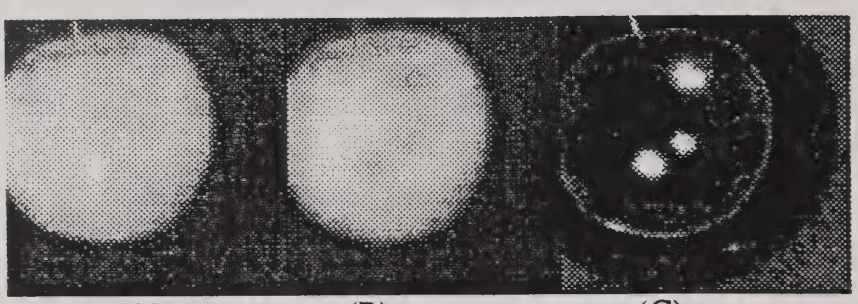

(A) (B) (C)

Figure 12. An Image of a Golden Delicious Apple with Cork Spot Captured at 1010nm (A), 740nm (B), and an Image with Cork Spot Damage Segmented by Subtracting A from B and Thresholding.(C).

Cracking

Fruit cracking occurs after periods of cloudy, rainy weather when rates of evaporation and transpiration are very low. Cultivars such as Stayman, Wealthy, and York Imperial are more

Figure 13. Mahalanobis Distance Versus Wavelength for Golden Delicious and Stayman Apples with Crack Damage.

susceptible for this kind of damage. The internal flesh grows at a more rapid rate than the outer skin and the skin is unable to expand at this same rate thus resulting in cracking. The Mahalanobis distance was the greatest for wavelengths of 720nm to 760nm for the 2 groups of Stayman and Golden Delicious apples tested (Figure 13). Crack damage often has localized dehydration or rot associated with it.

Subtracting two normalized images, the first captured at a center wavelength of 1010nm minus the second captured with a center wavelength of 740nm, crack damage can be segmented from undamaged tissue on Stayman and Golden Delicious apples by simple thresholding (Figure 14). Note that it is the cells around the dark crack that are detected due to their dehydrated state. Later you will see that if rot is present, it can be detected by the same process.

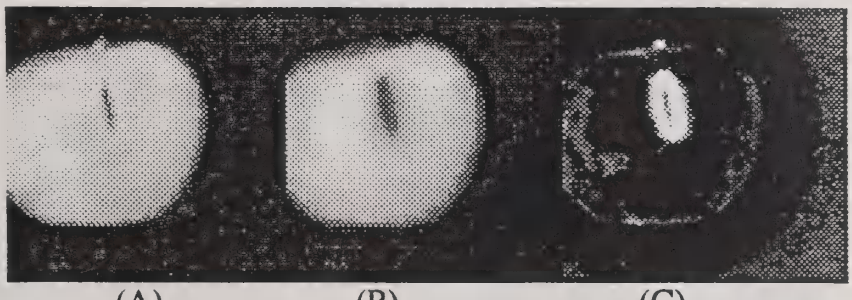

Figure 14. An Image of a Stayman Apple with Crack Damage Captured at 1010nm (A), 740nm (B), and the resulting image subtracting B from A segmenting the dehydrated cells around the edge of the crack.

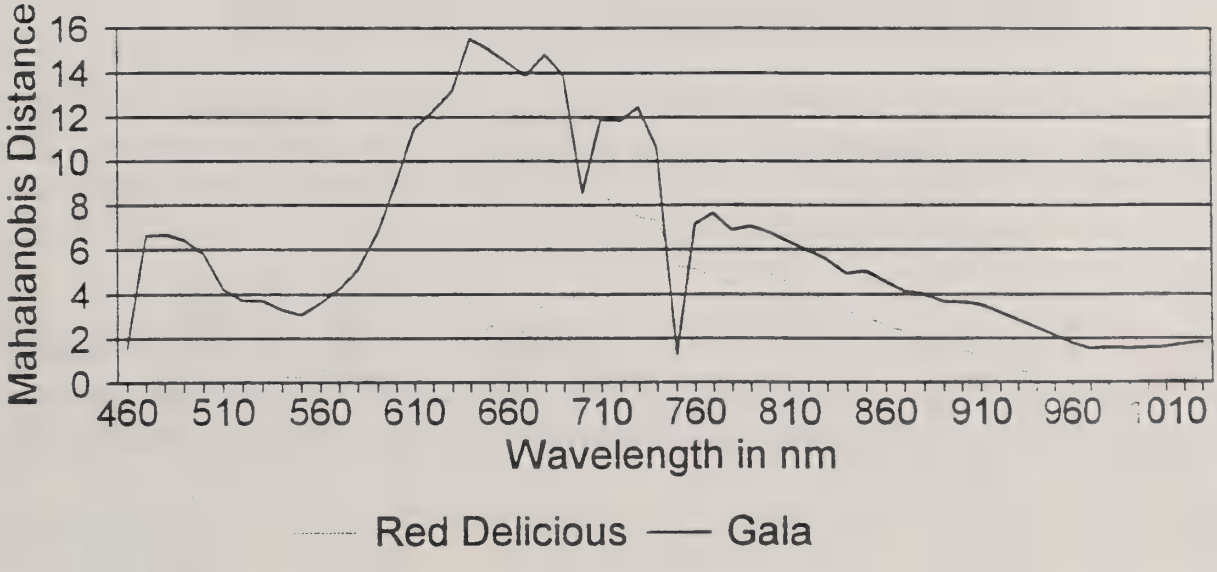

Figure 15. Mahalanobis Distance Versus Wavelength for Red Delicious and Gala Apples with Hail Damage.

Hail

Hail damage can occur anytime during the growing season. It has an appearance similar to cork spot with small sunken areas just under the skin of dead dehydrated cells. The Mahalanobis distance is the greatest for wavelengths between 700nm and 750nm (Figure 15). The Gala apples tested had a even greater Mahalanobis distance for wavelengths in the visible red region.

By subtracting a Red Delicious normalized apple image captured with a center wavelength of 740nm from a normalized image with a center wavelength of 1010nm, the result is an image that can easily be thresholded to segment the hail damaged areas. The damage on the 1010nm image has a reflectance equal or greater than the undamaged tissue while the reflectance of the damaged areas on the 740nm image is less than undamaged tissue (Figure 16).

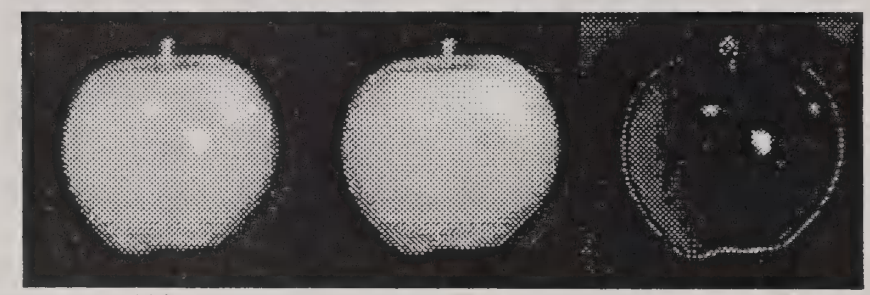

(A) (B) (C)

Figure 16. A Normalized Image of a Red Delicious Apple with Hail Damage Captured at 1010nm (A), 740nm (B), and the Resulting Image After Subtracting B from A and Thresholding (C).

Leaf Roller

Leaf roller damage is caused by the larvae consuming areas of skin and outer flesh. The discriminant analysis for both Red and Golden Delicious apples produced large Mahalanobis distances between classes of damaged and undamaged tissue for wavelengths between 700nm and 820nm. Very small Mahalanobis distances were found for wavelengths beyond 960nm (Figure 17). Large Mahalanobis distances for Golden Delicious apples were also produced for wavelengths in the color region.

By subtracting two normalized Golden Delicious images, the first taken at a center wavelength of 1010nm minus the second taken with a center wavelength of 740nm, leaf roller damage can be segmented from undamaged tissue on the 2 cultivars tested by simple thresholding (Figure 18).

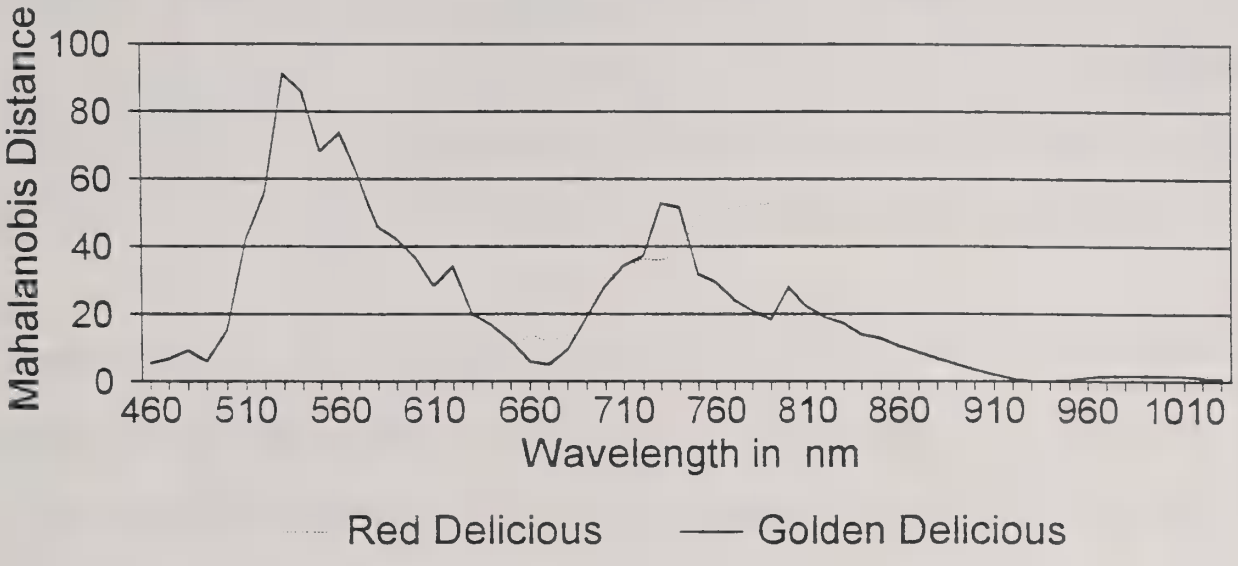

Figure 17. Mahalanobis Distance Versus Wavelength for Red and Golden Delicious Apples with Leaf Roller Damage.

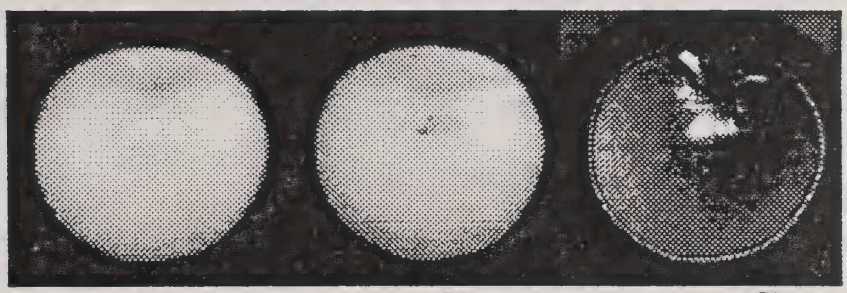

(A) (B) (C)

Figure 18. A Normalized Image of a Golden Delicious Apple with Leaf Roller Damage Captured at 1010nm (A), 740nm (B), and the Resulting Image After Subtracting B From A and Thresholding (C)

Rot

Rot comes in many forms and is present when organisms pass through the protective skin which has been damaged or through the open lenticels allowing passage of the organism into the moist fleshy tissue inside of the fruit. The distance between classes of damaged and undamaged Golden and Red Delicious apples was the greatest for wavelengths between 700nm and 750nm (Figure 19). The Mahalanobis distance was lowest for wavelengths beyond 960nm. The Golden Delicious apples also had higher Mahalanobis distances for most of the visible wavelengths as well.

If we subtract a normalized Crispin apple image captured at a center wavelength of 740nm from an image captured at a center wavelength of 1010nm, the resulting image can be used to segment the rot from undamaged tissue by simple thresholding (Figure 20).

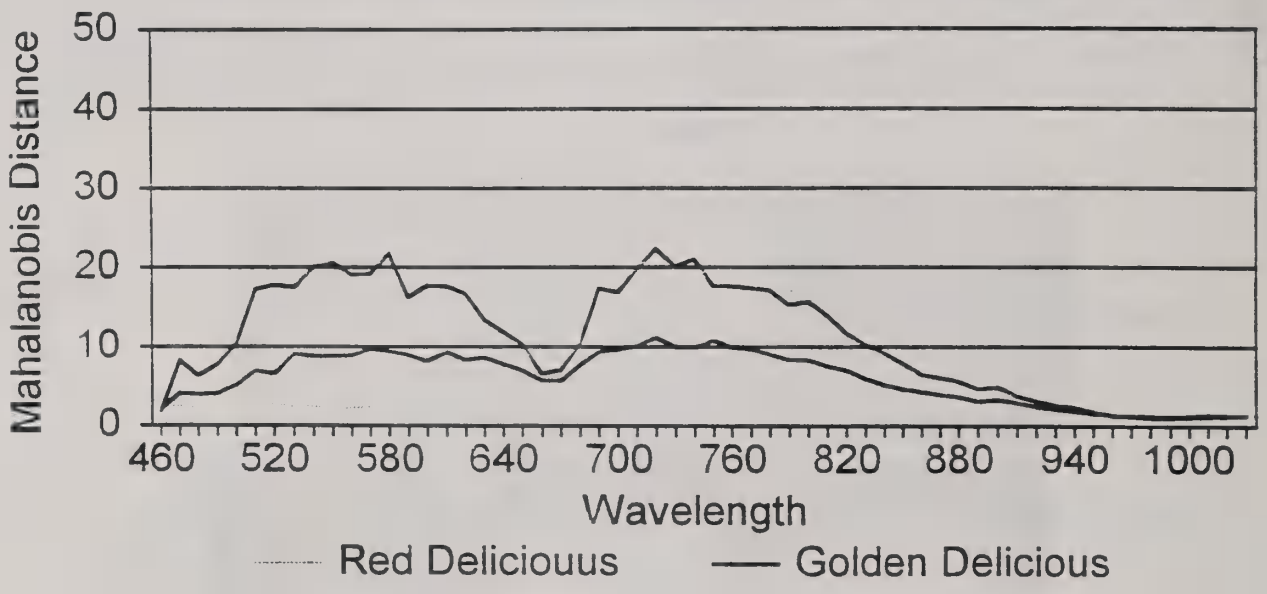

Figure 19. Mahalanobis Distance Versus Wavelength for Red and Golden Delicious Apples with Rot Damage.

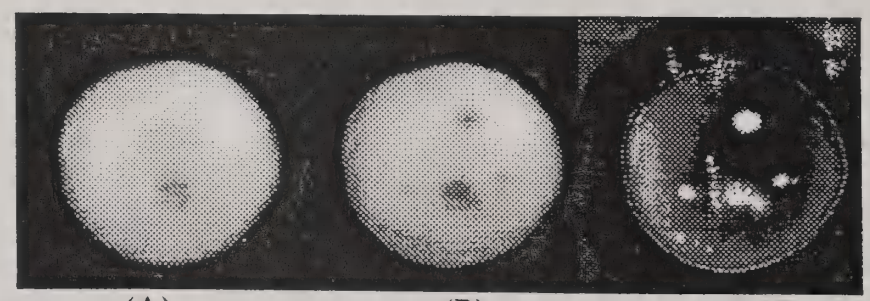

Figure 20. A Normalized Image of a Crispin Apple with Rot Damage Captured at 1010nm (A), 740nm (B), and the Resulting Image After Subtracting B From A and Thresholding (C).

Apple Scab

Apple scab is caused by a fungus and can appear during cool moist conditions anywhere apples are grown. The fungus enters through a rupture in the cuticle and produces brown or dark green lesions on the surface of the apple. For severe cases, the fruit shape can be altered causing poor peeling in automatic peeling machines. The Mahalanobis distance for Granny Smith, Red Delicious and McIntosh apples were very large for wavelengths between 700nm and 740nm (Figure 21). Granny Smith had Mahalanobis distances large enough for class separation between damaged and undamaged fruit also for most of the visible wavelengths. All of the cultivars tested had reduced Mahalanobis distances for wavelengths beyond 960nm.

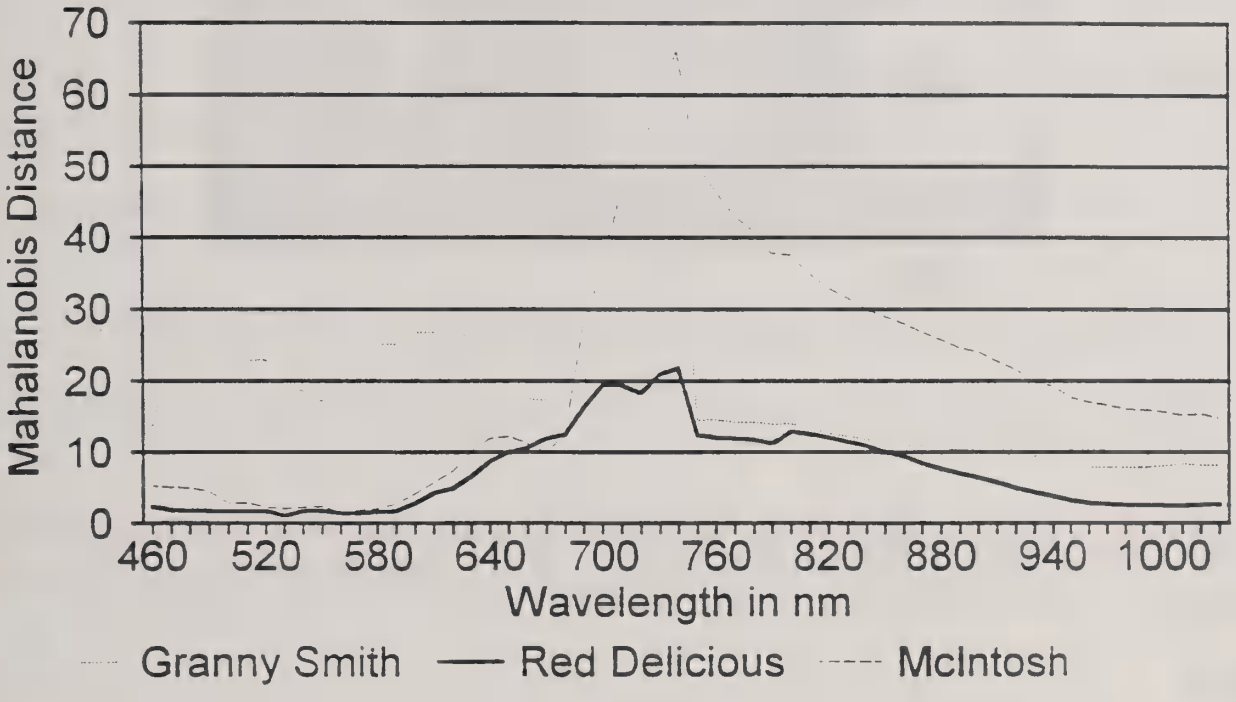

Figure 21. Mahalanobis Distance Versus Wavelength for Red Delicious, Granny Smith, and McIntosh Apples with Scab Damage.

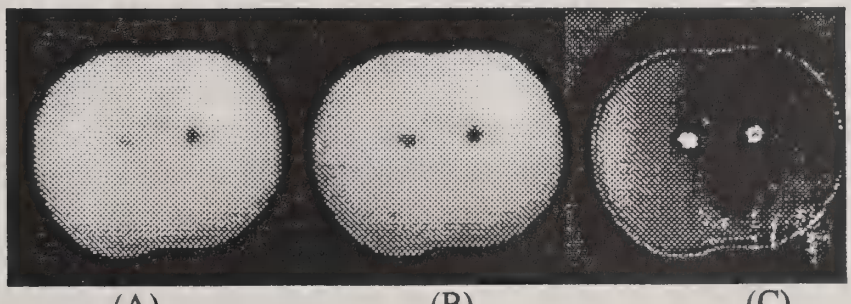

(A) (B) (C)

Figure 22. A Normalized Image of a McIntosh Apple with Scab Damage Captured at 1010nm (A), 740nm (B), and the Resulting Image After Subtracting B From A and Thresholding (C).

If we subtract a normalized McIntosh apple image captured at a center wavelength of 740nm from an image captured at a center wavelength of 1010nm, the resulting image can be used to segment the rot from undamaged tissue by simple thresholding (Figure 22).

While viewing apples at the processing plant, it became obvious that defects such as sooty blotch and severe flyspeck may not be ignored if automatic sorting is implemented for processed fruit. Figure 23 shows a Golden Delicious apple image with sooty blotch that has been processed as if checking for bruises. Severe sooty blotch has the potential of hiding other defects from a camera. By talking with the processors, we learned that they are becoming

(A) (B) (C)

Figure 23. Logically ANDED Image of Teflon Reference and 540nm Image of a Golden Delicious Apple With Sooty Blotch (A), 1010nm Image, and the Resulting Image After Subtraction of B From A Showing the Segmented Sooty Blotch (C).

concerned with this surface defect which is peeled away because they are presently processing apple skins and cores to obtain apple cider vinegar and feel that the sooty blotch fungus, *Gloeodes pomigena*, could contaminate this product.

Conclusions:

Images of unpeeled processing apples with damage from rot, bruising, cracks, codling moth, leaf roller, scab, hail, corking, and bitter pit requiring excessive trimming after peeling were successfully processed segmenting damaged tissue from undamaged tissue. Three wavelengths (540nm, 740nm, 1010nm) were found that simplified image processing to simple image subtraction and thresholding for unpeeled apples. In most cases an image at one of the three wavelengths had high contrast between damaged and undamaged tissue while an image at one of the other two wavelengths had low contrast. By subtraction of the high contrast image from the low contrast image and thresholding, segmentation of the damaged areas was completed. York spot on the York cultivar was not always segmented successfully at 740nm and the Mahalanobis distance measured indicated that a wavelength band with a center wavelength of 640nm should work better.

Unlike unpeeled apples, peeled apples had the greatest contrast between damaged and undamaged tissue for the visible wavelengths 500nm to 640nm and a near - infrared (NIR) band between 960nm and 1000nm as indicated by the magnitude of the Mahalanobis distance.

Sooty blotch was found to block the reflectance changes for some defects like bruising, but the processing industry indicated that better control of this surface defect is desired.

References:

1. Aneshansley, D. J., J. A. Throop, and B L. Upchurch. 1997. Reflectance spectra of surface defects on apples. *Proceedings Sensors for Nondestructive Testing Conference*, Orlando, Florida. February 18-21, 1997. Northeast Regional Agricultural Service, 152 Riley-Robb Hall. Cornell University, Ithaca, NY 14853 . pp - 143-160

2. Harper, J. K. and G. M. Greene II. 1993. Fruit characteristics influence prices received for processing apples. *Journal of Horticultural Science*, 28(11): 1125-1128.

3. Ladd, G. W. and M. B. Martin. 1976. Prices and demands for input characteristics. *Amer. J. Agr. Econ* 58(1):21-30.

4. Lancaster, K. J. 1971. Consumer demand: A new approach. Columbia Univ. Press, New York.

5. Lucas, R. E. B. 1975. Hedonic price functions. *Econ Inquiry* 13(1):157-178.

6. Throop, J. A. and D. J. Aneshansley. 1997. Apple damage segmentation utilizing reflectance spectra of the defect. ASAE Paper No. 973078, ASAE, St. Joseph, MI

7. Tronstad, R., L. S. Huthoefer, and E. Monke. 1992. Market windows and hedonic price analysis: An application to the apple industry. *J. Agr. Resources Econ.* 17(2):314-322.

Paper No. 973078
An ASAE Meeting Presentation

Apple Damage Segmentation Utilizing Reflectance Spectra of the Defect

James A. Throop, Daniel J. Aneshansley

Cornell University, Department of Agricultural and Biological Engineering, Ithaca, NY 14853

Written for presentation at the
1997 ASAE Annual International Meeting
Sponsored by ASAE

Minneapolis Convention Center
Minneapolis, Minnesota
August 10-14, 1997

Summary: Reflectance spectra from 22 defects commonly found on 10 different apple cultivars were measured and processed to identify 3 wavelength bands of 50 - 60nm in width for defect segmentation. A combination of image processing techniques and images of the same apple captured at these different wavelengths were described to accomplish the segmentation process.

Keywords: Apples, Apple Quality, Defects, Defect Detection, Image Analysis, Image Processing,

ASAE, 2950 Niles Rd., St. Joseph, MI 49085-9659 USA
Voice: 616.429.0300 FAX: 616.429.3852 E-Mail: <hq@asae.org>

Acknowledgments: This project is supported in part by USDA Cooperative Agreement 58-1931-5-019 with the ARS-USDA Appalachian Fruit Research Station, Kearneysville, WV, and by the Agricultural Experiment Station at Cornell University with Hatch Regional Project NE179 and Hatch Project 412. We would also like to acknowledge the continued assistance and expertise of Mr. Bill Anger of ARS-USDA Appalachian Fruit Research Station in this project.

Abstract:

The reflectance spectra for 22 defects found on 10 different apple cultivars was measured every 10nm for wavelengths between 460nm to 1030nm. Discriminant analysis was used to identify three wavelength regions, 540nm, 740nm, and 1010nm, which produced images with the highest and lowest contrast for damaged tissue with respect to undamaged tissue as indicated by the highest or lowest Mahalanobis distance respectively. Subtraction of an apple image with the defect having the highest contrast compared to undamaged tissue from an image of the same apple with little difference between damaged and undamaged tissue and thresholding easily segmented bitter pit, botryosphaeria rot, chemical, codling moth, corking, cracking, hail, leaf roller, rot, and scab damage.

Bruising, scald, punctures, sooty blotch, and fly speck had a lower reflectance for all near-infrared wavelengths. The lowest reflectance compared to undamaged tissue occurred for wavelengths between 960nm and 1030nm. Images captured with these defects were segmented by subtracting these images from a teflon reference image with intensity values approximating the values of undamaged tissue.

Defects such as russet, early frost damage, insect stings, blister spot, and powdery mildew are only skin deep and affect skin color. These defects appeared brighter on red apples and darker on yellow/green apples. This caused the defects to be undetectable on red/green varieties such as Empire. For monochoric apples such as Red or Golden Delicious, these defects were segmented by subtracting an image captured at 540nm from an image captured at 1010nm. The defect on the resulting image for yellow/green apples was segmented by simple thresholding. For red colored apples, the resulting image must be subtracted from a teflon reference image before thresholding. Blister spot was segmented in the same manner but a Sobel edge detector was applied to the resulting image before thresholding.

Sunburn was segmented on Red Delicious apples by subtraction of an image captured at 1010nm from an image captured at 540nm and thresholding.

Background:

The quality of apples in the retail market are greatly influenced by maturity at harvest, handling, picking, transportation, and storage. Dealers judge apple quality by physical features such as size, shape, color, appearance, and finger feel. Consumers decide to purchase based on eating qualities of the apple although quite often at the time of purchase only external appearance is available (S. Dhanaraj et. al. 1980). Although studies have shown that appearance has little to do with eating quality, it certainly plays a major part in the final decision to purchase (E. Hohn, 1990). The "juicy, crisp, and flavorful" part of the consumer's decision come from memory of the last time an apple was consumed.

Appearance is the major criteria for quality sorting of apples for consumers. Typical reasons for culling apples are shown in Table 1. Although many of the defects are from insect and disease, the largest number of fruit culled resulted from size and color (W. D. Gerling. 1983).

Table 1. Typical Factors Causing Culling of McIntosh Apples During the 1992 & 1993 Growing Seasons in the Hudson Valley, Highland, NY.

Factor	% of Sampled Fruit	% of Total Culls
Undersize	3.5	38.7
Color	6.9	35.0
Bruise	0.2	2.7
Mechanical	0.5	4.9
Stem Puncture	0.1	1.0
Hail	0.8	9.0
Malformed	0.3	3.3
Finish	0.3	2.7
Disease	0.1	0.7
Insect Damage	0.2	2.0
Total	11.9	100.0

Table 2. Average Percentage of Defective Apples According to Origin or Time of Occurrence of the Grade Defect.

Variety	Orchard	Harvest & Handling	Storage	All Sources
Delicious	20.3	9.1	1.7	28.1
Jonathan	22.0	13.7	4.6	35.8
McIntosh	19.2	21.0	0.1	35.1
Rome	31.1	17.9	1.9	41.2
All Varieties	23.8	13.4	2.2	35.8

Dewey et al. 1971 examined 18 lots of 6 cultivars of stored apples to determine the probable cause and origin of defects found on the apples and classified them into the following categories: (a) growing conditions, (b) harvest and handling conditions, and (c) storage or dumping operations (Table 2). Preharvest defects included small size, inadequate color, limb-rub, russeting, hail damage, and scab. The most serious defect during harvesting was bruising. Defects from storage included mostly rot, decay, and internal breakdown.

Dewey et. al. 1971 found that the number of 42-lb. bushels of orchard run fruit necessary to packout 40-lb. units of U. S. Fancy Michigan apples increased as the number of defects increased causing lower packout rates (Table 3). If the packout rate decreased from 95% to 35%, the storage, sorting and packing costs nearly tripled. Two chances for increasing profit were found: (1) improve fruit quality during production and harvesting, (2) do not store low grade fruit. If high speed automatic sorting was available, more apples could be sorted before storage to prevent storage of low grade fruit.

Table 3. The Effect of Packout Rate on the Number of 42-lb Orchard Run Bushels Required to Fill a U. S Fancy 40-lb. Unit.

Packout of Orchard Run Apples (Percent)	Yield of U. S. Fancy (Units per Orchard Bushel)
95	1.00
85	1.12
75	1.27
65	1.46
55	1.73
45	2.12
35	2.72

In spite of the fact that defect sorting represents a loss of product value, quality sorting of apples is necessary to provide the consumer with a quality apple with excellent appearance or other fruits will replace apples in the retail market.

Assessing apple quality, both for maturity and defects, by spectral reflectance dates back to the early 1940's (Lott, 1943). The recording of the reflectance from the apple surface of different wavelengths of light resulted in identifying particular wavelengths to define maturity (Bittner, et. al. 1968, bruising (Ingle and Hyde, 1968, Brown et. al., 1974, Fuzzen, 1981, Upchurch et. al. 1990), and other defects (Reid, 1976, Rehkugler et. al. 1989).

Aneshansley et. al. 1997 captured images with a video camera with a tunable bandpass filter in front of the camera lens. Images of the reflectance for center wavelengths between 460nm and 1030nm were captured in 10 nm intervals for 5 cultivars and 18 defects. Discriminant analysis was performed on the data and the classification error between damaged and undamaged tissue and the Mahalanobis distance for each defect were used to statistically identify the wavelengths which produced the greatest reflectance contrast between damaged and undamaged tissue. This paper is a continuation of this work.

Objectives:

Expand the present data base of images of the reflectance spectra of defects for additional cultivars and through discriminant analysis, define specific wavelength bands to insure maximum and minimum contrast in reflectance between damaged and undamaged tissue for each defect and determine if these wavelength bands work for different cultivars with the same defect.

Determine which defects can be quickly segmented by subtracting 2 images, one captured using a wavelength band that produces the highest contrast between damaged and undamaged tissue, and a second image captured that produces the lowest contrast between damaged and undamaged tissue. After the subtraction process, determine which defects can be segmented with simple thresholding.

If subtraction of two images and thresholding fails to segment the defect, attempt to define another image processing technique for segmentation.

Materials and Methods:

During the 1995 and 1996 harvest season, 18 - 22 damaged apples for 22 defects from 10 cultivars (York, Golden Delicious, Red Delicious, Stayman, Gala, Empire, Granny Smith, McIntosh, Crispin, and Rome Beauty) were harvested from orchards near the USDA Appalachian Fruit Research Station, Kearneysville, WV. The apples were held in common cold storage until 24 hours before images were captured (Table 4).

Two camera/lens/adjustable filter combinations were used. System 1 consisted of a CCD monochrome camera (Model 4900, Cohu Electronics, San Diego, CA) with its gain adjusted to full and equipped with a 25mm lens with the aperture set at f1.4. A tunable filter system (Model:VS-VIS3-20-MC-20-SQ, Cambridge Research & Instrumentation Inc., Cambridge, MA) was placed in front of the camera lens. The filter had variable attenuation control and was adjusted for 29 different wavelengths between 460nm to 750nm, both of which were controlled from the serial port of the image capture computer. For each wavelength selected the filter had a 20nm bandpass and a 20nm aperture diameter. System 2 consisted of a CCD monochrome camera (Model 4800, Cohu Electronics, San Diego, CA) equipped with a 25 mm lens with the aperture set at f1.4. A tunable filter system (Model:VS-NIR1-35-MC-20-RN, Cambridge Research & Instrumentation Inc., Cambridge, MA) was placed in front of the camera lens. The filter had variable attenuation control and was adjusted for 29 different wavelengths between 750nm to 1030nm, both of which were controlled from the serial port of the image capture computer. For each wavelength selected the filter had a 35nm bandpass and a 20nm diameter aperture. A white teflon cylinder 76mm diameter by 76mm high was placed in the field of view of both systems. For each wavelength tested, the correct attenuation setting for the neutral density portion of the variable filter allowing a camera output of 175 out 255 grey levels was recorded in a look up table. This assured that the camera output was normalized to a standard output grey level while viewing the teflon cylinder regardless of

Table 4. Table Showing the Defects Tested on the Left, Cultivars Tested on the Right, and the Cultivars Which Had the Defect in the Center.

Defect	Cultivars Tested (By Letter)	Cultivars
Bitter Pit	A, B	A. Red Delicious
Blister Spot	B, C	B. Golden Delicious
Botryosphaeria Rot	B	C. Crispin
Bruise	A, B	D. Gala
Chemical	B	E. Empire
Codling Moth	A, B, C, E, F	F. Stayman
Corking	B, F, G	G. York
Cracking	B, F	H. McIntosh
Fly Speck	A, B, E, I	I. Granny Smith
Frost (early)	B, F	J. Rome Beauty
Hail	A, D	
Leaf Roller	A, B	
Powdery Mildew	A, H	
Puncture	A, B, H	
Rot	A, B, C	
Russet	A, B, E, F, H	
Scab	A, B, H, I	
Scald	A	
Sooty Blotch	A, B, E	
Sting	A, B, C	
Sunburn	A	

changes in camera response due to wavelength or of changes in the transmission characteristics of the variable filter. System 1 and system 2 were each controlled by different PCI bus Alpha 275 MHz processor equipped computers (Model SYS-AXP275AN, BTG Micro Systems, Fairfax, VA and Model Cobra Cab 275, Carrera Computers Inc., Laguna Hills, CA) with frame grabber cards (Raptor-PCI, BitFlow, Woburn, MA) installed for image capture. Filter control was through the serial port via a subroutine running under image capture and processing software (Quantim, ZEDEC Technologies Inc., Burlington, NC). For every apple tested, this combination provided sequential filter adjustment and image capture for 58 images continuously for each of the different wavelengths tested. Images 256 pixels high by 256 pixels wide were captured in this study and were stored on a rewriteable 650 MB/disk PD/CD-ROM drive (Model:LF-1004AB, Panasonic Communications & Systems Co., Secaucus, NJ).

Diffuse lighting was produced by placing the apples inside of a 222mm diameter cylindrical white acrylic diffuser 406mm high with four tungsten lamps placed around the outside. The 40 watt lamps (model 40A, 40W, General Electric, Cleveland, Ohio) were placed in a 305mm per side square centered about the outside of the diffuser at a height of 184mm. To minimize

60 Hz fluctuations, the adjustable 120 VAC to the lamps was converted to adjustable 160 VDC (4V pk-pk ripple) by using a 10A bridge rectifier (GBPC-1004, General Instruments) and a capacitor filter (80 uf 450 VDC, 36DX-800F450DC, Sprague).

The average grey level intensity of undamaged and damaged areas 4 pixels wide by 4 pixels high were interactively located and recorded from the apple images. Discriminant analysis of the two classes of tissue (damaged and undamaged) was performed (Minitab 11.0, Minitab Inc., State College, PA). The classification error and Mahalanobis distance between class means were recorded for each 10nm change in center wavelength between 460nm and 1030nm. Whenever the classification error was the smallest for both classes, the Mahalanobis distance was the greatest indicating the greatest reflectance difference between damaged and undamaged tissue.

Results and Discussion:

Figure 1 is a typical graph showing the variation in Mahalanobis distance as the center wavelength changed from 460nm to 1030nm for Empires, Golden Delicious, and Stayman apples with codling moth damage. The greatest Mahalanobis distance occurred at 720nm - 740nm and the lowest at wavelengths above 950nm for all 3 cultivars shown. Further graphs of the Mahalanobis distance for other defects on different cultivars can be seen in Throop et. al. 1997 and Aneshansley et. al. 1997.

As a result of the discriminant analysis, 3 wavelength bands centered at 540nm, 740nm, and 1010nm were identified having either the highest or the lowest Mahalanobis distance,

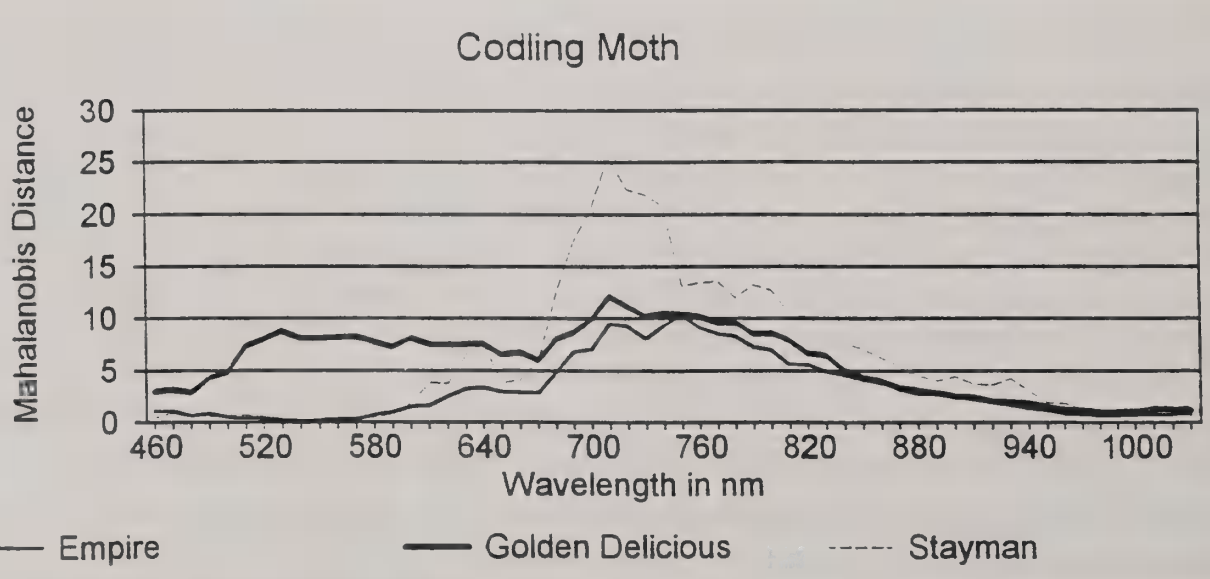

Figure 1. Mahalanobis Distance for Every 10nm Change in Center Wavelength for Empire, Golden Delicious , and Stayman Apples with Codling Moth Damage.

depending on the physical changes caused by the defect to the apple surface. Table 5 shows the defects with a solid line indicating the wavelength band with the highest Mahalanobis distances and the greatest contrast between damaged and undamaged tissue. If a dotted line is shown, this wavelength band had the lowest Mahalanobis distances indicating very low contrast between damaged and undamaged tissue. For defects like bruising, scald, fly speck, sooty blotch, and puncture damage, one wavelength band showed the greatest contrast for undamaged tissue but did not have a second wavelength band where the defect had a reflectance similar to undamaged tissue.

It was observed that the Mahalanobis distance remained nearly at the same level for adjacent wavelengths each side of the center wavelengths of 540nm, 740nm and 1010nm. Considering that wider wavelength bands would supply more light to the camera allowing more exposure flexibility during actual image capture on the grading line, 5 images were averaged together before the segmentation process was started. Apple images captured at a center wavelength of 520nm, 530nm, 540nm, 550nm, and 560nm and a bandwidth of 20nm were averaged

Table 5. Table of Defects Indicating by Solid Lines the Wavelength Band with Greatest Contrast and with Dotted Lines the Lowest Contrast Between Areas of Damaged and Undamaged Tissue.

Defect	Center Wavelength		
	540nm	740nm	1010nm
Bitter Pit		———	.....
Blister Spot	———		.....
Botryosphaeria Rot		———	.....
Bruise			———
Chemical		———	.....
Codling Moth		———	.....
Corking		———	.....
Cracking		———	.....
Fly Speck		———	
Frost (early)	———		.....
Hail		———	.....
Leaf Roller		———	.....
Powdery Mildew	———		.....
Puncture			———
Rot		———	.....
Russet	———		.....
Scab		———	.....
Scald			———
Sooty Blotch		———	
Sting	———		.....
Sunburn	———		.....

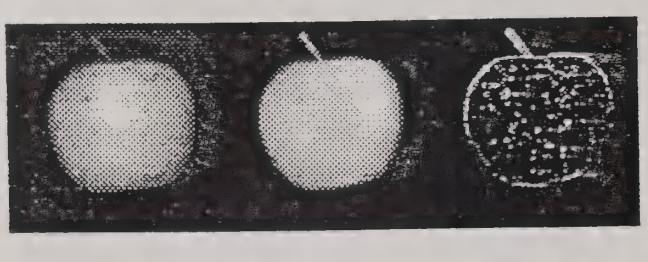

Blister Spot on Golden Delicious

Figure 2. A Golden Delicious Image Captured at 540nm, 1010nm, and the Resulting Image After Subtracting the 540nm From the 1010nm Image, Edge Detection with a Sobel Filter, and Low Pass Filter Using a 7 x 7 Kernel.

together to form a single image with a center wavelength of 540nm and an approximate band width of 50nm. Images captured at a center wavelength of 720nm, 730nm, 740nm, 750nm, and 760nm and a bandwidth of 35nm were averaged together to form a single image with a center wavelength of 740nm and an approximate bandwidth of 60nm. Similarly, images captured at a center wavelength of 990nm, 1000nm, 1010nm, 1020nm, 1030nm and a bandwidth of 35nm were averaged together to form an image with a center wavelength of 1010nm and an approximate bandwidth of 60nm. All images were normalized to an intensity of 220 grey levels.

Figure 2 shows a Golden Delicious apple image with blister spot captured at a center wavelength of 540nm (high defect contrast) and a second image captured at a center wavelength of 1010nm (low defect contrast). For every image where the defect has high contrast and low contrast with undamaged tissue, it is possible after image normalization to subtract the high defect contrast image from the low defect contrast image and apply simple thresholding to the resulting image to segment the defect. Blister spot segmentation starts by the subtraction of an image captured at 540nm from an image captured at 1010nm, but requires the resulting image to be filtered by a Sobel edge detector and low pass filter to remove the lenticels. The size of kernel used in the low pass filter is dependent on the size of blister spots and lenticels (Figure 2). For this group of apples a 7 x 7 kernel size was used.

Bitter pit, botryosphaeria rot, chemical, codling moth, corking, cracking, hail, leaf roller, rot, and scab damage was segmented by subtracting normalized apple images captured at 740nm from images captured at 1010nm and simple thresholding (Figure 3). These defects have a lower intensity value for the defective area at 740nm and an equal or higher reflectance than undamaged tissue for images captured at 1010nm. This wavelength, 1010nm, is near a water absorption band (960nm) in the near-infrared and the loss of internal cell fluid due to the defect is indicated by the higher reflectance than for undamaged tissue.

Bruising, scald, punctures, sooty blotch, and fly speck had grey levels different from undamaged tissue for all of the wavelengths tested. This was also indicated by the Mahalanobis distance which remained high for all near-infrared wavelengths tested with the highest values for wavelengths beyond 960nm. A reference image representing the general background of

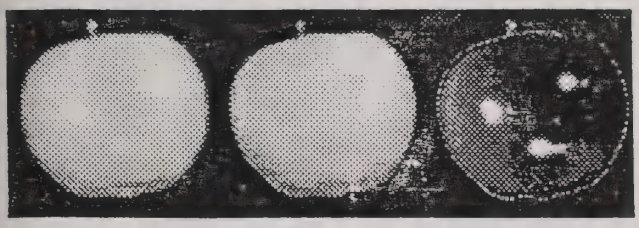

Bitter Pit on Red Delicious

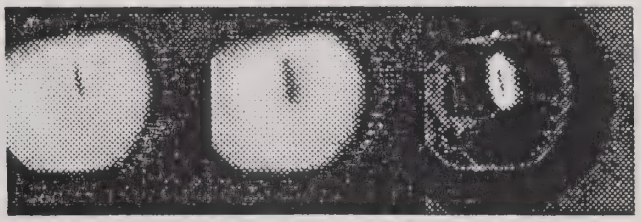

Cracking on Stayman

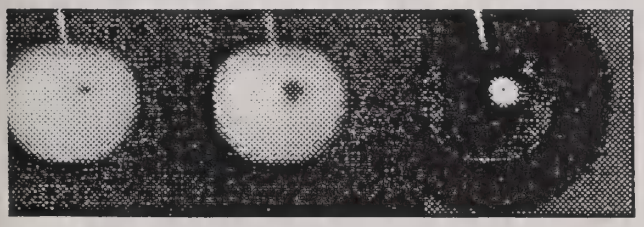

Botryosphaeria Rot on Golden Delicious

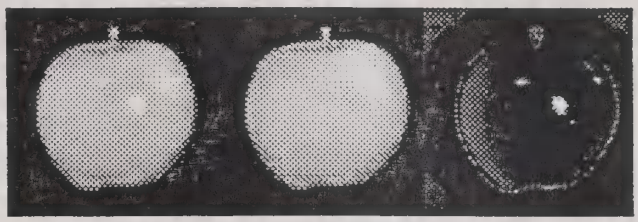

Hail on Red Delicious

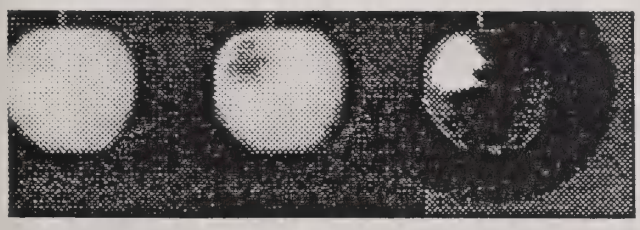

Chemical Spray on Golden Delicious

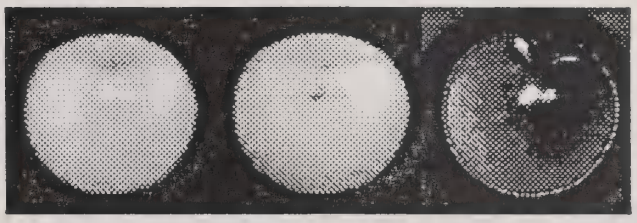

Leaf Roller on Golden Delicious

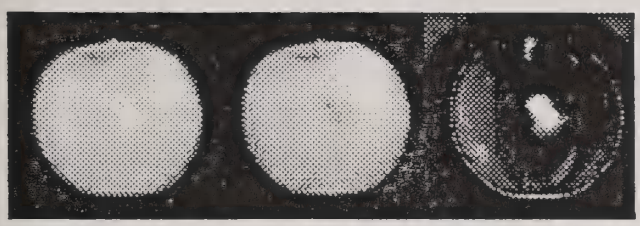

Codling Moth on Crispin

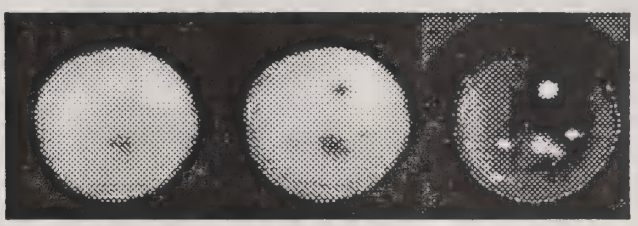

Rot on Crispin

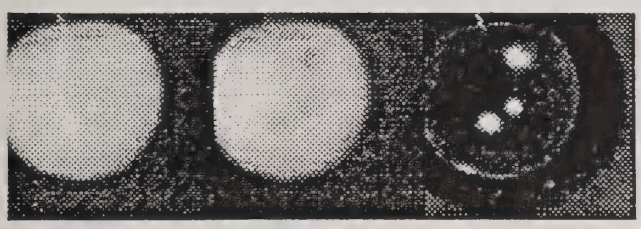

Corking on Golden Delicious

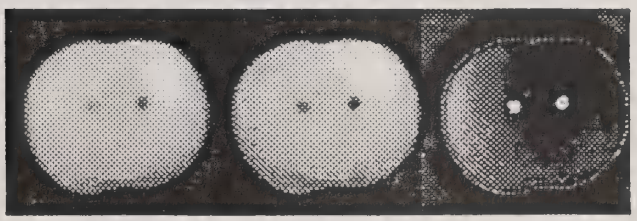

Scab on McIntosh

Figure 3. Images of Apples of Different Cultivars with Different Defects, the First in Each Series of 3 Views is a Low Contrast Image of the Defect Captured at 1010nm, the Second a High Contrast Image of the Defect Captured at 740nm, and the Third a View of the Segmented Defect After Subtraction of View 2 From View 1 and Thresholding.

undamaged tissue was created by capturing and normalizing an image of a teflon cylinder at a wavelength of 1010nm. Because the cylinder was a fixed size and the apples tested were of variable size, the image of the teflon cylinder was logically AND with the apple image captured at 540nm. The resulting image is now the same size as the apple being tested and has grey level values very similar to undamaged tissue. By subtracting apple images captured at 1010nm from this reference image and thresholding, bruising, punctures, scald, sooty blotch, and fly speck were segmented (Figure 4).

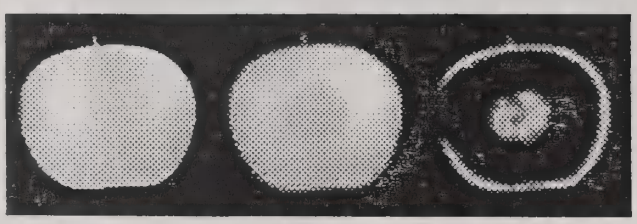

Bruise on Golden Delicious

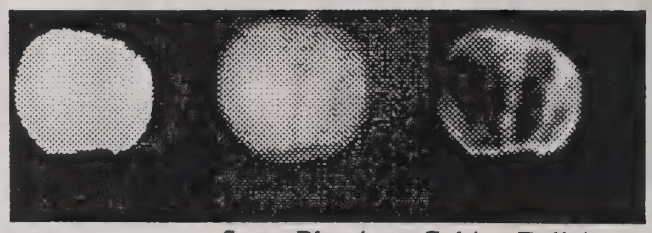

Sooty Blotch on Golden Delicious

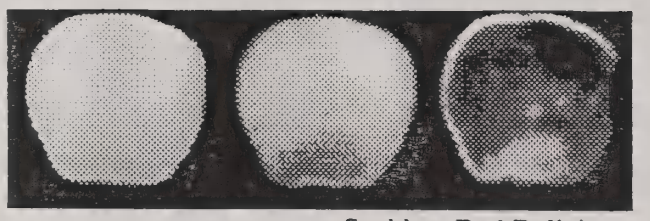

Scald on Red Delicious

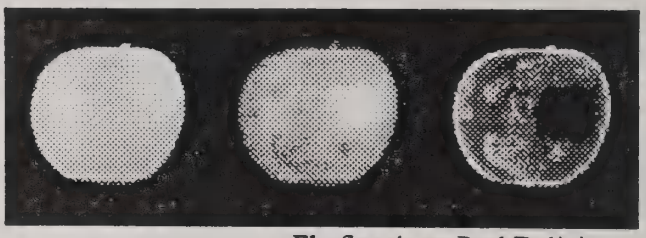

Fly Speck on Red Delicious

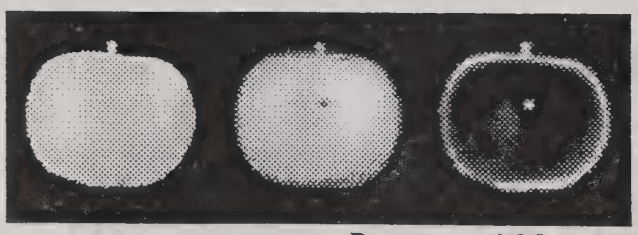

Puncture on McIntosh

Figure 4. Images of Apples of Different Cultivars with Different Defects. The First in Each Series of 3 Views is a Background Reference Image Captured of a Teflon Cylinder at 1010nm and Logically AND with an Image Captured at 540nm, the Second a High Contrast Image of the Defect Captured at 1010nm, and the Third a View of the Segmented Defect After Subtraction of View 2 From View 1 and Thresholding.

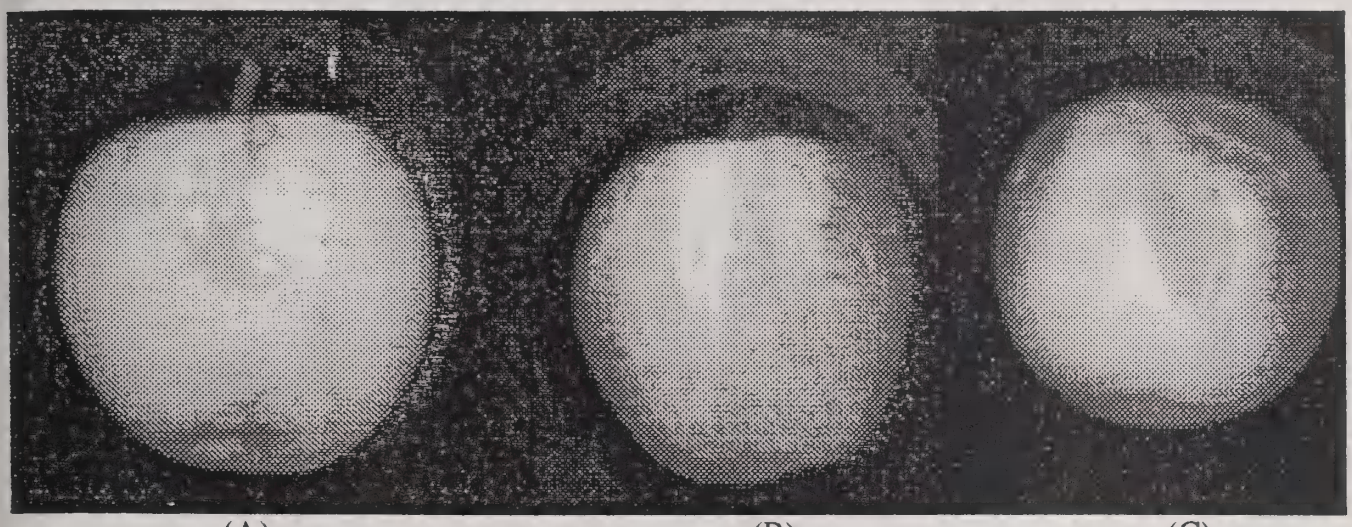

(A) (B) (C)

Figure 5. Images Captured at 540nm of Russet Damage on Golden Delicious (A), Red Delicious (B). and Empire (C) Apples.

Defect segmentation discussed so far has been quite successful because the defects have been of higher or lower contrast than undamaged tissue in the near - infrared wavelengths and variation in fruit color has not been a factor. Russet and defects which appear similar to russet such as early frost damage, insect stings, and powdery mildew are difficult to segment. The defect russet is only skin deep and mainly affects the skin color. For images captured at 540nm, the defect looks brighter than undamaged tissue on red apples while on yellow/green varieties the same defect appears darker than undamaged tissue (Figure 5). For images captured at 740nm and 1010nm, russet appears similar to undamaged tissue. The fact that the damage appears brighter on yellow/green apples and darker on red apples makes this defect difficult to segment on varieties such as Empires which can be both red and green on adjacent surfaces of the apple cheek (Figure 5).

Early insect stings not only may have a russet like appearance, but also can have local shape deformation as well. Figure 6 shows early insect stings with little shape deformation on Red Delicious and Golden Delicious apples but the Crispin apple not only has a patch of russet like cells visible but also is deformed with some pitting in the affected region. The russet areas are not visible in the images captured at 740nm but the pitted areas appear as dark spots.

Segmentation of russet like damage is possible from images captured of monochroic apples. Figure 7 shows segmentation of russet on both Golden and Red Delicious cultivars. The initial image processing for the red and yellow/green colored apples is the same at the start where an image captured at 540nm is subtracted from an image captured at 1010nm. The resulting

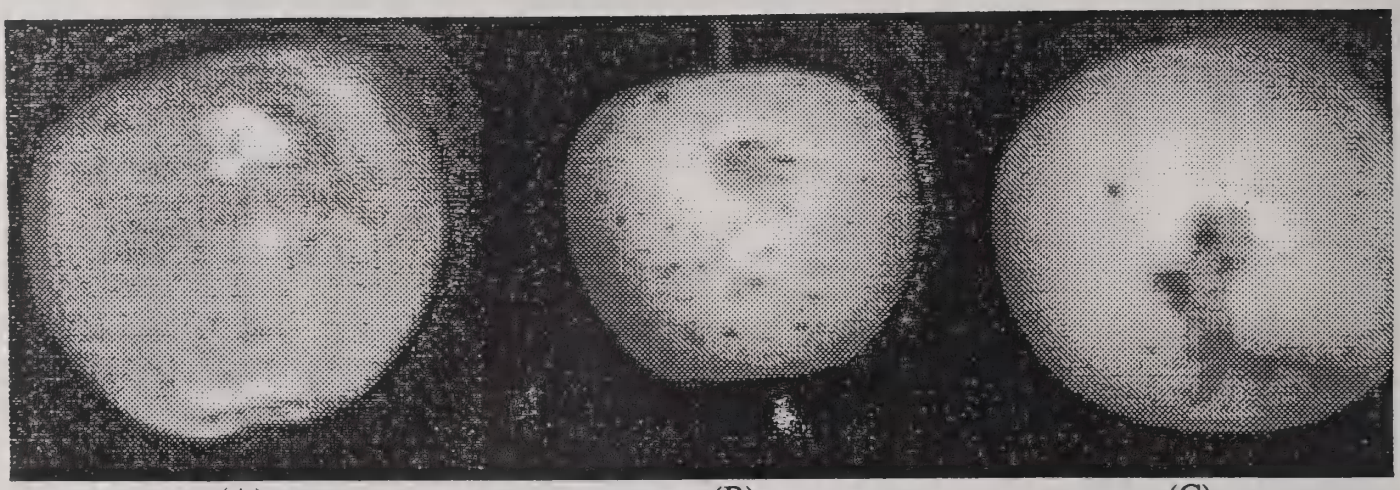

(A) (B) (C)

Figure 6. Images of Early Insect Stings Captured at 540nm on Red Delicious (A), Golden Delicious (B), and Crispin (C).

image is multiplied by a constant and simple thresholding is applied for russet segmentation on yellow/green apples. To segment russet like damage on red colored apples, the resulting image must be subtracted from the teflon reference image described earlier for bruising and simple thresholding applied (Figure 7). The same image process is used for early frost damage and early sting damage for defect segmentation (Figure 7).

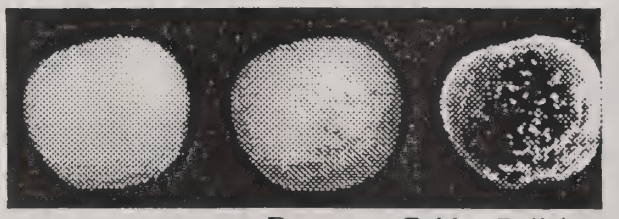

Russet on Golden Delicious

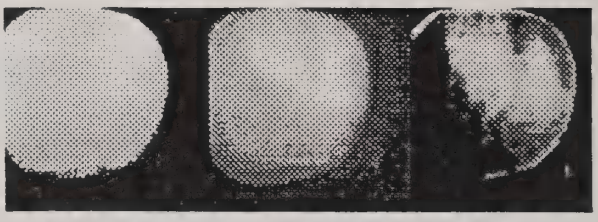

Early Frost Damage on Stayman

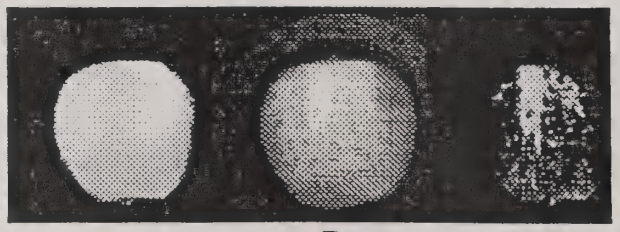

Russet on Red Delicious

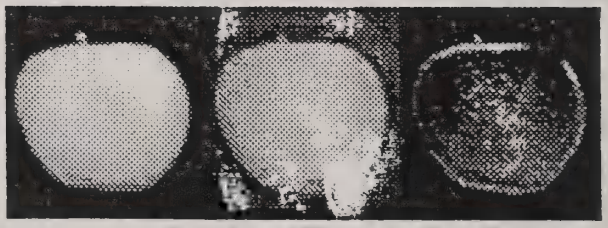

Powdery Mildew on Red Delicious

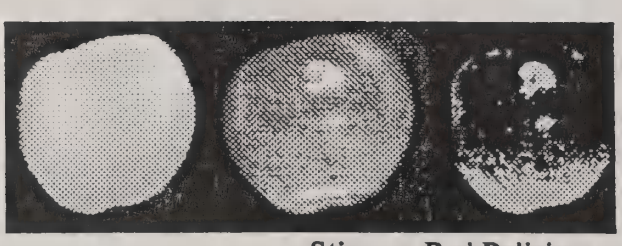

Sting on Red Delicious

Figure 7. Examples of Segmentation of Russet, Insect Sting, Early Frost Damage and Powdery Mildew on Monochromatic Apples.

Sunburn affects the skin color and can be detected in images captured at 540nm. A red apple image captured at 1010nm was subtracted from an image captured at 540nm. The resulting image was multiplied by a constant and logically AND with the 540nm image (Figure 8).

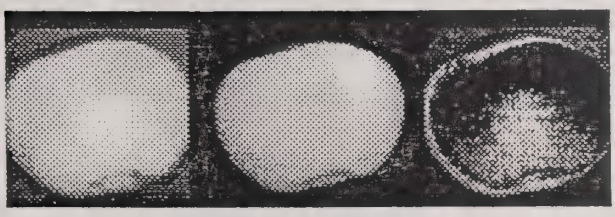

Sunburn on Red Delicious

Figure 8. A Red Delicious Apple with Sunburn Damage Captured at 540nm, 1010nm and the Resulting Image After Logically AND with the 540nm Image.

Conclusions:

Scab, bitter pit, botryosphaeria rot, chemical spray, codling moth, corking, cracking, hail, leaf roller, and rot damage were segmented from undamaged tissue by subtracting a normalized image captured at 740nm from a normalized image captured at 1010nm and simple thresholding. Type of cultivar is not a factor for segmentation.

Blister spot damage can be segmented by subtracting a normalized 540nm image from a normalized 1010nm and filtering with a Sobel and low pass filter kernel. This defect was only tested on green/yellow cultivars.

Bruising, scald, punctures, sooty blotch, and fly speck damage can be segmented by subtracting a normalized image captured at 1010nm from a reference image. The reference image is formed by logically AND of a normalized 540nm image with an image captured at 1010nm of a teflon cylinder. Type of cultivar is not a factor for segmentation.

Russet, early sting, early frost, and powdery mildew damage can be segmented on monochroic apple images captured at 540nm which are subtracted from a normalized image captured at 1010nm. Yellow/green apples are then segmented by simple thresholding. Red apples are subtracted from the teflon reference image described for bruise segmentation before simple thresholding is applied. Segmentation was only possible on monochroic apples.

Sunburn damage on red apples was segmented by subtracting a normalized image captured at 1010nm from a normalized image captured at 540nm and logically AND of the resulting image with the image captured at 540nm. Only had Red Delicious apples with sunburn damage but suspect that monochroic apples are required for segmentation.

References:

1. Aneshansley, D.J., J.A. Throop, and B.L. Upchurch. 1997. Reflectance spectra of surface defects on apples. *Proc. Sensors for Nondestructive testing*. Orlando Florida, Feb. 18-21, 1997. Northeast Regional Agricultural Service, 152 Riley-Robb Hall. Cornell University, Ithaca, NY 14853 pp 143-160.

2. Bittner, D.R. and K.H. Norris. 1968. Optical Properties of Selected Fruit vs. Maturity *Transactions of the ASAE*.11(4): 534-536.

3. Brown, G.K., L.J. Segerlind and R. Summit. 1974. Near-Infrared reflectance of Bruised Apples. *Transactions of the ASAE* 17(1): 17-19.

4. Daharaj, S., S.M. Ananthakrishna and U.S. Gouindarajan. 1970. Apple Quality: Development of Descriptive Quality Profile for Objective Sensory Evaluation. *Journal of Food Quality 4: 83-100.*

5. Dewey, D.H. and T.J. Schueneman. 1971. Quality and Packout of Storage Apples...Their Effects on Costs and Returns. Research report / Michigan State University, Agriculture Experiment Station, 147: 1-6.

6. Fuzzen, D.R. 1981. Parameters for Automatic Bruise Detection in Apples. *M.S. Thesis* University of Guelph.

7. Gerling, W.D. 1980. Cost of Growing and Harvesting Apples in Eastern N.Y. *Proceedings Annual Meeting N.Y. State Hort. Soc*, 126: 44-47.

8. Hohn, E. 1990. Quality Criteria of Apples. Acta Hortic, Wageningen: *International Society for Horticultural Science*, 285: 111-118.

9. Ingle, M. and J.F. Hyde. 1968. The Effect of Bruising on Discoloration and Concentration of Phenolic Compounds in Apple Tissue. *Proc. Amer. Soc. Hort. Sci.* 93: 738-745.

10. Lott, R.V. 1943. Some Spectral Curves of Maturing Apples. *Proc. Amer. Soc. Hort. Sci.* 43: 59-62.

11. Rehkugler, G.E. and J.A. Throop. 1989. Image Processing Algorithm for Apple Defect Detection. *Transactions of the ASAE* 32(1): 267-272.

12. Reid, W.S. 1976. Optical Detection for Skin, Bruise Flesh, Stem, Calyx. *Journal of Agric. Engng. Res.* 21(3): 291-295.

13. Throop, J. A. and D. J. Aneshansley. 1997. Inspection of processed fruit before and after peeling. ASAE Paper No. 976044. St. Joseph, MI.

14. Upchurch, B.L., A. Affeldt, W.R. Hruschka, K. H. Norris, and J.A. Throop. 1990. Spectrophotometric Study of Bruises on Whole Red Delicious Apples. *Transactions of the ASAE* 32(2): 585-589.

ELSEVIER

Postharvest Biology and Technology 10 (1997) 15–19

Postharvest Biology and Technology

Detecting internal breakdown in apples using interactance measurements

B.L. Upchurch [a,*], J.A. Throop [b], D.J. Aneshansley [b]

[a] *USDA-ARS, Appalachian Fruit Research Station, 45 Wiltshire Road, Kearneysville, WV 25430, USA*
[b] *Biological and Agricultural Engineering Department, Cornell University, Ithaca, NY 14853, USA*

Accepted 7 August 1996

Abstract

A technique using body transmittance in the 450- to 1050-nm region was evaluated as a non-destructive technique for identifying apples with internal breakdown. Apples with internal breakdown absorbed shorter wavelengths of light (<750 nm) more than good apples; however, light at longer wavelengths (>750 nm) was absorbed more by good apples than defective ones. A classifier based on the ratio between the light intensity at 720 and 810 nm was used to segregate apples with internal breakdown from good apples. Only 6.3% of the good apples were incorrectly classified; however, bruises on the apples contributed to the incorrect classification of good apples. None of the apples with severe internal breakdown were incorrectly classified. Apples with very slight internal breakdown contributed to most of the 12.0% error of misclassifying defective fruit as good. The number of misclassified apples was reduced by adjusting the cut-off; however, the number of good fruit that would be discarded increased.

Keywords: Light transmittance; Postharvest quality; Apple; Internal browning; Inspection

1. Introduction

Accurate non-destructive techniques for assessing the postharvest quality of fruits and vegetables would be an asset to the industry. Correct decisions about the quality of each item at harvest could reduce the postharvest losses by eliminating the storage and transportation of inferior quality produce. By identifying fruit that are past the optimum stage for long-term storage, these fruit can be marketed early prior to a degradation in quality. A fast non-destructive technique would provide an objective measurement of each fruit; therefore, each fruit would be of similar quality when it reached the consumer.

Internal defects, such as watercore, brown heart, internal browning, internal breakdown, or insect infestation, result in automatic rejection of the apple for fresh market. To identify the presence of internal defects, current practices involve a destructive test on a random sample. Each apple in the sample is cut in half and visually inspected. If an internal defect is present in a certain percentage of the samples, the complete 'lot' is rejected. To date, non-destructive technologies for inspecting the internal condition of each fruit either do not exist or are very limited in functionality and affordability.

A challenge to inspecting for internal defects is identifying a sensing technique that yields a detectable signal after penetrating deep into the product. Chen et al. (1989) used magnetic resonance imaging

* Corresponding author.

PII S0925-5214(96)00057-9

to obtain images of bruises on apples, peaches, pears, and onion, pits in olives and prunes, and worm damage in pears. Although magnetic resonance imaging exhibited positive results, it is costly and slow. Techniques, such as 1-dimensional profiles, are being developed to reduce processing time and costs (Zion et al., 1993). X-rays have been successfully used to detect split pits in peaches (Bowers and Dodd, 1988) and watercore in apples (Tollner et al., 1992).

Light transmittance measurements were used to measure internal defects in fruits and vegetables. Birth and Olsen (1964) and Throop et al. (1989) reported light transmission measurements for distinguishing watercored apples from good ones. Using a machine vision system to measure the light distribution through the apple, Throop et al. (1989) reduced the errors of misclassification caused by high light levels around the stem. The success of this technique was dependent upon the sensitivity of the camera (Throop et al., 1994) and the length of time the apples had been in storage prior to inspection (Upchurch et al., 1994).

Various factors contribute to the development of internal breakdown in apples. This is a term used to describe an internal disorder that is characterized by the browning and softening of the cortex tissue. The failure of the cell membranes to retain phenolic precursors of browning within the vacuole is the cause of browning related to internal breakdown (Porritt et al., 1982). However, the mechanisms behind the cellular disorganization is not fully understood. The accumulation of sorbitol or volatiles is a contributing factor. Accumulation of sorbitol around the vascular bundles is evident in apples with watercore; therefore, watercore apples have a higher probability of developing internal breakdown than good apples (Myers, 1983). High levels of carbon dioxide during storage caused internal breakdown in apples during the 1993 season (Anonymous, 1994; Warner, 1994).

Light transmittance has been the only technique reported for measuring the internal breakdown in fruits and vegetables. An optical density difference between 710 and 800 nm successfully detected internal browning in potatoes (Birth, 1960). Differences in the light transmittance at 600 and 740 nm were used to detect internal browning in apples; however, the technique was unable to detect apples with slight browning (Fukuda and Kubota, 1979).

Marketing apples with internal breakdown can negatively affect consumer acceptance. By inspecting each apple for this defect prior to shipping, only apples with internal breakdown would be rejected. The objective of this research was to evaluate an interactance measurement that could be used to detect the presence of internal breakdown in apples.

2. Materials and methods

'Delicious' apples were hand harvested in late October during the 1994 season from the orchards at the Appalachian Fruit Research Station, Kearneysville, WV. Apples harvested late in the season had a high probability of having watercore at harvest and developing internal breakdown during storage. These apples were stored at 0°C for 6 months which provided ample time for development of internal breakdown. Interactance measurements were recorded for 556 apples. A set of 136 apples were used as a calibration set. After developing the classifier, interactance measurements were recorded on 420 additional apples, and the performance of the classifier was evaluated. Interactance for each apple was measured with the apparatus shown in Fig. 1.

A DC light source and computer-controlled spectrograph provided the necessary instrumentation for recording the spectral content of the light traveling through the apple. The calyx-end of the apple was exposed to the light source by placing each apple on top of a 15 × 15 × 17 cm light box. To reduce the amount of light leaking around the sides of the fruit, a 7.6-cm diameter black sponge with an inverted conical surface was mounted between the light box and calyx of the apple. The calyx-end was illuminated through a 3.2-cm diameter opening at the top of the light box and sponge seal. A 160 VDC source was supplied to the envelope-type tungsten lamp in the light box. This DC voltage eliminated the 60 Hz fluctuations of AC powered light sources and was generated by converting 120 VAC to 160 VDC (4 V pk–pk ripple) by using a 10-A bridge rectifier (GBPC-1005, General Instruments) and an 80-μf 450 VDC capacitor filter (36DX-800F450DC, Sprague).

A fiber optic probe collected the energy exiting through the cheek of each apple. After placing the apple on the light box so that the light entered the

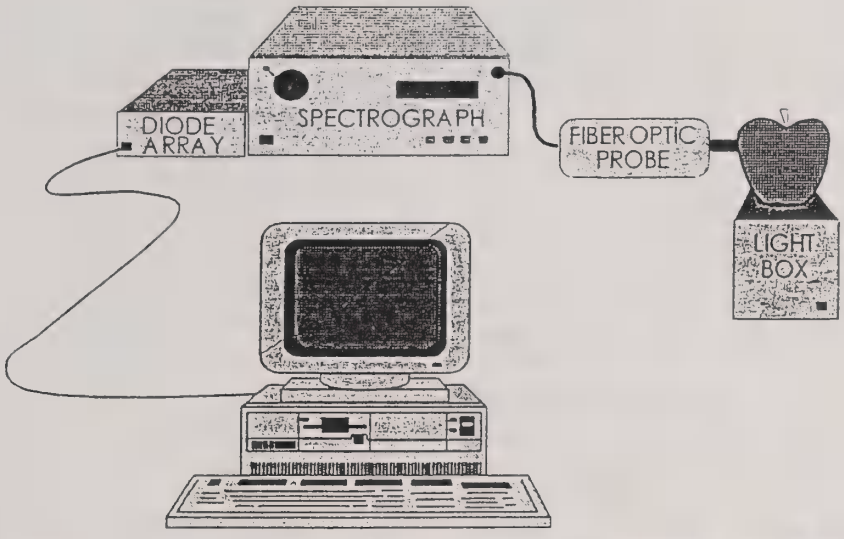

Fig. 1. Apparatus for measuring the spectral composition of the light transmitted through an apple.

calyx end, a 4-mm diameter fiber optic probe was placed in contact with the cheek midway between the stem and calyx ends. The site at which the probe contacted the apple was marked on the peel. Only one site was selected for each apple.

Spectral composition of the light transmitted through the apple was measured in the 450- to 1050-nm region. The other end of the probe was connected to the entrance port on a spectrograph (82-498, Jarrell-Ash). A 150 grooves/mm ruled grating (11-086 985-30-49-40, Jarrell-Ash) in the spectrograph yielded the required wavelength range. The spectral composition of the light exiting the spectrograph was measured with a silicon diode array (TN-6112, Tracor Northern). Extremely low light levels required a 500-μm entrance slit in the spectrograph and a 5-s exposure time for the diode array. This combination of grating and slit yielded a spectral resolution of 12 nm. The signal from the diode array was digitalized by a photodiode array acquisition system (TN-6600, Tracor Northern) with 14-bit resolution.

Each apple spectrum was converted to a percent transmittance prior to analysis. Before measuring the spectra of the apples, the transmittance through an 80-mm diameter Teflon cylinder was recorded as a reference. This measurement was only made once a day. The cylinder was centered on the light box, and the probe mounted 25 mm above the base of the cylinder for the measurement. A percent transmittance was calculated by dividing each apple spectrum by the reference spectrum.

A visual score that was indicative of the internal condition was assigned to each apple. The amount of browning was used as a measure of the internal breakdown. After measuring all apples, each fruit was sliced perpendicular to the stem calyx axis. A subjective score of (0) no, (1) slight, (2) moderate, or (3) severe browning was assigned to each apple. When the region of browning did not extend completely around the cut half, the location of the browning relative to the measurement site was recorded. For apples with no signs of browning, the calyx half of the apple was cut parallel to the core. This cut was essential to insure that no browning occurred around the calyx. If browning was present, a new score of slight browning was assigned. A classifier was developed to segregate the apples with internal breakdown (scores 1–3) from non-defective apples.

3. Results and discussion

Browning of the tissue within an apple affected the spectral content of the light transmitted through the fruit. The average transmission spectrum for each class of the calibration set is shown in Fig. 2. Generally, absorption at wavelengths between 720 and 750 nm was greater for apples with internal browning than apples without the defect. At wavelengths

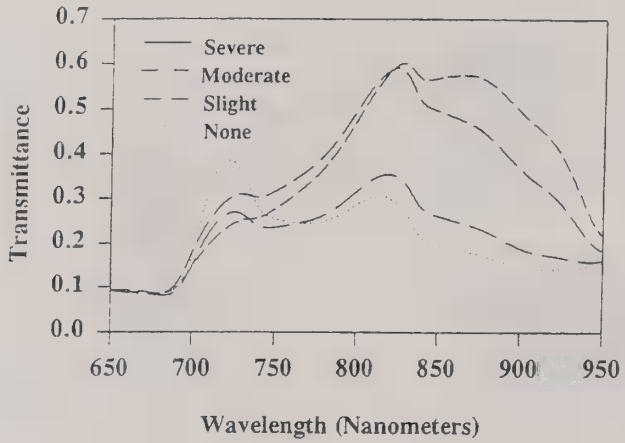

Fig. 2. Average spectral composition of the light transmitted through apples with and without internal browning.

above 750 nm, the transmittance was higher for defective apples. The degree of absorption by the apple was dependent upon the amount of browning present in the tissue.

A classifier for identifying apples with internal breakdown was developed based on the spectral characteristics of the transmittance. From Fig. 2, the amplitude of the transmittance at several wavelengths was dependent upon the internal condition of the apple. To minimize the influence of path length, a ratio between the transmittance at 720 and 810 nm was selected as the feature for discriminating between defective and good apples. The ratio decreased as the amount of browning increased and was correlated ($r^2 = 0.71$) with the degree of internal breakdown. Analysis of variance and subsequent mean separation with confidence intervals of the data ($F = 221.2$, $P < 0.0001$, ANOVA, SAS/LAB, SAS Institute, Inc., SAS, 1992) revealed three distinct classes, no browning, slight, and moderate/severe browning (Table 1). A lack of difference between the moderate and severe browning class could be attributed to the assignment of the subjective score.

A classifier based on the transmission ratio was developed for identifying apples with internal breakdown. Using the 95% confidence intervals for the class means (Table 1), apples with a ratio greater than or equal to one were classified as good apples, while any apple with a ratio less than one was classified as defective. The ratio feature was the performance of the classifier based on the ratio is

Table 1
Confidence intervals for the four classes of apples with and without internal browning. Scores represent the degree of internal browning (0, none; 1, slight; 2, moderate; and 3, severe) assigned to the calibration set

Score	Number of samples	95% Confidence interval[a]
0	28	1.24: 1.36 (a)
1	36	0.74: 0.85 (b)
2	53	0.49: 0.58 (c)
3	19	0.36: 0.51 (c)

[a]Confidence intervals with a different letter are significantly different at the 95% confidence level.

Table 2
Classification errors associated with separating apples into two classes, no internal browning and internal browning, using a feature based on the ratio between the transmittance at 710 and 820 nm. An apple with a ratio equal to or greater than 1.0 was classified as a good apple, while any apple with a ratio less than 1.0 was classified as defective

	Predicted good	Predicted brown
Actual good	237	16
Actual brown	20	147

shown in Table 2. Since any amount of browning would result in rejection of the apple, all of the apples with internal browning were combined into a single class. No effort was made to distinguish between the classes of browning. Only 16 out of the 253 (6.3%) good apples were misclassified as having browning, while 20 out of the 167 apples (12.0%) with browning were misclassified as good fruit.

Different factors contributed to the errors of classification. Some of the apples had large bruises in the vicinity of the region where the measurements were taken. Due to light scattering within the apple, browning within bruised tissue had a similar effect on the spectrum when the bruise was located within 45° of the site. Five of the sixteen good apples that were misclassified had large bruises. Classifying defective apples as good could be very costly. For the 20 apples identified as good, only 2 apples had a moderate browning score. The remaining 18 apples had very slight browning in a small area away from the site where the measurement was taken. Very slight browning is very difficult to detect if the damaged tissue is not located in the vicinity of the

measurement. A single measurement site was capable of detecting small areas of brown tissue provided the defective region was within 45° of the measurement site. By increasing the cut-off between classes, apples with slight browning would be correctly classified at the expense of increasing the percentage of good apples that would be rejected.

Transmittance is a non-destructive technique for identifying apples with internal breakdown; however, the technique is difficult to implement into an on-line inspection system. The integration time (5 s) required to improve the signal-to-noise ratio in the signal is too long for real-time inspection that requires less than 100 ms to measure the product. This time could be reduced by increasing the output of the light source; however, an increase in the output of the lamp causes an increase in the heat produced. There are techniques available to block the thermal energy while passing the shorter wavelengths. For apples, light must enter through the calyx end. Sufficient light transmittance by scattering was achieved only when the calyx end of the apple was directly illuminated. Differences between classes were reduced when the cheek of the apple was illuminated and the energy exiting the fruit was measured at the calyx (unpublished data, 1994). The integration time had to be increased to 10 s to improve the signal-to-noise ratio. Without knowing the orientation of the apple, this technique would not be reliable for detecting internal breakdown in apples.

4. Conclusions

Apples with internal breakdown were distinguished from good apples using a ratio of the transmittance at 720 and 810 nm. Setting a threshold of 1.0 for the ratio, only 6.3% of the good apples were misclassified. Bruises on these apples were the major contributor toward misclassifying good apples. Over 12.0% of the defective apples were classified as good; however, the tissue in most of these apples only had a brown tint or the browning was confined to a small area away from the measurement site.

References

Anonymous, 1994. Maturer Fugi more at risk for internal browning. Good Fruit Grower, 45(5): 27.

Birth, G.S., 1960. A nondestructive technique for detecting internal discolorations in potatoes. Am. Potato J., 87(2): 53–60.

Birth, G.S. and Olsen, K.L., 1964. Nondestructive detection of watercore in Delicious Apples. Proc. Am. Soc. Hort. Sci., 85: 74–84.

Bowers, S.V. and Dodd, R.B., 1988. Nondestructive testing to determine internal quality of fruit. Am. Soc. Agric. Eng., Paper No. 88–6569.

Chen, P., McCarthy, M.J. and Kauten, R., 1989. NMR for internal quality evaluation of fruits and vegetables. Trans. ASAE, 32(5): 1747–1753.

Fukuda, H. and Kubota, T., 1979. Nondestructive measurement of chlorophyll, watercore, and internal browning disorders in apple fruits by light transmission. Kaju Shikenjo: Bulletin of the Fruit Tree Research Station, 6(225): 27–34.

Myers, S.C., 1983. Watercore and internal browning in apples. Virginia Fruit, LXXI(9): 9–15.

Porritt, S.W., Meherink, M. and Lidster, P.D., 1982. Postharvest disorders of apples and pears. Publication 1737/E, Agriculture Canada, pp. 14–15.

SAS, 1992. SAS/LAB Software: User's Guide, Version 6. SAS Institute, Inc. Cary, NC.

Throop, J.A., Rehkugler, G.E. and Upchurch, B.L., 1989. Applications of computer vision for detecting watercore in apples. Trans. ASAE, 32(6): 2087–2092.

Throop, J.A., Aneshansley, D.J. and Upchurch, B.L., 1994. Camera system effects on detecting watercore in 'Red Delicious' apples. Trans. ASAE, 37(3): 873–877.

Tollner, E.W., Hung, Y.C., Upchurch, B.L. and Prussia, S.E., 1992. Relating x-ray absorption to density and water content with apples. Trans. ASAE, 35(6): 1921–1928.

Upchurch, B.L., Throop, J.A. and Aneshansley, D.J., 1994. Effects of storage duration on detecting watercore in apples using machine vision. Trans. ASAE, 37(2): 483–486.

Warner, G., 1994. Braeburn growers search for cause of brown heart. Good Fruit Grower, 45(5): 26, 59.

Zion, B., Chen, P. and McCarthy, M.J., 1993. Image analysis technique for detection of bruises in magnetic images of apples. ASAE Paper No. 93-3084, St. Joseph, MI.

United States Patent *5,855,270*
Throop , et al. **January 5, 1999**

Fruit orienting device

Abstract

A fruit or other produce orienting device, particularly suited for orienting apples, orients a piece of fruit with its stem axis horizontal so that it can undergo quality inspections. The device employs a cylindrical drive roller which engages the fruit on one side, and causes it to rotate, and a pair of freely rotating orienting rollers which engage the fruit across from the drive roller, and cause the fruit to achieve the desired orientation as it rotates. The first orienting roller is cone shaped with a tapered flat or concave surface so that it will steer the fruit toward the second, opposing roller, which has a thin disk shaped portion with a front surface that engages the fruit. The front surface of the disk shaped portion tends to align itself with the flat edge of the fruit at its stem or calyx end, and this causes the rotating fruit to be oriented quickly with its stem axis parallel to the roller axes, and then maintains the fruit in the correct orientation once it is achieved.

Inventors: **Throop; James A.** (Newfield, NY); **Aneshansley; Daniel J.** (Ithaca, NY); **Upchurch; Bruce L.** (Springfield, GA)

Assignee: **Cornell Research Foundation, Inc.** (Ithaca, NY); **U.S. Dept. of Agriculture** (Washington, DC)

Appl. No.: **735511**

Filed: **October 23, 1996**

Current U.S. Class: **198/394**; 198/387; 198/779; 209/912
Intern'l Class: B65G 017/32
Field of Search: 198/384,385,387,779 209/538,912

References Cited [Referenced By]

U.S. Patent Documents

Re26111	Nov., 1966	Amori	198/385.
2296645	Sep., 1942	Marsden	198/779.
2907440	Oct., 1959	Hait	198/387.
3011620	Dec., 1961	Amori	198/387.
3225892	Dec., 1965	Keesling	198/382.
3389730	Jun., 1968	Anderson et al.	198/436.
3403769	Oct., 1968	Anderson et al.	198/384.
3460668	Aug., 1969	Gerrans	198/779.
3575292	Apr., 1971	Roda	209/912.
3738474	Jun., 1973	Ellis	198/385.
4005774	Feb., 1977	Casanova Valero	198/384.
4169528	Oct., 1979	Amstad	198/385.
4482061	Nov., 1984	Leverett	209/912.
4706797	Nov., 1987	Carlson	198/394.
4730719	Mar., 1988	Brown et al.	198/387.
4746001	May., 1988	Tichy	198/387.
4981205	Jan., 1991	Cowlin	198/387.
5190137	Mar., 1993	Tas	198/779.

Foreign Patent Documents

591035	Jan., 1960	CA	198/387.
617769	May., 1961	CA	198/387.

Other References

Rehkugler, G. E. et al., "Apple Sorting With Machine Vision", Transactions of the ASAE Amer. Socity of Agricultural Eng., vol. 29(5), Sep.-Oct. 1986, pp. 1388-1397.
Rehkugler, G. E. et al., "Optical-Mechanical Bruised Apple Sorter", ASAE Publication 1-76, Quality Detection in Foods, American Socity of Agricultural Eng., Dec. 1974, 5 pages.

Primary Examiner: Bucci; David A.
Assistant Examiner: Tran; Thuy V.
Attorney, Agent or Firm: Jones, Tullar & Cooper

Goverment Interests

The present invention was made with Government support under Grant No. 58-1931-3-001, awarded by the USDA-ARS. The Government has certain rights in the invention.

Parent Case Text

This application is a continuation-in-part of application No. 08/491,805, filed Jun. 19, 1995, now abandoned.

Claims

What is claimed is:

1. A device for orienting generally spherical shaped objects having a longitudinal axis comprising:

a) a drive roller for engaging and rotating an object to be oriented;

b) a first orienting roller spaced from said drive roller and positioned parallel thereto, said first orienting roller having an outer end diameter larger than an inner end diameter, and an outer periphery thereof forming a tapered object engaging surface; and

c) a second orienting roller spaced from said first orienting roller, said second orienting roller having a disk shaped portion with a front surface for engaging an object to be oriented;

wherein, said drive roller and said first and second orienting rollers are positioned to engage a generally spherical object in three locations, and cause orientation of the object with its longitudinal axis in a generally horizontal direction.

2. The object orienting device of claim 1, wherein said drive roller is disposed for rotation on a first shaft, and said first and second orienting rollers are disposed for rotation on a second shaft which is spaced from, and parallel to, said first shaft.

3. The object orienting device of claim 2, wherein said first and second shafts are spaced from one another by approximately 4 to 5 inches.

4. The object orienting device of claim 2, wherein said first orienting roller has an inner end diameter of approximately 2 inches.

5. The object orienting device of claim 4, wherein said first orienting roller has an outer end diameter of approximately 3 inches.

6. The object orienting device of claim 2, wherein said first and second orienting rollers are spring loaded on said second shaft toward each other.

7. The object orienting device of claim 2, wherein said first orienting roller has a concave outer surface.

8. A method for orienting generally spherical shaped objects so that a longitudinal axis of each of said objects is disposed in a generally horizontal position comprising the steps of:

a) providing a rotatable drive roller for engaging and rotating an object to be oriented;

b) providing first and second spaced orienting rollers for engaging and orienting an object being rotated by said drive roller, said first and second orienting rollers being positioned for rotation about a common axis that is spaced from and parallel to a rotational axis of said drive roller, said first orienting roller having a tapered outer surface with an inner end diameter smaller than an outer end diameter, and said second orienting roller including a disk shaped portion with a flat front surface facing said first orienting roller;

c) engaging and rotating an object to be oriented with said drive roller; and

d) simultaneously engaging said object with said tapered outer surface of said first orienting roller and said flat front surface of said second orienting roller, wherein said tapered outer surface tends to direct said object into said flat front surface, and thereby cause orientation of said object with its longitudinal axis in a generally horizontal position.

Description

BACKGROUND OF THE INVENTION

The present invention relates in general to a fruit orienting device for use with automatic sorting equipment that properly positions fruit or other produce, such as apples, for quality inspections.

Considerable effort has been placed on developing nondestructive sensor techniques for sensing the internal and surface quality of apples. Examples of these techniques include optical imaging systems for detecting bruises and other surface defects on the apples, and firmness testing devices which determine the firmness of an apple by tapping its surface, and sensing resulting acoustic vibrations therein. To work properly, both of these techniques require that the tests be performed on the apple's cheek. In the optical imaging technique, this requires that the imaging system be able to discriminate between the bruises or other surface defects, and the apple's stem or calyx.

One known technique for discriminating between surface defects and the stem or calyx is to employ complicated algorithms which can differentiate the concave surfaces around the stem/calyx ends from blemishes on the rest of the convex apple surface. Unfortunately, the use of such complicated algorithms slows down the apple sorting process, and this is unacceptable because the fruit packing industry requests that apples must be sorted at rates of 6-10 apples per second.

A more promising solution to this problem is to orient the apples prior to being imaged so that only the apple cheeks will be viewed by the imaging optics. This usually necessitates that the apples be oriented on a conveying device with their stem axes horizontal so that the apples can be rolled beneath the imaging optics, first for a preinspection for proper orientation with a reroute of improperly oriented fruit back to the beginning of the orientation process, and then for an inspection of the apple cheeks for bruises and other surface defects. This appears to be the most promising technique, for it eliminates the need for time consuming complex algorithms. In addition, this technique must be employed with firmness measuring devices and other quality measuring devices since such devices do not employ any optical means by which the cheek of the apple can be discriminated from the stem or calyx.

Unfortunately, all previously known techniques for orienting apples so that their stem axes are horizontal do not reliably orient the apples in the desired manner. For example, one known device employs a plurality of rollers which contact an apple at three locations on its surface. One of the rollers is a

cylindrical roller that is driven to cause the apple to rotate so that its entire surface can be viewed by the imaging system. The other two rollers are positioned adjacent to the cylindrical roller on a common shaft, and are cone shaped with tapered apple engaging surfaces that tend to hold the apple between these two rollers. Although this device is capable of orienting various types of apples with their stem axes in a horizontal direction, it does not do so quickly and dependably, and often cannot maintain the proper orientation if and when it is achieved.

SUMMARY OF THE INVENTION

In view of the foregoing, it is the object of the present invention to provide an improved fruit orienting device which can quickly and dependably orient pieces of fruit, particularly apples, with their stem axes in a horizontal direction.

This and other objects of the invention are achieved through provision of an orienting device which comprises a drive roller for engaging a generally spherical piece of fruit or other produce on one side and causing it to rotate, and a pair of freely rotating orienting rollers that are positioned adjacent the drive roller in such a manner that they also engage the fruit. The first of the orienting rollers is cone shaped with one end diameter being larger than its other end diameter, thereby forming a tapered outer engaging surface that tends to direct the fruit into engagement with the second roller. Preferably, the outer surface of the roller is concave to better accommodate the spherical shape of the object (e.g. fruit or other produce) to be oriented, although the outer surface can also be flat and still produce good results. The second roller is disk shaped with a front engaging surface that contacts the flat edge of the fruit adjacent one of its ends. Both of the orienting rollers are preferably spring biased toward one another to allow lateral movement for varying sizes of fruit.

In contrast with the previously discussed known apple orienting device in which the two orienting rollers both comprise opposed cone shaped rollers, the use of the disk shaped roller in conjunction with the roller having the tapered concave or flat engaging surface in the present invention results in substantially improved orientation speed, accuracy and maintenance. This is because the disk roller's front surface forms a contact surface which can align itself with the fruit edge at the stem/calyx ends, thus providing quick horizontal orientation of the fruit, and stability to the revolving fruit once oriented.

BRIEF DESCRIPTION OF THE DRAWINGS

The features and advantages of the present invention will become more apparent from the following detailed description of a preferred embodiment thereof, taken in conjunction with the accompanying drawings in which:

FIG. 1A is a top view of a fruit or other produce orienting device constructed in accordance with a preferred embodiment of the present invention;

FIG. 1B is a front elevation of the fruit orienting device of FIG. 1A showing its rollers engaging a properly oriented apple;

FIG. 2 is a side view of the device of FIGS. 1A and 1B;

FIG. 3 is another top view of the device of FIG. 1A showing its rollers engaging a properly oriented apple;

FIG. 4 is a schematic illustration of a fruit conveyer employing a plurality of the orienting devices of

FIGS. 1-3;

FIGS. 5A and 5B are graphs illustrating experimental results obtained using the concave surfaced roller variation of the preferred embodiment of the present invention to orient apples, with FIG. 5A illustrating the percentage of apples properly oriented as a function of time for five different types of size 128 apples being rotated at 60 rpm, and FIG. 5B illustrating the percentage of apples properly oriented as a function of time for five different types of size 88 apples rotated at a speed of 60 rpm;

FIGS. 6A and 6B are graphs illustrating additional experimental results obtained using the concave surfaced roller variation of the preferred embodiment of the present invention to orient apples, with FIG. 6A illustrating the percentage of apples oriented from an axis of rotation perpendicular to the stem/calyx axis to an axis of rotation about the stem/calyx axis as a function of time for five different types of size 128 apples, and FIG. 6B illustrating the same results for five different types of size 88 apples;

FIGS. 7 and 8 are graphs illustrating experimental results obtained using flat surfaced roller variation of the preferred embodiment of the present invention to orient apples, with FIG. 7 illustrating the percentage of apples properly oriented as a function of time for five different types of apples and FIG. 8 illustrating the percentage of apples maintaining their proper orientation as a function of time; and

FIGS. 9 and 10 are graphs illustrating experimental results obtained using a known apple orienting device, with FIG. 9 illustrating the percent of apples correctly oriented as a function of time for five different types of apples, and FIG. 10 illustrating the percent of apples maintained in the correct orientation as a function of time.

DETAILED DESCRIPTION OF THE PREFERRED EMBODIMENT

Turning now to a detailed consideration of a preferred embodiment of the present invention, FIGS. 1-3 illustrate a fruit or other produce orienting device 10 comprising a cylindrical drive roller 12 which is rotated by a power source, such as a motor (not shown), through a drive belt 14. The cylindrical drive roller 12 preferably has a soft resilient (e.g. padded) surface, and is mounted on a first horizontal shaft 16. Preferably it has a length (e.g., 3.75 inches) that is somewhat greater than the typical height of the fruit to be oriented (e.g., an apple).

First and second orienting rollers 18 and 20 are mounted for free rotation on a second horizontal shaft 22, which is positioned parallel to the first shaft 16, and is spaced therefrom by a distance of preferably approximately 4-5 inches. The first orienting roller 18 is cone shaped with an inner end diameter 24 that is preferably approximately 2 inches, and an outer end diameter 26 that is preferably larger, for example, approximately 3 inches, thereby forming a tapered peripheral or outer engaging surface 27 which is tapered in the direction of the second orienting roller 20. The thickness of the cone shaped roller 18 is preferably approximately 1 inch. Preferably, the outer engaging surface 27 is concave in shape as illustrated to better accommodate the spherical shape of the fruit or other produce to be oriented, thereby further improving the orienting performance of the device 10 when used to orient cultivars, for example, which are difficult to orient. Alternatively, the outer engaging surface 27 can be flat as illustrated by the dashed lines in FIG. 1A, and still provide good results as discussed below in conjunction with FIGS. 7 and 8.

The second orienting roller 20 has a disk shaped portion 28 having a diameter approximately equal to that of the outer diameter 26 of the cone shaped roller 18. The disk portion 28 includes a rounded edge 30, and has a thickness of approximately 3/16 inches. A front, flat engaging surface 32 is formed generally perpendicular to the axis of the second horizontal shaft 22 for engaging the surface of the fruit to be

oriented. Preferably, both of the rollers 18 and 20 are spring loaded toward each other by a pair of compression springs 33 of equal length and spring rate which allow lateral movement for varying sizes of fruit.

As illustrated in FIGS. 2 and 3, the particular spacing and arrangement of the drive roller 12 and orienting rollers 18 and 20, enables the drive roller 12 to engage an apple 34 or other generally similar shaped object to be oriented and rotate the same, while the orienting rollers 18 and 20 engage the apple 34 on a generally opposite side thereof. As also illustrated in FIG. 3, the front engaging surface 32 of the disk shaped portion 28 is designed to engage one of the flat shoulder portions 35 of the apple 34 positioned adjacent its stem or calyx ends.

The two roller shafts 16 and 22 are fixed at their opposite ends to first and second conveyor chains 38. As illustrated in FIG. 4, a plurality of the devices 10 are preferably incorporated into a conveying apparatus 40 which conveys a plurality of pieces of fruit to be inspected past a sensor device 44, which by way of example can be an imaging device for visually inspecting the apple cheeks, a firmness testing device or any other device for sensing the apple's condition.

In operation, randomly oriented apples are conveyed onto a plurality of the devices 10, where they are each engaged at three locations on their surfaces by the drive roller 12 and the orienting rollers 18 and 20 of their corresponding device. As the apple is rotated by the drive roller 12, the cone shaped roller 18 tends to move the apple into engagement with the disk shaped roller 20. When this occurs, the apple has a tendency to seek a position where its largest diameter (its width) engages the drive roller 12 and one of its ends (stem or calyx) contacts the disk shaped roller 20, with the axis of rotation for the fruit lying along its shortest dimension, which is the apple's height. Because of these tendencies, the front engaging surface 32 of the disk shaped roller 20 tends to align itself with the flat edge of the apple at either the stem or calyx ends, and provides stability to the revolving apple once it is oriented.

Experiments were conducted to compare the orientation success rate of the preferred embodiment of the present invention using both concave and flat surfaced orienting rollers with that of the previously discussed known apple orienting device. The results of these experiments are illustrated in FIGS. 5-10, with FIGS. 5A, 5B, 6A and 6B illustrating the results obtained with the preferred embodiment of the present invention using a concave orienting roller, FIGS. 7 and 8 illustrating the results obtained with the preferred embodiment of the present invention using a flat surfaced orienting roller, and FIGS. 9 and 10 illustrating the results obtained using the known orienting device.

FIGS. 5A and 5B illustrate that the orienting device 10 with the concave surfaced orienting roller was able to orient 95 to 100% of various sizes of Cortland, Empire, Fuji, Jonagold, McIntosh and Rome apples within approximately 0.2 minutes. FIGS. 6A and 6B illustrate the experimental results obtained with various sizes of apples that are known to be difficult to orient because of a greater variation in both size and shape, including Golden Delicious, Granny Smith, Crispin, Red Delicious and small Galla apples. With the exception of large Granny Smith and Crispin apples, successful orientation was achieved 60 to 82 percent of the time.

Experiments were also conducted using the flat surfaced orienting roller variation of the preferred embodiment which performs well when used to orient the less difficult to orient types of apples. As illustrated in FIG. 7, the flat surfaced roller variation correctly orients the stem/calyx axis into the horizontal position (parallel to the axis of roller rotation) of Cortland, Jonagold, Idared and Empire apples 88 to 100% of the time, and within 12 seconds. Once oriented, the device 10 is virtually 100% successful at maintaining the proper orientation of the apples as illustrated in FIG. 8.

In contrast, experiments with the known orienting device employing a pair of opposed cone shaped rollers, indicate in FIG. 9 that this technique is successful at properly orienting the various types of apples 73-95% of the time after a period of 16-18 seconds. In addition, once the apples were oriented, many of them lost their orientation within 10 seconds as illustrated in FIG. 10.

It should be pointed out that neither the flat surfaced roller embodiment of the present invention nor the known orienting device were particularly successful at orienting Red Delicious apples as can be noted from a careful inspection of the graphs in FIGS. 7-10. This is because many Red Delicious apples tend to have an elongated pear shape with a much different fruit diameter at the stem end than at the calyx end, and the calyx end of this type of Red Delicious apple does not present a good shoulder surface for the flat surface 32 of the disk roller 20 to engage. However, as discussed above in conjunction with FIGS. 6A and 6B, the concave surfaced roller variation of the preferred embodiment works considerably better at orienting Red Delicious, and other difficult to orient, apples.

In conclusion, the present invention provides an improved fruit orienting device that is particularly suited for orienting fruit or other produce, such as apples, about to undergo a quality inspection. The device provides a substantially greater orientation success rate, achieves the proper orientation in less time and better maintains the orientation once achieved than any previously known fruit orientation devices. This is particularly significant when the device is employed with automatic apple sorting devices which must inspect large quantities of apples for bruises and other defects, and sort the apples accordingly in a fast, efficient and dependable manner.

Although the present invention has been disclosed in terms of a preferred embodiment, it will be understood that numerous other modifications and variations could be made thereto without departing from the scope of the invention as defined in the following claims. For example, although the invention is designed specifically for orienting fruit, specifically apples, it will be understood that it can also be employed for orienting other similarly shaped produce, such as vegetables. In fact, the present invention can be employed for orienting any generally spherical shaped object having some type of asymmetry, such as a stem, defining a longitudinal axis.

* * * * *

Paper No. 993205
An ASAE Meeting Presentation

Inspection Station Detects Defects on Apples in Real Time

by

J. A. Throop, D. J. Aneshansley

Cornell University, Department of Agricultural and Biological Engineering, Ithaca, NY 14853

B. Anger
USDA-ARS Appalachian Fruit Research Station
Kearneysville, WV 25430

Written for Presentation at the
1999 ASAE/CSAE-SCGR Annual International Meeting

Sheraton Centre
Toranto, Ontario, Canada
July 18-21, 1999

Summary: A design and implementation of a multispectral inspection station is presented. Apple images at four different wavelengths are captured through a common aperture. Design features include lighting, chromatic aberration correction, flat-field correction, apple presentation and conveyance, and defect segmentation. Example images at 4 wavelengths are shown with the results of defect segmentation.

Keywords: Apples, Apple Quality, Defects, Defect Detection, Image Analysis, Image processing, Automated Inspection, Grading

Acknowledgments: This project is supported in part by USDA Cooperative Agreement 58-1931-5-019 with the ARS-USDA Appalachian Fruit Research Station, Kearneysville, WV, and by the Agricultural Experiment Station at Cornell University with Hatch Regional Project NE179 and Hatch Project 412. Special thanks to Donald Peterson, Project Coordinator at ARS-USDA Appalachian Fruit Research Station, for his guidance and advice. Thanks also to Doug Caveney, Cornell University, and Scott Wolford, ARS-USDA Appalachian Fruit Research Station, for their fabrication knowledge and construction skills that make this research possible.

ABSTRACT

A design and its implementation are presented for an automatic apple defect sorting system utilizing elements from 25 years of past research. The design included methods for apple orientation, conveyance, and presentation to a camera at five apples per second.

Special optics and filters allow image capture of apple reflectance using three wavelength bands with center wavelengths of 540nm, 750nm, and 960nm and bandwidths of approximately 60nm. A fourth image captured included all visible and near infrared wavelengths that the camera array could detect. The camera captured all four images simultaneously through a common aperture device with selected optical filters added to obtain the desired wavelengths.

Lighting was designed to provide diffuse lighting at the required wavelengths to match the relative response of optics, filters, camera, and apple reflectance. This required the addition of compact fluorescent lamps to increase light for the 540nm wavelength.

A method for defining and capturing 6 regions of interest per apple as multiple apples conveyed laterally and rotated through the camera's field of view was presented.

Imaging software captured the regions of interest and applied flat-field correction to correct apple reflectance variation caused by surface curvature and lighting variation across the field of view. Average reflectance intensity was used to set threshold levels for defect segmentation. The size and shape of the segmented pixel clusters were used to select clusters that represented defects.

Example images of the four wavelength bands and the segmented defects were presented.

BACKGROUND

Past research has developed many of the elements required to construct a high-speed system for apple defect detection. Elements include apple orientation, stem/calyx identification, lighting, defining reflectance spectral characteristics, camera/optics design, and image processing.

Apple Orientation:

Placing the stem/calyx ends of an apple in a known position eliminates the need to locate them during the defect detection process. The stem/calyx regions can appear similar to defects on the apple surface making it difficult to differentiate from defects. One device consisted of a rotating inverted conical shaped transport cup with a hole in the bottom through which a small wheel rotated while contacting the fruit. When the stem or calyx moved to a position over the wheel, contact with the apple surface ended leaving the apple oriented with the stem/calyx in a vertical position (Keesling, 1965,

Rehkugler et. al. 1976). The apple was in the bottom of the cup making viewing of the apple surface difficult.

Current bicone roller conveyors were found to orient Red Delicious apples from Washington State to an axis of rotation passing through both the stem and calyx. Most varieties grown in other parts of the country tended to rotate about an axis perpendicular to the stem/calyx axis. A new device consisting of a vertical disk and a cone roller with a concave shape spring loaded towards each other in combination with a powered rotating padded cylindrical roller was built to convey apples while they oriented (Throop et. al., 1995, 1997, 1999). The device oriented 95% to 100% of Cortland, Empire, Jonagold, McIntosh, Rome, and small Fuji. Golden Delicious, Granny Smith, Crispin, and Gala oriented 60% to 82% of the time. The resulting apple position of the apple rotating about an axis passing through the stem/calyx regions was conducive for viewing the apple surface for defects.

Stem/Calyx Identification:

A method using two images: one image of the apple using diffuse lighting and a second using structured light distinguished the stem and/or calyx from other defects based on the curvature of the laser lines. However, no information was provided to describe conditions causing the algorithm to fail in the identification process (Yang, 1993,1996). A study using a structured light consisting of nine parallel lines of light found that identification errors increased to as high as 20% as the stem/calyx position moved towards the outer edges of the apple image (Campins et. al., 1997).

Lighting:

Lighting for manual sorting of apples has been and continues to be an issue in packing houses. Having enough light that is both diffuse to reduce glare and with the correct wavelengths aids workers in the sorting process (Brown, 1991). Automatic optical inspection of fruits and vegetables requires lighting system design that match the reflectance properties of the physiological character of the desired product and the performance characteristics of the optical system elements (Affeldt et. al., 1993).

Reflectance Spectral Characteristics:

Knowledge of the spectral reflectance properties of apples and their many defects define the design parameters of the lighting and the camera/optic systems. The reflectance spectra of 21 defects found on 10 apple cultivars were captured for wavelengths between 460nm and 1030nm in 10nm increments using an electrically adjustable filter. The Mahalanobis distance was used as a measure to find the greatest contrast between defect and undamaged tissue reflectance. Three wavelength bands 60nm wide with center wavelengths of 540nm, 740nm, and 1010nm provided that contrast for most defects (Aneshansley et. al. 1997, Throop et. al., 1997). The visible images captured for these studies did not include a near-infrared blocking filter for the adjustable visible filter. A new study undertaken in 1998-1999 has found a fourth wavelength band at 650nm that should be included (Unpublished Data, 1999). Images in this paper will not include this wavelength since apples with appropriate defects are not available until the 1999 harvest.

Camera/Optics Design:

The use of the response characteristics of a silicon sensor array in combination with filters to form an optical system sensitive to particular wavelengths has been used experimentally for bruise detection (Graf, 1981,1982). Optimizing lighting with respect to the camera response can maximize contrast between bruised and undamaged regions (Throop et. al., 1993). Knowledge of light wavelength emission and reflectance spectral characteristics is required to select the appropriate camera array response and filter combination. Transmission characteristics of the filter and lens also are important in optimizing sensory response, that is, matching the reflectance properties of the physiological character of the product and the performance characteristics of the optical/camera system (Affeldt et. al., 1993).

Image Processing:

Considerable effort has been used to expedite the segmentation of defects from the undamaged background of apple images. Most effort has been directed at bruise detection where the change in gray level intensity between bruised and undamaged tissue is less than 10%. A multivariable statistical classifier of each pixel in an apple image classified bruised from undamaged tissue (Graf et. al., 1981, 1982). A decrease in processing time and improved performance was found for a non-statistical processing approach. A low-pass filter was applied to the original image. The original gray level image was subtracted from the low-pass filtered image and the resulting image is thresholded to form a binary image. A form of contour - following is applied to each segmented cluster of pixels and a dimensionless measure of shape called the thinness ratio is found. Thresholding the thinness ratio selects the pixel clusters from the segmented image that are counted as damage (Throop, et. al., 1988). This processing method was applied to other defects besides bruising (Rehkugler et. al., 1989). Investigation of three methods of contour following for computational efficiency and accuracy of predicted pixel cluster area and perimeter length found that the method presently selected was best (Sagi et. al., 1991). Further research added processes to segment stored bruises whose reflectance had changed to greater than undamaged tissue. An experimental method for estimating gray level threshold values and minimum values for shape factor was found (Throop et. al., 1995). Images of the same apple at three wavelength bands 50nm – 60nm in width with center wavelength of 540nm, 740nm, and 1010nm were processed in a similar manner to segment 22 different defects found on 10 different apple cultivars (Throop et. al., 1997).

Combining the design elements into a machine capable of sorting apple defects at 5 apples per second is the subject of this paper.

OBJECTIVES

1. Present a design and its implementation for the inspection of apples incorporating the elements from past research with present day technology.

2. Discuss problems encountered in this process.

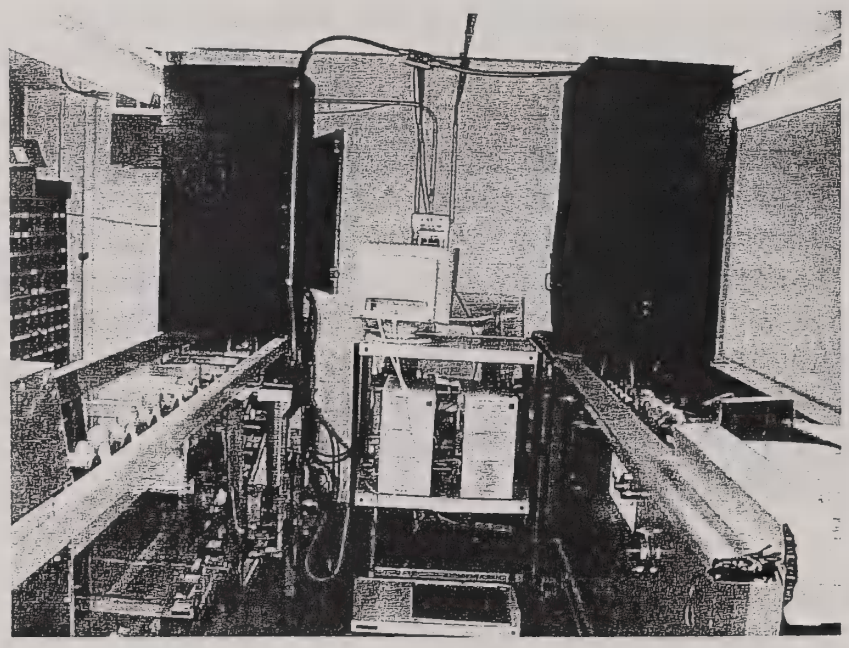

Figure 1. System 1 (right) using conventional bicone roller conveyor and system 2 (left) using an experimental conveyor.

MATERIALS AND METHODS

Apple Conveyance and Presentation:

Two conveying and orienting systems were developed to present apples to the camera in an oriented position with an axis of rotation common with an axis passing through the stem/calyx ends. Two systems were designed to accommodate orientation for different apple cultivar shapes.

System 1 used a typical bicone roller conveyor that orients elongated apples such as Red Delicious from Washington State. Agri-Tech Inc., Woodstock, VA, loaned the device to the research project (Figure 1). Modifications to the system included variable speed control of the linear travel speed of the conveyor and the rotational speed of the bicone rollers(253G-200E, Dart Control Inc., 6Z410, Datyon Electric Co.). Fiber optic sensors were added to the conveyor to trigger the camera when the apple was correctly positioned(FE5F-1MC6S-M, Honeywell Microswitch, Minneapolis, MN).

System 2 was built at Cornell University and could orient York, Stayman, Cortland, Empire, Fuji, Jonagold, McIntosh and Rome apples. It incorporated a new device consisting of a vertical disk and a cone roller with a concave shape spring loaded towards each other in combination with a powered rotating padded cylindrical roller described in the background (Figure 1). Variable speed control of the linear travel speed of the conveyor, variable speed control of the rotational speed of the bicone rollers, and fiber optic sensors similar to the first system were also added.

Image Capture System:

A scientific grade digital camera was selected that images at 30 frames per second with spatial resolutions of 1024x1024x12 bits (SMD-1M30, Silicon Mountain Design, Colorado Springs, CO). The camera was interfaced to the PCI computer bus by an image capture card with 4 MB VRAM (Raptor, Bitflow Inc., Woburn, MA). Data enters a 32-bit RS422 digital port that can be externally triggered at up to 40MHz. Dual ported 4 MB memory allows the host to access data during acquisition. The host was a 533MHz clocked 21164A Alpha processor equipped desktop computer using a Durango II motherboard with 4 MB cache and 512 MB memory with a Windows NT operating system (Aspen Systems Inc., Wheat Ridge, CO). Image capture and processing software was a custom version of QUANTIM software (ZEDEC Technologies, Morrisville, NC).

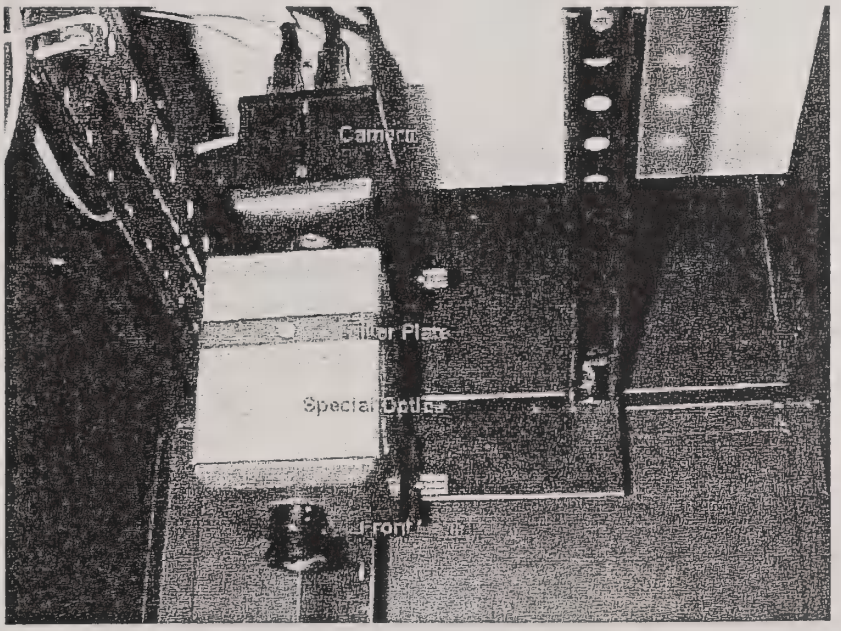

Figure 2. Common aperture device with a 6.5mm lens mounted on the front and the camera behind.

Filters and Optics:

A common aperture device was placed before the camera to project four spectral images of the apple on the single focal plane of the camera array (MSAI-04V, Optical Insights, LLC, Tucson, AZ). This device enabled simultaneous capture of spectrally discrete real – time images with a single camera (Figure 2). A 6.5mm high resolution Monofocal CCTV C-mount lens was mounted in front of the common aperture device (23FM65, Tamaron Industries, Farmingdale, NY). An F-mount to C-mount adapter coupled the device to the camera. The filter plate was fitted with four 2.54cm diameter holes to fit interference filters for the selected wavelength bands. Filter 1 was a green additive dichroic with 50% transmission starting at 505nm and ending at 575nm (CA-550-F, Corian Corp., Franklin, MA). Since this filter passes near-infrared, an infrared

cutoff filter was added (D53710, Edmund Scientic, Barrington, NJ). Filter 2 had a center wavelength of 750nm and a bandwidth of 65nm (750 IF 65, Cheshire County Optical Inc., Jaffrey, NH). Filter 3 was a long wave pass filter with a cut-on/off wavelength of 950nm (950FH90-25, Andover Corp., Salem, NH). Filter 4 initially passed all wavelengths. Neutral density filters were added as needed to normalize image intensity for the different wavelengths (ND010R/25, ND050R/25, ND070/25, Maier Photonics Inc., Manchester Center, VT)(03 FNG 040, Melles Griot, Irvine, CA). While design was underway for the machines, it was discovered that the visible wavelength data from the variable filter for measuring the spectral reflectance characteristics included near-infrared wavelengths. The previous test should have included a filter to block near infrared wavelengths. This information was not specified clearly in the filter documentation requiring a second set of images to be captured. A fourth wavelength band with a center wavelength of 650nm was discovered (Unpublished Data, 1999). In the future Filter 4 will have a center wavelength of 650nm and a 40nm bandwidth (650 IF 40, Cheshire County Optical Inc., Jaffrey, NH). Filter 2 and filter 4 were ordered with painted edges in place of standard metal ring mountings.

Lighting

A custom designed fixture composed of five 100W soft white incandescent lamps (Osram Sylvania, Danvers, MA) alternately spaced between four compact fluorescent lamps (DULUX EL23W, Osram Sylvania, Danvers, MA). A diffuser cut from 1.59mm thick white teflon sheet (Teflon TFE, Ain Plastics, Mount Vernon, NY) was applied on the conveyor side of a pair of fixtures for each machine (Figure 3). The incandescent lamps were powered by variable rectified AC voltage. Constant 115 volts AC powered the compact fluorescent lamps.

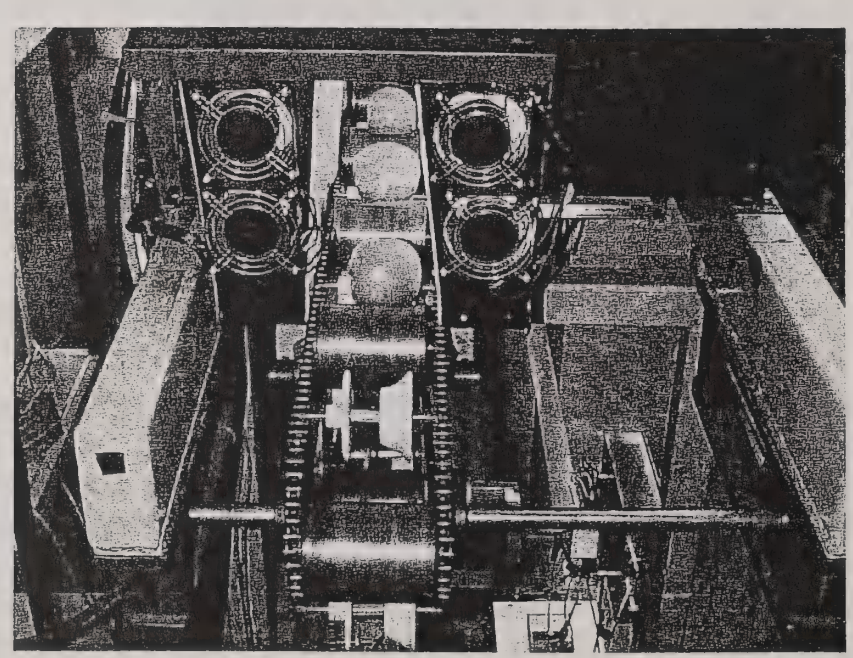

Figure 3. Custom lighting fixtures positioned on each side of the experimental conveyor.

RESULTS AND DISCUSSION

Relative System Response

Lighting, filter selection, and camera response all had to be considered together in order to obtain high quality images at the desired wavelengths. The relative response of the camera, transmitance of the filters, and light output from the incandescent and compact fluorescent lamps were graphically plotted for wavelengths between 400nm to 1000nm (Figure 4). The fluorescent lamps were added to increase the amount of available light in the 540nm bandwidth to counter the low camera response and incandescent lamp

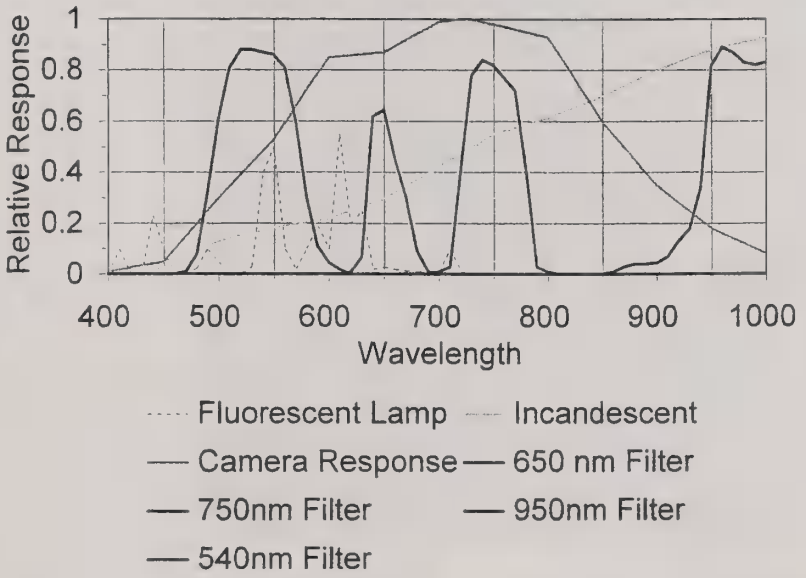

Figure 4. Graph showing the relative response for the different components that formed the imaging system.

emission in that range of wavelengths. The incandescent lamp's increasing emission as the wavelength increases supplied ample light for the 960nm wavelength even with the low camera response.

Region of Interest

Apples were conveyed through the camera field of view rotating about an axis passing through the stem/calyx ends. With the apples oriented to this position, it is possible to view most of the apple cheek with a single camera. This eliminates the stem/calyx ends from being identified as defects and enables placement of other cameras attuned to inspect the stem/calyx regions. Present research is currently focused on the apple cheek.

As the rotating apple passes through the 355.6mm field of view, images of 6 regions of interest across the field of view and around the rotating apple's perimeter are captured. The position of the six regions of interest must be established with respect to the conveyor position, the camera array position and the rotational speed of the apple. This

positioning process starts with the spatial location of an optical sensor monitoring the apple's position on the conveyor that provides an external trigger signal to the camera for image capture. Three white Delrin spheres 76.2mm diameter are placed adjacently

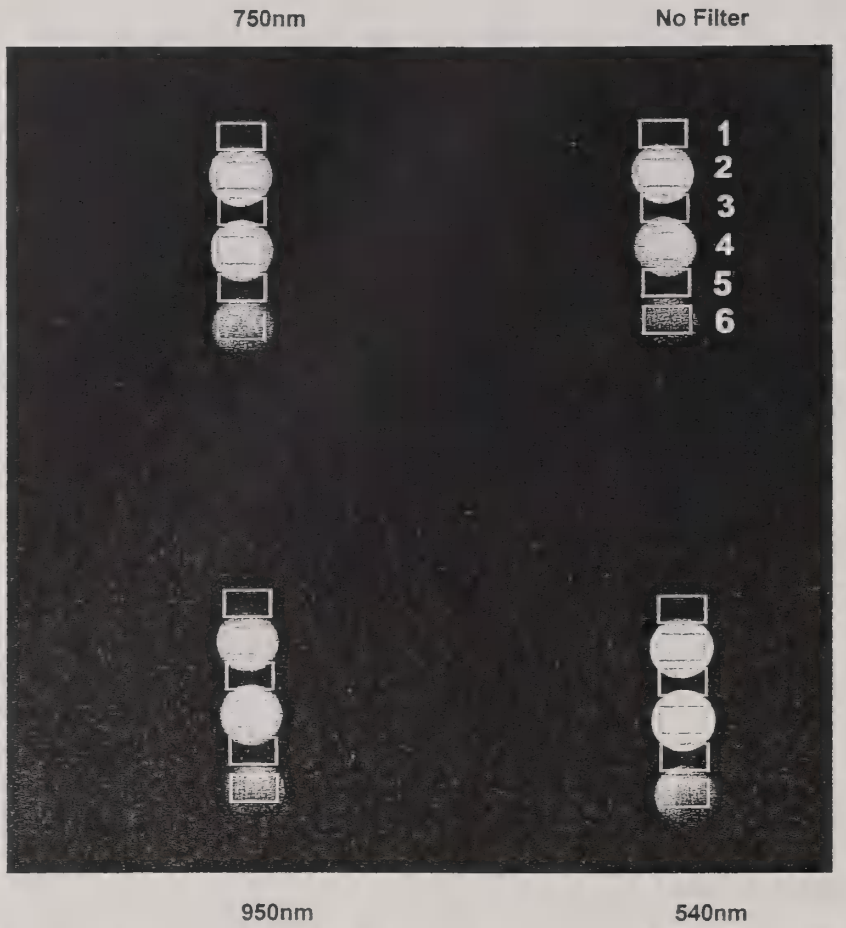

Figure 5. Simultaneous capture by the camera array of the three Delrin spheres passing through the field of view for the four wavelength bandwidths. Starting at the upper left quadrant of the image and rotating clockwise, the center wavelengths are 750nm, all wavelengths, 540nm, and 950nm respectively. The six regions of interest are drawn automatically centered on the spheres.

on the moving conveyor. Images of the spheres are captured as they passed through the camera's field of view at a distance of 578mm from the optics/camera (Figure 5). Software centers the six regions of interest on the Delrin spheres and the size of the regions are set based on the size of the apples to be inspected. The location of each region of interest is stored in a file and can be manually edited for fine-tuning if necessary. As apples pass through the camera field of view, pixel data from the six regions of interest are captured and displayed adjacent to each other. The resulting image depicts the reflectance for each wavelength band of the total apple surface excluding the stem/calyx ends. Although not implemented, the stem/calyx ends can be imaged by a single frame capture by separate miniature cameras during the time traveling past the initial camera.

Images are captured of a Teflon sphere with a black tape stripe every 60 degrees. If the proper rotational speed is set, the black stripe will appear at approximately the same

location in each region of interest. With proper spatial registration for each image at different wavelengths, only black lines without white edges or white lines without black edges will appear in the images formed by subtraction of various image pairs (Figure 6).

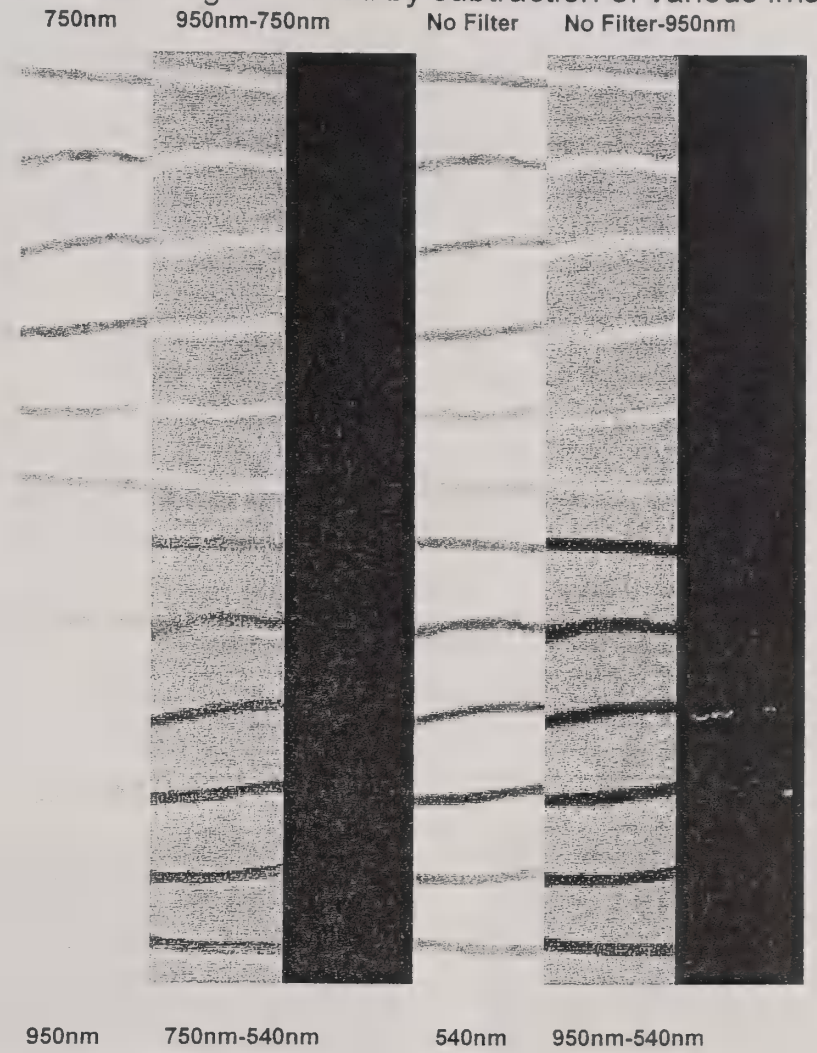

Figure 6. Image of Teflon sphere with tape stripe every 60 degrees checking for spatial and rotational alignment.

Flat Field Correction

An image of a white Teflon sphere 76.2mm diameter is captured for the four wavelength bandwidths. The image is used to manually place neutral density filters in combination with the bandpass filters making the gray level output for the Teflon reflectance normalized to 200. The gray level readings for a row of pixels across a region of interest for any wavelength band were found to be nearly uniform (Figure7). The gray level readings for a column of pixels read across all six regions of interest showed the curvature of the Teflon sphere as each region of interest boundary was crossed (Figure 8). If it is assumed that the teflon sphere approximates the reflectance of undamaged tissue on apples, an inversion of the Teflon image can be added to every apple image captured for flat field correction. The gray level readings across 6 regions of interest for an apple image for the 750nm wavelength after applying flat field correction as described no longer show the curvature of the apple at the boundaries of the regions of

interest (Figure 9). This simplifies the thresholding process while segmenting apple defects.

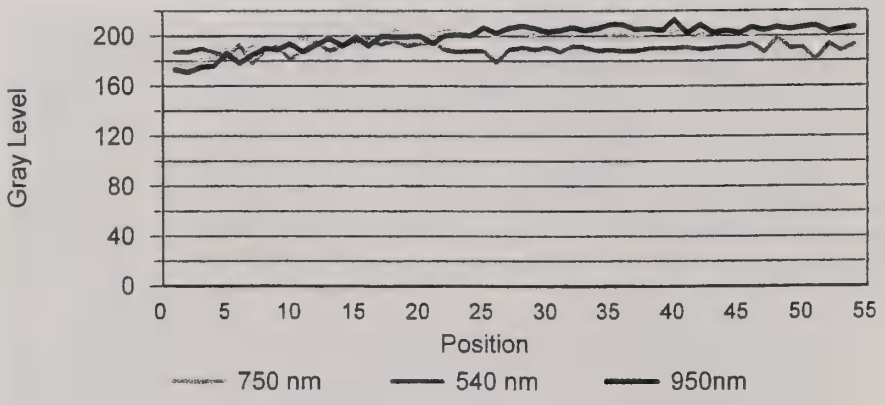

Figure 7. Plot of the camera output in gray level for a row of pixels across one region of interest.

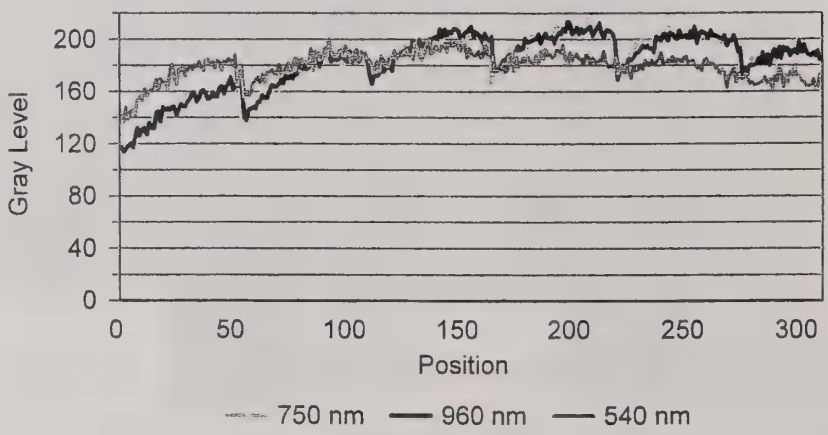

Figure 8. Plot of the gray level intensity of a column of pixels selected across all 6 regions of interest from an image captured of a teflon sphere.

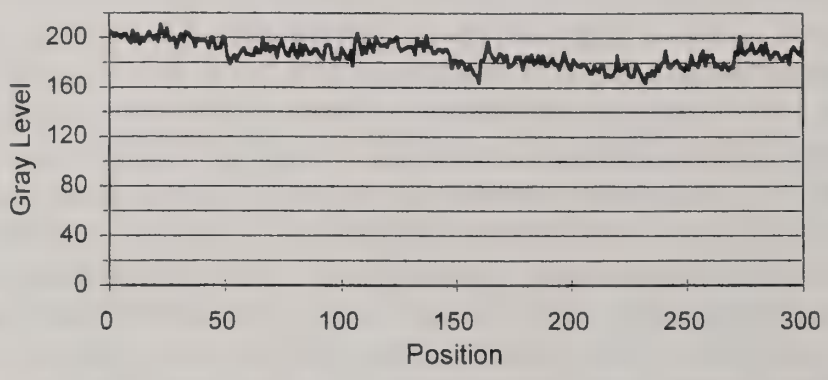

Figure 9. Plot of the gray level intensity of a column of pixels selected across 6 regions

of interest captured of an apple with flat field correction applied by adding the pixel values of the same regions of an inverted image captured of a teflon sphere.

Special Optics Adjustments

The special optics from Optical Insights were difficult to align and keep in alignment. The position of the images would not stay spatially matched between array quadrants and were difficult to readjust. The F-mount to C-mount adapter did not allow enough flexibility for alignment with the camera and was removed and replaced by two telescopes sleeves. The construction of the mounting box was poor and did not keep the vertical mounting plates holding the lenses and prism rigid and parallel. In addition, it was difficult to correctly position the filter plate when removed to add additional neutral density filters. The mounting box was reconstructed from aluminum plate with parallel slots machined to align the edges of the mounting plates. Adjustment screws in the x and y direction were added to center and lock the prism mounting plate and the filter holding plate in the optical path between the input and output lenses.

Chromatic Aberration

The index of refraction is a function of the materials forming the optical path and wavelength. As wavelength increases, the index of refraction decreases for the same

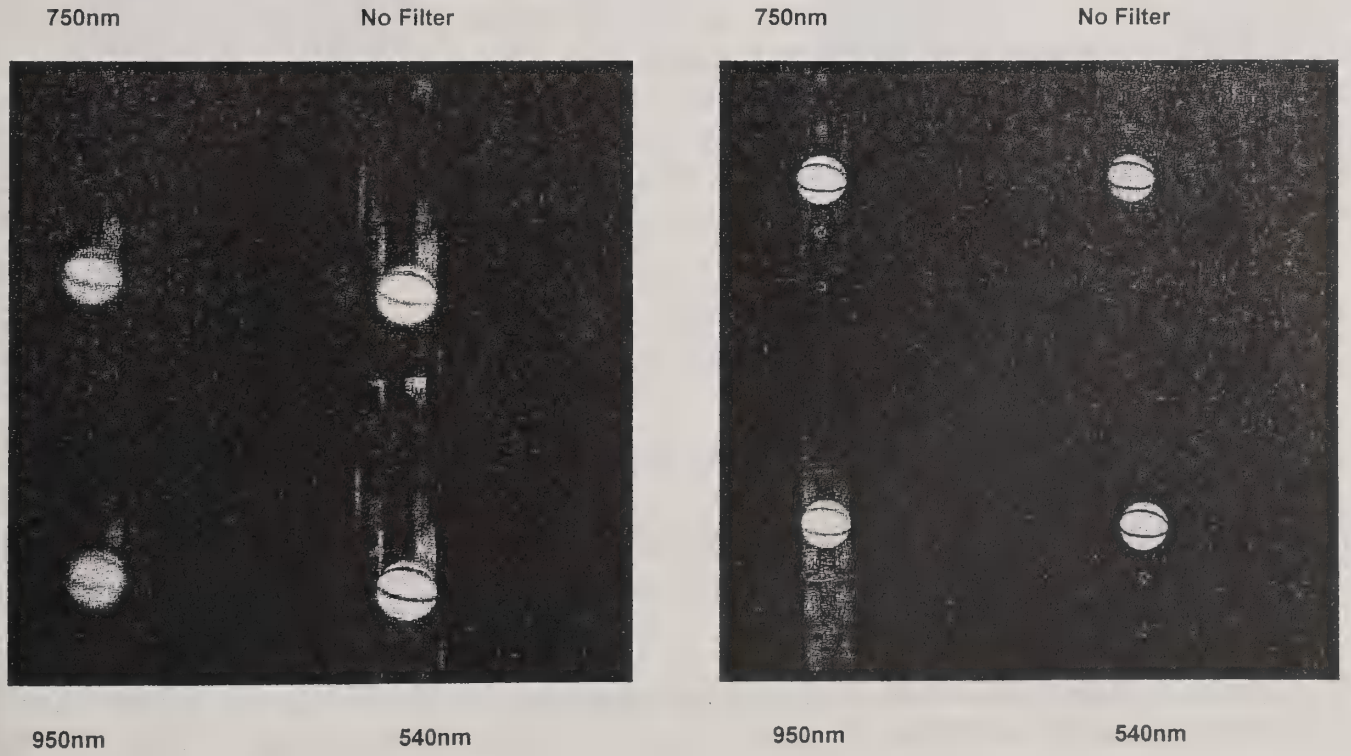

Figure 10. Image of Teflon sphere with a black stripe before (left) and after (right) chromatic aberration correction.

optical path. The index of refraction for the 540nm wavelength is higher, thus this image is focused closer to the rear lens of the special optics and further away from the camera array than images for 950nm wavelength (Figure 10 left). By adding elements that decrease the index of refraction for the shorter wavelengths, the focus point for the shorter wavelengths can be made to coincide with the 960nm wavelength (Figure 10 right).

Camera Adjustments

The SMD-1M30 camera provided 12-bit intensity resolution while 8-bit resolution was considered adequate. If the exposure exceeded 255 gray levels (8-bit) the lower 8 bits of interest would be set to 0 and bit 9 would rise to 1. The result was that if the camera saturated higher than 8 bits the image would darken instead of remaining at a saturated gray level of 255. Silicon Mountain Design provided additional interface circuitry to hold the gray level at 255 for the saturated condition. They also factory adjusted the camera gain to maximize sensitivity and to match each camera used in system1 and system 2.

Image Capture and Defect Segmentation

Images are captured and processed in a time period of 150ms. The machine with the commercial bicone roller conveyor can have as many as three apples in the camera's 355.6mm field of view during a single frame capture. This means that regions of interest for 3 different apples most be stored for every frame capture. Each apple passing through the field of view has a total of six regions of interest stored of its surface from six different frame captures. The machine with the experimental conveyor has a blank conveyor area between each apple reducing the flow rate by nearly one-half.

The processing steps are as follows:

1. Capture Image.
2. Add or Subtract Combinations of Images for Different Wavelengths.
3. Find Average Gray Level.
4. Adding +/- Value to Average Gray Level to Set High/Low Intensity Threshold.
5. Threshold Defect.
6. Erode or Dilate as Required.
7. Measure Segmented Defects.
8. Threshold Defects Based on Size or Shape Factors.
9. Record to File Defect Size in Pixels or Percent of Total Surface Area.

The processing steps are applied on images from any of the four wavelength bands. The processing can be tuned to look for expected specific defects or defects common on a particular cultivar. Some defects were easily segmented and were visible in more

blush on its cheek, some defects in the 540nm wavelength band can be masked by the coloring.

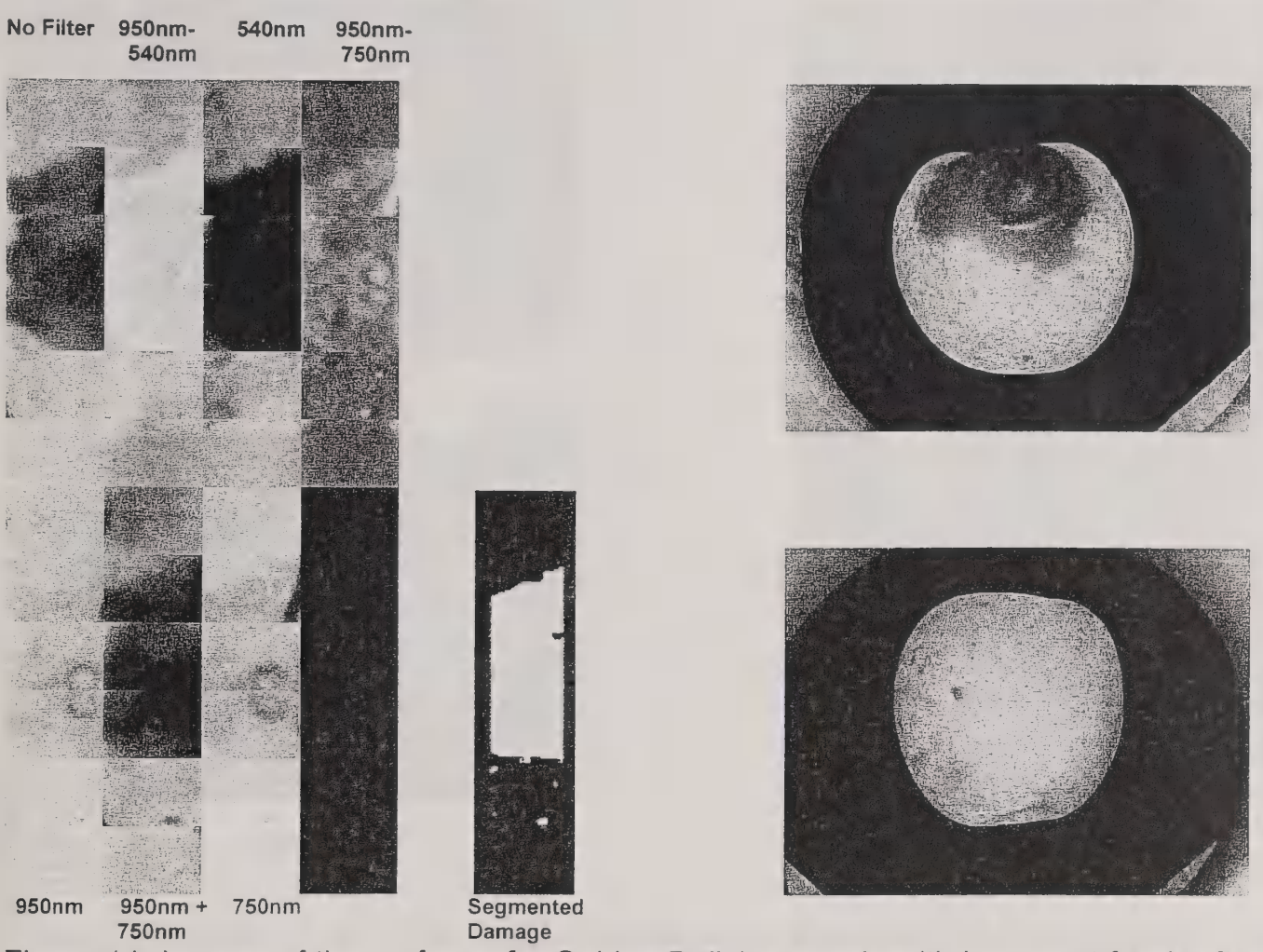

Figure 11. Images of the surface of a Golden Delicious apple with brown rot for the four wavelength bands, mathematical wavelength combinations, segmented damage, and visible wavelength views of each side of the apple (left).

Bitter pit on Red Delicious is best processed from images from the 750nm wavelength band. It is practically invisible in both the 950nm and the 540nm wavelength bands (Figure 12). Studies undertaken in 1999 indicate that even better contrast of bitter pit damage from undamaged tissue can be expected for the 650nm wavelength.

Bruising has the best contrast in the near-infrared wavelengths. The example shown is a Stayman apple removed from a bin right before processing. The bruise can be clearly seen in both the 750nm and 950nm images (Figure 13). For examples of other segmented defects using multiple wavelength images see Throop et. al., 1997.

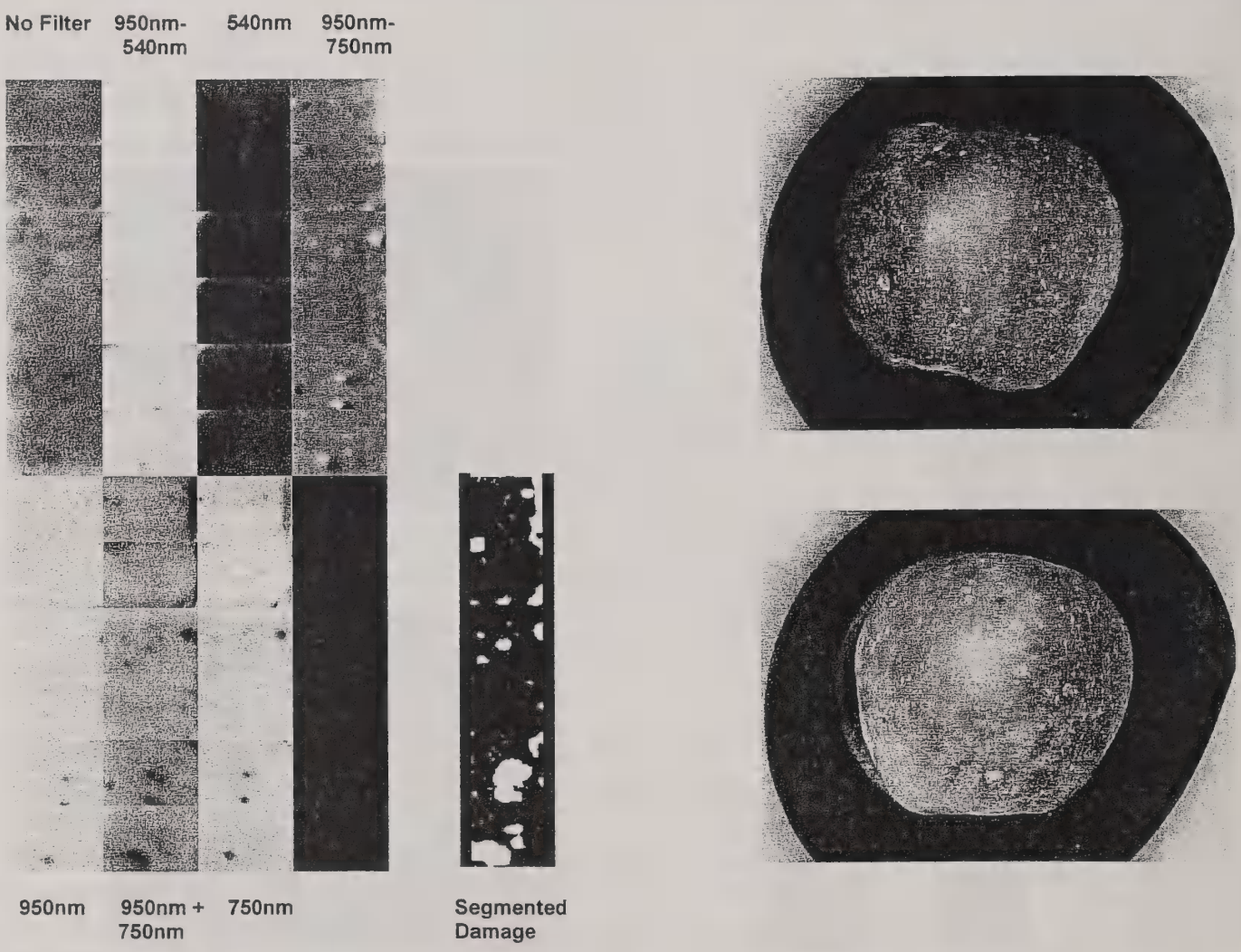

Figure 12. Images of the surface of a Red Delicious apple with bitter pit for the four wavelength bands, mathematical wavelength combinations, segmented damage, and visible wavelength views of each side of the apple (left).

Future Challenges

The addition of a user-friendly interface allowing the user to adjust sensitivity for the different threshold values while processing to detect the many different kinds of defects is necessary since some markets have stricter sorting requirements than others. Means for adjusting the region of interest size for different apple sizes and cultivars is necessary. More apple cultivars need to be oriented by redesign of the conveyor or stem/calyx identification needs to be added.

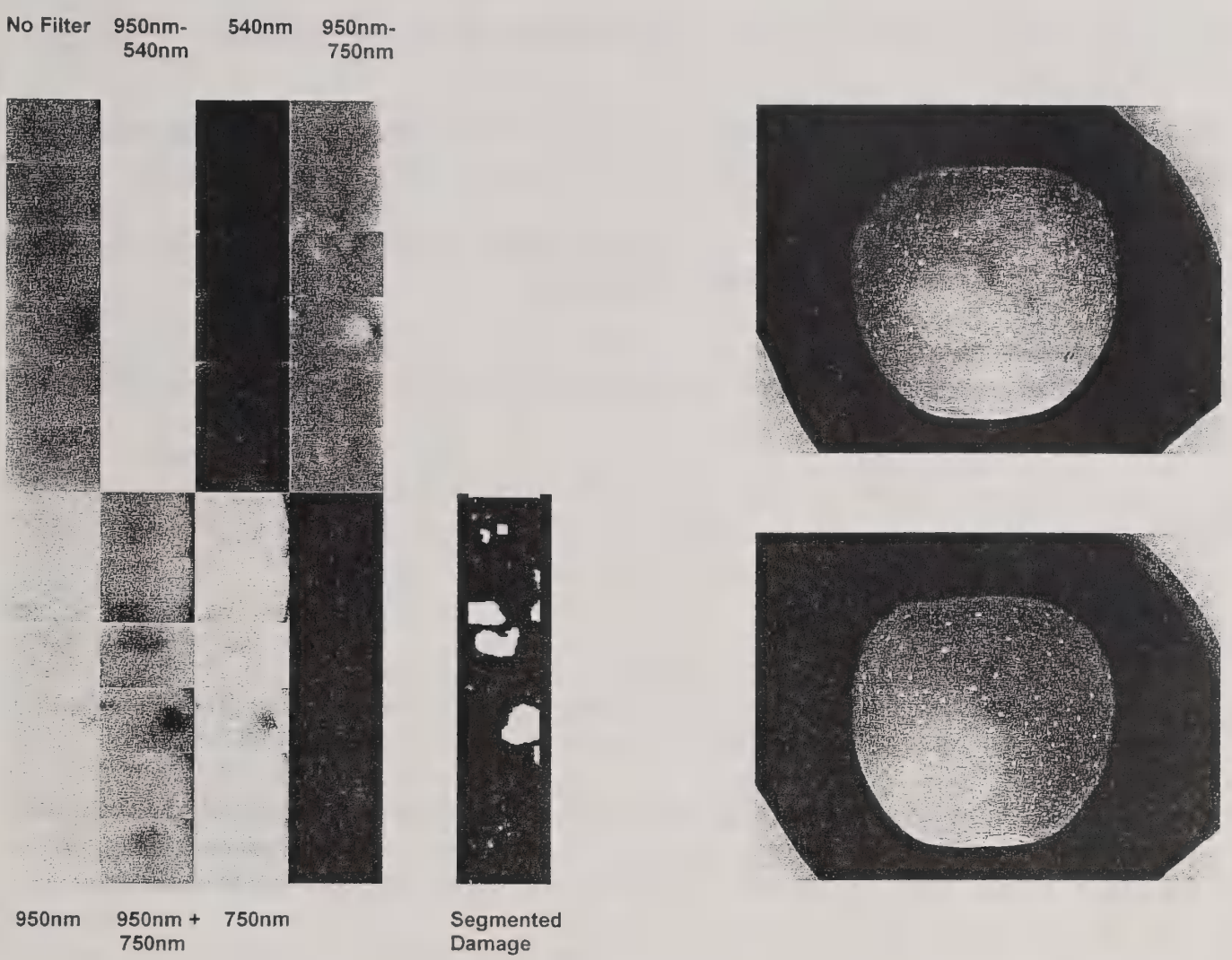

Figure 13. Images of the surface of a Stayman apple with bruising for the four wavelength bands, mathematical wavelength combinations, segmented damage, and visible wavelength views of each side of the apple (left).

CONCLUSIONS

The design and implementation of an inspection station to detect surface defects on apples is presented.

The systems capture multiple images of each rotating apple as they are conveyed through the inspection station at up to 5 apples a second. Special optics produce four identical spatial subimages in each quadrant of the captured frame. Each subimage has different wavelength characteristics

Concerns encountered in this process are discussed as follows:

1. Matching relative response of camera, filters, optics, and lighting to a wide variety of apple cultivars and their defects.

2. Setting the regions of interest to capture the surface of an apple traveling laterally and rotating through the camera's field of view.

3. Providing flat field correction to adjust for variation in reflectance caused by apple surface curvature.

4. Chromatic aberration correction enabling focusing of multiple images captured through a common aperture at different wavelengths.

5. Defect segmentation using features of reflectance for different wavelengths, thresholding based on average reflectance intensity, and segmented feature size and shape.

Example apple images captured at four wavelength bands and a segmented image are presented.

REFERENCES

Affeldt, H. A. and R. D. Heck. 1993. Illumination Methods for Automated Produce Inspection: Design Considerations. *Transactions ASAE,* Vol10(6):871-880.

Aneshansley, D.J., J.A. Throop & B.L. Upchurch. 1997. Reflectance Spectra of Surface Defects on Apples. In Sensors for Nondestructive Testing: Measuring the Quality of Fresh Fruits and Vegetables. Northeast Regional Agricultural Engineering Service Publication No. 97, Ithaca, N.Y. 14853.

Brown, G. K. 1991. Lighting for the Manual Sorting of Apples and Sweet Cherries. ASAE Paper No. 913553, ASAE, St. Joseph, MI. pp 12.

Campins, J., J. A. Throop, D. J. Aneshansley. 1997. Apple Stem and Calyx Identification for Automatic Sorting. ASAE Paper No. 973079, ASAE, St. Joseph, MI. pp 12

Graf, G. L., G. E. Rehkugler, W. F. Millier and J. A. Throop. 1981. Automatic detection of surface flaws on apples using digital image processing. ASAE Paper No. 813537, ASAE, St. Joseph, MI

Graf, G. L. 1982. Automatic detection of surface blemishes on apples using digital image processing. Ph. D. thesis. Cornell University, Ithaca, NY 267p.

Keesling, T. B. 1965. Fruit Processing Method. *U. S. Patent No. 3225892.* 15 p. Commissioner of Patents and Trademarks, Washington, D. C.

Rehkugler, G. E. and J. A. Throop. 1976. Optical – Mechanical Bruised Apple Sorter. *Quality Detection in Foods,* compiled by J. J. Gaffney, ASAE, St. Joseph, MI, pp 185-188.

Rehkugler, G. E. and J. A. Throop. 1989. Image processing algorithm for apple defect detection. *Transactions of the ASAE* 32(1):267-272.

Sagi, Z. and J. A. Throop. 1991. Evaluation of computational algorithms for measurement by cluster segmentation. ASAE Paper No. 913053, ASAE, St. Joseph, MI. pp 19.

Throop, J. A. and G. E. Rehkugler. 1988. Image processing system for detecting bruises on fruit. *U. S. Patent No. 4741042.* Commissioner of Patents and Trademarks, Washington, D. C.

Throop, J. A., D. J. Aneshansley, and B. L. Upchurch. 1995. An image processing algortithm to find new and old bruises. *Transactions of the ASAE.* Vol. 11(5):751-757.

Throop, J. A., D. J. Aneshansley, B. L. Upchurch. 1995. Apple Orientation on Automatic Sorting Equipment. ASAE Paper No. 956176, ASAE. St. Joseph,MI pp 20.

Throop, J.A., D.J. Aneshansley, B.L. Upchurch. 1997. Apple Orientation on Automatic Sorting Equipment. In Sensors for Nondestructive Testing: Measuring the Quality of Fresh Fruits and Vegetables. Northeast Regional Agricultural Engineering Service Publication No. 97, Ithaca, N.Y. 14853.

Throop, J. A., and D. J. Aneshansley, 1997. Apple Damage Segmentation Utilizing Reflectance Spectra of the Defect. ASAE Paper No. 973078, ASAE, St. Joseph, MI pp. 17.

Throop, J. A., D. J. Aneshansley, B. L. Upchurch. 1999. Fruit Orienting Device. *U. S. Patent No. 5,855,270.* 19 p. Commissioner of Patents and Trademarks, Washington, D. C.

Yang, Q. 1993. Finding Stalk and Calyx of Apples using Structured Light. *Computers And Electronics in Agriculture*, Vol(8), pp 31-42.

Yang, Q. 1996. Apple Stem and Calyx Identification with Machine Vision. *Journal of Engineering Research,* Vol(63), pp. 229-236.